March 2021

Heterogeneous Performance Modeling with Applications in Healthcare and Reliability Engineering

Xuxue Sun
University of South Florida

Heterogeneous Performance Modeling with Applications in Healthcare and Reliability Engineering

by

Xuxue Sun

A dissertation submitted in partial fulfillment
of the requirements for the degree of
Doctor of Philosophy
Department of Industrial and Management Systems Engineering
College of Engineering
University of South Florida

Major Professor: Mingyang Li, Ph.D.
Tapas K. Das, Ph.D.
Susana K. Lai-Yuen, Ph.D.
Hongdao Meng, M.D., Ph.D.
Wenjun Cai, Ph.D.

Date of Approval:
February 28, 2021

Keywords: Performance Outputs, Latent Heterogeneity, Prediction Accuracy, Bayesian Statistics, Estimation Algorithm

Dedication

This dissertation is dedicated to my dear parents for their unconditional support in all my endeavors.

Acknowledgments

First of all, I would like to express my deepest appreciation to my major advisor, Dr. Mingyang Li. I am more than grateful that he can give me the opportunity to join in the PhD program at University of South Florida. It is his guidance and patience that makes me go through those hard times. His innovation, passion and rigorous attitudes have set an great example for me in research.

The dissertation would not be successfully completed without my committee members. I would like to express my heartfelt thanks to Dr. Tapas K. Das, Dr. Susana K. Lai-Yuen, Dr. Hongdao Meng and Dr. Wenjun Cai for their generous advice, guidance and great support through my doctoral study.

I would like to show my sincere appreciation to Dr. Nan Kong and Prof. Dr.-Ing. Dr. med. Steffen Leonhardt for their enormous encouragement on my Ph.D. study and their valuable advice in my research. I would also like to thank Dr. Kathryn Hyer for her kind support and great offering of research opportunities. May her soul rest in peace.

Moreover, I gratefully acknowledge the financial support from NSF Grant CMMI-1825761. I also want to express my gratitude to Dr. Kingsley Reeves, Dr. Lu Lu, and Allison Torres-Sabetti for their continued support.

Last but not the least, I would like to express my deepest gratitude to my family. This dissertation would not have been possible without their warm love, continued patience, and endless support. I would also like to thank my friends in China and abroad for their great support: Dr. Yuxin Wen, Dr. Xiaorong Ding, Dr. Zhiyuan Wan, Dr. Zhifan Gao, Dr. Liqin Su, Dr. Wujun Si, Tatapudi Hanisha, Xufei Liu and Yanqing Kuang.

Table of Contents

List of Tables iv

List of Figures v

Abstract viii

Chapter 1 Introduction 1
1.1 Background and Motivation 1
1.2 Literature Review 6
1.3 Overview of Dissertation 10
1.4 Organization of This Dissertation 18

Chapter 2 Heterogeneous Healthcare Utilization Modeling and Evaluation 21
2.1 Introduction 21
2.2 Methodological Framework 23
2.2.1 Framework Overview 23
2.2.2 Modeling of Heterogeneous Time-to-readmission Data 25
2.2.3 Modeling of Heterogeneous Length-of-stay Data 28
2.2.4 Predictive Analytics Integrated Simulation 31
2.3 Case Study 33
2.4 Concluding Remarks 43

Chapter 3 Heterogeneous Service Demand Modeling and Evaluation 44
3.1 Introduction 44
3.2 Framework Overview 47
3.3 Individual Heterogeneity Modeling of Service Demand 49
3.3.1 Module I: Heterogeneous Service Utilization Modeling 49
3.3.2 Module II: Heterogeneous Service Need Characterization 50
3.3.3 Module III: Facility-level Service Demand Simulator 55
3.4 Module IV: Temporal Heterogeneity Modeling of Service Demand 56
3.4.1 Model Formulation 56
3.4.2 Model Estimation 59
3.5 Data-driven Two-Phase NH Resource Planning 62
3.5.1 Module V: Capacity Planning 63
3.5.2 Module VI: Workforce Planning 64
3.6 Case Study 66
3.6.1 Data Description 66

3.6.2 Prediction Performance Evaluation and Comparison 68
3.6.3 Validation of Simulation Model 71
3.6.4 Decision Performance Evaluation and Comparison 73
3.6.5 What-if Scenarios with Different Resident Compositions 76
3.6.6 Results of Temporal Heterogeneity Model 80
3.6.6.1 Prediction Performance Evaluation 80
3.6.6.2 Model Interpretation 82
3.6.6.3 Staffing Decision Performance Comparison 84
3.6.6.4 What-if Scenarios Analysis 87
3.7 Concluding Remarks 90

Chapter 4 Heterogeneous Tribological Degradation Performance Modeling 91
4.1 Introduction 91
4.2 Methodological Framework 95
4.2.1 Framework Overview 95
4.2.2 Model Formulation 96
4.2.3 Material Statistical Descriptor 99
4.2.4 Model Estimation 102
4.3 Real Case Study 107
4.3.1 Experimental Data Description 107
4.3.2 Functional Covariates Extraction 109
4.3.3 Performance Comparison with Alternative Approaches 111
4.3.4 Model Interpretation 115
4.4 Conclusion Remarks 118

Chapter 5 Heterogeneous Corrosion Performance Modeling 120
5.1 Introduction 120
5.2 Framework Overview 123
5.3 Model Formulation 124
5.3.1 Physical Background 124
5.3.2 Individual-level Degradation Performance Modeling 127
5.3.3 Population-level Degradation Performance Modeling 130
5.4 Model Estimation 133
5.4.1 Individual-level Model Estimation 134
5.4.2 Population-level Model Estimation 136
5.4.3 Reliability Analysis 139
5.4.4 Discussion 140
5.5 Case Study 142
5.5.1 Case I: Corrosion-induced Degradation of Al-alloy 142
5.5.1.1 Individual-level Performance Evaluation 142
5.5.1.2 Population-level Performance Evaluation 145
5.5.2 Case II: Corrosion-induced Degradation of Mg-alloy 149
5.6 Conclusion Remarks 150

Chapter 6 Conclusion and Future Work 152

References 156

Appendix A Copyright Permissions 171
A.1 Permission for Chapter 2 171
A.2 Permissions for Chapter 3 and Chapter 4 173
A.3 Permission for Chapter 5 174

Appendix B Supplemental Materials 175
B.1 Appendix for Chapter 4 175
B.1.1 Details of Vector Form of Proposed Model 175
B.1.2 Derivation of Eq. (4.31) 177
B.1.3 Derivation of Eq. (4.32), Eq. (4.33) and Eq. (4.34) 178
B.2 Appendix for Chapter 5 180
B.2.1 Derivations of Eq. (5.38) and $K_1(R,\omega)$-$K_4(R,\omega)$ 180
B.2.2 Derivation of $r_{1i}(\omega,R_i)$-$r_{4i}(\omega,R_i)$ 182

List of Tables

Table 1.1 Summary of different model specifications 19

Table 2.2 Parameters estimation results of proposed readmission model 34

Table 2.3 Estimation results of hospital LOS model 39

Table 2.4 Simulation settings in different scenarios 41

Table 3.5 Identifying variables in the service need characterization system 52

Table 3.6 Estimation results of proposed LOS model 69

Table 3.7 Staffing decision comparison of real practice and proposed model 72

Table 3.8 Descriptions of different capacity strategies 73

Table 3.9 Descriptions of different staffing strategies 74

Table 3.10 Resource planning decision comparison among different scenarios 77

Table 3.11 Modeling features of different staffing strategies in comparison 85

Table 4.12 Different degradation performance modeling approaches 112

Table 4.13 Model comparison results 113

Table 4.14 Model parameter estimation results 115

Table 5.15 Estimation results of individual-level model 144

List of Figures

Figure 1.1 Heterogeneous time-to-readmission data 3

Figure 1.2 Heterogeneous trajectory data 4

Figure 1.3 Heterogeneous corrosion performance assessment signals 5

Figure 1.4 Organization of the dissertation 20

Figure 2.5 Service utilizations among different healthcare facilities 24

Figure 2.6 Overview of proposed modeling framework 25

Figure 2.7 State chart for agent-based simulation of elderly individuals 32

Figure 2.8 Healthcare service utilization variations 33

Figure 2.9 Posterior density plots of model parameters 35

Figure 2.10 Individual unobserved heterogeneity of time-to-readmission data..... 36

Figure 2.11 Facility-specific individual unobserved heterogeneity..... 37

Figure 2.12 Upper limits validation of hospital and NH CIF..... 37

Figure 2.13 Personalized risk analysis 38

Figure 2.14 Individual unobserved heterogeneity of hospital LOS 40

Figure 2.15 Number of individuals using care services in different scenarios..... 42

Figure 3.16 Overview of the proposed framework and decision support system..... 48

Figure 3.17 Service need heterogeneity characterization system 51

Figure 3.18 Fitting performance of the service need groups..... 54

Figure 3.19 Decision tree of service need classification system 54

Figure 3.20 Extracted resident-level information..... 67

Figure 3.21 Comparison of survival curves based on different approaches..... 70
Figure 3.22 Comparison of simulated resident volume at different scales 71
Figure 3.23 Performance comparison among different capacity strategies..... 73
Figure 3.24 Performance comparison among different staffing strategies..... 75
Figure 3.25 Graphical user interface of the decision support platform 80
Figure 3.26 Goodness-of-fit performance evaluation 81
Figure 3.27 Predictions of individual service need trajectories 81
Figure 3.28 Effects of individual characteristics on the baseline service need 82
Figure 3.29 Covariates effects on temporal evolution of service need 83
Figure 3.30 Effects of individual characteristics on determining membership 84
Figure 3.31 Comparison of prediction performance of different strategies 86
Figure 3.32 Staffing supply comparison of different strategies 86
Figure 3.33 Understaffing amount comparison of different strategies..... 87
Figure 3.34 Total labor cost comparison of different strategies 88
Figure 3.35 Daily staffing level comparison of different residents compositions..... 89
Figure 3.36 Total labor cost comparison of different residents compositions 89
Figure 4.37 Overview of proposed modeling framework 95
Figure 4.38 Visualization of proposed bi-level degradation model 99
Figure 4.39 TEM image and diagrams of its functional descriptor 100
Figure 4.40 The testing environment of the investigated accelerated wear test 108
Figure 4.41 Degradation performance outputs of four test units 108
Figure 4.42 TEM micrographs of two different material types.....109
Figure 4.43 Extracted functional descriptors.....110
Figure 4.44 Prediction performance comparison among different models.....115
Figure 4.45 Effects of internal material characteristics among all test units.....116

Figure 4.46 Interaction effect among all test units.....117
Figure 4.47 Quantification of individual latent heterogeneity 118
Figure 5.48 Overview of the proposed degradation modeling framework 124
Figure 5.49 Conventional EIS based physical models 126
Figure 5.50 Proposed model based on fractional order system dynamics.....128
Figure 5.51 Graphical representations of proposed models 133
Figure 5.52 Performance comparison of different modeling approaches.....143
Figure 5.53 Results comparison based on different estimation methods 144
Figure 5.54 Estimated degradation rates comparison 146
Figure 5.55 Prediction performance evaluation of population-level model.....147
Figure 5.56 Quantification of parameter uncertainty and population variability 148
Figure 5.57 K-M curves for individual units RUL and population average RUL 148
Figure 5.58 Prediction comparison results of individual unit of Mg-alloy 149
Figure 5.59 Quantification of uncertainty and variability for Mg units.....150
Figure 5.60 Reliability estimates of individual units and underlying population.....150

Abstract

In both health systems engineering and reliability engineering, individual units, such as patients and product units, often exhibit highly heterogeneous performance due to the influences of various observed individual characteristics and unobserved/unknown factors. Successful modeling of the heterogeneous performance of individual units is of great importance. It will not only facilitate the identification and quantification of influencing factors for improving performance of individual units, but also improve prediction accuracy of their future performance. This will further facilitate better decisions, such as cost-effective and adaptive healthcare resource planning decision, and proactive maintenance policy at reduced cost. However, due to the highly complex data structure of the heterogeneous performance of individual units, heterogeneous performance modeling is challenging. Most of existing models often have restrictive modeling assumptions with limited modeling flexibility. In this dissertation, a generic modeling framework is established with a series of statistical models to characterize three major types of heterogeneous performance data in health systems engineering and reliability engineering, namely the heterogeneous time-to-event data, the heterogeneous trajectory data and the heterogeneous frequency response data. First, a modeling approach of heterogeneous time-to-event data is proposed to characterize the time-to-discharge and time-to-readmission observations of older adults. The proposed model improves service utilization modeling of individual older adults by considering individual latent heterogeneity as well as multiple types of healthcare settings. Second, a modeling approach of heterogeneous trajectory data with latent heterogeneity is proposed to characterize the heterogeneous service demand of nursing home residents. The proposed approach improves prediction accuracy of ser-

vice demand of individual resident and further improves resource planning decisions via integration of the predictive models with computer simulation and stochastic optimization. Third, a modeling approach of heterogeneous trajectory data with covariates is proposed to characterize the heterogeneous tribological degradation performance data of deteriorating test units of cooper alloys. The proposed model improves prediction accuracy of degradation performance by considering mixed-type covariates as well as latent heterogeneity within each test unit. Last, a modeling approach of heterogeneous frequency response data is proposed to characterize the heterogeneous corrosion performance assessment data of corroding aluminum alloys in frequency domain. Both the individual latent heterogeneity and nonlinear fractional order system dynamics are considered to improve reliability assessment and prediction performance of individual test units. Real case studies in both health systems engineering and reliability engineering are considered to illustrate the effectiveness of the proposed modeling framework as well as the developed approaches, and further demonstrate their superior performances as well as benefits to stakeholders in both health systems engineering and reliability engineering.

Chapter 1

Introduction

1.1 Background and Motivation

Due to the influences of various observed individual characteristics and unobserved (or unknown) factors, the individual units (e.g., patients, product units) in health systems engineering and reliability engineering often exhibit highly heterogeneous patterns of performance outputs. For instance, in health systems engineering, individual patient often exhibits heterogeneous service utilization and health outcome, due to the influences of various observed individual characteristics (e.g., demographics, health conditions) and unobserved factors (e.g., service quality of the healthcare provider, care quality of caregiver), which are not available from the existing data (e.g., administrative claims data). Similarly, in reliability engineering, the individual product unit often exhibits highly heterogeneous reliability performance, such as time-to-failure observations and degradation performance trajectories, due to the influences of various observed individual characteristics of product units (e.g., material properties, operating conditions) and unobserved factors (e.g., unknown manufacturing errors and variations, unverified design changes).

Successful modeling of heterogeneous performance of individual unit is of great importance in both health systems engineering and reliability engineering. First, a better heterogeneous performance model will enrich the scientific understanding of the subject of interest for potential performance improvement by identifying and quantifying the influence of potential contributing factors. In health systems engineering, different risk/protective factors which influence the heterogeneous health outcome of individual patient can be identified through the heterogeneous performance modeling and they will

inform healthcare providers to provide more personalized treatment and/or care to improve the outcomes of patients. In reliability engineering, different reliability accelerating/decelerating factors can be identified and quantified based on the heterogeneous performance model. As a result, reliability engineers will be able to improve the reliability growth and maximize the product reliability based on the modeling outputs. Second, a better heterogeneous performance model will improve the prediction accuracy of the performance outputs. In health systems engineering, it will allow the healthcare providers to better predict how different individual patients will utilize healthcare resources differently or allow the doctors to better anticipate how the health outcomes of individual patients will respond differently to the same treatment. In reliability engineering, the heterogeneous performance model will improve the product reliability assessment and the prediction accuracy of failure occurrence as well. Third, with the improved prediction accuracy of performance outputs, the developed heterogeneous performance model can further facilitate the decision making of relevant stakeholders when the available resources are limited. In health systems engineering, with the improved prediction performance of service demand, healthcare provider will be able to achieve better personalized care delivery to meet the heterogeneous service demand of individual patients at reduced costs. In reliability engineering, with the improved prediction accuracy of failure occurrence, reliability engineers will be able to develop more proactive and cost-effective maintenance strategies to maximize the product reliability at field operation stage. To further demonstrate the importance of heterogeneous performance modeling, I will show three motivating examples as follows with different types of performance data which are commonly investigated in health systems engineering and reliability engineering.

The first example is the heterogeneous time-to-event data. The event can be discharge or re/admission in health systems engineering or product failure in reliability engineering. As shown in Figure 1.1, the time-to-readmission observations of residents in assisted living facility are correlated within the same individual and exhibit hetero-

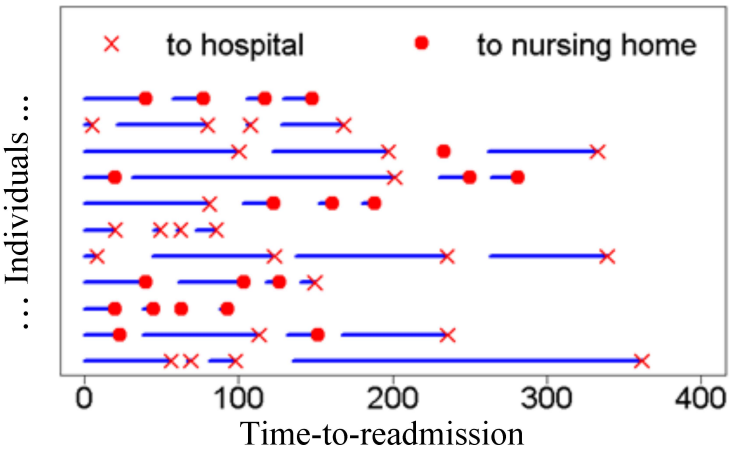

Figure 1.1: Heterogeneous time-to-readmission data

geneous patterns among different individuals. Besides, the readmission events also involve multiple competing healthcare facilities, such as hospital and nursing home (NH), as shown in Figure 1.1. Successful modeling of heterogeneous time-to-event data in health systems engineering (e.g., time-to-readmission and time-to-discharge) is of great importance to achieve high-quality care delivery and cost-effective healthcare resource preparedness. For example, adequate modeling of heterogeneous time-to-readmission data can help to identify the influencing factors of readmission to healthcare facilities (e.g., re/hospitalization). Better understanding of these risk/protective factors can help to better analyze individual patterns of service utilization of different healthcare settings and identify the individuals with high need and high cost. The adequate model of heterogeneous time-to-readmission data can also improve the prediction accuracy of personalized risk of re/hospitalization and NH placement. Moreover, the modeling of time-to-readmission data in health systems engineering can facilitate proper healthcare resource preparedness and care delivery decision to improve health outcomes of elderly individuals, and further inform reimbursement policy. Similarly, successful modeling of heterogeneous time-to-event data in reliability engineering (e.g., time-to-failure) can provide reliability growth opportunities by identifying important influencing factors in affecting product reliability and further can improve the reliability assessment and failure predic-

tion of engineering products. The developed model with improved prediction accuracy enables more proactive maintenance plans and/or warranty policies to be designed.

The second example is the heterogeneous trajectory data. The trajectory data are repeated measurements in temporal domain, which often exhibit heterogeneous evolution patterns among different individual units. For example, the longitudinal observations of

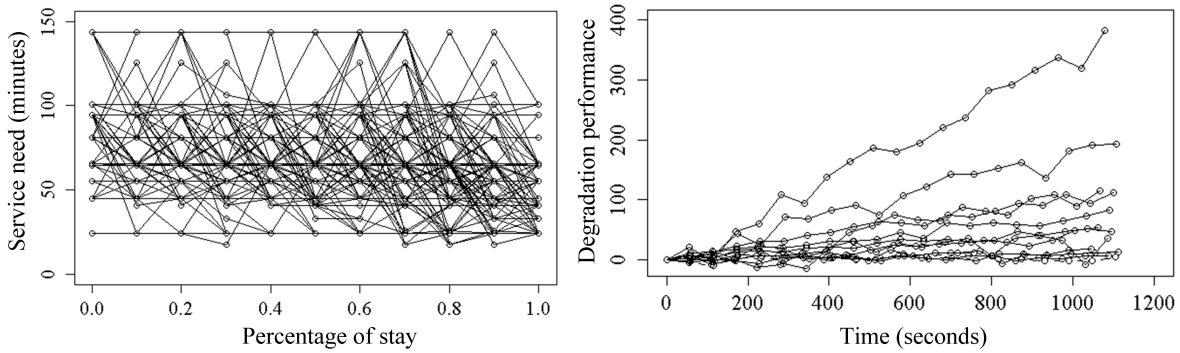

(a) Service need trajectories of nursing home residents

(b) Tribological degradation performance outputs of material test units

Figure 1.2: Heterogeneous trajectory data

service need (measured by the amount of nursing care needed in minutes) for NH residents are temporally evolving and exhibit temporal heterogeneity patterns among different individuals, as shown in Figure 1.2a. Another example is the tribological degradation performance measurements of material test units, which are highly heterogeneous among different test units, as shown in Figure 1.2b. Successful characterization of such heterogeneity is essential to investigate the temporal dynamics and temporal evolution patterns of the trajectory data. The modeling of heterogeneous trajectory data can help to identify the influencing factors which affect the temporal evolution of heterogeneous performance (e.g., service need evolution of nursing care, tribological degradation performance) and quantify their effects as well. The modeling framework can further help to capture the increasing/decreasing patterns of trajectory data and improve the prediction accuracy of dynamic evolution of heterogeneous performance. With the improved predictive analytics and higher modeling fidelity, the adequate modeling of heterogeneous trajectory data

in health systems engineering can further provide managerial insights and inform better decisions about healthcare resource planning. Similarly, successful modeling of trajectory data in reliability engineering can inform better experimental design about material reliability testing and better maintenance policy.

The third example is the heterogeneous frequency response data. The frequency pro-

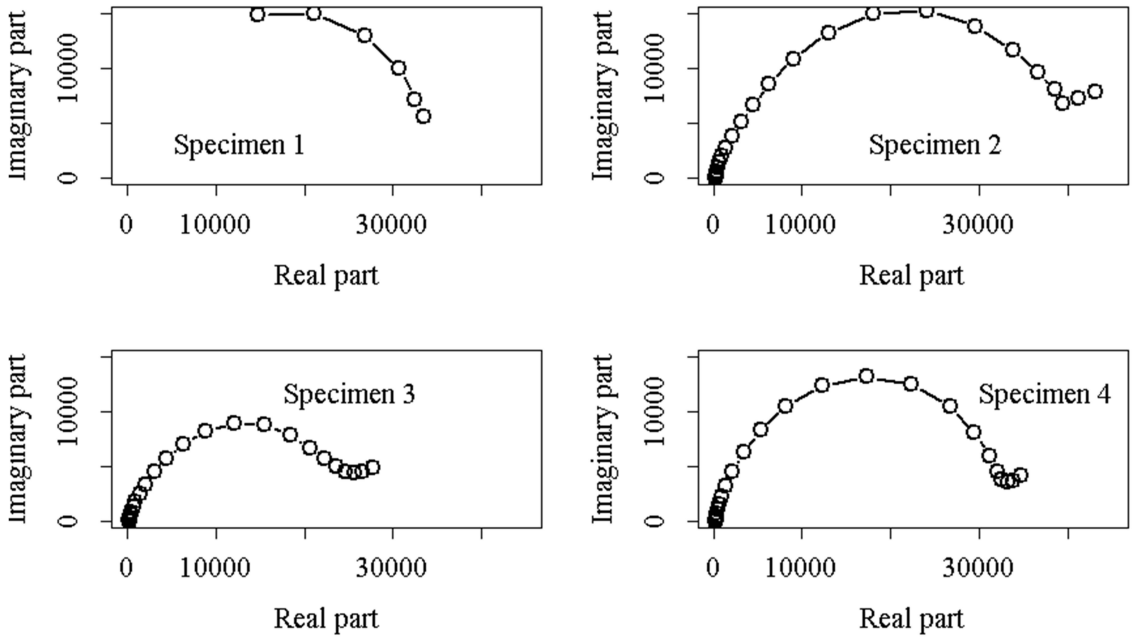

Figure 1.3: Heterogeneous corrosion performance assessment signals

files are nonlinear signal measurements in frequency domain and often exhibit heterogeneous patterns among different individual units. For example, the corrosion performance assessment signals of material units of aluminum alloy measured in frequency domain are highly nonlinear and heterogeneous among different material units, as shown in Figure 1.3. Successful modeling of such heterogeneous and nonlinear frequency response data in reliability engineering can help to identify important accelerating/decelerating factors and quantify their influences on product degradation performance. The adequate modeling of heterogeneous frequency response data in reliability engineering can also improve the prediction accuracy of remaining useful life and failure occurrence of mission-critical components/systems, and further improve product reliability assessment. Further, the predictive model of heterogeneous frequency response data with improved ac-

curacy can benefit the cost-effective design of experiments for accelerated testing at research and development stage and also facilitate the optimal maintenance decisions at field operation stage. The heterogeneity modeling approach of frequency response data in reliability engineering can be extended to health systems engineering for analyzing physiological signals, such as electroencephalogram (EEG) signals, which will further facilitate care delivery decisions and inform better treatment decisions to improve the health outcomes of patients.

1.2 Literature Review

The scope of this dissertation is focusing on the heterogeneous performance modeling in both health systems engineering and reliability engineering. Specifically, this dissertation work will investigate the modeling of three major types of heterogeneous performance data often encountered in both health systems engineering and reliability engineering, namely (i) the heterogeneous time-to-event data, (ii) the heterogeneous trajectory data, and (iii) the heterogeneous frequency response data. This section will provide a comprehensive literature review of the existing modeling approaches for these common types of performance data.

The time-to-event data is a generic type of performance data which measures the time duration until the event of interest occurs. This type of performance data commonly appears in both health systems engineering and reliability engineering. For instance, the observations of time-to-discharge from hospital and the observations of time-to-readmission to multiple competing healthcare facilities are examples of the time-to-event data in health systems engineering. In reliability engineering, the time-to-event data can refer to the time-to-failure data of product units. The time-to-event observations in both health systems engineering and reliability engineering are highly heterogeneous among different individual units and often exhibit within-individual dependency, as previously illustrated in Figure 1.1. Such heterogeneous performance is influenced by the

observed individual characteristics, such as individual socio-demographics and health conditions in health systems engineering, and individual characteristics of product unit in reliability engineering. The within-individual dependency can be ascribed to the influence of unobserved/unknown factors, such as the detailed physiological information of individual patient which is not available from high-level claims data in health systems engineering, and unknown material properties due to measurement limitations in reliability engineering. To characterize such complex time-to-event data in health systems engineering and reliability engineering, different analytical methods have been developed. Some existing studies use parametric/non-parametric distribution-based methods (Zonderland et al., 2015; Méndez-González et al., 2017) to analyze time-to-event data at aggregate population level. These methods fail to consider the influence of individual characteristics on heterogeneous performance data and they are incapable of personalized analysis. To account for the influence of individual covariates, some existing models incorporate individual observed characteristics and investigate their effects on heterogeneous performance of time-to-event data, such as linear and generalized linear models (Lee et al., 1993; Bender et al., 2018; Verburg et al., 2014). For instance, the existing literature in health systems engineering utilize individual demographics and clinical diagnoses to characterize the heterogeneous time-to-readmission data (Salamzadeh et al., 2003) and time-to-discharge data (Gardner et al., 2007). However, these models with observed covariates fail to consider the individual unobserved heterogeneity due to the lack of available information (e.g., detailed health information in administrative claims data). Although some recent studies incorporate latent variables to capture individual unobserved heterogeneity, such as frailty models (Rondeau et al., 2003, 2006), their estimation procedures are developed for population-level analysis and cannot estimate individual-specific latent variables. Moreover, most existing literature often focus on single type of event, e.g., single type of healthcare settings for individual readmission in health systems engineering (Zonderland et al., 2015; Salamzadeh et al., 2003), and they fail to consider

multiple cause-specific competing types of event of interest. There is a need to develop a generic analytical framework to address the above gaps and to characterize the heterogeneous time-to-event data in both health systems engineering and reliability engineering.

The trajectory data is another important type of performance data to be investigated in this dissertation. The longitudinal trajectory consists of repeated measurements from same subject in temporal domain. It is a generic data type in health systems engineering and reliability engineering, which can be used to represent different performance responses, such as the service need trajectories of NH residents in health systems engineering, and tribological degradation performance trajectories of material test units in reliability engineering. The trajectory data in both health systems engineering and reliability engineering is heterogeneous among different individual units and often exhibits diverse temporal evolution pattern, as previously illustrated in Figure 1.2 (a) and (b). Many existing studies often assume a homogeneous population and utilize population parameters to characterize the trajectory data, such as continuous stochastic process (Ye and Xie, 2015; Chen and Ye, 2018) and Markov-based models (Kharoufeh et al., 2010; Bian et al., 2015). For instance, the population dynamics models (Dadlani et al., 2014) in population health study assume the individuals are from same population and often use population parameters to characterize the heterogeneity of disease propagation. Similarly, in reliability engineering, Kharoufeh and Cox (2005) focus on characterizing the heterogeneity of degradation performance outputs as a whole without explicitly incorporating covariates as additional inputs. These approaches neglect the influence of individual covariates and fail to explain part of the heterogeneity of the trajectory data. To characterize heterogeneous trajectory data with covariates, many existing models often consider single type of covariates. For example, Bagdonavicius and Nikulin (2001) only considers scalar covariates which represent the aggregate-level material characteristics. Similarly, Park et al. (2017) only considers scalar covariates of external environmental conditions in their model to capture degradation performance heterogeneity in reliability engineer-

ing. On the other hand, Si et al. (2019) only considers functional covariate of detailed material microstructure information in their degradation model for reliability study. For another example in health systems engineering, many existing models consider time-invariant covariates only to capture the heterogeneous temporal evolution patterns of disability/functional performance trajectories (Chiu and Wray, 2011; Zimmer et al., 2012). The above models fail to consider multiple types of covariates (e.g., scalar and functional, time invariant and time-varying) and their potential interaction. Moreover, most existing literature fail to address the latent heterogeneity induced by the unobserved factors shared within each individual unit. In some recent studies which consider the influence of unobserved factors, they either utilize discrete latent variable only, such as mixture model in health systems engineering and reliability engineering (Yuan and Ji, 2014; Sakib et al., 2017), or use continuous latent variable only, such as random growth model in health systems engineering (Laird and Ware, 1982) and degradation path model in reliability engineering (Meeker et al., 1998). Most existing models fail to consider both types of latent variables, namely discrete and continuous latent variables, and they are not able to capture both individual-level latent heterogeneity and sub-population level heterogeneity. In addition, most existing studies in both health systems engineering and reliability engineering focus on the modeling of one-dimensional trajectory data and they are not applicable for handling multi-dimensional trajectory data. There is a need to develop a generic modeling framework to address the above gaps and to characterize both temporal dynamics and temporal heterogeneity of trajectory data with observed covariates and latent heterogeneity in both health systems engineering and reliability engineering.

The frequency response data is the third type of performance data that will be investigated in this dissertation. The frequency profiles are nonlinear assessment signals measured in frequency domain. For instance, the corrosion performance data of aluminum alloy in reliability engineering are nonlinear frequency responses and can be collected via non-destructive testing technique to account for the latent nature of degradation state of

corroding units of aluminum alloy. The frequency response data is highly heterogeneous among different material test units, as previously illustrated in Figure 1.3. To investigate the corrosion-induced degradation process of the test units and to assess the latent degradation performance of corroding aluminum alloy units, several physical models based on frequency response data have been established, including Randles circuit model (Alavi et al., 2016) and failed coating model (Bierwagen et al., 2003). However, these models are less generic and less flexible to characterize the highly nonlinear relationship between frequency responses and the latent degradation state. Besides, the existing physical models have two major limitations. First, the least squares estimation method which is mainly considered in the existing literature fails to quantify model parameters uncertainty due to the limited sample size of data. Second, many existing studies are mainly restricted to analyzing degradation behavior of an individual test unit and often fail to account for the degradation performance variability of the underlying population from which multiple test units are drawn. Moreover, when a test unit has sparse measurements, it is difficult to assess its individual degradation performance. Although Bayesian statistics provides appealing estimation and inference framework (Gelman et al., 2013) to address the aforementioned estimation challenges, it cannot be directly adopted due to its empirical nature and the complex physical failure mechanism of corroding units. It will be desirable to integrate physical models with Bayesian statistics to improve the modeling accuracy and reliability assessment as well. There is a need to develop a modeling framework to capture the heterogeneity of the highly nonlinear frequency responses data and to quantify both the parameters uncertainty and population variability.

1.3 Overview of Dissertation

This dissertation focuses on advancing the modeling of heterogeneous performance in health systems engineering and reliability engineering with three different types of performance data, namely the heterogeneous time-to-event data, the heterogeneous tra-

jectory data and the heterogeneous frequency response data. To address the research gaps mentioned in previous section, I propose a generic modeling framework of heterogeneous performance of individual units in both health systems engineering and reliability engineering, manifested as

$$
\begin{aligned}
y_{ij} &\sim f(y \mid \boldsymbol{x}_i, Z_i, \boldsymbol{\Theta}), \forall i = 1, ..., N, j = 1, ..., m_i \\
Z_i &\sim G(z \mid \boldsymbol{\Phi}), \forall i = 1, ..., N
\end{aligned} \tag{1.1}
$$

where y_{ij} refers to the j^{th} performance observation/measurement of individual unit i. For instance, in health systems engineering, y_{ij} can represent either the j^{th} hospital time-to-discharge observation of individual patient i, or the service need observation of nursing care of NH resident i at day j as well. In reliability engineering, y_{ij} can be specified as the tribological degradation performance measurement of individual material unit i at time index j, or the corrosion performance assessment of test unit i at frequency j. $f(\cdot)$ is a function mapping which links observed covariates and latent factors with performance response, and it can be manifested as parametric/nonparametric and linear/nonlinear model. $\boldsymbol{x}_i$ is a vector of observed characteristics of individual unit i, and it can be either the time-invariant characteristics, time-varying characteristics, or the functional covariates in spatial domain. For instance, $\boldsymbol{x}_i$ can refer to individual demographics, clinical diagnosis, and therapy intensity level of individual patient i in health systems engineering. Alternatively, it can also represent the time-varying health conditions of elderly adults i. In reliability engineering, $\boldsymbol{x}_i$ can refer to the environmental/accelerated conditions of individual material unit i in an accelerated degradation test, or the individual material properties of test unit i as well. $\boldsymbol{\Theta}$ is a set of unknown model parameters. Z_i is a latent variable (Bentler and Weeks, 1980) which is a random quantity that cannot be observed directly. In the proposed generic framework, I utilize Z_i to capture the unobserved heterogeneity induced by the unobserved/unknown factors shared within individual unit i. $G(\cdot)$ is a density

function for Z_i with parameters $\mathbf{\Phi}$. The latent variable Z_i can be specified as a continuous random variable which accounts for individual unobserved heterogeneity. It can also be specified as discrete random variable which captures sub-population level heterogeneity. Moreover, Z_i can become more than one dimension, such as mixed type (e.g., both discrete and continuous) latent variables, which capture both individual unobserved heterogeneity and grouping patterns of performance data. For instance, Z_i can represent the unobserved factors shared within each patient in health systems engineering due to the lack of detailed physiological information in claims data. In reliability engineering, Z_i can refer to the unmeasurable/unknown factors shared within each individual material unit due to measurement limitations. With the above formulation, the proposed modeling framework can jointly capture the observed heterogeneity and unobserved heterogeneity at different levels (e.g., individual level and sub-population level). Attributed to the generic formulation, several important classes of statistical models, such as frailty model and mixture model, can be viewed as special cases of the proposed modeling framework. Besides, the proposed modeling framework has appealing features in practice, such as improved prediction accuracy and sound model interpretability. Moreover, in this dissertation, I further develop the model estimation algorithms by addressing various technical challenges during model estimation. With such generic model formulation and flexible modeling capability, the proposed framework can be applicable for modeling different types of heterogeneous performance data in health systems engineering and reliability engineering. Under the proposed framework, the detailed contributions and advancements of the specific modeling approach developed in each chapter are elaborated as follows from both methodological development and application perspectives.

As mentioned in previous section, many existing modeling approaches of time-to-event data often consider the influence of observed covariates only and mainly focus on a single type of critical event. These approaches fail to consider the influence of unobserved/unknown factors and they are not able to account for multiple competing

types of critical events in both health systems engineering and reliability engineering. To fill the gaps and to address the research need of modeling heterogeneous time-to-event data, in chapter 2, I employ the proposed generic modeling framework and develop specific statistical model and estimation algorithm to jointly quantify the observed heterogeneity and the unit-specific latent heterogeneity. Considering the problems of time-to-readmission and time-to-discharge modeling in health systems engineering as examples, the response variables y_{ij}'s refer to the correlated time-to-readmission observations and time-to-discharge observations of patient i, respectively. The individual observed covariates $\boldsymbol{x}_i$ refer to individual demographics and health conditions of each patient i. I then develop survival model to manifest the function mapping $f(\cdot)$. $\boldsymbol{\Theta}$ is a set of unknown parameters related to the specified survival model. The unknown model parameters can be facility-specific to account for the multiple types of competing healthcare settings (e.g., hospital, nursing home) involved in the critical events (e.g., discharge event, readmission event). The latent variable Z_i follows continuous distribution and it captures the unobserved heterogeneity of each patient i due to the lack of detailed physiological information in administrative claims data. Z_i can be facility-specific as well to account for the multiple competing types of healthcare settings. Further, I develop estimation algorithm under Bayesian framework to jointly estimate the influences of observed covariates and unobserved factors. With the integrated Bayesian estimation technique and latent survival analysis, I advance the heterogeneous time-to-event data modeling approach in this dissertation to account for both observed heterogeneity and unobserved heterogeneity. In addition to the methodological contribution, the proposed work also has contribution in the application of health systems engineering. As compared to many existing studies which focus on a particular disease group and/or single type of healthcare settings (e.g., hospital), I investigate multiple competing types of healthcare settings and study the elderly adults with multiple disease diagnoses in this dissertation.

The second type of heterogeneous performance data I want to investigate in this dissertation is the heterogeneous trajectory data. First, I study the application problem of service demand modeling of NH residents in health systems engineering. As mentioned in previous section, many existing studies use descriptive analytics and/or simple predictive analytics to capture individual service demand of NH residents. Some existing methods with predictive analytics characterize heterogeneous individual service demand via considering the influence of observed covariates or utilizing single type of latent variable. Most existing studies fail to account for temporal evolution dynamics and temporal heterogeneity of service demand. Many existing models fail to consider both observed heterogeneity and unobserved heterogeneity of service demand at both sub-population level and individual level. To fill the gaps and to address the research need of modeling trajectory data in health systems engineering, in chapter 3, I employ the proposed generic framework and develop service need trajectory model by incorporating both observed heterogeneity and mixed-type latent heterogeneity to characterize the temporal dynamics and temporal heterogeneity of individual service need evolution. Specifically, considering the problem of modeling service need trajectory of NH residents, the response variables y_{ij}'s refer to the repeated observations of individual daily service need of NH resident i in temporal domain. The individual observed covariates $\boldsymbol{x}_i$ refer to both of the individual time-invariant characteristics and time-varying characteristics of NH resident i, such as individual demographics, health conditions, functional performance limitations and therapy intensity level. The proposed model considers mixed-type latent heterogeneity and uses both continuous and discrete latent variables to capture both individual-level unobserved heterogeneity and sub-population level temporal evolution patterns. The underlying service need evolution is captured by both observed covariates and mixed-type latent variables, and further linked with observed service need trajectory via longitudinal model $f(\cdot)$. I also develop model estimation algorithm to jointly quantify the influence of observed covariates and the mixed-type latent heterogeneity of individual service

need evolution. Further, I integrate the developed predictive analytics with simulation model to capture the temporally evolving heterogeneous service demand of NH residents. Moreover, I improve NH resource (e.g., capacity, staffing) planning decisions to achieve better system performance via incorporating predictive analytics integrated simulation into data-driven decision analytics. In this dissertation, I also investigate how the demand heterogeneity of NH residents will influence the resource planning decisions. In addition to the methodological contributions, the proposed work in this dissertation also has several contributions from application perspective. The staffing decisions in many existing literature are ratio-based and most of them neglect the service demand heterogeneity among different individuals. There is also a lack of analytics-based decision support tools for NH resource planning. The proposed work in this dissertation considers the heterogeneous and temporally evolving service demand and further achieves adequate NH staffing decision based on the characterized service demand. Besides, I develop an analytics-based decision support platform to facilitate managerial decisions in response to the varied service demand of varied residents census compositions.

Along the research line of heterogeneous trajectory data modeling, I further investigate the tribological degradation performance modeling in reliability engineering. As mentioned in previous section, many existing degradation models either consider the scalar covariate of the external environmental condition only, or solely the functional covariate of the internal material information. Most existing models fail to consider both the scalar and functional covariates as well as their potential interaction. Besides, many approaches in existing literature fail to consider the influence of unobserved factors shared within each unit. To fill the gaps and to address the research need of modeling heterogeneous trajectory data with covariates in reliability engineering, in chapter 4, I employ the proposed framework and develop a generic degradation model with mixed-type covariates and latent heterogeneity to capture the heterogeneous tribological degradation performance. Specifically, the response variables y_{ij}'s refer to the repeated measurements

of tribological degradation performance of test unit i in temporal domain during an accelerated wear test. The individual observed covariates $\boldsymbol{x}_i$ are mixed-type covariates of material unit i which embrace both the scalar covariates of accelerated conditions and the functional covariates of material characteristics. The continuous latent variable Z_i captures the latent heterogeneity of each test unit i due to the influence of unobserved/unknown factors shared within each unit. I develop a bi-level degradation model to characterize the heterogeneous degradation performance. At response level, I linearize the function mapping via polynomial basis functions. At coefficient level, I then decompose the basis coefficient into five parts to quantify both the influences of mixed-type covariates and their interaction as well as continuous latent heterogeneity. Further, I develop estimation algorithm to address the estimation challenges. In this work, I employ finite basis approximation technique to address the infinite dimensionality of functional covariates. In addition, I use data augmentation technique to address the issue of joint estimation of mixed-type covariates and latent variable, and further develop the estimation procedure under expectation maximization framework. With the above model and algorithm development, the propose approach accounts for the influences of observed mixed-type covariates, which represent both the environmental/accelerated conditions and material microstructure characteristics, and the influence of their potential interaction as well as the influence of unobserved factors. In addition to the methodological contributions, the proposed work in this dissertation also achieves problem-wise advancements. As compared to many existing studies which may neglect the internal factors of material information, the proposed work considers both internal material information and external environmental conditions for accelerated degradation tests. Besides, the proposed work considers multiple types of material microstructure characteristics as compared to previous studies which only consider single material type.

In addition to the above modeling approaches of characterizing the heterogeneous time-to-event data and the heterogeneous trajectory data, I also investigate the model-

ing of heterogeneous performance data in frequency domain. As mentioned in previous section, many existing studies are based on physical models and only consider simple system dynamics. Most of these models fail to capture the complex physical failure mechanism and they are not able to characterize the highly nonlinear relationship between frequency responses and the latent degradation state. Besides, the conventional estimation methods in most existing studies could quantify neither the parameter uncertainty nor the population variability due to the limited sample size of data. Moreover, the sparse measurements also make the individual degradation performance assessment difficult. Although Bayesian statistics provide appealing estimation and inference framework to address the above estimation challenges, it cannot be directly adopted due to its empirical nature. To fill the gaps and to address the research need of modeling heterogeneous and nonlinear frequency response data, in chapter 5, I employ the proposed generic modeling framework and develop a physical-statistical model with integrated fractional order system dynamics and Bayesian statistics. Considering the problem of modeling degradation performance of corroding units of aluminum alloy, the response variables y_{ij}'s refer to the nonlinear corrosion performance assessment signals of test unit i in frequency domain. The individual observed covariates $\boldsymbol{x}_i$ refer to the frequencies of stimulus applied on each unit i. To establish the adequate nonlinear relationship between frequency responses and the latent degradation state, I then incorporate fractional order system dynamics to manifest the highly nonlinear function mapping $f(\cdot)$. The continuous latent variable Z_i captures the influence of unobserved/unknown factors shared within unit i. In this dissertation work, I propose Bayesian hierarchical model with integrated nonlinear fractional order system dynamics and Bayesian statistical inference to characterize population-level degradation performance and to capture the complex physical failure mechanism of corroding units. I develop estimation algorithm under Bayesian framework to quantify both parameter uncertainty and underlying population variability, and also to enable information sharing among different test units drawn from same

population. The proposed modeling framework of frequency response data can improve the prediction accuracy of remaining useful life and improve the reliability assessment of product unit as well. In addition to the methodological contributions, the proposed work also has contribution from the application perspective. As compared to the conventional approaches in corrosion degradation study which are either physical models or statistical models only, the proposed work incorporates both physical engineering knowledge and Bayesian statistics into a physical-statistical model for characterizing the highly nonlinear and heterogeneous frequency response data.

Overall, the proposed framework is generic for characterizing different types of heterogeneous performance data in both health systems engineering and reliability engineering. Under this framework, the model development details in each chapter for handing different types of performance data are summarized in Table 1.1.

1.4 Organization of This Dissertation

The dissertation is organized as follows. Chapter 1 introduces the background and significance of heterogeneous performance modeling in health systems engineering and reliability engineering. Chapter 1 also gives the literature review and introduces the proposed modeling framework as well as key features of the specific modeling approaches developed in each chapter for characterizing different types of heterogeneous performance data. Chapter 2 proposes a Bayesian modeling approach of heterogeneous time-to-event data with competing risk to characterize the heterogeneous service utilization of elderly individuals in different healthcare settings. Chapter 3 proposes a series of heterogeneous service demand modeling approaches to characterize heterogeneous length of stays and heterogeneous service need trajectories of NH residents and further integrates the predictive analytics with computer simulation and stochastic optimization to achieve optimal NH resource planning. Chapter 4 proposes a degradation model with mixed-type covariates and continuous latent variables to characterize the heterogeneous

Table 1.1: Summary of different model specifications

Domain	Healthcare		
Performance	time-to-discharge/time-to-readmission	Data structure	time-to-event data
Model specification details under the proposed framework in chapter 2			
y_{ij}'s	time-to-discharge/time-to-readmission observations		
$\boldsymbol{x}_i$	individual demographics and health conditions		
Z_i	continuous latent variable, capturing latent heterogeneity due to the lack of detailed physiological information		
$f(\cdot)$	survival model		
$\boldsymbol{\Theta}$	facility-specific unknown model parameters		
Performance	service need trajectory	Data structure	trajectory data
Model specification details under the proposed framework in chapter 3			
y_{ij}'s	service need observations in temporal domain		
$\boldsymbol{x}_i$	individual demographics, health conditions, functional performance limitations, therapy intensity		
Z_i	mixed-type (both continuous and discrete) latent variable, capturing temporal heterogeneity at both individual level and sub-population level		
$f(\cdot)$	longitudinal model		
$\boldsymbol{\Theta}$	unknown model parameters		
Domain	Reliability		
Performance	tribological degradation performance	Data structure	trajectory data
Model specification details under the proposed framework in chapter 4			
y_{ij}'s	tribological degradation performance measurements in accelerated wear test		
$\boldsymbol{x}_i$	mixed-type covariates (both scalar covariates of accelerated conditions and functional covariates of material characteristics)		
Z_i	continuous latent variable, capturing the influence of unobserved factors shared within each test unit		
$f(\cdot)$	longitudinal model		
$\boldsymbol{\Theta}$	unknown model parameters		
Performance	corrosion performance assessment signals	Data structure	frequency profiles
Model specification details under the proposed framework in chapter 5			
y_{ij}'s	corrosion performance measurements in frequency domain		
$\boldsymbol{x}_i$	frequency stimulus on each test unit		
Z_i	continuous latent variable, representing the latent degradation rate and capturing the influence of unobserved factors shared within each test unit		
$f(\cdot)$	hierarchical model with fractional order system dynamics		
$\boldsymbol{\Theta}$	unknown model parameters, including population sharing parameters		

tribological degradation performance of test units in an accelerated wear test. Chapter 5 proposes a hybrid degradation model via integrating Bayesian hierarchical models with fractional order system dynamics to characterize the heterogeneous frequency profiles of

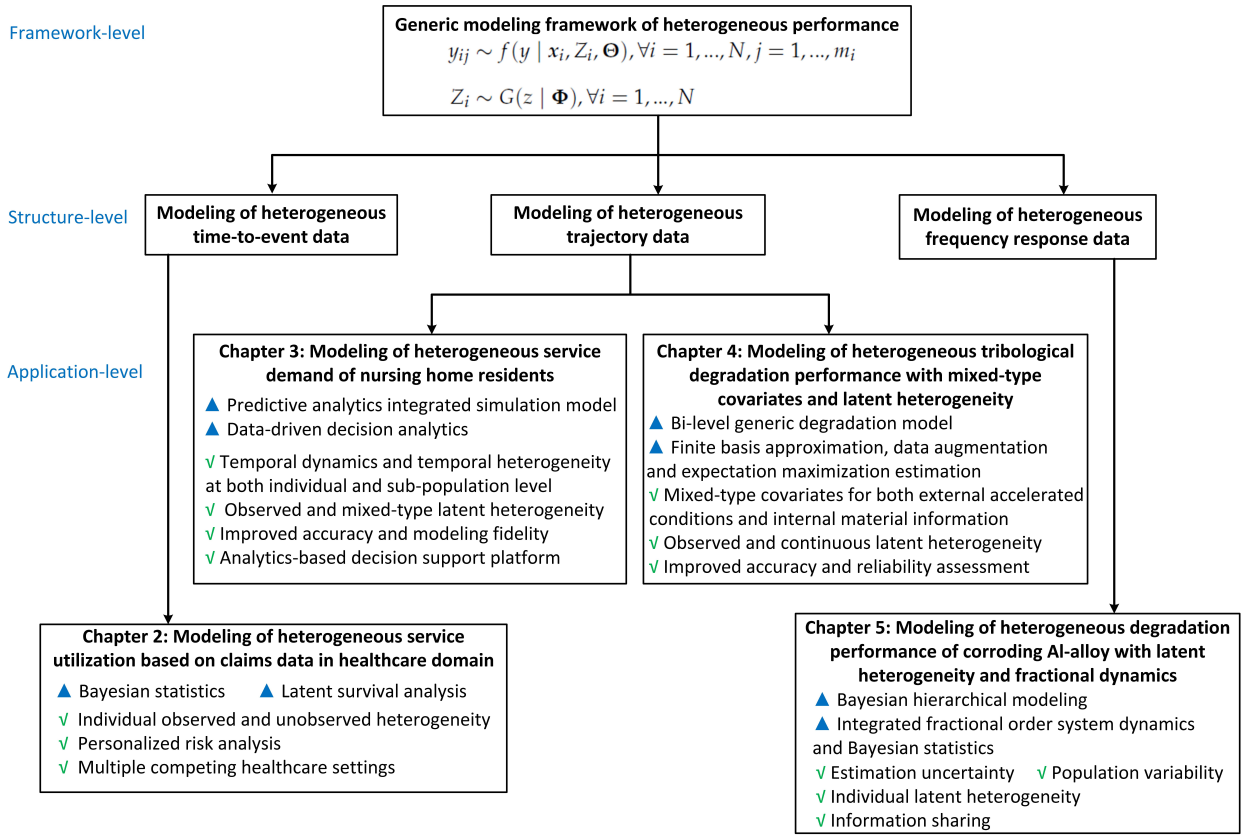

Figure 1.4: Organization of the dissertation

corroding units of aluminum alloy. Chapter 6 concludes the dissertation with some directions for future research. Figure 1.4 gives an organization diagram of the dissertation.

Chapter 2

Heterogeneous Healthcare Service Utilization Modeling and Evaluation of Older Adults with Latent Survival Analysis

2.1 Introduction

To achieve high quality healthcare service delivery and cost-effective resource management among different healthcare service facilities is one of the important and essential objectives in the current healthcare research and practice[1]. The increasing healthcare demand of the elderly due to the rapid population aging and high prevalence of diseases and disabilities, coupled with the costly and limited resources available in healthcare facilities, pose great challenges in current U.S. healthcare systems to ensure high quality of care. The service utilization of healthcare facility is a key measure of healthcare service demand. The pursuit of match between healthcare demand and resource requires a deep understanding of the relationship between the service utilization of healthcare facility and the various individual characteristics of aging population. Healthcare administrative claims data, originally generated for administrative and billing purpose, contains important information, such as healthcare time-to-readmission and length of stay (LOS), which can be leveraged to investigate the service utilization under different healthcare settings. They provide valuable tracking information for admissions and discharges of elderly individuals with different health conditions and demographics. Since healthcare service utilization may be affected by various individual characteristics and different types of healthcare facilities, such as acute care and long-term care facilities, may also have differ-

[1]This chapter was published in IEEE (Sun et al., 2017a) and World Scientific (Sun et al., 2017b). Copyright permissions from the publishers are included in Appendix A.

ent influencing factors, it will be desirable to develop data-driven models to analyze individual's time-to-readmission and LOS from historical administrative claims data. Claims data and electronic health records are two popular data sources for researchers to examine healthcare utilization patterns and cost of care. Electronic health records contain detailed individual health information while they are highly fragmented across different healthcare facilities due to various reasons, such as lack of compatibility of different data warehouse, lack of standardization of data formats, and privacy and security of data sharing (Fernández-Alemán et al., 2013). As compared to electronic health records, claims data are standard data sources for billing and administrative purposes with more compatible information but less individual detailed information. These important information of varied individual characteristics may contribute to the highly heterogeneous service utilization of elderly individuals while they are not available from claims data. Consequently, there may be many potentially influencing factors shared within each individual but they are unobserved. These unobserved factors may also affect individuals' healthcare service utilization and need to be quantified explicitly. Thus, an efficient and effective statistical model needs to be developed to capture such unobserved heterogeneity and to quantify the influence of observed individual characteristics on healthcare service utilization of different types of facilities.

Several challenges are involved in modeling heterogeneous time-to-event observations of elderly individuals from administrative claims data. In the context of this work, an event can refer to "readmission" or "discharge", and thus time-to-event observations become time-to-readmission or LOS observations. Both time-to-readmission and LOS data in practice exhibit right-skewness. This right-skewness makes the normality assumption in conventional statistical modeling approaches invalid. To address the right-skewness issue and to explore the influences of different factors, many statistical modeling approaches have been investigated (Bernatz et al., 2015; Jasti et al., 2008). However, these methods only consider heterogeneity induced by observed factors. They ignore the

unobserved heterogeneity, which quantifies the effect of unobserved factors due to the aforementioned unavailability of many individual detailed information in claims data. Some approaches are developed recently to address the issue of unobserved heterogeneity (Kansagara et al., 2011; Lee, 2012). However, these existing studies mainly employ non-Bayesian estimation method, such as maximum likelihood estimation method. They can only assess the average healthcare utilization over a population and fails to provide an individualized model for every individual care recipient. Non-Bayesian methods also have issues in unknown parameter estimation when sample size is small. In addition, most of the previous studies only consider single type of healthcare facility, and fail to address the multiple types of competing healthcare facilities.

Moreover, in the healthcare system, patients' behaviors directly affect the utilization of different healthcare resources (e.g., facility and personnel). The allocation of healthcare resources conversely impact the individuals' decisions on healthcare service selection. In addition, the individuals' health condition and service requirements are dynamically changing over time. To evaluate the performance of such complex healthcare systems, agent-based simulation (ABS) paradigm can be adopted according to its capability of modeling individual objects (e.g., patients) and their interactions in a dynamic environment. To better model the agents based on individuals' characteristics and their decisions on healthcare facility selection, there is a need to develop a predictive analytics integrated simulation model which integrates ABS and statistical models.

2.2 Methodological Framework

2.2.1 Framework Overview

To address aforementioned challenges and research needs, we propose a data-driven simulation approach with latent survival analysis that integrates Bayesian statistical modeling and ABS to evaluate the service utilizations of different healthcare facilities. As shown in Figure 2.5, the individuals transit from community dwelling to different health-

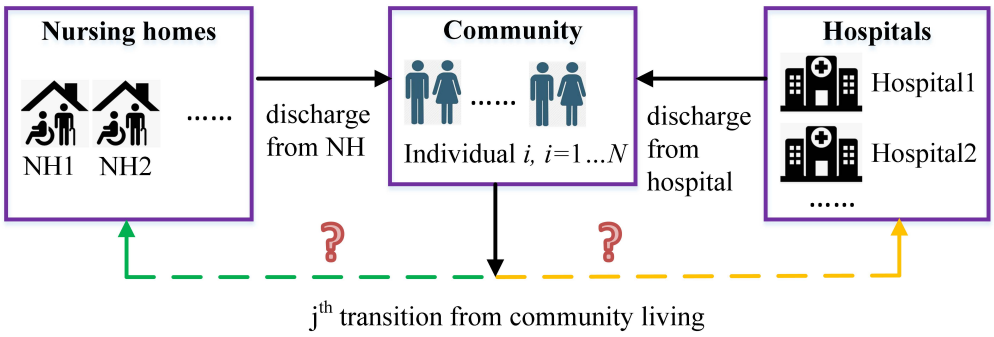

Figure 2.5: Service utilizations among different healthcare facilities

care facilities. The service selection of a typical healthcare facility is latent before the individual is readmitted to one of the multiple competing healthcare facilities. In particular, we consider two types of healthcare settings, namely, the acute care setting, such as hospitals, and long-term care setting, such as nursing homes (NHs).The proposed predictive models can capture the latent individual factors due to unavailable physiological information and the latent readmitted healthcare facility due to service selection. The developed statistical models can jointly estimate the facility specific individual observed and unobserved heterogeneity, and capture both within-individual dependency and between-individual independency. For each individual, multiple individual characteristics, such as ethnic group, age, gender, availability of caregiver, and health condition, are considered to model the time-to-readmission and LOS observations in the hospital and NH. An ABS model is then developed to simulate the individuals' time-to-readmission and LOS in the hospital and NH. The readmission and discharge events of each individual are driven by the Bayesian individualized models. We further define healthcare facility utilization as the simulation output. As illustrated in Figure 2.6, the proposed framework integrates the Bayesian modeling approach and ABS for healthcare systems with a heterogeneous population. The Bayesian modeling approach is employed to estimate each individual's time-to-readmission to different types of healthcare facilities and his/her stay in each type of healthcare facility. The ABS model is then developed to simulate each

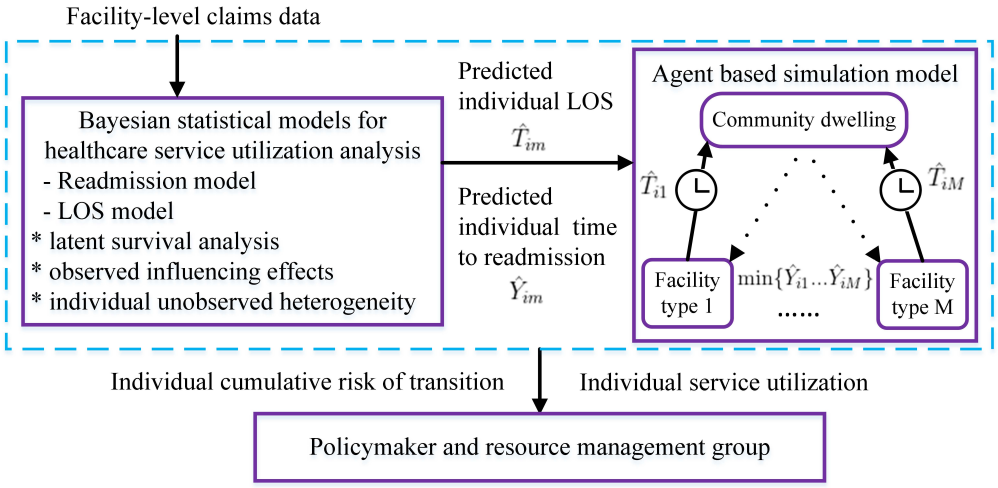

Figure 2.6: Overview of proposed modeling framework

individual's readmission and discharge events and further to evaluate service utilization of different types of healthcare facilities.

2.2.2 Modeling of Heterogeneous Time-to-readmission Data

Consider a heterogeneous population of N elderly individuals, and each individual i can be readmitted to one of M different healthcare facilities, namely, type m facility, $i = 1...N, m = 1...M$. Denote the j^{th} time-to-readmission observation of type m facility of an elderly individual i as T_{ij}, $j = 1...m_i$, where m_i is the total number of readmissions to healthcare facility m of individual i. To account for the uncertainty and variability of individualized multi-types facility readmission, an advanced statistical modeling approach needs to be developed. Several issues involved in the statistical modeling and analysis of time-to-readmission data should be addressed: (i) the data right-skewness which invalidates the conventional normality assumption; (ii) the consideration of both within-individual dependency and between-individual independency; (iii) the individualized model of considering both individual facility-specific observed and unobserved heterogeneity; and (iv) the competing risk of individuals requesting for healthcare services among multiple types of healthcare facilities.

To simultaneously address the aforementioned issues, we develop a data-driven individualized multi-type healthcare facility readmission model with latent survival analysis. The facility-specific readmission risk, $r_{im}(t)$, can be expressed as

$$r_{im}(t) = \lim_{\Delta t \to 0} \frac{\Pr(t \leq T_{ij} \leq t + \Delta t, J_{ij} = m \mid T_{ij} \geq t)}{\Delta t}, i = 1...N, m = 1...M, j = 1...m_i \quad (2.2)$$

where J_{ij} is an indicator taking value m if the target facility of j^{th} readmission of individual i is type m. $r_{im}(t)$ captures the instantaneous probability of individual i being readmitted to healthcare facility m at time t. The model can be further formulated by hazard regression, written as

$$r_{im}(t) = r_m^b(t) \exp(\boldsymbol{\beta}_m^{\mathrm{T}} \boldsymbol{x}_i + \gamma_{im}), i = 1...N, m = 1...M \quad (2.3)$$

where $r_m^b(t)$ is the baseline readmission rate to type m healthcare facility of an individual in the absence of facility-specific individual observed and unobserved heterogeneity. $\boldsymbol{\beta}_m$ and $\boldsymbol{x}_i$ are vectors of facility-specific covariate coefficient and covariates, which represent the facility-specific individual observed heterogeneity. γ_{im} is a random factor and is used to quantify the facility specific individual unobserved heterogeneity. Weibull hazard function can be assumed for $r_m^b(t)$ due to its flexibility in modeling right-skewness data, i.e., $r_m^b(t) = \lambda_m k_m t^{k_m - 1}$ where λ_m and k_m are facility-specific rate parameter and shape parameter of Weibull distribution respectively. The overall probability of no readmission to any facilities for individual $i, i = 1...N$ is then given by

$$S_i(t) = \exp\left(-\int_0^t \sum_{m=1}^{M} r_{im}(v)dv\right) = \exp\left[-\sum_{m=1}^{M} \lambda_m t^{k_m} \exp(\boldsymbol{\beta}_m^{\mathrm{T}} \boldsymbol{x}_i + \gamma_{im})\right] \quad (2.4)$$

The probability density function of facility-specific time-to-readmission can be expressed as $f_{im}(t) = r_{im}(t)S_i(t), i = 1...N, m = 1...M$. Denote $\boldsymbol{D}$ as the set of all available data, i.e., $\boldsymbol{D} = \{t_{ij}, \boldsymbol{x}_i, i = 1...N, j = 1...m_i\}$, and $\boldsymbol{\Theta}$ as a collection of all unknown parameters, i.e.,

$\boldsymbol{\Theta} = \{\lambda_m, k_m, \boldsymbol{\beta}_m, m = 1...M\}$. The marginal likelihood function can be obtained as

$$L(\boldsymbol{\Theta} \mid \boldsymbol{D}) = \prod_{i=1}^{N} \int_0^{\infty} ... \int_0^{\infty} \prod_{m=1}^{M} \prod_{j \in I_m} f_{im}(t_{ij}) \pi(\gamma_{i1}) ... \pi(\gamma_{iM}) d\gamma_{i1} ... d\gamma_{iM} \tag{2.5}$$

where I_m is an index set of all readmission records that the target facility of individual i is type m. $\pi(\cdot)$ represents an arbitrary probability density function. Conventional estimation methods, such as maximum likelihood estimation method, fail to carry out the estimation of all γ_{im}'s, since they will be integrated out in the marginal likelihood function maximization. To achieve the joint estimation of both the unknown parameters and all γ_{im}'s, we develop estimation algorithm under Bayesian framework. The joint posterior of $\boldsymbol{\Theta}$ and γ_{im}'s can be expressed as

$$\pi\left(\boldsymbol{\Theta}, \{\gamma_{im}\} \mid \boldsymbol{D}\right) \propto \prod_{i=1}^{N} \left[\prod_{m=1}^{M} \left(\prod_{j \in I_m} f_{im}(t_{ij}) \right) \right] \cdot \pi\left(\boldsymbol{\Theta}\right) \tag{2.6}$$

The above joint posterior can further be derived as

$$\pi\left(\boldsymbol{\Theta}, \{\gamma_{im}\} \mid \boldsymbol{D}\right) \propto L\left(\boldsymbol{\Theta} \mid \boldsymbol{D}, \{\gamma_{im}\}\right) \cdot \pi\left(\boldsymbol{\Theta}\right) \cdot \prod_{i=1}^{N} \prod_{m=1}^{M} \pi(\gamma_{im}) \tag{2.7}$$

where $\pi(\boldsymbol{\Theta})$ is joint prior density function of unknown parameters. $L\left(\boldsymbol{\Theta} \mid \boldsymbol{D}, \{\gamma_{im}\}\right)$ is joint likelihood function and can be calculated as

$$L\left(\boldsymbol{\Theta} \mid \boldsymbol{D}, \{\gamma_{im}\}\right) = \prod_{i=1}^{N} \left[\prod_{m=1}^{M} \prod_{j \in I_m} r_{im}(t_{ij}) \cdot \prod_{j=1}^{m_i} S_i(t_{ij}) \right] \tag{2.8}$$

Markov Chain Monte Carlo (MCMC) method (Roberts and Sahu, 1997) can be employed to obtain the posteriors of all unknown parameters and all γ_{im}'s. The sampling algorithm can be summarized as below. $\tau_{\max}$ is the maximum number of iterations in the sampling. It is noticed that the total time-to-readmission data of all individuals contribute

Algorithm 1 Sampling algorithm for parameter estimation of proposed model

Initialization: $\boldsymbol{\Theta}$ and $\{\gamma_{im}\}$ as $\boldsymbol{\Theta}^0 \leftarrow \{\{\lambda_m^{(0)}\}, \{k_m^{(0)}\}, \{\boldsymbol{\beta}_m^{(0)}\}\}$ and $\{\gamma_{im}^0\}$
for $\tau \leftarrow 1$ to $\tau_{\max}$ **do**
Draw samples $\gamma_{im}^{(\tau)} \sim \pi\left(\gamma_{im} \mid \boldsymbol{D}_i, \{\lambda_m^{(\tau-1)}\}, \{k_m^{(\tau-1)}\}, \{\boldsymbol{\beta}_m^{(\tau-1)}\}\right)$, i=1...N,m=1...M
Draw samples $\lambda_m^{(\tau)} \sim \pi\left(\lambda_m \mid \boldsymbol{D}, \{\gamma_{im}^{(\tau)}\}, \{k_m^{(\tau-1)}\}, \{\boldsymbol{\beta}_m^{(\tau-1)}\}\right)$,m=1...M
Draw samples $k_m^{(\tau)} \sim \pi\left(k_m \mid \boldsymbol{D}, \{\gamma_{im}^{(\tau)}\}, \{\lambda_m^{(\tau)}\}, \{\boldsymbol{\beta}_m^{(\tau-1)}\}\right)$,m=1...M
Draw samples $\boldsymbol{\beta}_m^{(\tau)} \sim \pi\left(\boldsymbol{\beta}_m \mid \boldsymbol{D}, \{\gamma_{im}^{(\tau)}\}, \{\lambda_m^{(\tau)}\}, \{k_m^{(\tau)}\}\right)$,m=1...M
end for

to the estimation of facility specific unknown parameters, while time-to-readmission data to any facilities of individual i contribute to the estimation of γ_{im}'s.

Based on the estimated parameters, individual cumulative risk can be analyzed. The cumulative probability of readmission to a specific healthcare facility m of individual i over time can be represented as $F_{im}(t) = \int_0^t f_{im}(v)dv$ where $F_{im}(t)$ is essentially a representation of cumulative incidence function (CIF). The upper limits of $F_{im}(t)$ quantify the eventual probability that readmission to healthcare facility m will happen on individual i. The upper limits of $F_{im}(t)$ approximate to proportion value $\frac{m_i}{\sum_m m_i}$ where m_i is the number of readmission to healthcare facility m for individual i, and $\sum_m m_i$ is the total number of readmission events of individual i.

2.2.3 Modeling of Heterogeneous Length-of-stay Data

Based on the above developed model, we can analyze personalized risk of readmission to any types of healthcare facilities. When an individual is readmitted to a specific healthcare facility, the individual stays in that facility and utilize healthcare service for a certain time. We can employ Bayesian statistical modeling techniques to characterize individual dwelling duration in a specific healthcare facility Consider a population of n elderly individuals in a studied healthcare facility and let a random variable Y_{ij} represent the j^{th} LOS of an elderly individual i in that facility, $i = 1...n, j = 1...u_i$, where u_i is the total number of times that individual i is discharged from healthcare facility of inter-

est. Denote y_{ij} as an actual observation of Y_{ij}, the observed LOS data can be expressed as $\{y_{ij}, i = 1...n, j = 1...u_i\}$. To account for both the effects of observed individual characteristics (e.g., age, race, health conditions, etc.) and latent effects due to unavailable clinical information, we develop a personalized LOS model under Bayesian framework with latent survival analysis. The individual LOS in a specific healthcare facility can be determined by the following model

$$\begin{aligned} d_i(t) &= \lim_{\Delta t \to 0} \frac{\Pr(t \leq Y_{ij} \leq t + \Delta t \mid Y_{ij} \geq t)}{\Delta t} \\ &= d^b(t) \exp(\boldsymbol{\alpha}^{\mathrm{T}} \boldsymbol{w}_i + \delta_i), \forall i = 1...n, j = 1...u_i \end{aligned} \tag{2.9}$$

where $d^b(t)$ is the baseline discharge rate of an individual from studied healthcare facility in the absence of influences of all observed individual characteristics and unobserved factors. We use Weibull hazard to represent the baseline discharge rate due to its flexibility in modeling right-skewed data, i.e., $d^b(t) = \nu\zeta t^{\zeta-1}$, where ν is rate parameter and ζ is shape parameter of Weibull distribution. $\boldsymbol{w}_i$ and $\boldsymbol{\alpha}$ are vectors of covariates and corresponding coefficients to represent individual characteristics and to quantify their effects, respectively. δ_i is a random variable with continuous distribution function $G(\cdot)$, i.e., $\delta_i \sim G(\cdot), \forall i$. δ_i is incorporated to capture the individual latent heterogeneity of the unobserved factors due to unavailable detailed individual information. $d_i(t)$ can be interpreted as the instantaneous probability of being discharged from the facility of interest of individual i at time t given this individual is still in the health care setting. It can measure how likely an individual will be discharged from hospital. A larger value of $d_i(t)$ indicates a shorter LOS of individual patient i and vice versus.

To estimate the above LOS model, we utilize available data $\boldsymbol{D}^l$, i.e., $\boldsymbol{D}^l = \{y_{ij}, \boldsymbol{w}_i, i = 1...n, j = 1...u_i\}$. Denote $\boldsymbol{\Theta}^l$ as a collection of all unknown parameters in the proposed LOS model, i.e., $\boldsymbol{\Theta}^l = \{\nu, \zeta, \boldsymbol{\alpha}\}$. To estimate $\boldsymbol{\Theta}^l$, the conventional non-Bayesian estimation method, e.g., maximization likelihood estimation, can be employed to maximize the

marginal likelihood function, i.e., $\hat{\boldsymbol{\Theta}}^l = \arg\max_{\boldsymbol{\Theta}^l} L(\boldsymbol{\Theta}^l \mid \boldsymbol{D}^l)$. The marginal likelihood function $L(\boldsymbol{\Theta}^l \mid \boldsymbol{D}^l)$ can be expressed as

$$L(\boldsymbol{\Theta}^l \mid \boldsymbol{D}^l) = \prod_{i=1}^{n} \int_0^{\infty} \prod_{j=1}^{u_i} \left(\nu\zeta y_{ij}^{\zeta-1} \exp\left[\delta_i + \boldsymbol{\alpha}^{\mathrm{T}} \boldsymbol{w}_i - \nu y_{ij}^{\zeta} \exp(\boldsymbol{\alpha}^{\mathrm{T}} \boldsymbol{w}_i + \delta_i) \right] \right) \pi(\delta_i) d\delta_i \quad (2.10)$$

where $\pi(\cdot)$ represents an arbitrary probability density function. As shown in Eq. (2.10), all δ_i's are integrated out in the marginal likelihood function and therefore, they cannot be estimated. However, δ_i's carry important information to quantify the individual LOS. To overcome such limitation in the conventional non-Bayesian method, Bayesian inference is considered since (i) both of the $\boldsymbol{\Theta}^l$ and δ_i's can be estimated; (ii) exact inference of $\boldsymbol{\Theta}^l$ and δ_i's can be achieved through obtaining their posterior densities while in non-Bayesian method, point estimate is often obtained and confidence intervals are approximated based on the asymptotic theory. Under the Bayesian framework, the joint posterior $\pi(\boldsymbol{\Theta}^l, \{\delta_i\}_{i=1}^n \mid \boldsymbol{D}^l)$ can be derived as

$$\begin{aligned} &\pi(\boldsymbol{\Theta}^l, \{\delta_i\}_{i=1}^n \mid \boldsymbol{D}^l) \propto L(\boldsymbol{\Theta}^l \mid \{\delta_i\}_{i=1}^n, \boldsymbol{D}^l) \cdot \prod_{i=1}^{n} \pi(\delta_i) \cdot \pi(\boldsymbol{\Theta}^l) \\ &= \prod_{i=1}^{n} \prod_{j=1}^{u_i} \left(\nu\zeta y_{ij}^{\zeta-1} \exp\left[\delta_i + \boldsymbol{\alpha}^{\mathrm{T}} \boldsymbol{w}_i - \nu y_{ij}^{\zeta} \exp(\boldsymbol{\alpha}^{\mathrm{T}} \boldsymbol{w}_i + \delta_i) \right] \right) \cdot \prod_{i=1}^{n} \pi(\delta_i) \cdot \pi(\boldsymbol{\Theta}^l) \end{aligned} \quad (2.11)$$

where $L(\boldsymbol{\Theta}^l \mid \{\delta_i\}_{i=1}^n, \boldsymbol{D}^l)$ is the joint likelihood function and $\pi(\boldsymbol{\Theta}^l)$ is the joint prior density of a collection of unknown parameters. Prior independence is often assumed, i.e., $\pi(\boldsymbol{\Theta}^l) = \pi(\nu)\pi(\zeta)\pi(\boldsymbol{\alpha})$. We further employ MCMC sampling method (Roberts and Sahu, 1997) to obtain the posterior densities of $\boldsymbol{\Theta}^l$ and all δ_i's. The full conditional poste-

rior densities can be explicitly derived as

$$
\begin{aligned}
&\pi(\delta_i \mid \boldsymbol{D}^l, \nu, \zeta, \boldsymbol{\alpha}) \propto \exp\left[u_i\delta_i - \nu S_i \exp(\delta_i)\right] \cdot \pi(\delta_i), \forall i \\
&\pi(\nu \mid \boldsymbol{D}^l, \{\delta_i\}_{i=1}^n, \zeta, \boldsymbol{\alpha}) \propto \nu^{\sum_{i=1}^n u_i} \exp\left[-\sum_{i=1}^n \nu S_i \exp(\delta_i)\right] \cdot \pi(\nu) \\
&\pi(\zeta \mid \boldsymbol{D}^l, \{\delta_i\}_{i=1}^n, \nu, \boldsymbol{\alpha}) \propto \zeta^{\sum_{i=1}^n u_i} \exp\left[(\zeta-1)\sum_{i=1}^n\sum_{j=1}^{u_i} \log(y_{ij}) - \sum_{i=1}^n \nu S_i \exp(\delta_i)\right] \cdot \pi(\zeta) \\
&\pi(\boldsymbol{\alpha} \mid \boldsymbol{D}^l, \{\delta_i\}_{i=1}^n, \nu, \zeta) \propto \exp\left[\sum_{i=1}^n u_i \boldsymbol{\alpha}^{\mathrm{T}} \boldsymbol{w}_i - \sum_{i=1}^n \nu S_i \exp(\delta_i)\right] \cdot \pi(\boldsymbol{\alpha})
\end{aligned} \tag{2.12}
$$

where $S_i = \sum_{j=1}^{u_i} y_{ij}^{\zeta} \exp(\boldsymbol{\alpha}^{\mathrm{T}} \boldsymbol{w}_i)$. Since $\zeta > 0$ and $\nu > 0$, their prior distributions can be specified as gamma distribution or log-normal distribution (McGilchrist and Aisbett, 1991). For δ_i's and $\boldsymbol{\alpha}$, there are no such positiveness restrictions and normal prior density is often selected. Based on the above equations, we can draw the samples from the derived posterior densities sequentially and update parameter estimates iteratively. Since the full conditional posterior densities in Eq. (2.12) are not from common distributions, e.g., distributions from the exponential family, Metropolis-Hasting algorithm (HASTINGS, 1970) can be employed to draw the corresponding samples.

2.2.4 Predictive Analytics Integrated Simulation

With the developed Bayesian statistical models in previous sections, we further develop a predictive analytics integrated ABS model to simulate the readmission and discharge events of each individual who has potential healthcare service needs for multiple types of healthcare facilities. The flow chart of ABS model is illustrated in Figure 2.7. In the simulation model, we assume that all of the elderly individuals are in the community dwelling status before being readmitted to any types of healthcare facilities. Individuals in this status do not need any healthcare services. However, an individual may need a certain type of healthcare service (e.g., care service in NH) over time, and can be readmitted to the corresponding healthcare facility to receive service. An individual's probability

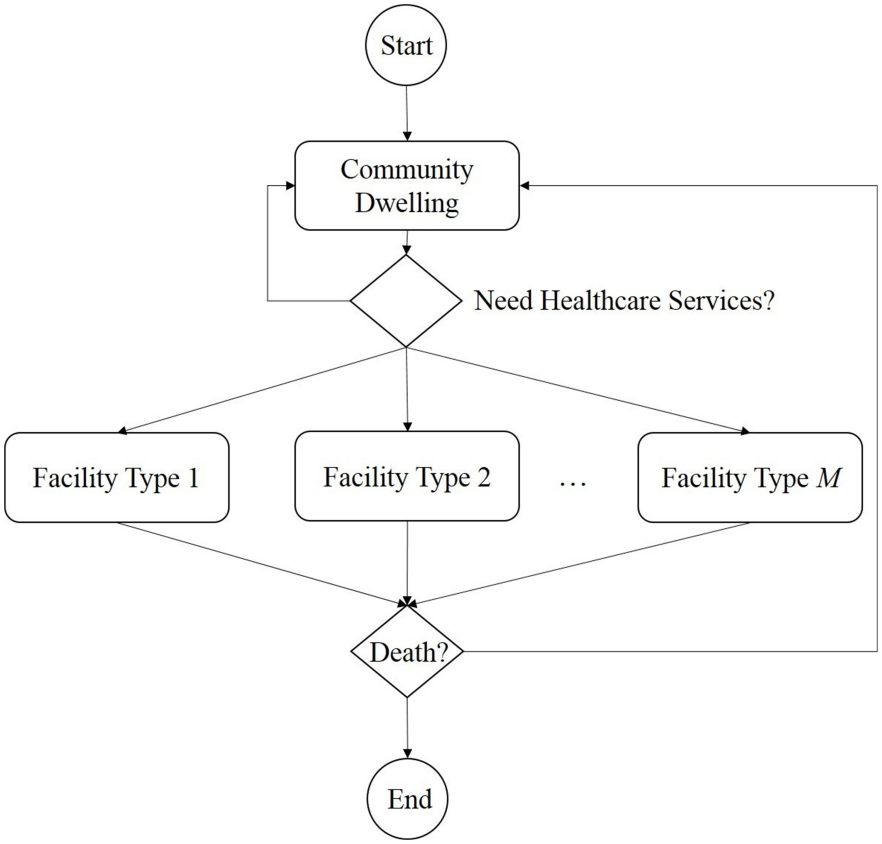

Figure 2.7: State chart for agent-based simulation of elderly individuals

of readmission to a certain type of healthcare facility is time-dependent and is driven by the individualized readmission model, as described in Eq. (2.3). The status of an individual is then changed to the corresponding type of the facility. The individual stays in that status for a certain time, and the dwelling duration in that facility is driven by the individual LOS model, as shown in Eq. (2.9). After being discharged from the healthcare facility, an individual transit back to community dwelling status or exits the simulation when he/she reaches a randomly generated death age. The individual healthcare service demand of an agent is driven by the proposed statistical models and can be characterized by the ABS simulation model. The simulation outputs include the number of individuals in each type of healthcare facility throughout the entire simulation horizon. Animations include the visualizations of states transition of agents and the real-time plots of number of individuals in various healthcare facilities.

2.3 Case Study

To illustrate the proposed approach and demonstrate its effectiveness, a real case study is provided based on a subset of the Florida's Medicare and Medicaid claims data (Meng et al., 2013). The real data contain details of readmission and discharge records of multiple types of healthcare facilities. The readmission records of 217 elder people and the discharge records of 1529 elderly individuals in total are utilized to extract the facility-specific time-to-readmission data and individual LOS data. Two facility types, namely, hospital and NH are considered in this study. As shown in Figure 2.8, the individual

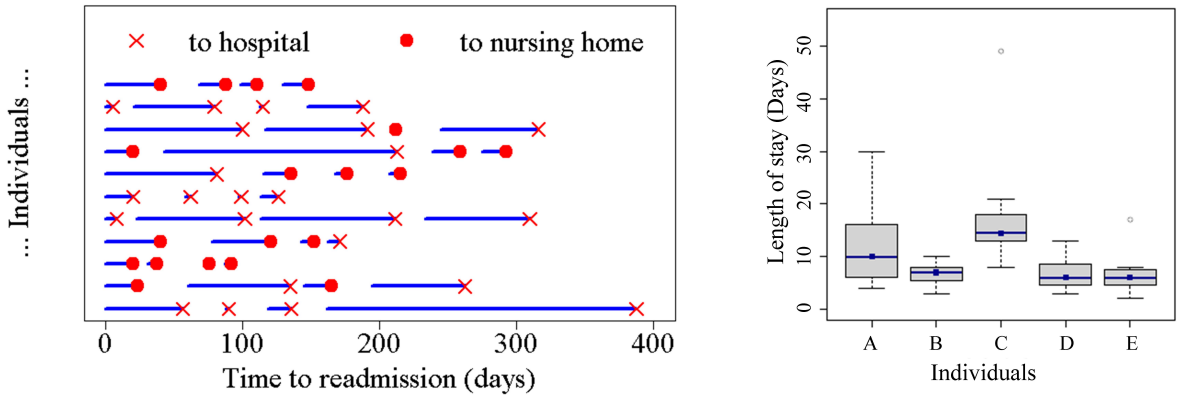

(a) Individual time-to-readmission

(b) Individual LOS

Figure 2.8: Healthcare service utilization variations

facility-specific time-to-readmission and individual LOS exhibit heterogeneity. To account for such individual heterogeneity, we employ the developed statistical models and incorporate both observed individual characteristics as well as unobserved factors. The individual characteristics available in the data set include binary variables, such as gender indicator, and categorical variables, such as Assisted daily living (ADL) total score and Charlson comorbidity index as well as ethnicity group, and continuous variables, such as age. Classical variable selection methods, such as random forest based method, can be used to select the significant covariates. In proposed readmission model, five covariates are selected to estimate the proposed statistical models, including the indicator of white

ethnic group x_1, age x_2, female indicator x_3 and caregiver indicator x_4, and score for total help in activities of daily living x_5. Ten facility-specific covariates coefficients are involved in the readmission model. Totally 14 unknown parameters and 217 individual γ_{i1}'s, γ_{i2}'s can be jointly estimated using Algorithm 1. In the proposed individual LOS model, six covariates are selected for model development, including dummy variables w_1-w_3 which represent the ethnic groups of "white", "black" and "hispanic" while the baseline ethnic group is "other", w_4, w_5 and w_6 which represent age, gender and Charlson comorbidity index, respectively. The estimates of unknown parameters of individual LOS model and all δ_i's can be jointly obtained under Bayesian estimation framework.

Table 2.2: Parameters estimation results of proposed readmission model

Parameters	Posterior mode	2.5%	25%	50%	75%	97.5%
k_1	1.36538	1.19000	1.29700	1.35800	1.42700	1.58200
k_2	1.10523	0.94020	1.04600	1.10300	1.16100	1.28400
λ_1	0.00102	0.00013	0.00053	0.00104	0.00199	0.00681
λ_2	0.00102	0.00007	0.00042	0.00106	0.00255	0.01302
β_{11}	-0.46868	-0.83680	-0.59130	-0.46760	-0.34450	-0.10750
β_{12}	-0.37511	-0.89031	-0.54450	-0.37440	-0.20400	0.13600
β_{22}	0.02201	-0.00812	0.01171	0.02188	0.03220	0.05241
β_{52}	0.74749	0.22840	0.56680	0.74540	0.92540	1.28500

As no prior knowledge is available, non-informative priors are assumed for parameters. To be specific, normal priors are assigned for all facility-specific covariates coefficients $\boldsymbol{\beta}_m$, and inverse gamma distributions are assumed for shape parameters k_1 and k_2. The point estimate and interval estimate of some estimated unknown parameters in the readmission model are summarized in Table 2.2. The facility-specific shape parameters k_1 and k_2 are larger than 1, which indicates that both the individualized instantaneous probability of readmission to hospital and NH will increase over time. λ_1 and λ_2 can be interpreted as the baseline average hospital readmission and NH readmission respectively, in the absence of effects from individual observed covariates and unobserved het-

erogeneity. As shown in Table 2.2, β_{11} has strong negative effect on hospital readmission, which implies that the "caucasian" ethnic group is less likely to be readmitted to hospital, compared to other ethnic groups. Although β_{12} is not significantly different from zero at 95% credible interval, it still contains rich information. β_{12} has negative effect at 50% credible, and shows strong concentration on negative values. This implies that the white ethnic group is less likely to be readmitted to NH. β_{22} neither has a significant effect at 95% credible interval. However, it is significantly positive at 50% credible interval. When an individual gets older, the probability of readmission to NH becomes higher. β_{52} is significantly positive at 95% credible interval, which implies that the individual who needs more help in activities of daily living is more likely to be readmitted to NH and thus has shorter time-to-readmission to NH. The density plots of $\hat{\beta}_{11}$ and $\hat{\beta}_{52}$ are shown in Figure 2.9, which consistently depict the strong negative tendency and the strong positive tendency at 95% credible interval respectively.

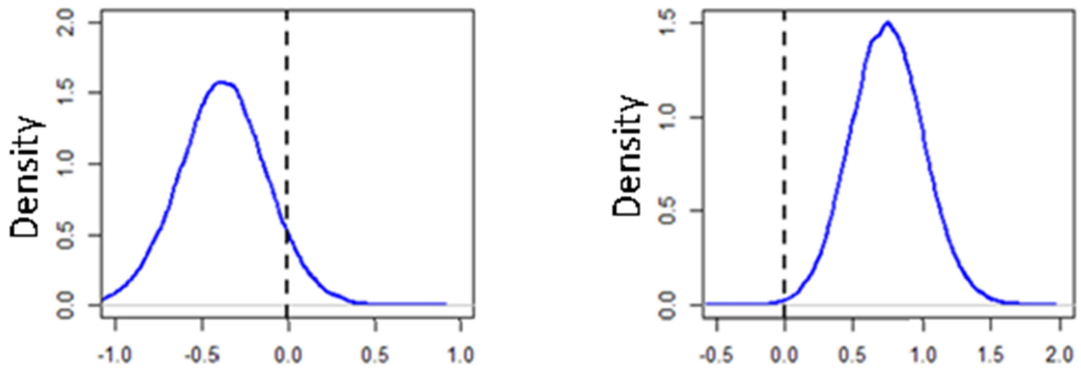

(a) β_{11} (b) β_{52}

Figure 2.9: Posterior density plots of model parameters

In addition to the unknown parameters of the proposed readmission model, the individual latent heterogeneity can also be quantified. The positive value of facility-specific individual unobserved heterogeneity indicates that individual is more likely to be readmitted to a specific facility, and thus has a shorter time-to-readmission, and vice versus. As shown in Figure 2.10a, individual C has relatively longer time-to-readmission to NH, compared to the other individuals. Individual A has relatively shortest time-to-

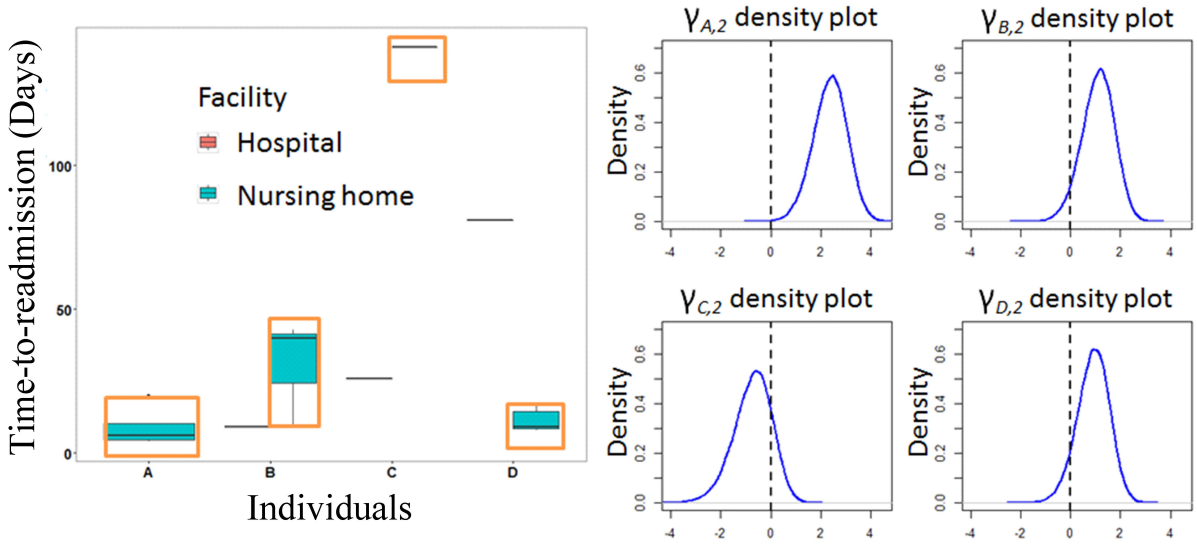

(a) Time-to-readmission of four individuals (b) Density plots of NH-specific γ_{i2}'s

Figure 2.10: Individual unobserved heterogeneity of time-to-readmission data

readmission to NH. As illustrated in Figure 2.10b, the density plot of γ_{C2} concentrates on negative values, and it indicates that individual C is less likely to be readmitted to NH, and thus has longer time-to-readmission to NH. All of γ_{i2}'s for the other individuals exhibit a strong tendency on positive values, and particularly γ_{A2} has largest positive posterior mode among all individuals. The results inferred from γ_{i2}'s are consistent with the real data, that is, individuals A, B, D are more likely to be readmitted to NH and has relatively shorter time-to-readmission to NH than individual C, and individual A is relatively most likely to be readmitted to NH due to the effect from strongest positive concentration and largest posterior mode of γ_{A2}. The hospital-specific and NH-specific individual latent heterogeneity of all individuals are illustrated in Figure 2.11. The hospital-specific unobserved heterogeneity γ_{i1}'s are approaching to 0, indicating that the majority of individual heterogeneity can be explained by the observed individual covariates. On the other side, the NH-specific γ_{i2}'s are significantly different than 0, which implies that individual time-to-readmission to NH is influenced by the unobserved factors due to information unavailability issue in the raw health claims data.

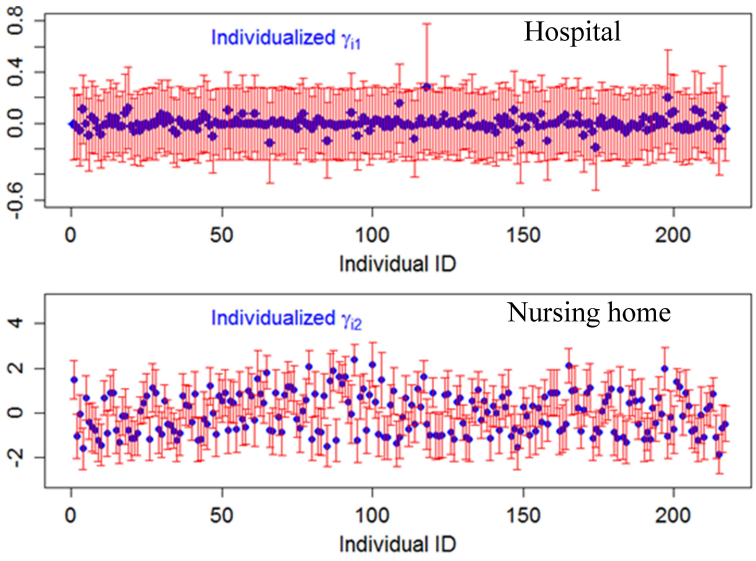

Figure 2.11: Facility-specific individual unobserved heterogeneity

Based on the estimated unknown parameters and facility specific individual unobserved heterogeneity, individualized competing risk analysis can be carried out for the proposed readmission model. The facility-specific individual cumulative incidence function can be obtained and the upper limits of hospital CIF and NH CIF can be calculated. The upper limits theory in context of readmission can be interpreted as upper limits of specific healthcare facility CIF should equal to the proportion of number of readmissions to corresponding healthcare facility over total number of readmissions. As shown in Fig-

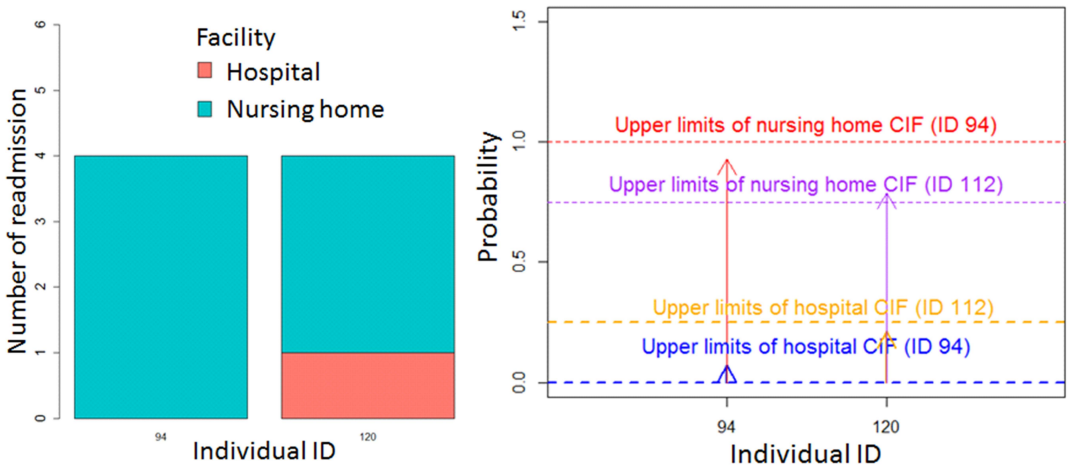

(a) (b)

Figure 2.12: Upper limits validation of hospital and NH CIF

ure 2.12, the upper limits of NH CIF for both two individuals approximate to the proportion of number of readmissions to NH over total number of readmissions respectively. Upper limits of hospital CIF can also be validated. Moreover, the personalized cumulative risk curve and probability of no readmission over time can be obtained. As shown in

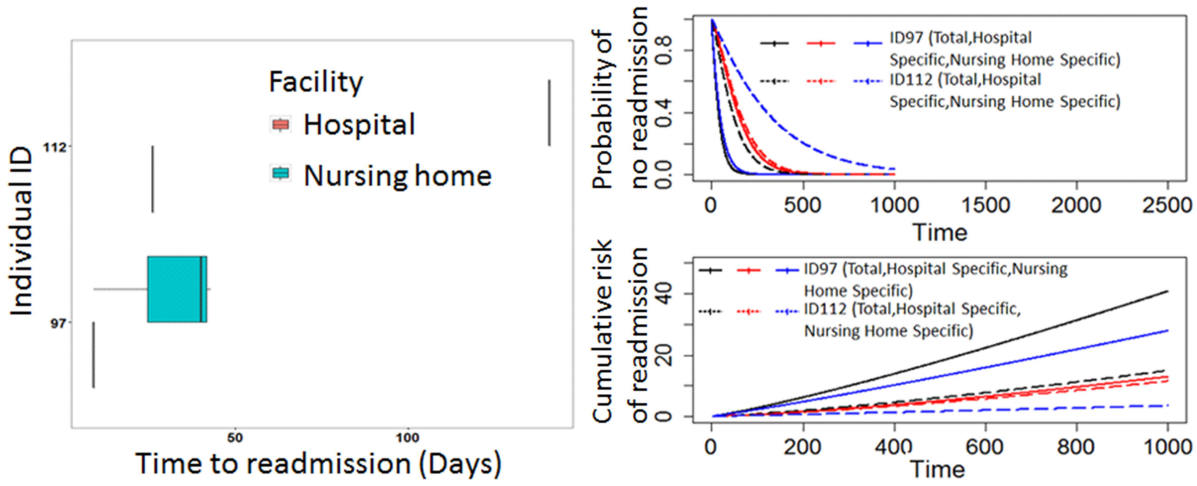

(a) (b)

Figure 2.13: Personalized risk analysis

Figure 2.13b, the total hospital-specific and NH-specific cumulative risks of readmission of individual with ID 97 are all larger than the ones of individual with ID 112, which are consistent with real data in Figure 2.13a.

Further, we carry out joint estimation of unknown parameters and all δ_i's in the proposed individual LOS model for healthcare facility of interest. The estimation results of hospital LOS model are summarized in Table 3.6, including point estimates (e.g., posterior mean), posterior quantiles (e.g., 25% posterior quantile) and interval estimate (e.g., 95% credible interval). The Bayesian estimation approach provides a rich information summary to quantify both the uncertainty of estimated parameters and variability among different individuals. As shown in Table 3.6, the parameter α_1 is significant and has a positive effect on hospital LOS based on 95% credible interval. This implies that compared to the baseline ethnic group "other", the individuals in "white" group will have shorter stay in hospital. Although the other covariates are not significantly from zero at 95% credible

Table 2.3: Estimation results of hospital LOS model

Parameters	Posterior mean	2.5%	25%	50%	75%	97.5%
α_1	0.31793	0.08485	0.23900	0.31790	0.39642	0.54990
α_2	0.24265	-0.16460	0.10340	0.24315	0.38350	0.64870
α_3	-0.06581	-0.33660	-0.16100	-0.06627	0.02705	0.21630
α_4	0.00215	-0.00811	-0.00141	0.00217	0.00570	0.01247
α_5	0.07670	-0.11680	0.01062	0.07645	0.14260	0.27190
α_6	-0.03613	-0.12060	-0.06472	-0.03530	-0.00802	0.04617
ν	0.00958	0.00357	0.00634	0.00861	0.01187	0.02100
ζ	1.93879	1.85100	1.90800	1.93900	1.96900	2.02700

interval, posteriors can still give rich and useful information. For instance, α_6 has a negative significance based on 50% credible interval. As the value of w_6 increases when the health condition of an individual becomes worse, the negative value of the coefficient α_6 indicates that individual with more severe health condition will be less likely discharged and thus has a longer stay in hospital. The estimated parameter $\hat{\zeta} > 1$ implies that the instantaneous probability of hospital discharge of an individual will increase over time. $\hat{\nu}$ can be perceived as the baseline average instantaneous discharge rate in the absence of influences of all δ_i's and all $\boldsymbol{w}_i$'s. The individual unobserved heterogeneity of all individuals can be simultaneously obtained by the estimation procedure of proposed LOS model, as described in Section 2.2.3. Figure 2.14 illustrates the estimation results of all δ_i's. The quantified individual latent heterogeneity is significantly different from 0, which implies that hospital LOS is impacted by unobserved individual factors. A positive value of δ_i indicates that an individual will be more likely discharged and thus has a shorter hospital LOS, and vice versus. Furthermore, we compare the goodness-of-fit performance of proposed LOS model with conventional models without considering individual unobserved heterogeneity. The deviance information criterion (DIC) (Spiegelhalter et al., 2002) is employed to evaluate the goodness-of-fit. A lower DIC value indicates a better goodness-of-fit. The DIC of the proposed model and the conventional model are 11380

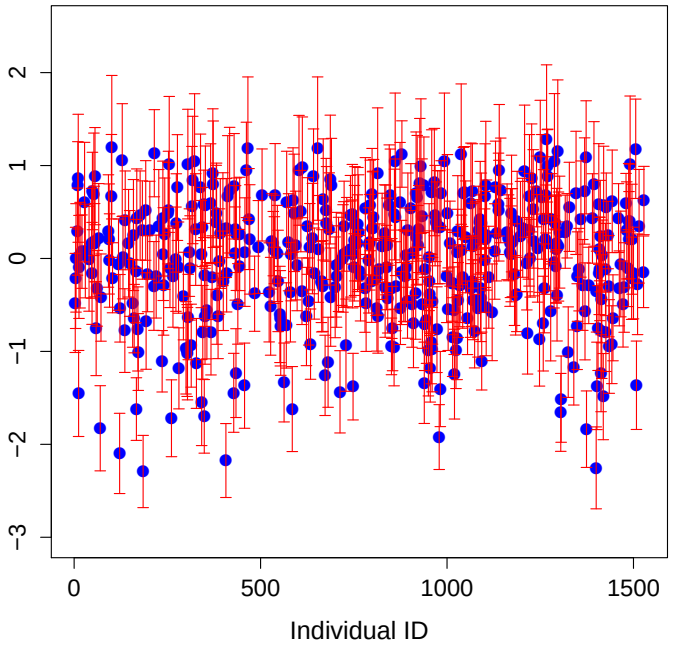

Notes: dots represent for posterior mean and bars represent for posterior mean $\pm$ standard deviation of δ_i's

Figure 2.14: Individual unobserved heterogeneity of hospital LOS

and 12070, respectively. Thus, the proposed LOS model considering individual latent heterogeneity achieves better goodness-of-fit to the data. Similarly, the individual NH LOS model of all elderly adults in NH can also be estimated based on the available data using the procedure demonstrated in Section 2.2.3.

Based on the above developed statistical model, we integrate predictive analytics with simulation model. The data-driven ABS model is developed in AnyLogic environment. Based on the data used in our case study, each agent in the simulation model has three possible states, including the state of an agent being in the community (no healthcare service needed), the state of an agent being in NH, and the state of an agent being in hospital. The data-driven simulation model is flexible enough to incorporate other types of healthcare facilities and individual attributes if the corresponding data is available. The individualized facility-specific probability of readmission can be quantified by Eq. (2.3) and individual LOS in facility of interest can be captured by Eq. (2.9). In the experiment, we

create 2 scenarios with different population cohort and varied individual characteristics. Table 2.4 shows the variables of individual characteristics as simulation inputs in differ-

Table 2.4: Simulation settings in different scenarios

Scenario 1			
Variables	Region 1	Region 2	Region 3
x_1	uniform_discr(0,1)	uniform_discr(0,1)	uniform_discr(0,1)
x_2,w_4	uniform_discr(45,55)	uniform_discr(55,65)	uniform_discr(65,75)
x_3	uniform_discr(0,1)	uniform_discr(0,1)	uniform_discr(0,1)
x_4	uniform_discr(0,1)	uniform_discr(0,1)	uniform_discr(0,1)
x_5	uniform_discr(0,5)	uniform_discr(0,5)	uniform_discr(0,5)
$[w_1, w_2, w_3]$	uniform_discr(0,1) $w_1 + w_2 + w_3 = 1$	uniform_discr(0,1) $w_1 + w_2 + w_3 = 1$	uniform_discr(0,1) $w_1 + w_2 + w_3 = 1$
w_5	uniform_discr(0,1)	uniform_discr(0,1)	uniform_discr(0,1)
w_6	uniform_discr(0,5)	uniform_discr(0,5)	uniform_discr(0,5)
Scenario 2			
Variables	Region 4	Region 5	Region 6
x_1	1	0	0
x_2,w_4	uniform_discr(65,75)	uniform_discr(65,75)	uniform_discr(65,75)
x_3	uniform_discr(0,1)	uniform_discr(0,1)	uniform_discr(0,1)
x_4	uniform_discr(0,1)	uniform_discr(0,1)	uniform_discr(0,1)
x_5	uniform_discr(0,5)	uniform_discr(0,5)	uniform_discr(0,5)
$[w_1, w_2, w_3]$	[1, 0, 0]	[0, 1, 0]	[0, 0, 1]
w_5	uniform_discr(0,1)	uniform_discr(0,1)	uniform_discr(0,1)
w_6	uniform_discr(0,5)	uniform_discr(0,5)	uniform_discr(0,5)

ent scenarios. In Scenario 1, 3 geographic regions (Regions 1-3) with different population age distribution are modeled to study the impact of age on healthcare service utilizations of different facilities. In Scenario 2, another 3 geographic regions (Regions 4-6) with different ethnic groups are modeled to study the effects of ethnicity on healthcare service utilization. Each region is designed to host a population of 150 individuals (agents) that may need healthcare services from NH and hospital. The steady state of simulation can be reached in about 3 years for each scenario. Consequently 5 years are simulated and

1865 samples are collected in total. The simulation results for all 6 regions are statistically significant. Figure 2.15a and Figure 2.15b show the healthcare service utilization results

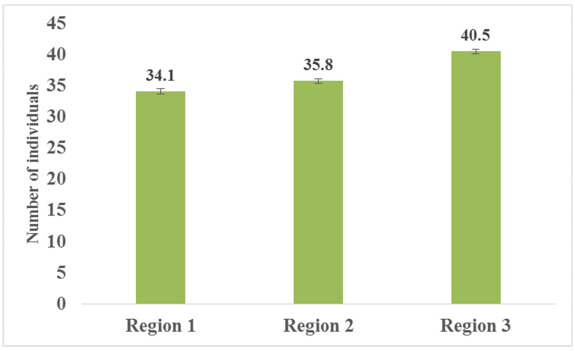

(a) Number of individuals in nursing home in Regions 1-3

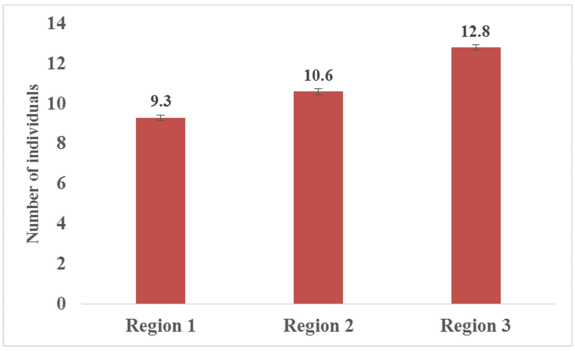

(b) Number of individuals in hospital in Regions 1-3

(c) Number of individuals in nursing home in Regions 4-6

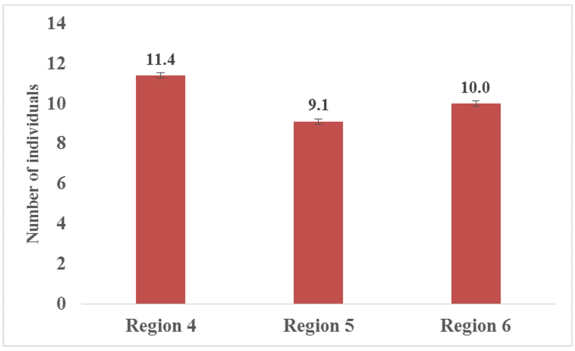

(d) Number of individuals in hospital in Regions 4-6

Figure 2.15: Number of individuals using care services in different scenarios

for Scenario 1. When the average age of the population increases, the utilizations of both NHs and hospitals increase. However, when the individuals are relatively young (e.g., in Regions 1 and 2), their utilization of NH service shows a slower increase compared to that from older individuals. These results indicate that the individuals in the region with an older population tend to have a higher healthcare service utilization. Figure 2.15c and Figure 2.15d show the healthcare service utilization results for Scenario 2. The white people (Region 4) tend to stay in NHs compared to African American and Hispanic people. When comparing African American people (Region 5) and Hispanic people (Region 6), African American people tend to utilize healthcare service in NHs, while Hispanic people

tend to go to hospitals. These results reveal that healthcare service utilizations of different facilities are affected by the ethnicity.

2.4 Concluding Remarks

In this work, a data-driven simulation approach with latent survival analysis is proposed to model and to evaluate healthcare service utilization of both acute care facility and long-term care facility. In the proposed approach, a Bayesian statistical modeling approach is proposed to analyze complex data structures of individuals' time-to-readmission and LOS observations by incorporating varied individual observed characteristics (e.g., gender) and unobserved factors based on real administrative claims data. Joint estimation of individual observed effects and individual latent heterogeneity is carried out under Bayesian estimation framework. An ABS model is further developed to study the readmission and discharge events of individuals based on the individualized Bayesian statistical models. We conduct a real case study based on Florida's Medicare and Medicaid claims data to evaluate the performance of proposed approach. The predictive analytics integrated simulation results reveal that 1) the healthcare facilities in the region with an older population tend to have a higher utilization, and 2) the healthcare facility utilization is affected by the ethnicity. Our future research works are to study additional observed factors for statistical modeling and incorporate the impact of healthcare facility capacity and payment policies, such as reimbursement policies, on individuals' healthcare service selection to produce more realistic results.

Chapter 3

An Analytics-based Capacity and Staffing Decision Support System under Heterogeneous Service Demand of Nursing Home Residents

3.1 Introduction

The elderly population in the United States has a rapid growth in recent years[2]. Along with the demographic shift in the elderly population, there is a considerable increase in the prevalence of aging-related disabilities, multiple chronic diseases and functional limitations/losses among older adults. Consequently, their needs for nursing care and personal assistance are dramatically increasing in healthcare systems, especially in modern nursing homes (NHs) which are mainly responsible for caring frail and vulnerable elderly population. Modern NHs provide 24/7 formal care to frail older adults with a variety of skilled personal medical care and living assistance. Different types of nursing staff in NH, such as certified nurse assistant (CNA), registered nurse (RN), and license practical nurse (LPN), provide various care services, including post-acute health care, specialized medical services, restorative and rehabilitation services, assistance with activities of daily living and end-of-life care. Although there are multiple different types of nursing care supplies, the aging-related issues of NH residents consequently trigger escalating nationwide NH workforce shortage and insufficient care resources as well as public financing shortfall (Janiszewski Goodin, 2003). On one hand, the shortage in available beds and nursing staff will arouse concerns on care accessibility of NH residents (Hyer et al., 2011; Spilsbury et al., 2011) and undermine their quality of life (Park and Stearns, 2009; Konet-

[2]Portions of this chapter were arxiv preprint (Sun et al., 2021b). Copyright permission from the publisher is included in Appendix A.

zka et al., 2008). Specifically, there are over 45 million Medicare-eligible aging adults with potential needs of NH care services, as compared to the insufficient nationwide supply of 1.7 million available NH beds (National Center For Health Statistics, 2019). Moreover, there is nationwide severe shortage of CNAs and over 90% of NHs are understaffed. On the other hand, excessive supplies in capacity and workforce may lead to a waste of resource and increase financial burden of NH providers. The unused beds will incur unnecessary healthcare expenditures and overstaffing will reduce the profitability of NH providers. To meet the excessive service demand of NH residents, it will be highly desirable to develop a cost-effective solution for NH resource planning which can ensure both the quality of care for NH residents and the profitability for NH providers.

Nevertheless, successful NH resource planning is challenging due to the highly heterogeneous and complex service demand of NH residents. The complexities of heterogeneous service demand lie in three aspects. First, different NH residents may have varied individual characteristics (Manton et al., 1985), such as diverse socio-demographics, various clinical diagnoses and chronic conditions, and different functional performance limitations (e.g., physical, mental and cognitive performance limitations and losses). Consequently, NH residents have diverse service needs. Per diem staff-time of certain care service may vary among different NH residents. For example, daily CNA staff-time ranges from 30 to 200 minutes (Centers For Medicare & Medicaid Services, 2013) among different individuals. Moreover, NH residents have diverse needs (e.g., skilled nursing care, restorative care, physical therapy, etc.) on different types of nursing staff and aides due to varied individual health conditions. The daily staff-time of different types of care services also varies among residents. Second, the resident-level service utilization, such as dwelling duration, is heterogeneous among NH residents. Specifically, different NH residents may have diverse length-of-stay (LOS) (Liu et al., 1991) with multiple competing and correlated discharge dispositions (e.g., hospital, community, etc.) due to different individual characteristics. For example, NH residents may be discharged to community

in a few weeks due to recovery, or stay in NH longer for several months or years due to further deterioration of their health conditions. Even during their stays, some NH residents may be transferred to acute care settings (e.g., hospital) due to the occurrence of critical events and emergencies (e.g., falls, infections, etc.). Third, resident-level functional performance limitations, such as activities of daily living (ADL) score, and health conditions as well as therapy intensity are time-varying. Consequently, the service need of NH residents may also changes over time and exhibits diverse temporal patterns. The resident-level service need may decrease over time due to recovery after receiving treatments and less needs of nursing care and assistance are required, or may increase over time due to health deterioration and more needs of daily living assistance are required. There is a research need to improve NH capacity and workforce planning in response to such heterogeneous and temporally evolving service demand of NH residents.

Existing NH resource planning approaches in nursing literature and industrial practice were mainly based on personal experiences and subjective judgment of NH administrators (Mueller et al., 2006; Zhang and Grabowski, 2004), and/or often relied on government regulations, such as minimum staff-to-resident (SR) ratio enforced by federal/state agencies (Bowblis, 2011; Bowblis and Ghattas, 2017). Many of them adopted one-size-fits-all policies based on aggregated measures, such as SR ratio and hours per patient day, which neglected service demand heterogeneity of different individuals. There was a lack of both data-driven framework and practical analytics-based decision support system to inform NH administrators of proper and managerial resource planning decisions. There is a need to develop an evidence-based analytical framework for NH capacity and workforce planning via taking the aforementioned complexities of service demand heterogeneity into account. On the other side, extensive works in the field of healthcare system and operations research focused on acute care settings, such as intensive care units (Ridge et al., 1998), emergency units (Kunkel and McLay, 2013) and hospitals (Ma and Demeulemeester, 2013; Burdett and Kozan, 2016; Siferd and Benton, 1992; Bard and

Purnomo, 2005; Kim and Mehrotra, 2015; Yankovic and Green, 2011; Punnakitikashem et al., 2013). There is few research focusing on long-term care (LTC) settings (Li et al., 2016; Zhang et al., 2012), such as LTC network and NH facilities. The existing studies often simplified the service demand via assuming a homogeneous population of NH residents and neglecting the complexity of heterogeneous service demand of NH residents (Bard and Purnomo, 2005; Kim and Mehrotra, 2015). Many of them considered the distribution-based LOS model without incorporating individual characteristics (Bard and Purnomo, 2005; Kim and Mehrotra, 2015; Burdett and Kozan, 2016; Siferd and Benton, 1992; Li et al., 2016). Some works utilized patient volume to quantify service demand without accounting for individual differences among patients (Siferd and Benton, 1992; Kim and Mehrotra, 2015). Further, most existing methods failed to account for temporal dynamics and temporal heterogeneity in service demand modeling. There is a need to better understand and characterize the complex and heterogeneous service demand of NH residents, and further to develop an integrated evidence-based decision support system for NH capacity and workforce planning under heterogeneous service demand of NH residents. To fill the above gaps and to address the research needs, I propose a data-driven integrated framework and analytics-based decision support system for NH resource planning in this chapter. The details will be described in the following sections.

3.2 Framework Overview

To determine the "right" amount of resources (e.g., number of beds and number of nursing staff) with proper scheduling in response to the heterogeneous and temporally evolving service demand of NH residents, I propose a data-driven modeling framework and decision support system. The proposed framework integrates advanced statistical modeling, computer simulation and stochastic optimization. It embraces several key modules, as illustrated in Figure 3.16. In Module I, I develop an individual NH LOS model to quantify heterogeneous service utilization of NH residents. In Module II, I then

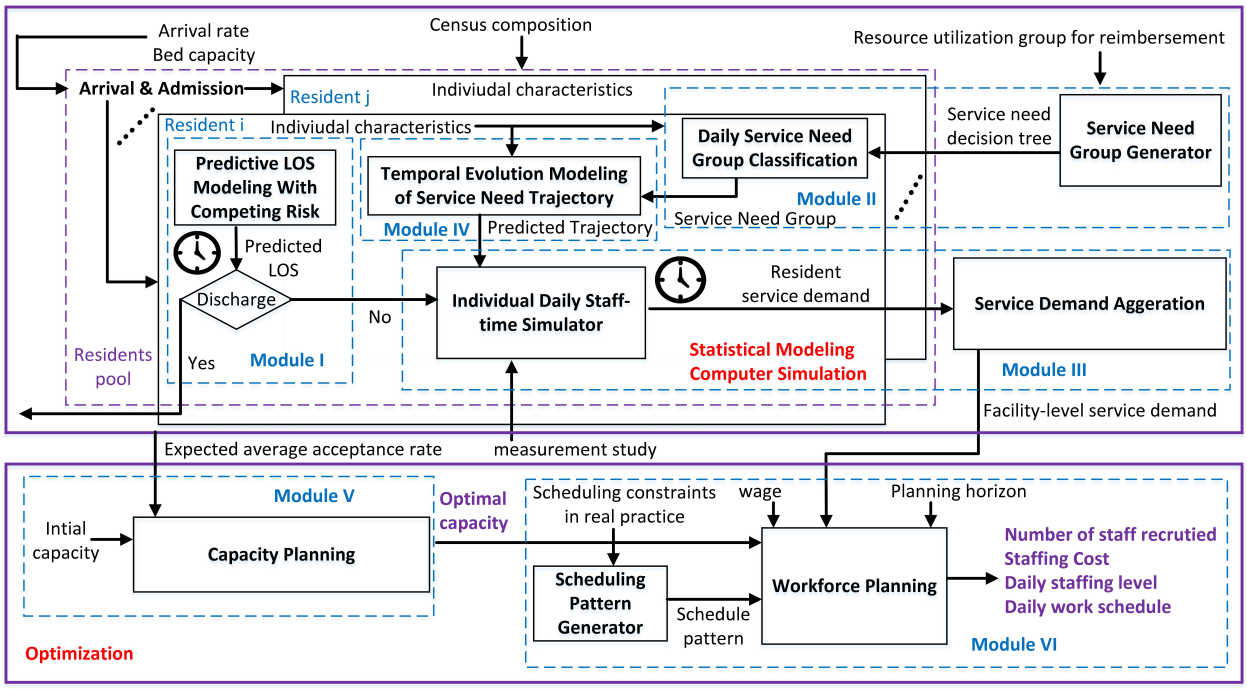

Figure 3.16: Overview of the proposed framework and decision support system

incorporate domain knowledge and develop a service need classification system to capture individual heterogeneity of service need of NH residents. In Module III, I further integrate computer simulation with developed predictive analytics to obtain facility-level service demand. In Module IV, I enhance the predictive analytics and propose a temporal heterogeneity modeling approach to characterize heterogeneous and temporally evolving service demand of NH residents at higher granularity. To meet the simulated service demand, I further develop a two-phase optimization approach to achieve optimal capacity planning decision (Module V) and optimal workforce planning (Module VI). Moreover, I develop a practical user-friendly decision support platform to facilitate managerial decision making for NH administrators. The details of proposed modeling framework are elaborated in the following sections.

3.3 Individual Heterogeneity Modeling of Service Demand

3.3.1 Module I: Heterogeneous Service Utilization Modeling

LOS is a critical measure of service utilization of NH residents. Due to the varied individual characteristics, LOSs differ considerably among residents. Further, NH residents will be either discharged back to their residential community due to recovery or transferred to higher-level acute care settings, such as hospital, due to the occurrence of critical events (e.g., fall, and infection, etc.). To improve the LOS prediction accuracy in presence of such individual heterogeneity with multiple competing discharge dispositions, I develop a semi-parametric predictive model with competing risk. The predictive model can better quantify and predict the service utilization of NH residents. In addition to the superior prediction accuracy, the developed model also achieves sound model interpretability by identifying the disposition-specific contributing factors and quantifying their effects on NH service utilization. Considering a heterogeneous population of N elderly NH residents and M discharge dispositions, T_{im} is denoted as LOS of resident i with discharge disposition m, $i = 1...N, m = 1...M$. The proposed LOS model can be formulated as

$$\begin{aligned}\gamma_{im}(t|\boldsymbol{x}_i) &= \frac{\lim_{\Delta t\to\infty}\Pr(t \le T_{im} < t+\Delta t | T_i^{\min} \ge t, \boldsymbol{x}_i)}{\Delta t} \\ &= \gamma_m^b(t)\exp\left(\boldsymbol{\beta}_m^{\mathrm{T}}\boldsymbol{x}_i\right), \quad i = 1...N, m = 1...M \end{aligned} \tag{3.13}$$

where $T_i^{\min} = \min(T_{i1}, ..., T_{im}, ..., T_{iM})$. $\gamma_{im}(\cdot)$ refers to the resident-specific NH discharge risk of disposition m and $\gamma_m^b(\cdot)$ is the baseline NH discharge risk of disposition m, $m = 1...M$. $\boldsymbol{\beta}_m$ and $\boldsymbol{x}_i$ represent the disposition-specific covariates coefficients and the individual characteristics (e.g., demographics, clinical diagnoses, functional performance, etc.), respectively. The proposed predictive LOS model with competing risk can be perceived as a special case of the time-to-event model described in Chapter 2. The latent variable is not considered here because only single LOS observation is available for each NH resi-

dent. It is not applicable to capture the within-individual dependency of correlated LOS observations, as compared to the model in Chapter 2. Based on the above formulation in Eq. (3.13), we can further estimate model parameters and quantify the effects of influencing factors. The original likelihood function has complex structure due to multiple discharge dispositions, making model parameters estimation challenging. To address the estimation issue, the augmented variables $\Delta_{im}, i = 1...N, m = 1...M$ are introduced to indicate the discharge disposition type and further to decouple the likelihood function. $\Delta_{im} = 1$ if resident i is discharged to disposition m and $\Delta_{im} = 0$ otherwise. Given the augmented data $\mathbf{D} = \{t_i, \Delta_{im}, \boldsymbol{x}_i\}_{i=1}^{N}$ and a set of unknown parameters $\boldsymbol{\Theta} = \bigcup_m \boldsymbol{\Theta}_m$ where $\boldsymbol{\Theta}_m$'s are mutually exclusive and $\boldsymbol{\Theta}_m = \{\gamma_m^b(\cdot), \boldsymbol{\beta}_m\}, m = 1...M$, the original likelihood can be decomposed into multiple disposition-specific likelihood functions as

$$\begin{aligned} L(\boldsymbol{\Theta}|\mathbf{D}) &= \prod_{i=1}^{N}\prod_{m=1}^{M}\left\{\gamma_m^b(t_i)\exp(\boldsymbol{\beta}_m^{\mathrm{T}}\boldsymbol{x}_i)\exp\left[-\sum_{m=1}^{M}\int_0^{t_i}\gamma_m^b(\tau)\exp(\boldsymbol{\beta}_m^{\mathrm{T}}\boldsymbol{x}_i)d\tau\right]\right\}^{\Delta_{im}} \\ &= \prod_{m=1}^{M} L_m(\boldsymbol{\Theta}_m \mid \mathbf{D}) \end{aligned} \tag{3.14}$$

where $L_m(\boldsymbol{\Theta}_m|\mathbf{D}) = \prod_{i\in I_m}\gamma_m^b(t_i)\exp(\boldsymbol{\beta}_m^{\mathrm{T}}\boldsymbol{x}_i)\exp\left[-\sum_{m=1}^{M}\int_0^{t_i}\gamma_m^b(\tau)\exp(\boldsymbol{\beta}_m^{\mathrm{T}}\boldsymbol{x}_i)d\tau\right]$ is the disposition-specific likelihood function and I_m is the index set of all NH residents who are discharged to disposition m. To estimate model parameters, partial likelihood maximization is first used to obtain the estimates of $\boldsymbol{\beta}_m$, e.g., $\hat{\boldsymbol{\beta}}_m = \arg\max_{\boldsymbol{\beta}_m} L_m(\boldsymbol{\Theta}_m|\mathbf{D})$. Further, to address the estimation issue of nonparametric component, Efron morris estimator (Efron and Morris, 1973) is employed to estimate $\gamma_m^b(\cdot)$.

3.3.2 Module II: Heterogeneous Service Need Characterization

In real practice, the daily service need of NH residents can be quantified as per diem staff-time needed (in minutes) on each type of caregivers (e.g., CNA). Due to diverse chronic conditions (e.g., vascular disease, osteoporosis, dementia and depression), multi-

functional (e.g., physical and cognitive) limitations, and different types of therapies (e.g., audiology, occupational and/or physical therapy) and treatments (e.g., radiation, dialysis and/or skin treatment) received, residents service need can be highly heterogeneous. For example, per diem CNA staff-time varies from 30 minutes to 200 minutes among different NH residents with varied health conditions and therapy service level. To characterize

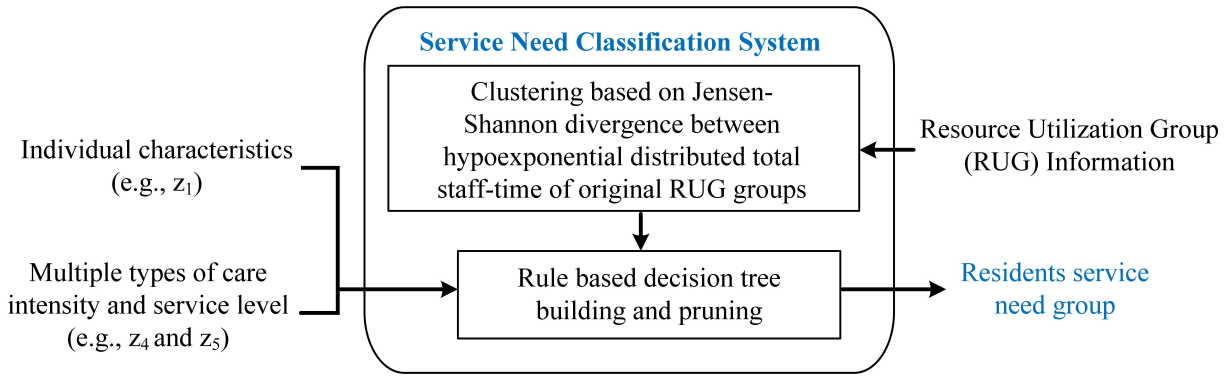

Figure 3.17: Service need heterogeneity characterization system

the heterogeneous service need of NH residents, I develop a service need classification system, as shown in Figure 3.17. In this work, I particularly use CNA service need as an example to illustrate the classification system because CNAs account for the majority (over 60% in average) of nursing staff in U.S. NHs. Without losing generality, the proposed approach can be applied to any other types of caregivers in a NH as well (e.g., RN, LPN). In the proposed classification system, I incorporate NH domain knowledge, such as national Staff Time and Resource Intensity Verification (STRIVE) Project (Centers For Medicare & Medicaid Services, 2013) and resource utilization group (RUGs) (Dellefield, 2006). The raw RUG system is a patient classification system for reimbursement purpose which categorizes NH residents into multiple service need groups. Each service need group comprises NH residents with similar resource usage level. For residents in each of the raw service need groups, STRIVE project, one of the most recent national staff-time projects, further provides staff-time information based on nationwide measurement study. Specifically, STRIVE provides nationwide reference values of average daily

staff-time needed based on the aggregation of raw staff-time measurements (collected using personal digital assistants) of approximately 97,000 NH residents from more than 200 representative high-quality NHs across different states. For each service need group, STRIVE contains (i) daily average staff-time spent directly with or on behalf of a resident; and (ii) daily average staff-time proportion spent indirectly for supporting the delivery of care for a resident. The former is defined as direct care, which involves activities such as feeding, helping dress, giving medications, charting for a resident, calling a physician about a resident, etc. The latter is defined as indirect care, which involves activities such as stocking medication cabinet, performing administration, participating in training sessions, taking time for breaks and meals, etc. Due to a lack of actual staff-time measure-

Table 3.5: Identifying variables in the service need characterization system

Variable	Variable Description	Value	Value Description
z_1	Activities of daily living (ADL) score: functional disability	0-1	Independent, no or few needs of daily living assistant
		2-5	Dependent, need daily living assistance
		6-10	Dependent, need medium level daily living assistance
		11-14	Highly dependent, need high level daily living assistance
		15-16	Most dependent, need highest level daily living assistance
z_4	Rehabilitation services level: level of therapy services for speech, audiology, occupational and physical therapy	0	No: without rehabilitation services
		1	Low
		2	Medium
		3	High
		4	Very high
		5	Ultra-high
z_5	Extensive medical services level: level of medical services	0	No: without extensive medical services
		1	Tracheostomy care, AND ventilator/respirator
		2	Tracheostomy care, OR ventilator/respirator
		3	Isolation for active infectious disease

ments at our studied NH, I incorporate STRIVE project to quantify the "representative" daily staff-time needed in minutes. I utilize the identifying variables in original RUGs classification system and develop a modified service need classification system to charac-

terize service need heterogeneity of NH residents, as shown in Table 3.5. The identifying variables include (i) the resident-level ADL scores which measure the level of functional assistance or support required by the resident, and (ii) care intensity such as the rehabilitation service level and extensive medical care service level.

As aforementioned, the raw RUG classification system is designed for reimbursement policy making. Thus, NH residents in different raw groups may have similar patterns of daily service need of different types of caregivers. To reduce the complexity of raw classification system and to characterize service need heterogeneity of NH residents, I modify the raw RUG classification system. To ensure modeling simplicity and practical convenience (van Eeden et al., 2016), I consider exponential distribution with single parameter to model daily staff-time of direct care and indirect care, and further assume they are independent. The total staff-time then follows hypoexponential distribution with two different rate parameters. To capture similar patterns of total staff-time among NH residents, I perform clustering on total staff-time of original RUG groups. Specifically, I employ hierarchical clustering approach (Dhillon et al., 2003) and use Jensen-Shannon divergence (JSD) as similarity measure (Lin, 1991). The number of target service need groups is obtained by minimum number of groups which can satisfy the condition that maximum within-cluster JSD is not exceeding tolerance ϵ_c, expressed as $N^* = \arg\min N \in \mathbf{Z}^+ : \left\| \{D_{p_i,p_j}\}_{i,j \in c_k} \right\|_\infty \leq \epsilon_c, k = 1, ..., N$ where $D_{p_i,p_j} = -\int \frac{p_i+p_j}{2} \log \frac{p_i+p_j}{2} d\mu + + \frac{1}{2} \int p_i \log p_i d\mu + \frac{1}{2} \int p_j \log p_j d\mu$ with p_i and p_j as distributions of average daily staff-time of original RUG group i and j, and c_k is a index set of original groups which belong to cluster k. In this study, I use $\epsilon_c = 0.002$ as the criterion to determine final number of service need groups. Further, the group-specific parameters for total staff-time are obtained based on the mean of the rate parameters of all raw RUG groups within cluster. The effectiveness of clustering results is evaluated via Cramer-Von Mises (CVM) test (Stephens, 1970). The p-values of all groups based on CVM test are larger than 0.5. This strongly indicates that the hypoexponential distribution with fitted group parameters achieves satisfactory goodness-

of-fit performance. As shown in Figure 3.18, the total mean staff-time is increasing when

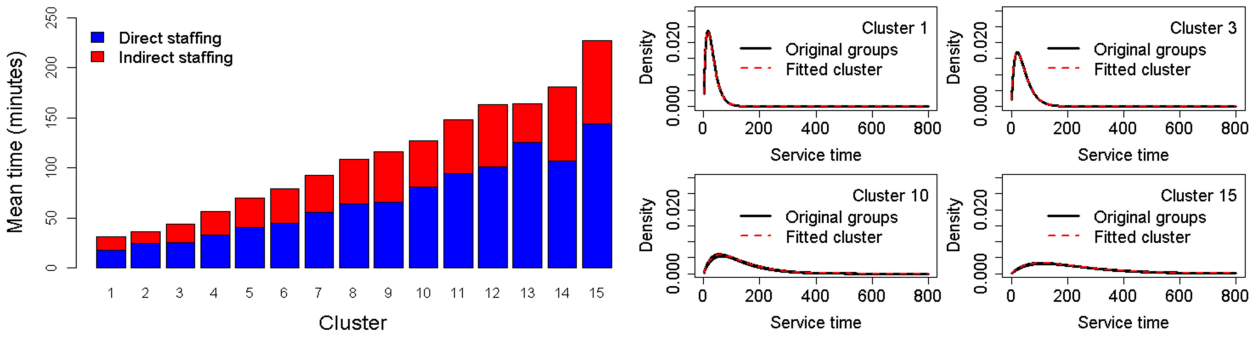

Figure 3.18: Fitting performance of the service need groups

the group index becomes larger and the distributions of total staff-time among different groups are significantly different. To further characterize the service need heterogeneity

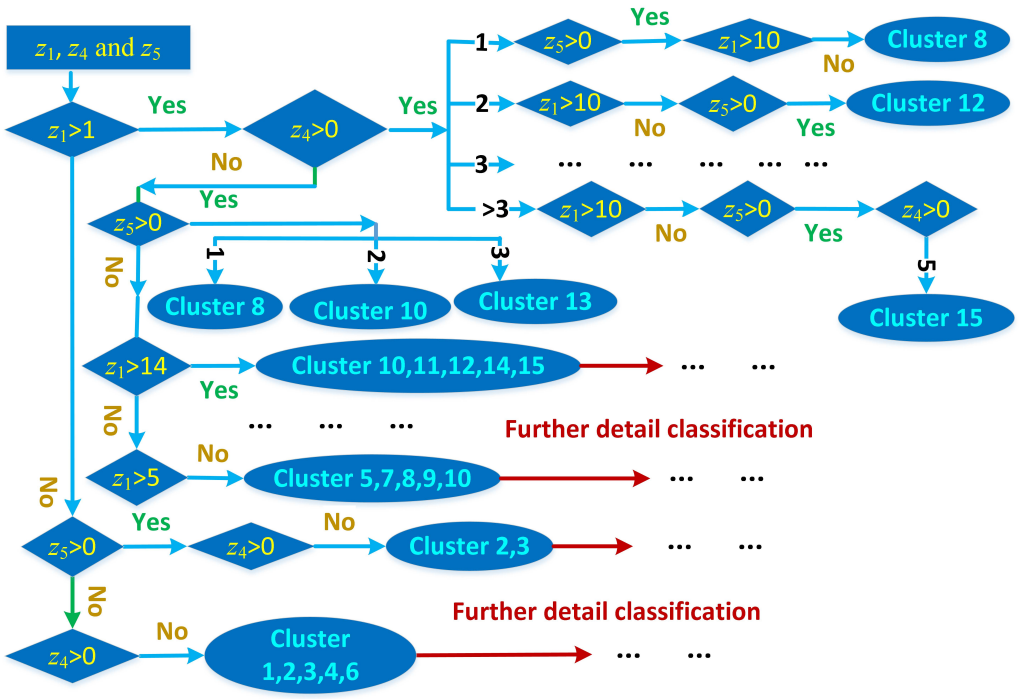

Figure 3.19: Decision tree of service need classification system

among different NH residents, I employ Apriori algorithm (Agrawal et al., 1994) to learn the association rules among identifying variables and service need groups. I then construct and prune a classification tree (Gehrke et al., 1999). The tree-based classification diagram is illustrated in Figure 3.19. When the resident ADL score is larger, the service

need group index becomes larger, which implies that the residents need of CNA service becomes larger. It is because, in a typical NH, CNAs are mainly responsible for providing daily living assistance (e.g., dressing, feeding and bathing) for NH residents. Besides, CNAs also assist residents with their rehabilitation plans, such as assisting residents with physical or occupational therapy activities established by the therapists. As shown in Figure 3.19, when resident has higher rehabilitation service level, the CNA service need tends to become larger. In addition, when resident extensive medical care becomes more intensive, the resident need more CNA service, as depicted in Figure 3.19. It is because that CNAs also provide tracheostomy care and ventilator care (e.g., ventilation equipment setup) under verification and supervision from RN or LPN. Overall, the proposed classification system can characterize service need heterogeneity of NH residents with no loss on fitting performance and can ensure the modeling fidelity for demand simulation.

3.3.3 Module III: Facility-level Service Demand Simulator

With the above predictive analytics, I further integrate with computer simulation to predict facility-level service demand of a heterogeneous population of NH residents for NH resource planning. In the predictive analytics integrated simulation model, daily arrivals for short-stayers and long-stayers are simulated. For each newly admitted short-stay resident, I employ the developed predictive LOS model in Section 3.3.1 to predict individual NH LOS and the discharge disposition. Due to the limited number of observations of discharge events for long-stay residents, distribution-based model is used to predict NH LOS for newly admitted long-stayers. For each NH resident, the individual service need group is identified based on the developed classification system in Section 3.3.2. For each resident within the identified service need group g, we extract group-specific daily average staff-time of direct care and indirect care, denoted as y_g^1 and y_g^2 respectively. For modeling convenience, we assume the daily staff-time of direct and indirect care are independent and consider exponential distribution with single param-

eter to model them. The group-specific rate parameters of total staff-time then become $\lambda_g^s = \frac{1}{y_g^s}, s = 1, 2$ where $s = 1$ represents direct care and $s = 2$ represents indirect care. For each resident i who belongs to service need group g, denoted as $I_i = g$, the resident-level daily service demand ξ_i measured by total staff-time in minutes is further simulated, i.e., $\xi_i = \sum_{s=1}^{2} \xi_i^s, s = 1, 2$ where $\xi_i^s \mid I_i = g \sim Expo(\lambda_g^s)$. The total daily staff-time of resident i in service need group g can then be simulated on a daily basis from hypo-exponential distribution (van Eeden et al., 2016), i.e., $\xi_i \mid I_i = g \sim HypoExp(\lambda_g^1, \lambda_g^2)$. Such resident-level daily service demand is repeatedly simulated for each NH resident until the end of his/her NH stay. Further, the simulated resident-level service demand is aggregated to obtain facility-level service demand of a heterogeneous population of N NH residents, denoted as ξ, i.e., $\xi = \sum_{i=1}^{N} \xi_i$. The generated facility-level demand will be utilized in Module VI for workforce planning.

3.4 Module IV: Temporal Heterogeneity Modeling of Service Demand

3.4.1 Model Formulation

In the above demonstrated paradigms of residents service demand simulation, we assume the daily average service need of both direct care and indirect care are time-invariant. However, the individual daily average service need may vary over time in real world. As shown in Section 3.3.2, the resident-level daily living assistance and therapy intensity level as well as the varied individual health conditions determine individual daily service need on CNAs. Due to recovery or deterioration of health condition, the individual daily service need of NH residents may vary over time based on the time-varying individual characteristics and care intensity. As a result, the daily service demand may exhibit temporally evolving patterns within NH stay of each resident. The temporal evolving patterns of individual service demand among different residents may also be considerably different. Thus, I propose a generic modeling approach with mixed-type

(e.g., both discrete and continuous) latent variables to characterize temporal dynamics and temporal heterogeneity of resident-level daily service demand.

Let us consider a heterogeneous population of N elderly NH residents, and m_i observations of daily staff-time of direct care and indirect care are collected over time for each resident i. To capture temporal dynamics and heterogeneity of daily average service need, we denote $\boldsymbol{y}_i^s = [y_{i1}^s, y_{i2}^s, ...y_{im_i}^s]^{\mathrm{T}}, \forall i = 1...N, s = 1, 2$ as the service need trajectory of resident i where $y_{ij}^s = y_{I_{ij}}^s(t_{ij}), \forall j = 1...m_i$ refers to the observed daily average service need of resident i at time t_{ij} for care type s. I_{ij} is an indicator of service need group of resident i at time t_{ij} and it may vary over time. We assume that the heterogeneous population consists of K sub-populations and each NH resident belongs to one single sub-population. NH residents within each sub-population exhibit similar temporal patterns of service need trajectories while residents among different sub-populations exhibit different patterns of service need trajectories. Given that resident i belongs to sub-population k, the observed service need trajectory of resident i can be modeled as

$$y_{ij}^s \mid \delta_i = k = H_s(\Lambda_k(t_{ij}) + \epsilon_{ij}; \boldsymbol{\eta}^s), \forall i = 1...N, j = 1...m_i, s = 1, 2, k = 1...K \tag{3.15}$$

where y_{ij}^s is observed daily average service need of resident i at time t_{ij}. A discrete latent variable δ_i with $P(\delta_i = k) = \pi_k$ is introduced to indicate the membership of resident i where π_k is the proportion of sub-population k in the overall population. $\delta_i = k$ indicates the service need trajectory of resident i belongs to sub-population k. With the categorical latent variable δ_i, we can capture sub-population-level latent heterogeneity of service need trajectory of NH residents. $\Lambda_k(t)$ represents the latent service need evolution of residents in sub-population k. $\epsilon_{ij} \sim N(0, \sigma_\epsilon^2)$ refers to the error term where σ_ϵ^2 is the variance. The function mapping $H_s(\cdot)$ is a link function with parameters $\boldsymbol{\eta}^s = [\eta_1^s \quad \eta_2^s], s = 1, 2$ that describes the relationship between the observed service need evolution of direct care and indirect care (represented by observed service need trajectories) and the latent service

need evolution. For modeling simplicity and ease of interpretation, linear link function is considered and can be expressed as

$$H_s^{-1}(y_{ij}^s \mid \delta_i = k) = \frac{y_{ij}^s - \eta_1^s}{\eta_2^s} = \Lambda_k(t_{ij}) + \epsilon_{ij}, \forall i = 1...N, j = 1...m_i, s = 1, 2, k = 1...K \quad (3.16)$$

Further, the nonlinear latent service need evolution of sub-population k can be explicitly characterized as

$$\Lambda_k(t_{ij}) = \boldsymbol{\theta}_{ki}^{\mathrm{T}} \boldsymbol{\phi}(t_{ij}) + \mu_i, \forall i = 1...N, j = 1...m_i, k = 1...K \quad (3.17)$$

where μ_i is continuous latent variable, i.e., $\mu_i \sim N(0, \sigma_u^2)$ where σ_u^2 is the variance. μ_i is introduced to capture individual-level latent heterogeneity and to reflect the correlations of observations of resident i. $\boldsymbol{\phi}(t_{ij})$ and $\boldsymbol{\theta}_{ki}^{\mathrm{T}}$ refer to a vector of basis functions and a vector of corresponding basis coefficients respectively. To capture the nonlinear pattern of service need evolution, we can specify $\boldsymbol{\phi}(t_{ij})$ as polynomial basis functions with maximum order Q, i.e., $\boldsymbol{\phi}(t_{ij}) = [1 \quad t_{ij} \quad ... \quad t_{ij}^Q]^{\mathrm{T}}$. Then the basis coefficients can be written as $\boldsymbol{\theta}_{ki} = [\theta_{ki0} \quad \theta_{ki1} \quad ... \quad \theta_{kiQ}]^{\mathrm{T}}$ and the basis expansion becomes $\boldsymbol{\theta}_{ki}^{\mathrm{T}} \boldsymbol{\phi}(t_{ij}) = \sum_{q=0}^{Q} \theta_{kiq} t_{ij}^q$. The basis coefficient θ_{kiq} can further be formulated as

$$\theta_{kiq} = \alpha_{kq} + \boldsymbol{\beta}_{kq}^{\mathrm{T}} \boldsymbol{x}_i, \forall k = 1...K, i = 1...N, q = 0...Q \quad (3.18)$$

where α_{kq} is sub-population-specific intercept for the decomposed q^{th} basis coefficient. $\boldsymbol{x}_i = [x_{i1}...x_{iP}]^{\mathrm{T}}$ is a vector of individual covariates of resident i and $\boldsymbol{\beta}_{kq} = [\beta_{kq1}, ..., \beta_{kqP}]^{\mathrm{T}}$ represents the corresponding sub-population-specific coefficients of individual covariates in the decomposed q^{th} basis coefficient.

Based on the above formulation with mixed-type latent variable, the temporal dynamics of service need evolution can be captured, and the temporal heterogeneity of service need trajectory, including sub-population-level heterogeneity and individual-level

heterogeneity, can be characterized as well. In addition to the modeling flexibility, the proposed model has appealing interpretability. For example, $\theta_{ki0} = \alpha_{k0} + \boldsymbol{\beta}_{k0}^{\mathrm{T}} \boldsymbol{x}_i$ captures the baseline service need of resident i who belongs to sub-population k upon NH admission. α_{k0} represents the average baseline service need in the absence of individual characteristics. The individual covariates $\boldsymbol{x}_i$ (e.g., ADL, therapy intensity) and the corresponding coefficients $\boldsymbol{\beta}_{k0}$ capture the influences of individual factors on baseline service need. Another example is the decomposition of basis coefficient when $q = 1$, as shown in Eq. (3.18). $\theta_{ki1} = \alpha_{k1} + \boldsymbol{\beta}_{k1}^{\mathrm{T}} \boldsymbol{x}_i$ characterizes the slope of latent service need evolution. α_{k1} is the average slope of latent service need evolution in the absence of individual covariates. $\boldsymbol{\beta}_{k1}$ captures the temporal effects of baseline individual characteristics on the slope. In this work, we consider $Q = 1$ and use linear basis function to avoid overfitting, i.e., $\boldsymbol{\phi}(t_{ij}) = [1 \;\; t_{ij}]^{\mathrm{T}}$ and $\boldsymbol{\theta}_{ki} = [\theta_{ki0} \;\; \theta_{ki1}]^{\mathrm{T}}$. The latent service need evolution is manifested as

$$\begin{aligned}\Lambda_k(t_{ij}) &= \theta_{ki0} + \theta_{ki1} t_{ij} + \mu_i \\ &= \alpha_{k0} + \boldsymbol{\beta}_{k0}^{\mathrm{T}} \boldsymbol{x}_i + \alpha_{k1} t_{ij} + \boldsymbol{\beta}_{k1}^{\mathrm{T}} \boldsymbol{x}_i t_{ij} + \mu_i, \forall i = 1...N, j = 1...m_i, k = 1...K \end{aligned} \tag{3.19}$$

With the above model specification, the density function of observed service need trajectory can further be manifested. $f(y_{ij}^s \mid \delta_i = k)$ is essentially a Gaussian density function, and its mean and variance can be calculated respectively as

$$\begin{aligned}&\mathbb{E}(y_{ij}^s \mid \delta_i = k) = \eta_1^s + \eta_2^s \alpha_{k0} + \boldsymbol{\beta}_{k0}^{\mathrm{T}} \boldsymbol{x}_i \eta_2^s + \eta_2^s \alpha_{k1} t_{ij} + \boldsymbol{\beta}_{k1}^{\mathrm{T}} \boldsymbol{x}_i t_{ij} \eta_2^s, \\ &\mathbb{V}(y_{ij}^s \mid \delta_i = k) = (\eta_2^s)^2 (\sigma_u^2 + \sigma_\epsilon^2), \forall i = 1...N, j = 1...m_i, s = 1, 2, k = 1...K \end{aligned} \tag{3.20}$$

3.4.2 Model Estimation

With the above generic formulation for temporal heterogeneity modeling of service need trajectory, I further employ numerical optimization techniques for model estimation. To estimate the proposed model, let $\boldsymbol{D} = \{y_{ij}^s, t_{ij}, \boldsymbol{x}_i, \forall i = 1...N, j = 1...m_i, s = 1, 2\}$ denote

the set of all available data of N NH residents. We then denote a collection of unknown model parameters as $\boldsymbol{\Theta} = \{\alpha_{k0}, \alpha_{k1}, \boldsymbol{\beta}_{k0}, \boldsymbol{\beta}_{k1}, \sigma_u^2, \sigma_\epsilon^2, \eta_1^s, \eta_2^s, \pi_k, \forall k = 1...K, s = 1, 2\}$. The joint likelihood function of the proposed model can be explicitly expressed as

$$
\begin{aligned}
L(\boldsymbol{\Theta} \mid \boldsymbol{D}) &= \prod_{i=1}^{N} \prod_{s=1}^{2} \left(\sum_{k=1}^{K} \pi_k \prod_{j=1}^{m_i} f\left(y_{ij}^s \mid \delta_i = k, \boldsymbol{\Theta} \right) \right) \\
&= \prod_{i=1}^{N} \prod_{s=1}^{2} \left[\sum_{k=1}^{K} \pi_k \prod_{j=1}^{m_i} \left(2\pi \mathbb{V}(y_{ij}^s \mid \delta_i = k) \right)^{-\frac{1}{2}} \exp\left(- \frac{\left(y_{ij}^s - \mathbb{E}(y_{ij}^s \mid \delta_i = k) \right)^2}{2\mathbb{V}(y_{ij}^s \mid \delta_i = k)} \right) \right]
\end{aligned} \tag{3.21}
$$

The model parameters estimation can be achieved by maximizing the log-likelihood, i.e., $\hat{\boldsymbol{\Theta}} = \arg\max l(\boldsymbol{\Theta} \mid \boldsymbol{D})$ where $l(\boldsymbol{\Theta} \mid \boldsymbol{D}) = \log L(\boldsymbol{\Theta} \mid \boldsymbol{D})$ is the log-likelihood function. I further employ Levenberg-Marquardt algorithm to solve this nonlinear optimization problem. At each iteration τ, the gradient and Hessian matrix of the log-likelihood function are computed as $g(\boldsymbol{\Theta}^\tau) = \nabla l(\boldsymbol{\Theta}^\tau \mid \boldsymbol{D})$ and $H^\tau = \mathbb{J}(g(\boldsymbol{\Theta}^\tau))$, respectively, where $\mathbb{J}$ is the Jacobian matrix. Further, the diagonal-inflated Hessian matrix is calculated to update model parameters. The estimation algorithm is summarized in Algorithm 2. The convergence criterion C1 is used to ensure parameter stability and C2 is used to ensure log-likelihood stability. C3 is introduced based on size of the derivatives. With the developed estimation procedure, both the influences of observed covariates and mixed-type (e.g.,discrete and continuous) latent variables can be jointly quantified.

Further, we perform the post-analysis on the estimated model to investigate the influences of different potential contributing factors on mixing proportions. The total number of groups K^* can be obtained via model selection and the estimated mixing proportions $\hat{\pi}_k, \forall k = 1...K^*$ can then be obtained. Further, the posterior probability that the service

Algorithm 2 Parameter Estimation Algorithm of Temporal Heterogeneity Model

Initialization: $\boldsymbol{\Theta}_0$, $\tau \leftarrow 0$, $\iota \leftarrow 0.01$, $\rho \leftarrow 0.01$, $\zeta \leftarrow 1$, $\varepsilon_1 = \varepsilon_2 = \varepsilon_3 = 10^{-4}$,
while $\tau < \tau_{max}$ and stop flag is false **do**
Calculate gradient $g(\boldsymbol{\Theta}^\tau)$ and Hessian matrix H^τ at current iteration
Calculate diagonal-inflated Hessian $\tilde{H}^\tau$ at current iteration as
$(\tilde{H}^\tau)_{ij} = \begin{cases} H_{ij}^\tau, & \text{if } i \neq j \\ H_{ii}^\tau + \iota \left[(1-\rho)\left|H_{ii}^\tau\right| + \rho \text{tr}(H^\tau)\right], & \text{o.w.} \end{cases}$
if $(\tilde{H}^\tau)$ is positive-definite **then**
$\iota \leftarrow 0.9\iota$, $\rho \leftarrow 0.9\rho$
else
$\iota \leftarrow 1.1\iota$, $\rho \leftarrow 1.1\rho$
end if
Check convergence is achieved using three criteria simultaneously:
C1: $\sum_{j=1}^{|\boldsymbol{\Theta}|}(\boldsymbol{\Theta}_j^\tau - \boldsymbol{\Theta}_j^{\tau-1})^2 \leq \varepsilon_1$
C2: $\left|l(\boldsymbol{\Theta}^\tau \mid \boldsymbol{D}) - l(\boldsymbol{\Theta}^{\tau-1} \mid \boldsymbol{D})\right| \leq \varepsilon_2$
C3: $g(\boldsymbol{\Theta}^\tau)^{\mathrm{T}}(H^\tau)^{-1}g(\boldsymbol{\Theta}^\tau)/|\boldsymbol{\Theta}| \leq \varepsilon_3$
if any of C1-C3 is not satisfied **then**
Update parameter estimates as
$\boldsymbol{\Theta}^{\tau+1} = \boldsymbol{\Theta}^\tau - \zeta(\tilde{H}^\tau)^{-1}g(\boldsymbol{\Theta}^\tau)$
$\tau = \tau + 1$
else
set stop flag as true
end if
end while

need trajectory of resident i belonging to sub-population k can be obtained as

$$\begin{aligned} P_{ik} &= Pr(\delta_i = k \mid \boldsymbol{D}, \hat{\boldsymbol{\Theta}}) \\ &= \frac{\hat{\pi}_k \prod_{s=1}^{2}\prod_{j=1}^{m_i} f(y_{ij}^s \mid \delta_i = k, \hat{\boldsymbol{\Theta}})}{\sum_{l=1}^{K^*}\hat{\pi}_l \prod_{s=1}^{2}\prod_{j=1}^{m_i} f(y_{ij}^s \mid \delta_i = l, \hat{\boldsymbol{\Theta}})}, \forall i = 1...N, k = 1...K^* \end{aligned} \tag{3.22}$$

With the obtained posterior probability, we then investigate the influences of individual characteristics on membership. The probability of service need trajectory of resident i belonging to sub-population k can be expressed as

$$\hat{P}_{ik} = \frac{\exp(\boldsymbol{\chi}_k^{\mathrm{T}}\boldsymbol{\nu}_i)}{\sum_l^{K^*}\exp(\boldsymbol{\chi}_l^{\mathrm{T}}\boldsymbol{\nu}_i)}, \forall i = 1...N, k = 1...K^* \tag{3.23}$$

where ν_i is a vector of individual covariates of resident i and χ_l's $\forall l = 1...K^*$ are the corresponding sub-population-specific coefficients for membership modeling. With the estimated coefficients $\hat{\chi}_l$, we can quantify the effects of individual covariates on determining membership. In addition, for a newly admitted NH resident, the probability of his/her service need trajectory belonging to a specific sub-population can be evaluated based on the observed individual covariates, as described in Eq. (3.23). Based on the estimated probabilities, the membership of service need trajectory of the newly admitted residents can further be determined. With the determined membership, we can then predict individual service need trajectory over time based on the proposed model in Eq. (3.15).

With the above modeling approach for characterizing temporally evolving and heterogeneous patterns of service need, I employ the similar simulation procedure (as described in Section 3.3.3) to incorporate the developed predictive analytics into the computer simulation model. Specifically, with the quantified daily staff-time needed for direct care and indirect care over time, denoted as y_{ij}^1 and y_{ij}^2 respectively, the hypoexponentially distributed individual daily service demand can be simulated with parameters $\lambda_{ij}^1 = \frac{1}{y_{ij}^1}$ and $\lambda_{ij}^2 = \frac{1}{y_{ij}^2}$. The predictive analytics integrated simulation approach can capture non-stationary patterns of residents service demand over time. The individual service demand is then aggregated to obtain facility-level demand for NH resource planning.

3.5 Data-driven Two-Phase NH Resource Planning

Based on the characterized facility-level service demand, we further develop a two-phase decision analytics module to determine optimal resource planning decisions at different time scales, such as annual bed capacity at strategic level, bi-monthly number of nursing staff to be recruited at tactical level, and daily working schedules as well as daily staffing level at operational level. The details are elaborated as follows.

3.5.1 Module V: Capacity Planning

In the first phase, the goal of capacity planning is to search for the optimal bed capacity such that the service quality measure of interest can be ensured. In this work, we consider average daily acceptance level as NH service quality measure. The optimal capacity planning problem can be expressed as

$$\kappa_p = \arg\min\{\kappa \in \mathbf{Z}^+ : Pr(\bar{\boldsymbol{\alpha}}_T(\kappa) \geq \tau_c) \geq \eta\} \tag{3.24}$$

where κ_p is the minimum required bed capacity and $\bar{\boldsymbol{\alpha}}_T(\kappa)$ is the mean of a vector of daily acceptance level over the planning horizon T with fixed capacity κ, i.e., $\boldsymbol{\alpha}_T(\kappa) = \{\alpha_t(\kappa)\}_{t=1}^T$. τ_c is service quality criterion and η is the quantile threshold. To account for

Algorithm 3 Optimal Capacity Planning

Initialization: $\kappa_p \leftarrow \kappa_0$, $\zeta \leftarrow 0.5\kappa_0$, $m \leftarrow 1$, $v \leftarrow 1$, $T \leftarrow 365$, $N \leftarrow 500$, $r \leftarrow 500$, $\tau_c \leftarrow$85%, $\eta \leftarrow 95\%$
  while $m \leq N$& $v = 1$ **do**
    for $j \leftarrow 1$ to r **do**
      obtain daily acceptance level at current simulation run j as $\{\alpha_t^j(\kappa_p)\}_{t=1}^T$ with simulation parameters κ_p and T
      $\bar{g}_j = \frac{1}{T}\sum_{t=1}^T \alpha_t^j(\kappa_p)$
    end for
    calculate $p = Pr(\bar{g} \geq \tau_c)$
    if $p < \eta$ **then**
      update $\zeta \leftarrow 0.5\kappa_p$ and $\kappa_p = \lceil \kappa_p + \zeta * (\eta - p) \rceil$
    else
      $v = 0$
    end if
    $m \leftarrow m + 1$
  end while

the uncertainty of residents flow and to achieve desired facility-level performance, I employ simulation-based heuristic search to determine the minimum required number of beds at the desired service quality level. The optimal capacity algorithm is summarized in Algorithm 3. In each iteration, I perform 500 replication runs to simulate NH arrivals,

admission and discharge events, and then obtain 500 samples of daily average acceptance rate based on simulation outputs. We then check if current capacity decision achieves satisfactory accessibility performance, as described in Eq. (3.24). If the stopping condition is not satisfied, the current bed capacity will be updated and the performance with a new capacity decision will be evaluated. The iterative searching process continues until we find the optimal capacity that can achieve the desired performance criterion. The developed solution algorithm can achieve a desired level of care accessibility (e.g., average daily acceptance rate at 85% or above) while can maintain the utilization performance (e.g., bed occupancy rate) as well.

3.5.2 Module VI: Workforce Planning

With the simulated facility-level service demand and the determined optimal annual capacity in previous sections, an integrated staffing and scheduling (ISS) optimization model is further formulated to minimize the overall labor cost and to meet the heterogeneous service demand of NH residents. To reduce the combinatorial complexity of working schedules in real practice, I apply dynamic programming to generate the scheduling patterns based on NH industrial knowledge, as described by *PATTNGEN* in Algorithm 4. $\boldsymbol{A}_{P\times T}$ is a matrix of all generated scheduling patterns, $\boldsymbol{A}_{it} = 1$ if scheduling pattern i contains working day t, and $\boldsymbol{A}_{it} = 0$ otherwise. The objective of workforce planning is to achieve optimal staffing and scheduling decision at reduced total labor cost. The total labor cost includes planned staffing cost for staff recruitment, understaffing penalty cost for calling temporary nursing staff (e.g., nurse as needed or agency aides) to satisfy the unmet demand, and overstaffing penalty cost due to unnecessary planned additional staffing. We denote the understaffing penalty cost as c_u and denote overstaffing penalty cost as c_v. We use $\boldsymbol{x} = [x_1, ..., x_P]^{\mathrm{T}}$ to represent a vector of decision variables where x_i is number of staff need to be recruited for scheduling pattern i, and use $\boldsymbol{c} = [c_1, ..., c_P]^{\mathrm{T}}$ to represent a vector of staffing cost where c_i is the staffing cost of schedul-

Algorithm 4 Optimal Workforce Planning

function PATTNGEN(x, $\mathbf{\Gamma}$, t_c, T_s, $\boldsymbol{\eta}$, v_{pf}, $\tilde{t}_1$, $\tilde{t}_2$)
  if $|\boldsymbol{\eta}| = t_c$ **then**
    $\mathbf{\Gamma} \leftarrow \mathbf{\Gamma} \cup \boldsymbol{\eta}$
  else
    for $j \leftarrow x$ to T_s **do**
      $c \leftarrow$ total number of working days allocated at weekend
      if $c \leq \tilde{t}_1$ **then**
        $c \leftarrow$ bi-weekly total number of working days
        if v_{pf}=2 AND $c \leq \tilde{t}_2$ OR $v_{pf} = 1$ **then**
          $\boldsymbol{\eta} \leftarrow \boldsymbol{\eta} \cup j$
          PATTNGEN(j+1, $\mathbf{\Gamma}$, t_c, T_s, $\boldsymbol{\eta}$, v_{pf}, $\tilde{t}_1$, $\tilde{t}_2$)
        end if
      end if
    end for
  end if
end function
procedure STAFFDECISIONMAKER
  PATTNGEN(1, $\boldsymbol{A}$, β_{ft}, T, Ξ, 1, $\tilde{t}_{wk}$, $\tilde{t}_{pt}$)
  for each $\beta \in \boldsymbol{\beta}_{pt}$ **do**
    $\Xi \leftarrow \{\}$
    PATTNGEN(1, $\boldsymbol{A}$, β, T, Ξ, 2, $\tilde{t}_{wk}$, $\tilde{t}_{pt}$)
  end for
  simulate individual daily service demand of NH residents
  aggregate resident-level demand to obtain facility-level demand as $\boldsymbol{\xi} = [\xi_1, ..., \xi_T]^{\mathrm{T}}$
  solve the following model by sample average approximation:
  $\min_{\boldsymbol{x} \subseteq \mathbb{Z}_+^p} \quad \boldsymbol{c}^{\mathrm{T}}\boldsymbol{x} - c_u \mathbb{E}_{\boldsymbol{\xi}} \left[[(\boldsymbol{s} - \boldsymbol{\xi})^-]^{\mathrm{T}} \mathbb{1}_T \right] + c_v \mathbb{E}_{\boldsymbol{\xi}} \left[[(\boldsymbol{s} - \boldsymbol{\xi})^+]^{\mathrm{T}} \mathbb{1}_T \right]$
  where $(\boldsymbol{d})^- = [\min(d_1, 0), ..., \min(d_T, 0)]^{\mathrm{T}}$ and $(\boldsymbol{d})^+ = [\max(d_1, 0), ..., \max(d_T, 0)]^{\mathrm{T}}$
  $\boldsymbol{s} = [s_1, s_2, ..., s_T]^{\mathrm{T}}$ and $s_t = K\left(\sum_{i=1}^{P} \boldsymbol{A}_{it} x_i\right)$
end procedure

ing pattern $i, i = 1...P$. Given the planning horizon T, we can then define a loss function as $L(\boldsymbol{\xi}, \boldsymbol{x}) = \boldsymbol{c}^{\mathrm{T}}\boldsymbol{x} - c_u \sum_{t=1}^{T}(s_t - \xi_t)^- + c_v \sum_{t=1}^{T}(s_t - \xi_t)^+$ where the operators $(\cdot)^-$ and $(\cdot)^+$ are denoted as $(d)^- = \min(d, 0)$, $(d)^+ = \max(d, 0)$. ξ_t refers to the random facility-level service demand at day t, $t = 1...T$. s_t refers to the staffing supply in minutes at day t and can be further expressed as $s_t = K\left(\sum_{i=1}^{P} \boldsymbol{A}_{it} x_i\right)$, where P is total number of generated scheduling patterns and K is the daily supply (in minutes) per staff. Then the goal of NH workforce planning is to determine number of nursing staff need to be recruited for each scheduling pattern that can minimize the expected loss function. The NH ISS optimization problem is described in Algorithm 4. To account for the stochastic uncertainty of service demand, I employ sample average approximation method (Kleywegt et al., 2002) to solve the ISS optimization model.

3.6 Case Study

3.6.1 Data Description

I evaluate the prediction performance and decision performance of proposed framework based on the de-identified electronic health records of NH residents (Saliba et al., 2012) from our industrial collaborator (Greystone Healthcare Management Corp.). The real data contains details of admission and discharge records, and rich resident-level health assessment information, including but not limited to socio-demographics, disease diagnoses, functional performances limitations (e.g., physical limitation and cognitive impairments, etc.), and care intensity as well as service level. In this work, totally 677 residents are considered. More than 80% of residents are over 65 years old. Based on the admission and discharge records, the resident-level LOS information is extracted. As illustrated in Figure 3.20a, the extracted resident-level dwelling duration is heterogeneous with different discharge dispositions. In addition, the diseases and chronic conditions among NH residents are diverse, as shown in Figure 3.20b. Over 90% of the NH residents have at least one type of chronic diseases (e.g., cancer, and hypertension, etc.) and

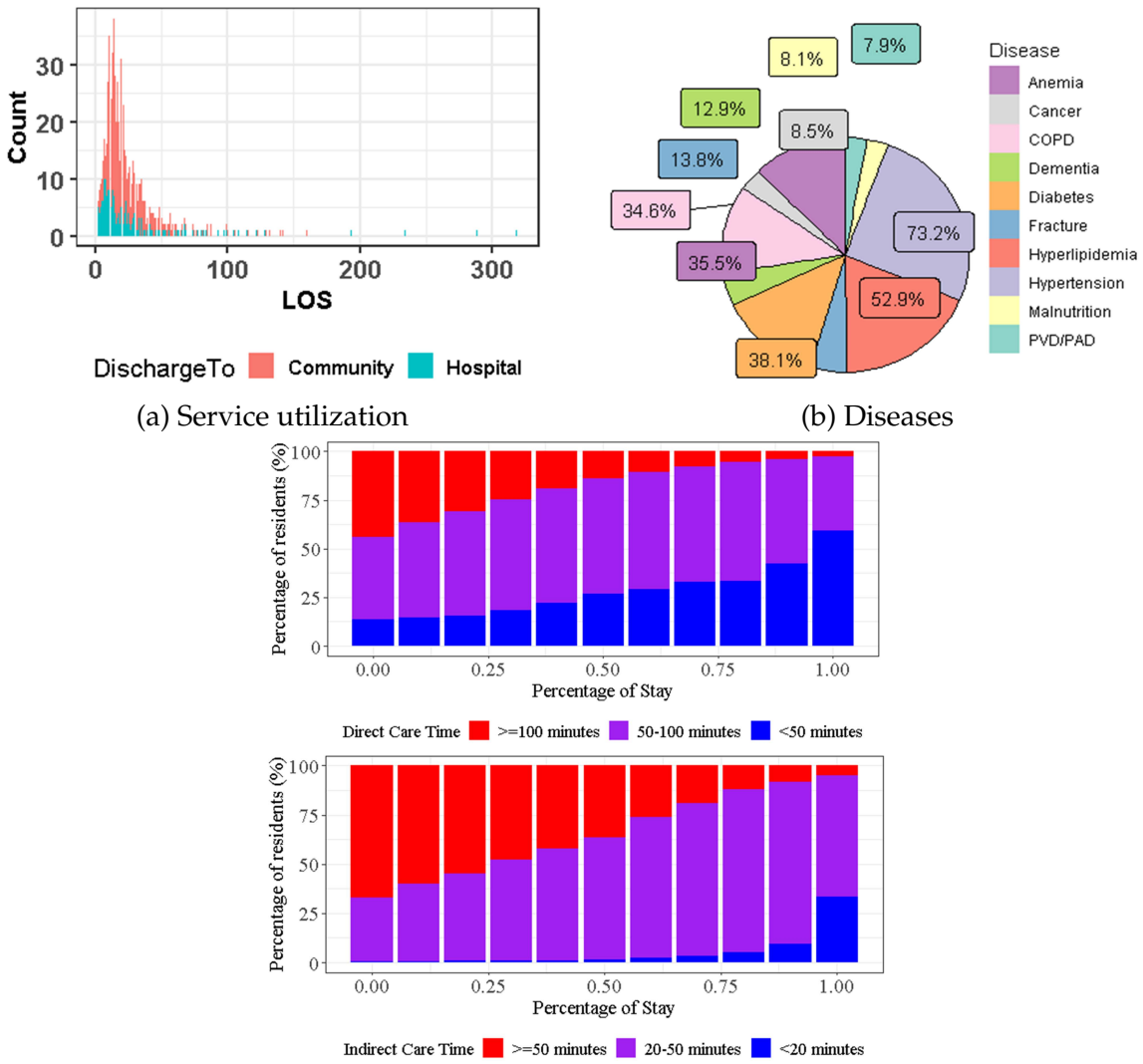

(a) Service utilization (b) Diseases

(c) Service need of direct care and indirect care

Figure 3.20: Extracted resident-level information

many residents even have multiple chronic conditions. About 38% of residents have diabetes mellitus and about 35% of residents have anemia condition. Besides, over 60% of residents are diagnosed with skin problems, such as pressure ulcers and skin tears. Over 90% of residents need skin care and treatment procedure. Moreover, about 5% of residents are diagnosed with acute conditions such as obstructive uropathy. Further, the ADL score of NH residents are also available from the data set. It measures the level of functional assistance or support required by the residents. A higher ADL score means that the resident is more physically dependent and needs more daily living assistance.

In the real data, over 90% of residents need daily living assistance (e.g., ADL is larger than 1). Among the residents who need daily living assistance, 20% of them have more physical disabilities and are highly dependent, and thus need most daily living assistance (e.g., ADL from 11 to 16). Besides, the resident-level information also includes the varied service need level and care intensity among different types of services. Over 95% residents need rehabilitation therapy service during their stay. On the other hand, less than 5% residents need extensive medical care service. Due to the varied individual functional performance and care service needed, the service demand of each resident (quantified in staff-time needed) is highly heterogeneous and also fluctuates over time. As shown in Figure 3.20c, the extracted facility-level compositions of direct care and indirect care over time reflect the heterogeneous and temporally evolving service demand of NH residents.

3.6.2 Prediction Performance Evaluation and Comparison

Based on the acquired data, I first model simulation inputs, such as daily arrivals and LOSs of NH residents, and evaluate their prediction performances. Based on the LOS observations and definitions of short stay as well as long stay from Centers for Medicare & Medicaid Services, we classify NH residents into short-stay residents (e.g., LOS $\leq$ 100 days) and long-stay residents (e.g., LOS > 100 days). Short-stay residents mainly receive rehabilitation therapy service and post acute care while long-stay residents mainly receive long-term custodial care in a NH. Negative binomial distribution is used to model the arrivals of short-stay residents, i.e., NB(r, p). The goodness-of-fit performance is evaluated by Chi-square test. The p-value of the estimated NB$(\hat{r}, \hat{p})$ is 0.3, which indicates a satisfactory goodness-of-fit performance. On the other side, I use Poisson distribution to model the arrivals of long-stay resident, i.e., Pois(λ). The p-value of Chi-square test is 0.67, which also indicates a satisfactory goodness-of-fit performance.

Further, I apply the developed LOS model to analyze the real LOS observations. Two major discharge dispositions are considered, e.g., community and hospital (about 61% of

residents are discharged to community and 24% of residents are re/hospitalized). Other discharge dispositions, such as transferring to another NH or death, are negligible and thus discarded. In the real NH data, more than 90% of residents are short-stay residents (e.g., LOS $\leq$ 100 days) while the others stay longer than 100 days. I employ the predictive LOS model (as described in Section 3.3.1) with incorporating individual characteristics and multiple competing discharge dispositions to analyze NH LOS of short-stay residents. I employ variable selection techniques and identify 16 covariates to model the heterogeneous LOS, including both time-to-discharge to community and time-to-discharge to hospital. As shown in Table 3.6, the ADL score exhibits a significant negative effect on

Table 3.6: Estimation results of proposed LOS model

Community specific covariates	Type	Coefficients	p-value
ADL	Numeric	-0.1134	<1e-6
Summary score of mental health	Numeric	-0.0341	0.05589
Total mood severity score	Numeric	-0.1433	0.00047
Cancer	Binary	-0.4356	0.00722
Anemia	Binary	-0.2026	0.0367
Hypertension	Binary	-0.5592	<1e-6
Benign prostatic hyperplasia	Binary	-0.5148	0.00027
Renal failure	Binary	-0.3303	0.01363
Multidrug-resistant organism	Binary	-0.6281	0.03305
Hip fracture	Binary	-0.6041	0.00957
Other fracture	Binary	-0.4213	0.00091
Non-Alzheimer's Dementia	Binary	-0.4478	0.00139
Hemiplegia or hemiparesis	Binary	-0.8457	0.00041
Malnutrition	Binary	-0.5564	0.00448
Hospital specific covariates	Type	Coefficients	p-value
ADL	Numeric	0.0872	0.00026
Anemia	Binary	0.4821	0.00727
Obstructive uropathy	Binary	1.0283	0.00079
Diabetes mellitus	Binary	0.5031	0.00311
Malnutrition	Binary	0.4162	0.08115

the time-to-discharge to community. With a higher ADL score, the resident needs more daily living assistance and thus stays in NH longer. It is because the resident either needs more time to restore his/her functional performance, or changes from short-term rehabilitation stay into long-term care stay due to unsuccessful recovery. The proposed LOS model also identifies other significant factors, including varied disease conditions, such as anemia, diabetes, and obstructive uropathy, etc. These factors have significant positive effects on rehospitalization risk. The quantified effects of these contributing factors on re/hospitalization risk can better inform NH administrators to focus on the most at-risk NH residents with more targeted resource allocated.

Based on the developed model, I further evaluate its prediction performance and compare with alternative modeling approaches, namely LOS model without considering multiple discharge dispositions. Specifically, I compare the Kaplan-Meier survival curves (Akritas, 1986) between predicted samples of two LOS models and observed samples. As

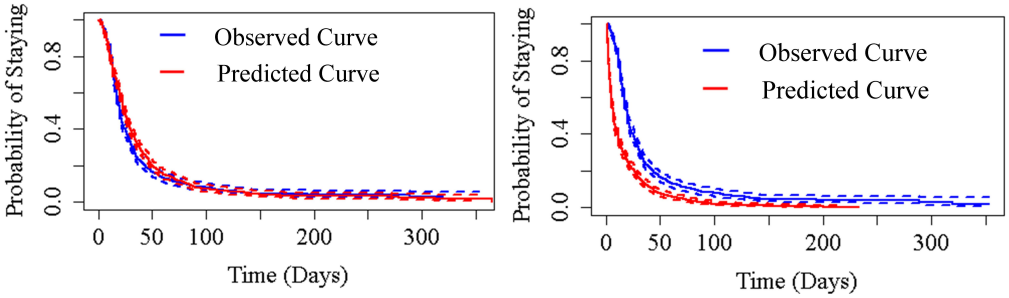

(a) Proposed model (b) Alternative model

Figure 3.21: Comparison of survival curves based on different approaches

shown in Figure 3.21a, the K-M curve of predicted LOS samples based on the proposed model is close to the K-M curve of observed LOS samples. This demonstrates satisfactory predictive distribution accuracy of the developed LOS model. On the other side, the model without considering multiple discharge dispositions results in LOS underestimation, as shown in Figure 3.21b. Overall, the developed LOS model can successfully capture LOS heterogeneity with multiple competing discharge dispositions and improve LOS prediction performance. For long-stay residents, most of them stay much longer

than the selected one-year time period. Thus, few completed discharge events are observed. I simply use log-normal distribution to capture such right-censored observations. The p-value of Chi-square test is 0.26 and thus the estimated model of LOSs for long-stay residents is also validated.

3.6.3 Validation of Simulation Model

With the above predictive analytics, I further integrate them with high-fidelity simulation to predict facility-level service demand of NH residents. To validate the simu-

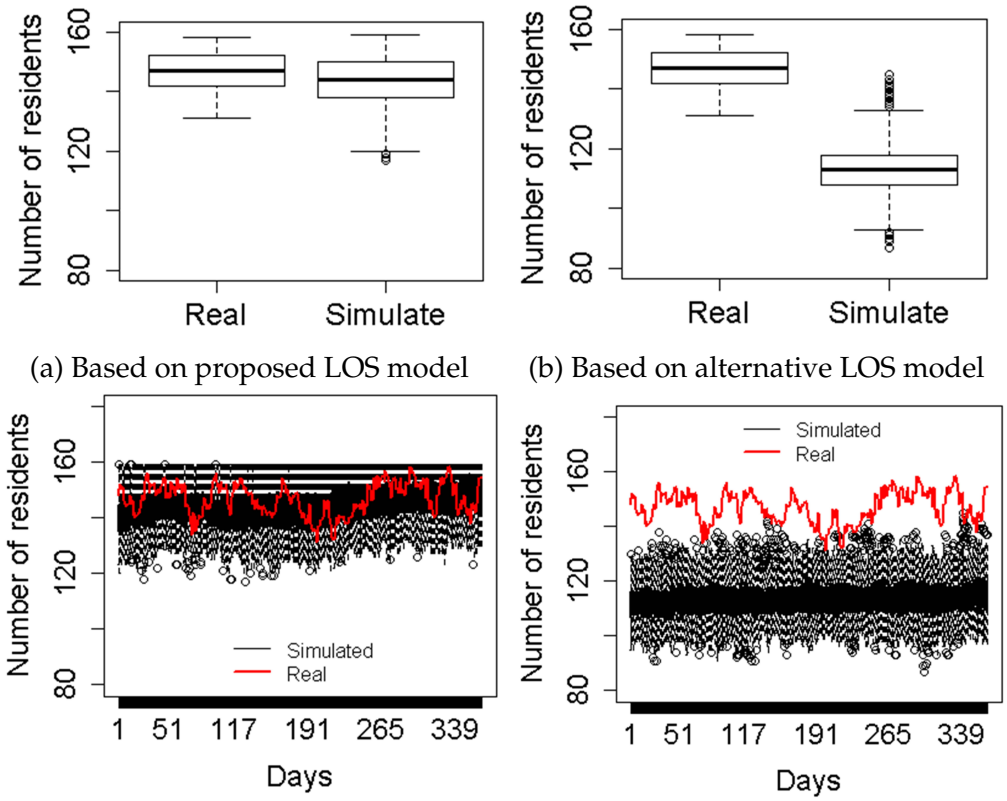

(a) Based on proposed LOS model (b) Based on alternative LOS model

(c) Based on proposed LOS model (d) Based on alternative LOS model

Figure 3.22: Comparison of simulated resident volume at different scales

lation model, I compare the simulated outputs of daily resident volume with the actual observed resident volume. As shown in Figure 3.22a, the simulated samples of daily resident volume exhibit a similar distribution to the real data. Moreover, I use two-sample Kolmogorov-Smirnov (KS) test to compare their statistical differences and a p-value of

0.52 implies that there is no statistically significant difference between the two. The results demonstrate the superior prediction performance of the proposed approach at facility level. On the other hand, the simulation outputs of model without considering competing discharge dispositions fail to achieve satisfactory prediction results, as shown in Figure 3.22b, with a p-value of <2.2e-16 in the KS test. The conventional model which neglects multiple discharge dispositions will result in LOS underestimation and a lower-than-actual resident volume. Such prediction inaccuracy will propagate to resource planning, and further induce the inappropriate capacity and workforce planning decisions with unsatisfactory performance (e.g., inadequate capacity, and large understaffing cost). To further provide validation of the simulation outputs at a finer scale, I compare the simulated daily number of residents over time (under multiple replication runs) based on the proposed approach with the real data. As shown in Figure 3.22c, 95% confidence bands of the simulated resident volume can fully cover the observed daily number of residents over time. On the other hand, the simulation outputs based on LOS model without considering multiple discharge dispositions have lower-than-actual daily number of residents over time than actual data, as shown in Figure 3.22d.

Further, I validate the developed simulation model by comparing the simulated and observed system performance (e.g., daily staffing level, average planned staffing cost per day). The comparison results are summarized in Table 3.7. The average planned staffing

Table 3.7: Staffing decision comparison of real practice and proposed model

Cost Analysis	Real Practice (min/mean/max)	Simulation
Average planned staffing cost per day	2.9K / 4.2K / 5.2K	3168-4224
Daily staffing level	32/46/57	36-48

cost per day and the daily staffing level from the proposed model are covered by the lower and upper bounds of observed performance. This further justifies the validity of the proposed predictive analytics integrated simulation model for demand simulation.

3.6.4 Decision Performance Evaluation and Comparison

With the characterized service demand from the proposed predictive analytics integrated high-fidelity simulation, I further implement the proposed two-phase optimization module for NH resource planning. For capacity planning, I employ heuristic search method to find the optimal bed capacity with the desired performance level, as described in Section 3.5.1. To evaluate the capacity decision performance, I compare the proposed

Table 3.8: Descriptions of different capacity strategies

Strategies	Description
C1	The maximum capacity of NHs in the state of Florida
C2	The average capacity of NHs in the state of Florida
C3	The maximum capacity of NHs from our industry collaborator
C4	The average capacity of NHs from our industry collaborator

capacity strategy with other alternative strategies, as shown in Table 3.8. As compared

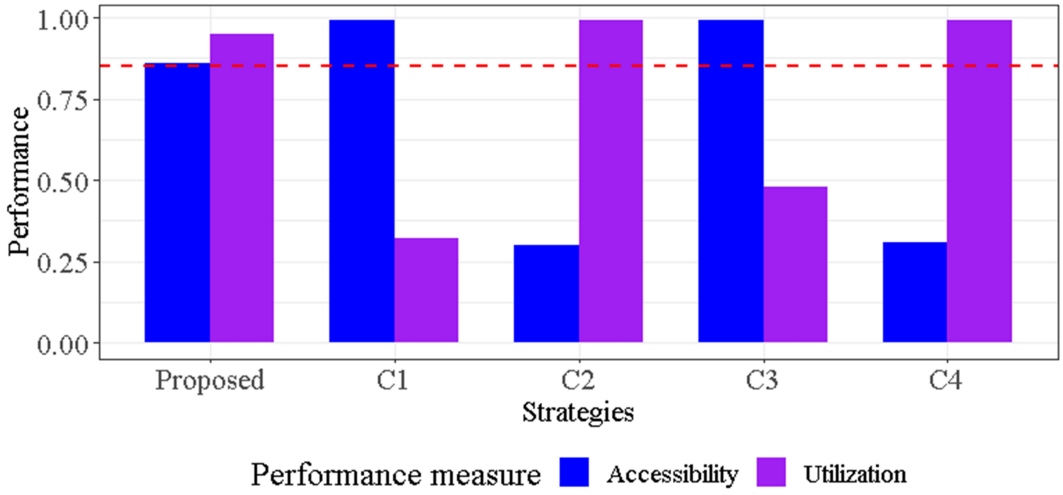

Figure 3.23: Performance comparison among different capacity strategies

to the other capacity strategies (e.g., C1-C4), the proposed capacity strategy can achieve the desired accessibility level (e.g., average daily acceptance rate 85% or above) at largest bed utilization performance with minimum required number of beds, as shown in Figure 3.23. On the other side, the other strategies either fail to achieve the desired quality

level of care accessibility (e.g., C2 and C4), or fail to maintain a satisfactory bed utilization performance (e.g., C1 and C3). Moreover, I evaluate the performance of capacity decision from LOS model which neglects multiple competing discharge dispositions. The required number of beds derived from LOS model without considering multiple discharge dispositions is 100, which is much smaller as compared to the capacity from propose strategy due to the underestimated LOS and lower resident volume. The average daily acceptance rate based on such capacity decision becomes less than 30% and it fails to achieve the desired care accessibility level. Overall, the proposed capacity strategy can achieve desired quality level of care accessibility and can maintain bed utilization performance as well with minimum required number of beds.

With the optimal annual capacity obtained, I further evaluate the performance of proposed ISS decision making model. Without losing generality, workforce planning decision of CNAs is considered since CNAs provide the most direct and essential care to the NH residents. I compare the proposed ISS strategy for CNA workforce planning with

Table 3.9: Descriptions of different staffing strategies

Strategies	Description
M1	Facility-implemented SR ratio-based staffing without scheduling patterns
M2	State-regulated SR ratio-based staffing without scheduling patterns
M3	Facility-implemented SR ratio-based ISS
M4	State-regulated SR ratio-based ISS
M5	Need-based ISS without incorporating predictive analytics
M6	Need-based ISS without incorporating stochastic uncertainty of demand

alternative staffing strategies, as described in Table 3.9. As compared to the other staffing strategies (e.g., M1-M6), the proposed ISS strategy achieves the smallest total labor cost, as shown in Figure 3.24, due to the following three reasons. First, the proposed strategy accounts for the heterogeneous service need of NH residents while the SR ratio-based strategies (e.g., M1-M4) fail to consider the service need heterogeneity. The strategies

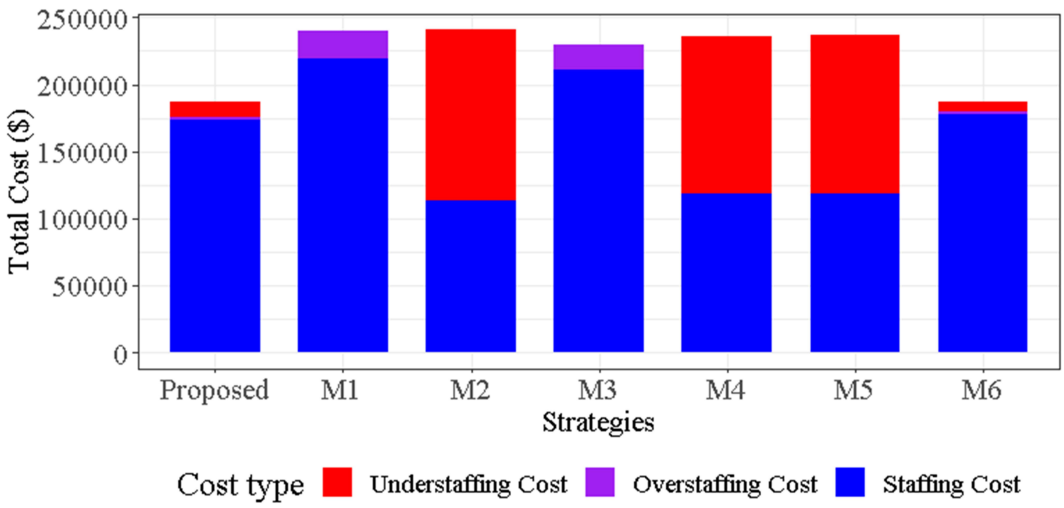

Figure 3.24: Performance comparison among different staffing strategies

with minimum SR ratio elicited from industry practice (e.g., M1 and M3) result in significantly larger overstaffing cost. On the other side, the strategies with minimum SR ratio enforced by state regulation (e.g., M2 and M4) lead to significantly larger understaffing cost. As compared to the SR ratio-based staffing strategies without considering scheduling patterns (e.g., M1 and M2), the SR ratio-based ISS strategies (e.g., M3 and M4) which incorporate scheduling patterns can achieve smaller total cost. All of these above strategies result in larger unmet service demand, and further induce larger cost than the proposed need-based ISS strategy. Second, the proposed strategy accounts for heterogeneous LOS of NH residents via the developed LOS predictive model. I compare the proposed strategy with other need-based strategy (e.g., M5) without incorporating the improved LOS predictive analytics and further investigate the impact of LOS heterogeneity on ISS decisions. Due to the underestimated LOS and the smaller bed capacity, the strategy M5 underestimates service demand, and results in significantly larger understaffing cost than the proposed strategy, as shown in Figure 3.24. Third, the proposed strategy accounts for the stochastic uncertainty of service demand via stochastic optimization. I compare the proposed strategy with other need-based strategy (e.g., M6) based on deterministic optimization to investigate the impact of stochastic demand uncertainty on ISS decisions.

The strategy M6 which fails to consider service demand uncertainty leads to larger total labor cost than the proposed strategy. The value of stochastic solution is 242. Overall, the proposed need-based ISS strategy can successfully meet with the heterogeneous service demand and achieve the smallest total labor cost.

3.6.5 What-if Scenarios with Different Resident Compositions

Given the above resident composition, the proposed work demonstrates superior performances on both capacity and workforce planning decisions. In real practice, the current strategies may need to be adjusted when the resident composition varies considerably, such as in the same NH but at different seasonal/yearly period or across different NH facilities. Thus, I generate different what-if scenarios of resident composition to investigate how the resource planning decisions may vary. Particularly, I investigate the impacts of LOS heterogeneity and service need heterogeneity on resource planning decisions. The actual resident composition scenario in Section 3.6.1 is considered as baseline scenario (S1). I then generate five more alternative scenarios, including

- worse health conditions scenario (S2): as compared to S1, half of residents have diabetes mellitus and the percentage of residents having anemia increases to 50%. Over 50% of residents have acute condition, such as obstructive uropathy.
- less physically dependent scenario (S3): 90% of residents are less physically dependent (e.g., ADL from 0 to 1) and can either live independently or require less daily living assistance. The mean of ADLs decreases 80% as compared to S1.
- more physically dependent scenario (S4): 90% of residents are more physically dependent (e.g., ADL from 11 to 16) and require more daily living assistance. The mean of ADLs increases 80% as compared to S1.

- less rehabilitation therapy need scenario (S5): residents have the same ADLs and health conditions as those in baseline scenario. However, the percentage of residents who need rehabilitation decreases 50% as compared to S1.
- more extensive medical service need scenario (S6): as compared to S1, residents have the same ADLs, health conditions and therapy need. However, the percentage of residents who require extensive medical care increases to 90%.

Based on the constructed scenarios, I investigate the effects of different census compositions on service demand and further investigate the effects of LOS heterogeneity and service need heterogeneity on capacity and workforce planning decisions. The performance comparison results among different scenarios are summarized in Table 3.10. The resident-level service utilization quantified by LOS and service demand quantified by daily staff-time needed in minutes may vary in response to the varied resident composition. Consequently, the capacity and workforce planning decisions will be affected by the varied service utilization and daily service demand. For example, the residents in S2 have shorter NH stay than S1 due to the increasing likelihood of being re/hospitalized. Such increasing likelihood is attributed to the increasing percentage of residents having acute conditions (e.g. anemia, diabetes mellitus and obstructive uropathy), which impose significantly positive effects on the re/hospitalization risk (as shown in Table 3.6). Consequently, the residents are more likely to be re/hospitalized more quickly for the acute

Table 3.10: Resource planning decision comparison among different scenarios

Scenario	Optimal Capacity	Total Labor Cost	Planned Staffing Cost
S1	156	187007	173888
S2	148	178607	167552
S3	146	131249	123904
S4	167	240451	224928
S5	156	180247	167904
S6	156	225031	208736

condition treatment and thus have shorter NH stay. Due to the decreased residents volume, the optimal capacity in S2 decreases, as shown in Table 3.10. Nevertheless, the service need in S2 has no change because the individual functional performance and therapy intensity keep the same as compared to S1. With the joint effects of less residents staying in NH and unaltered daily service need, the facility-level service demand decreases as well, and further the planned staffing cost and total labor cost also decrease. In addition to the health conditions, the varied functional performance among different scenarios also affects residents NH LOS and daily service need, and further influences capacity and workforce planning decisions. For example, the residents in S3 have decreasing ADL score and thus need less daily living assistance. With the joint effects of increased likelihood of being discharged to community and decreased likelihood of re/hospitalization, the residents in S3 tend to stay shorter and the residents volume decreases accordingly. Consequently, the optimal capacity in S3 decreases as compared to S1. The daily service need also decreases due to less care services are needed. The facility-level service demand decreases because of both shorter stay and less service need. Further, the total labor cost and planned staffing cost in S3 decrease as well. On the other side, the residents in S4 become more physically dependent with larger ADL scores and thus need more daily living assistance during NH stay. The residents in S4 tend to stay longer because of the joint effects of decreased likelihood of being discharged to community and increased re/hospitalization risk, as shown in Table 3.6. As a result, the optimal capacity in S4 increases significantly with increased residents volume. The daily service need also increases in response to the increased ADL scores. The facility-level service demand increases due to the increased service utilization (measured in LOS) and the increased daily service need. As compared to S1, more CNAs need to be recruited in S4 to meet such increased facility-level demand. Consequently, the total labor cost and planned staffing cost in S4 become significantly larger. Moreover, the care intensity of different types of service also varies among different scenarios and induces varied service need and further affects

workforce planning decision. For example, the rehabilitation need of NH residents in S5 decreases 50% as compared to S1, and thus the service need becomes less. Nevertheless, the service utilization of NH residents (measured in LOS) in S5 are the same as S1, different from the varied service utilization among scenarios S2-S4. Thus, there is no difference in capacity decision of S5 as compared to S1 due to the unchanged resident volume. However, the planned staffing cost in S5 becomes smaller as compared to S1 and the total labor cost decreases due to the decreased service need. Fewer CNAs are needed to meet the decreased service demand in S5. On the other side, the need for extensive medical care increases in S6, and consequently the characterized service need increases as compared to S1. Despite increased residents service need, the individual characteristics related to service utilization in S6 are the same as compared to S1. Thus, the optimal capacity in S6 is the same as compared to S1 due to the unaltered residents volume. With the increased daily service need and unchanged service utilization, the facility-level service demand increases. Consequently, more CNAs are needed to meet the increased demand in S6 and thus the planned staffing cost as well as total labor cost become larger as compared to S1. Overall, the proposed framework is flexible to analyze different what-if scenarios of different resident census compositions and can suggest adaptive optimal resource planning decisions to NH administrators.

With the above demonstrated effectiveness of proposed approach, I develop a practical user-friendly decision support platform to facilitate managerial decision making for NH administrators, as shown in Figure 3.25. The analytics-based decision support system for NH resource planning can deliver rich decisions at different time scales, including strategic decision, such as annual bed capacity decision, tactical decision, such as bi-monthly staff recruitment decision (e.g., number of nursing staff need to be recruited), and operational decision, such as daily staffing levels as well as daily working schedules.

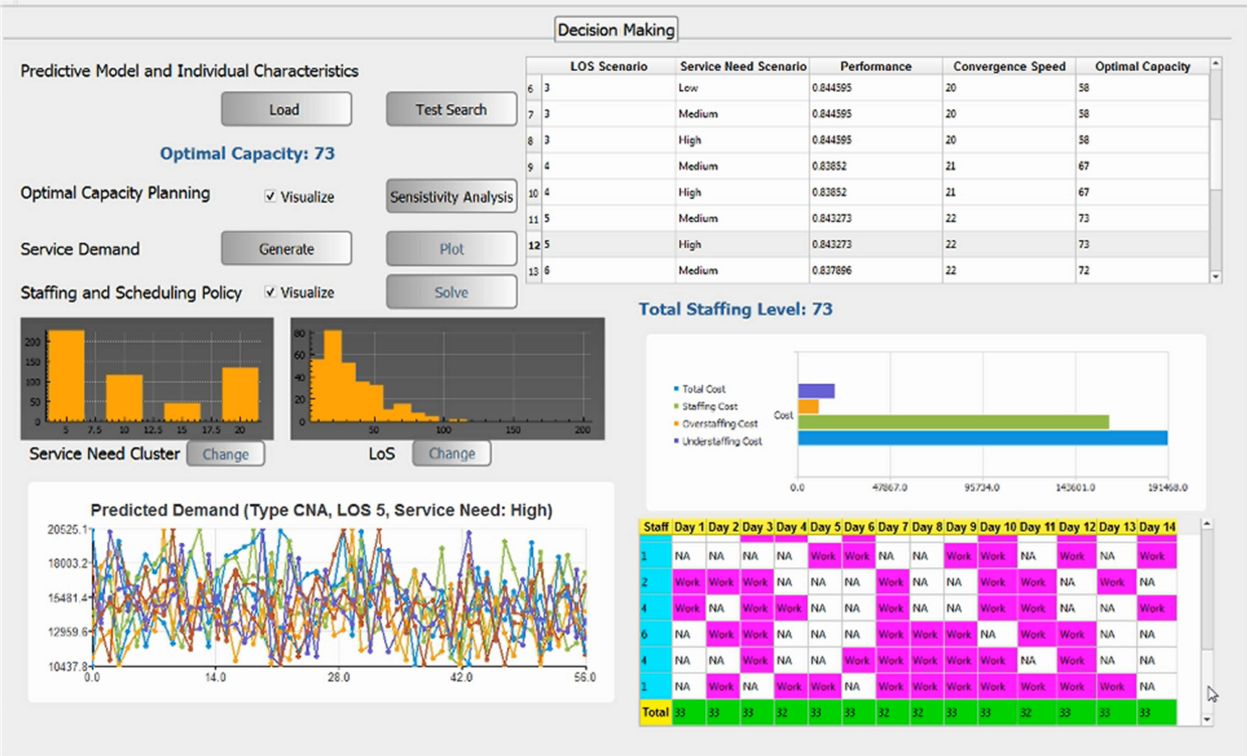

	LOS Scenario	Service Need Scenario	Performance	Convergence Speed	Optimal Capacity
6	3	Low	0.844595	20	58
7	3	Medium	0.844595	20	58
8	3	High	0.844595	20	58
9	4	Medium	0.83852	21	67
10	4	High	0.83852	21	67
11	5	Medium	0.843273	22	73
12	5	High	0.843273	22	73
13	6	Medium	0.837896	22	72

Staff	Day 1	Day 2	Day 3	Day 4	Day 5	Day 6	Day 7	Day 8	Day 9	Day 10	Day 11	Day 12	Day 13	Day 14
1	NA	NA	NA	NA	Work	Work	NA	NA	Work	Work	NA	Work	NA	Work
2	Work	Work	Work	NA	NA	NA	Work	NA	NA	Work	Work	NA	Work	NA
4	Work	NA	Work	Work	NA	NA	Work	NA	NA	Work	Work	NA	NA	Work
6	NA	Work	Work	NA	NA	NA	Work	Work	Work	NA	Work	Work	NA	NA
4	NA	NA	Work	NA	NA	Work	Work	Work	Work	Work	NA	Work	NA	NA
1	NA	Work	NA	Work	Work	NA	Work	Work	Work	Work	Work	Work	Work	NA
Total	33	33	33	32	33	33	32	32	33	33	32	33	33	33

Figure 3.25: Graphical user interface of the decision support platform

3.6.6 Results of Temporal Heterogeneity Model

3.6.6.1 Prediction Performance Evaluation

With the above proposed decision support platform for NH resource planning, I further enhance the demand modeling via considering temporal heterogeneity, as demonstrated in Eq. (3.15). In this work, we consider resident-level ADL and therapy intensity as the individual covariates to characterize the daily service need evolution. I first compare the goodness-of-fit performance among models with different number of sub-populations. We consider the performance criteria, such as log-likelihood, Akaike information criterion (AIC) and Bayesian information criterion (BIC). As shown in Figure 3.26, the model with 8 sub-populations can achieve the largest log-likelihood and the smallest AIC and BIC values. Thus, we select the estimated model with 8 sub-populations and further investigate the prediction performance based on the selected model. We predict

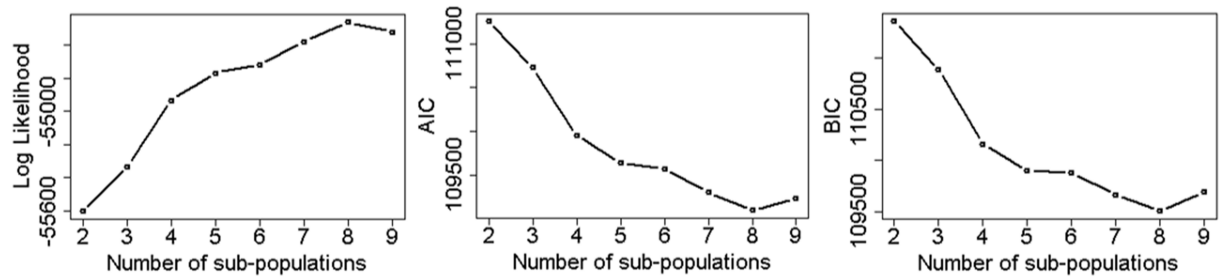

(a) Log-likelihood (b) AIC (c) BIC

Figure 3.26: Goodness-of-fit performance evaluation

the individual daily service need trajectories of direct care and indirect care with the incorporated individual characteristics. As illustrated in Figure 3.27, the temporal evolving

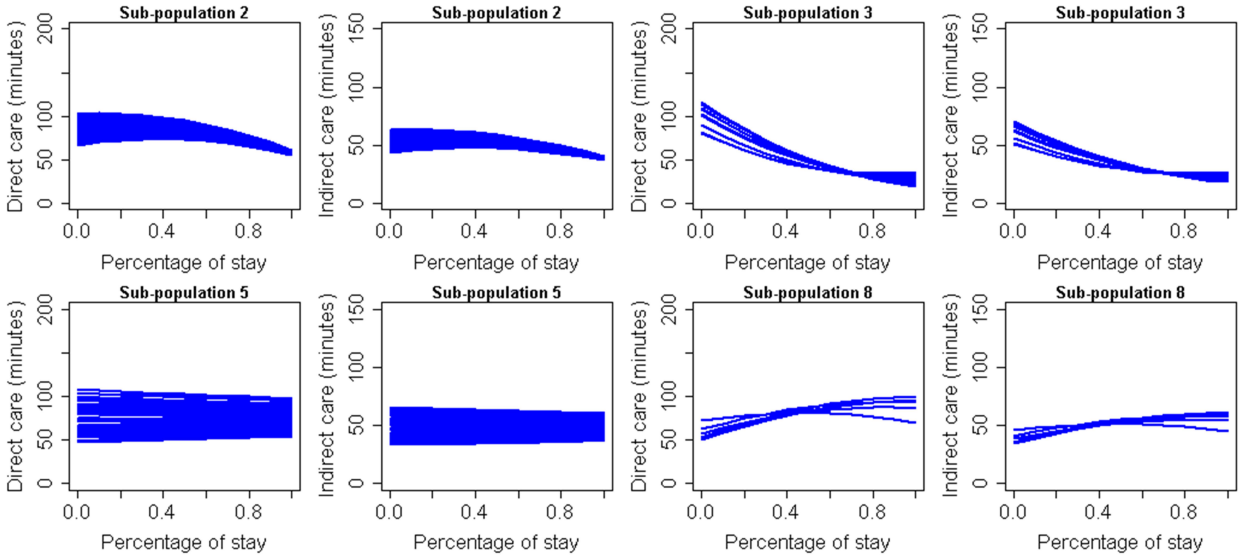

Figure 3.27: Predictions of individual service need trajectories

patterns of predicted service need trajectories among different sub-populations are significantly different. For instance, the decreasing pattern of service need trajectories in sub-population 3 indicates that the residents in sub-population 3 have reasonably good recovery of functional performance during NH stay and thus their daily service need trajectories exhibit decreasing pattern. The individual heterogeneity of temporally evolving service need can be further explained by the influences of individual characteristics. The influence of individual covariates is also sub-population-specific. In other words,

the individual characteristics will have different influences on the service need evolution of different individuals in different sub-populations. The details of model interpretation will be elaborated as follows.

3.6.6.2 Model Interpretation

Further, I investigate the significance of individual covariates and their effects on the evolving patterns of service need trajectories. As shown in Eq. (3.15), $\boldsymbol{\beta}_k$ captures the sub-

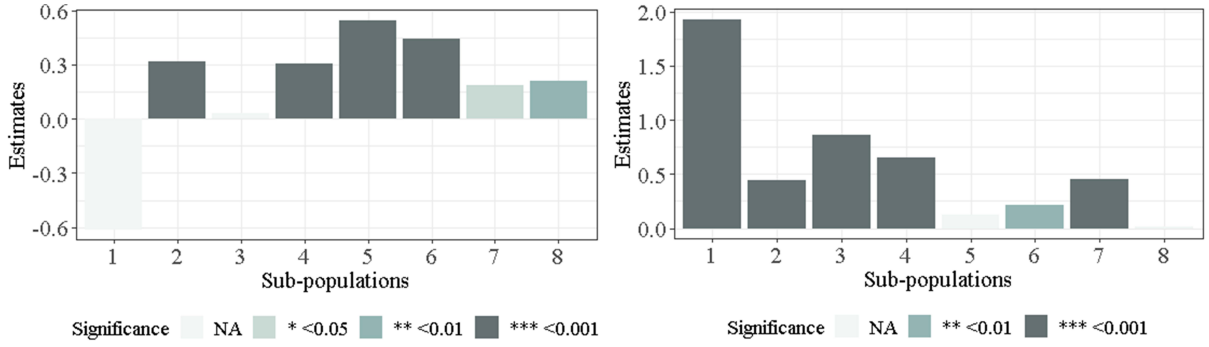

(a) ADL (b) Rehabilitation

Figure 3.28: Effects of individual characteristics on the baseline service need

population-specific effects of baseline individual characteristics on the underlying service need evolution. Specifically, β_{1k} and β_{2k}, $k = 1...K$, refer to the effects of individual ADL score and rehabilitation level on the baseline service need of a resident upon his/her NH admission, respectively. The estimation results of $\boldsymbol{\beta}_k$ are illustrated in Figure 3.28. The ADL scores and rehabilitation level have significant impacts on the underlying baseline service need in some sub-populations. The ADL score exhibits positive effect on baseline service need in most of the sub-populations, as shown in Figure 3.28a. This indicates that the underlying baseline service need of a resident increases when the resident is more physically dependent and needs more daily living assistance at the beginning of NH stay. Similarly, as shown in Figure 3.28b, the positive effect of therapy intensity implies that a resident tends to have more service need when the baseline care intensity of rehabilitation becomes larger. In addition, I also investigate the interaction effect of individual

covariates on the temporal patterns of underlying service need evolution. As illustrated

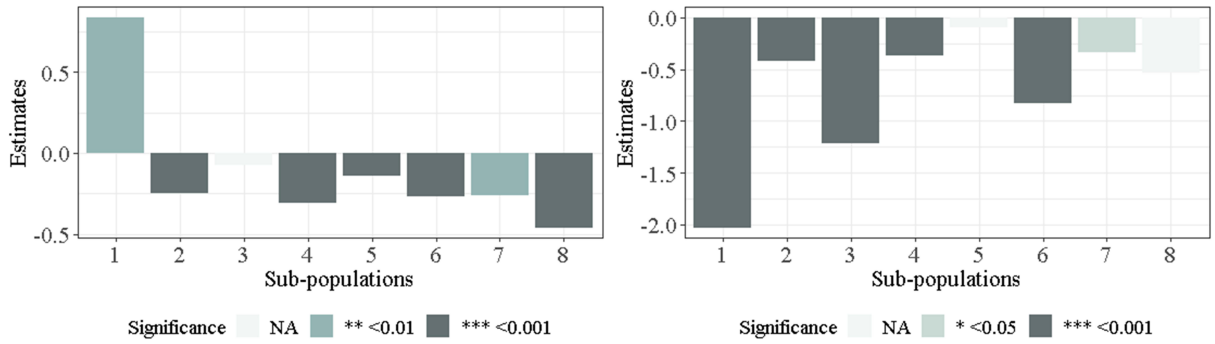

(a) ADL (b) Rehabilitation

Figure 3.29: Covariates effects on temporal evolution of service need

in Figure 3.29a, the ADL score in many sub-populations has significant negative effect on the underlying temporal evolution of resident daily service need. This implies that a resident with a higher baseline ADL score tends to experience an explicit decreasing pattern of his/her service need during NH stay due to explicit recovery. Similarly, as shown in Figure 3.29b, the rehabilitation level in some sub-populations has significant negative effect on the underlying daily service need evolution. This indicates that a resident with a higher rehabilitation level tends to experience a more explicitly decreasing pattern of his/her service need during NH stay due to the explicit recovery.

Moreover, I perform the post-analysis on the identified sub-populations, as described in Section 3.4.2, and investigate the effects of individual characteristics on determining membership. We consider individual characteristics such as individual demographics, primary diagnoses, cognitive functioning status, mental health condition, skin condition, pain condition, functional performance score and number of medications prescribed. Based on the statistical significance of individual covariates, we finally identify three contributing factors, including the ADL score, the indicator of having any skin problems and the level of required skin care. The residents compositions in different sub-populations are diverse. For example, over 30% of residents in sub-population 7 require no or less daily living assistance (e.g., ADL is smaller than 2) while none of the residents in sub-

population 7 are highly dependent (e.g., ADL from 11 to 16). On the other side, half of residents in sub-population 8 are highly dependent and need most daily living assistant while none of the residents are least dependent. Over 70% of residents in sub-population 4 have skin problems while the percentage of residents having skin conditions decreases to half in sub-population 8. In this work, we select sub-population 8 as reference sub-population to explore the effects of individual covariates on membership. As shown in

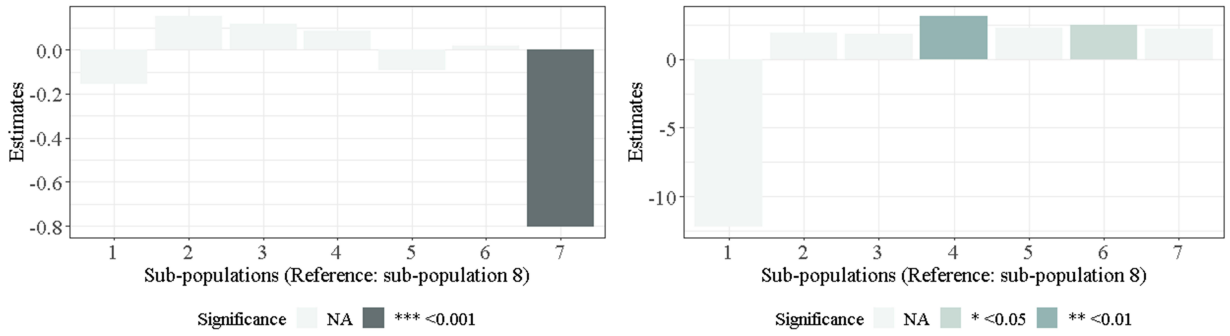

(a) ADL

(b) Skin conditions

Figure 3.30: Effects of individual characteristics on determining membership

Figure 3.30a, the effect of ADL score on sub-population 7 membership is significantly negative. This implies that when the ADL score of a resident becomes larger, the service need evolution pattern of the resident less likely belongs to sub-population 7 as compared to sub-population 8. On the other side, the indicator of having skin problems has significant positive effect on sub-population 4 membership, as shown in Figure 3.30b. This implies that the daily service need evolution of a resident tends to belong to sub-population 4 other than sub-population 8 if the resident has skin problems.

3.6.6.3 Staffing Decision Performance Comparison

Based on the above developed predictive model, we can capture the temporal evolution pattern of heterogeneous service need among NH residents. Further, we simulate service demand over time with the characterized temporally evolving and individually heterogeneous service need of NH residents. I employ the workforce planning algorithm

developed in Section 3.5.2 to achieve optimal ISS decisions. To evaluate the decision performance of proposed approach and to investigate the impact of temporal heterogeneity modeling on staffing decision performance, I compare the proposed work with other alternative strategies. M1 is ratio-based strategy which neglects baseline service need

Table 3.11: Modeling features of different staffing strategies in comparison

Strategy	Need-based	Sub-population level heterogeneity	Temporal dynamics	Individual heterogeneity
M1	✖	✖	✖	✖
M2	✔	✖	✖	✖
M3	✔	✔	✖	✖
M4	✔	✔	✔	✖
M5 (Proposed)	✔	✔	✔	✔

heterogeneity and temporal dynamics as well as temporal heterogeneity among different NH residents. On the other side, strategies M2-M5 account for baseline service need heterogeneity and use different models to characterize temporal complexity of service need. Strategy M2 assumes that service need of NH residents belongs to a single homogeneous population while strategy M3 allows the residents' service need belonging to different sub-populations. Both of M2 and M3 strategies further assume that the residents' service need is time invariant. On the contrary, strategies M4 and M5 account for temporal dynamics of service need. The proposed strategy M5 incorporates individual characteristics to capture the temporal evolving patterns of residents' service need while M4 only uses time basis to characterize temporal evolution pattern. The modeling features of different strategies are summarized in Table 3.11.

First, I evaluate the prediction performance of all strategies based on service need modeling. As compared to the alternative strategies M2-M4, the proposed strategy can achieve superior prediction performance. The average mean squared error over trajectories based on the proposed approach is the smallest, as illustrated in Figure 3.31. With the predicted service need trajectories of different strategies, I integrate computer simu-

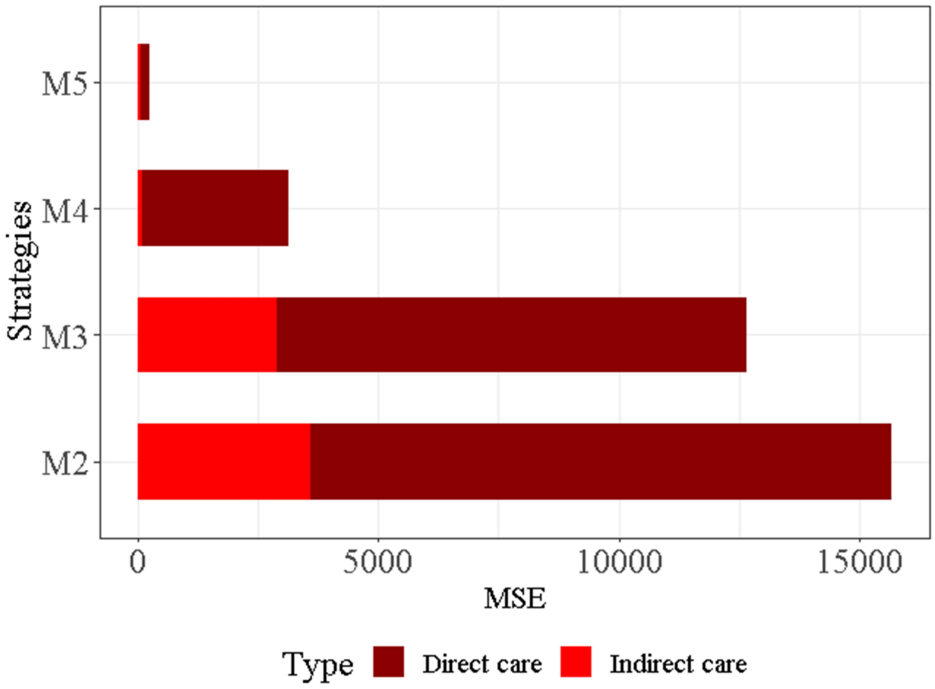

Figure 3.31: Comparison of prediction performance of different strategies

lation to simulate daily staff-time needed for each NH resident. We refer to the simulated service demand from real observations of trajectories as ground-truth. Further, I evalu-

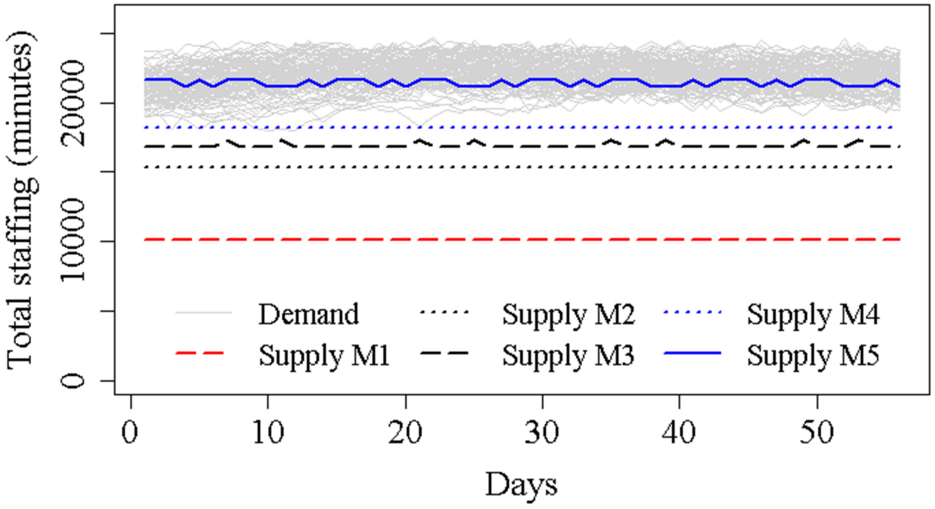

Figure 3.32: Staffing supply comparison of different strategies

ate and compare the decision performances of different strategies based on the simulated service demand of each strategy. The proposed strategy can meet the real demand and achieve the best performance at smallest total labor cost. All of the alternative strate-

gies lead to larger unmet demand, as shown in Figure 3.32. The strategy M1 with state

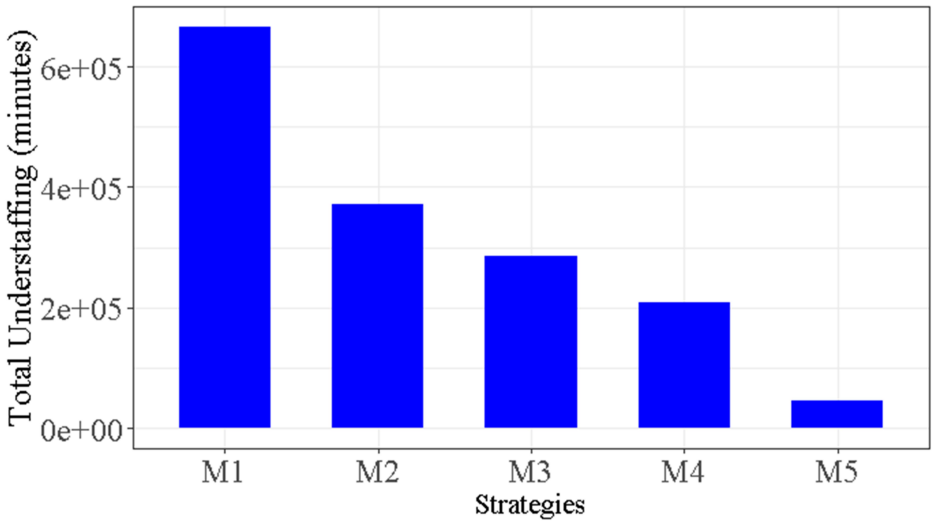

Figure 3.33: Understaffing amount comparison of different strategies

regulated ratio utilizes resident volume to determine staffing level and it results in significant unmet demand due to inadequate minimum SR ratio. The strategies M2-M4 involve prediction inaccuracy in service need trajectories and lead to service demand underestimation as well. The predictive modeling inaccuracy further propagates to decision making and induces inadequate staffing supply with significant unmet demand. As shown in Figure 3.33, the alternative strategies induce significantly larger understaffing amount as compared to the proposed strategy. The larger unmet demand induces significantly larger penalty cost among the alternative strategies and leads to the larger total labor cost, as shown in Figure 3.34. The proposed strategy is capable of predicting accurately the temporal evolution of service need of NH residents and suggesting adequate staffing decision at lowest total labor cost.

3.6.6.4 What-if Scenarios Analysis

In real practice, the resident census composition may vary over time within the same NH facility or differ across different NH facilities. To demonstrate that the proposed work can accommodate different resident census composition scenarios, I perform what-

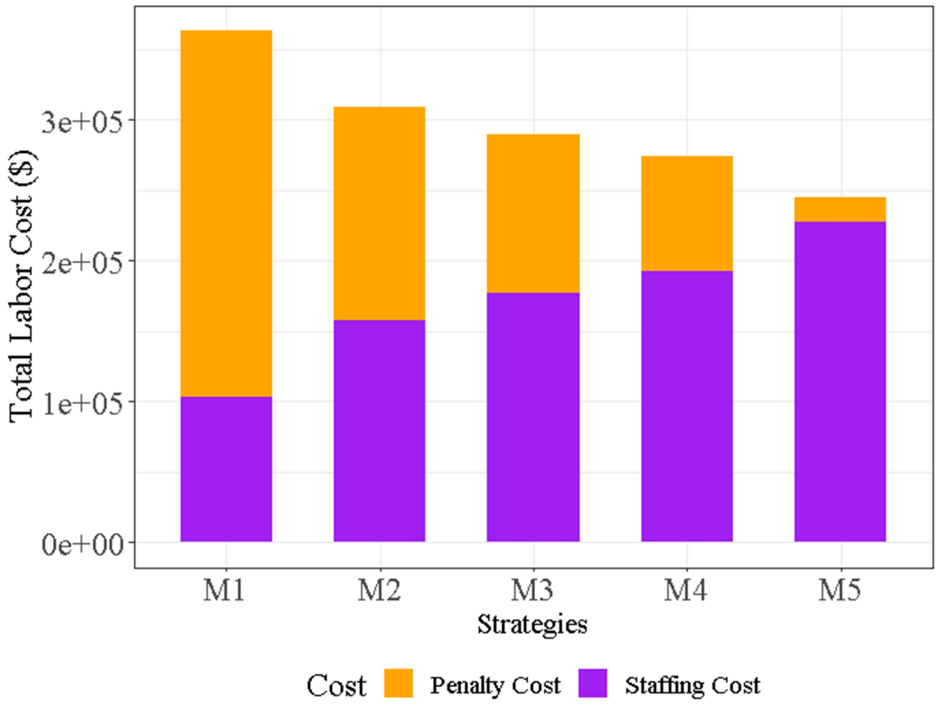

Figure 3.34: Total labor cost comparison of different strategies

if analysis in this section to investigate how staffing decision may vary among different census composition scenarios. I create different scenarios to illustrate the effectiveness of proposed work in capturing the temporal dynamics as well as temporal heterogeneity of service need and suggesting the corresponding optimal staffing decisions in an adaptive manner. The actual resident composition scenario is considered as baseline scenario (S1). I then generate another scenario S2 with a larger portion (e.g., 30%) of residents experiencing recovery pattern of functional performance and decreasing service need trajectories, as compared to a lower proportion (e.g., 3%) in S1. The simulated service demand at facility level becomes significantly lower in S2 than that in S1, as shown in Figure 3.35. Consequently, the staffing supply will be adjusted with a lower number of nursing staff to be recruited, leading to the lower total labor cost, as shown in Figure 3.36. Such results further indicate the importance of adaptively adjusting the staffing supply in response to varied resident census compositions. The one-size-fits-all staffing policies which are adopted in federal/state regulation and/or industrial practice cannot appropriately ad-

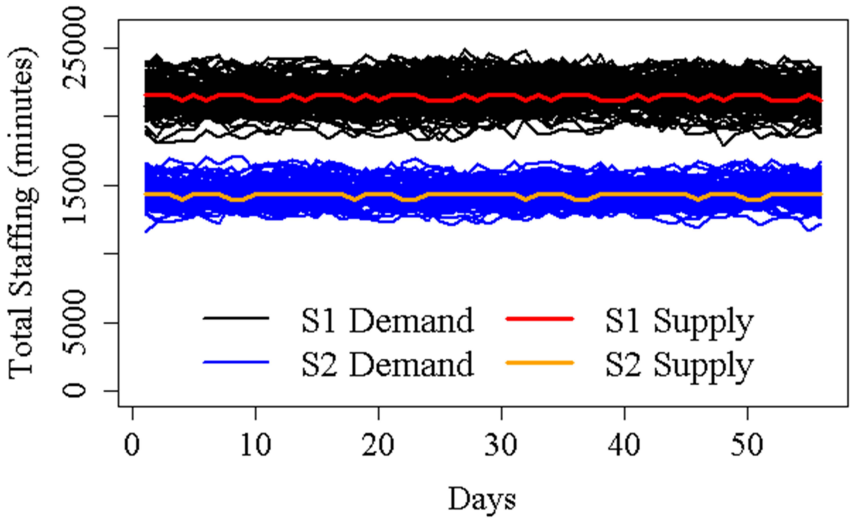

Figure 3.35: Daily staffing level comparison of different residents compositions

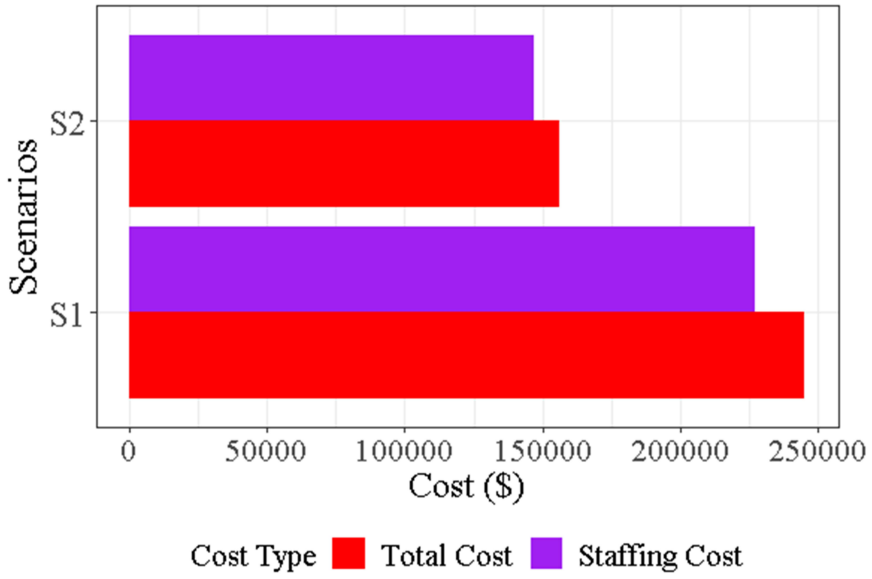

Figure 3.36: Total labor cost comparison of different residents compositions

just the staffing strategy. The conventional approaches fail to adapt in response to different census composition scenarios in same facility or among different facilities. On the other side, the proposed work will provide suggestions about staffing decision to NH administrators in an adaptive manner under different resident composition scenarios.

3.7 Concluding Remarks

In this chapter, I present a methodological innovation of characterizing the complexities of heterogeneous service demand of NH residents and improving the performance of resource planning decisions to meet such complex service demand. Specifically, I introduce an analytics-based decision support system to facilitate NH resource planning under heterogeneous and temporally evolving service demand of NH residents. The novel integration of advanced predictive analytics, computer simulation, and applied stochastic optimization as well as domain knowledge in real practice addresses a series of data and decision complexity in NH resource preparedness and care delivery. The proposed work is able to characterize both individual heterogeneity and temporal heterogeneity of service demand of NH residents with higher granularity. The proposed predictive analytics integrated simulation allows accurate prediction of service demand. The developed prescriptive analytics tools further provide optimal planning decisions with rich managerial insights. The derived operational policy for resource planning is implementable and actionable. The proposed framework is beneficial to multiple stakeholders in NH industry, such as facilitating adaptive managerial decision making of NH administrators, and improving health outcomes of NH residents.

In this work, we assume that the resident composition will not vary within each planning horizon and each NH resident belongs to one sub-population with the fixed membership during the planning horizon. However, the resident composition may vary within the planning horizon under extreme scenario, such as pandemic. Besides, each NH resident may also belong to multiple different sub-populations due to the change of dynamics. There is an opportunity of considering the mixed membership of NH residents in demand modeling and investigating the dynamics change within the planning horizon in the future work. Moreover, I will investigate caregiver assignment decision in future under the developed decision support system.

Chapter 4

Tribological Degradation Performance Modeling with Mixed-type Observed Heterogeneity and Latent Heterogeneity

4.1 Introduction

Accurate modeling of degradation performance data is of great importance for achieving accurate reliability assessment and failure prediction nowadays for highly reliable product units with few and zero failure observations[3]. Due to the varied product characteristics and the influences of many factors throughout the product design, manufacturing and operational phases, product units often exhibit highly heterogeneous degradation performance over time. To account for such degradation performance heterogeneity and to improve reliability assessment accuracy, many existing degradation models focused on modeling degradation performance data with covariates by incorporating various external influencing factors and quantifying their influences (Meeker and Escobar, 2014; Gorjian et al., 2010). At design phase, by investigating external factors, such as design settings or accelerated conditions (e.g., accelerated voltage, load, temperature), reliability engineers are able to either identify the most appropriate design changes for reliability improvement or achieve cost-effective reliability evaluation via analysis of accelerated degradation testing data. At operational phase, by investigating external factors, such as field operating conditions (e.g., usage rate, field temperature), reliability engineers are able to implement more accurate failure prognosis and initialize cost-effective condition-based maintenance actions. However, there is limited research to further extract and in-

[3]This chapter was arxiv preprint (Sun et al., 2021a). Copyright permission from the publisher is included in Appendix A.

corporate reliability relevant material characteristics of product units as internal factors and integrate them with external factors (e.g., accelerated/environmental conditions) for improving prediction accuracy of degradation performance outputs.

With the advancement of sensing technologies and material property characterization techniques, such as scanning electron microscope and transmission electron microscope (Goodhew and Humphreys, 2000), rich material characteristics of product units, such as microstructure information, become readily available or can be easily accessible. To extract rich characteristics information from material microstructure images, engineers often utilize informative material descriptors, such as two-point correlation function, radial distribution function and lineal-path function (Torquato, 2002). Many of these material descriptors are represented in the functional form rather than the scalar form. For instance, the two-point correlation is a functional feature curve over spatial distance to describe the spatial heterogeneity of material microstructure at microscopic scale, which often reflects the reliability-related product properties at macroscopic level (e.g., strength, hardness). Incorporating such functional covariates as internal reliability influencing factors and integrating them together with other external factors have a great opportunity for improving degradation performance modeling accuracy as compared to the existing models which only consider external factors. It will also help to improve the understanding of how material characteristics will influence the degradation performance of the product and further identify feasible material processing strategies to modify material settings for degradation-induced failure mitigation and reliability improvement. After considering the influences of both internal and external observed factors, it is still possible that the degradation performance within each product unit may be highly correlated due to the latent heterogeneity. Such latent heterogeneity is essentially caused by the influences of many unobserved/unknown factors shared within each unit. There is a need to develop a generic modeling framework which can simultaneously incorporate the mixed-type covariates (e.g., both functional covariates of internal material informa-

tion and scalar covariates of external accelerated/environmental conditions) and latent heterogeneity to improve the prediction accuracy of degradation performance modeling.

In the existing literature of reliability data modeling, different statistical/stochastic models have been developed to analyze different types of reliability data with covariates, such as failure counts data with covariates (Debón and Garcia-Díaz, 2012; Lyu and Chen, 2008) and time-to-failure data with covariates (Zhang and Xie, 2011; Peng et al., 2013; Li et al., 2017a). They mainly considered the scalar covariates that represent the external influencing factors, such as voltage, load, temperature and humidity, while they failed to incorporate internal factors, such as material characteristics information. In addition to the above reliability data types, degradation data is another important type of reliability data. For degradation data modeling in general, different data-driven models have been developed, such as continuous stochastic process (Ye and Xie, 2015; Ye and Chen, 2014; Gebraeel, 2006; Shafiee et al., 2015), Markov-based models (Kharoufeh et al., 2010; Shu et al., 2010), and general path models (Yuan et al., 2016; Lu and Meeker, 1993). Many of these modeling approaches mainly focused on characterizing the heterogeneity of degradation performance outputs as a whole without explicitly incorporating covariates as additional inputs to explain part of the heterogeneity. To characterize degradation performance heterogeneity with covariates, existing degradation models often considered scalar covariates that represent external factors, such as environmental conditions (Zhao et al., 2018; Fang et al., 2020; Ye et al., 2015). There is limited recent studies which account for the influences of material characteristics on degradation performance output. Park et. al. (Park et al., 2017) incorporated a scalar covariate into degradation performance modeling which represented the aggregate-level material information. Si et. al. (Si et al., 2019) considered functional covariate in their degradation model and incorporated detailed material microstructure information. However, these approaches failed to jointly consider both the mixed-type (i.e., functional and scalar) covariates and their potential in-

teraction. The latent heterogeneity caused by the influences of unobserved factors shared within each product unit was not addressed in these models as well.

To address the above research gaps, we propose a generic statistical degradation performance modeling framework to account for both the observed mixed-type covariates and the latent heterogeneity. The mixed-type covariates consist of (i) the functional covariates which capture the internal material microstructure characteristics of product units, and (ii) the scalar covariates which capture the external environmental conditions elevated in the context of accelerated degradation test. Moreover, a model estimation algorithm is developed to jointly quantify the influences of mixed-type covariates and the latent heterogeneity, and further to examine the potential interaction between functional and scalar covariates. Functional data analysis and data augmentation techniques are employed to address a series of estimation challenges, such as the infinite dimensionality of functional covariates and joint estimation of observed factors' effects and latent variable. To demonstrate the effectiveness of the proposed approach, we present a real case study using accelerated tribological degradation data of Cu-alloy test units and demonstrate the superior performance of proposed model over several alternative degradation performance modeling approaches.

The rest of this paper is organized as follows. Section 4.2 describes the formulation of proposed degradation modeling framework and introduces the concepts of functional material descriptor, followed by a detailed elaboration of the developed algorithm of model estimation. Section 4.3 presents a real case study to illustrate the proposed work and further demonstrate its superior performance (e.g., accurate prediction performance, appealing model interpretation) over several alternative models. Section 4.4 draws the conclusive remark of this paper.

4.2 Methodological Framework

4.2.1 Framework Overview

To capture the influences of both environmental conditions and material characteristics as well as the latent effects of unobserved factors, we propose a generic degradation performance modeling framework with mixed-type covariates and latent heterogeneity, as shown in Figure 4.37. For each material unit, the degradation performance outputs

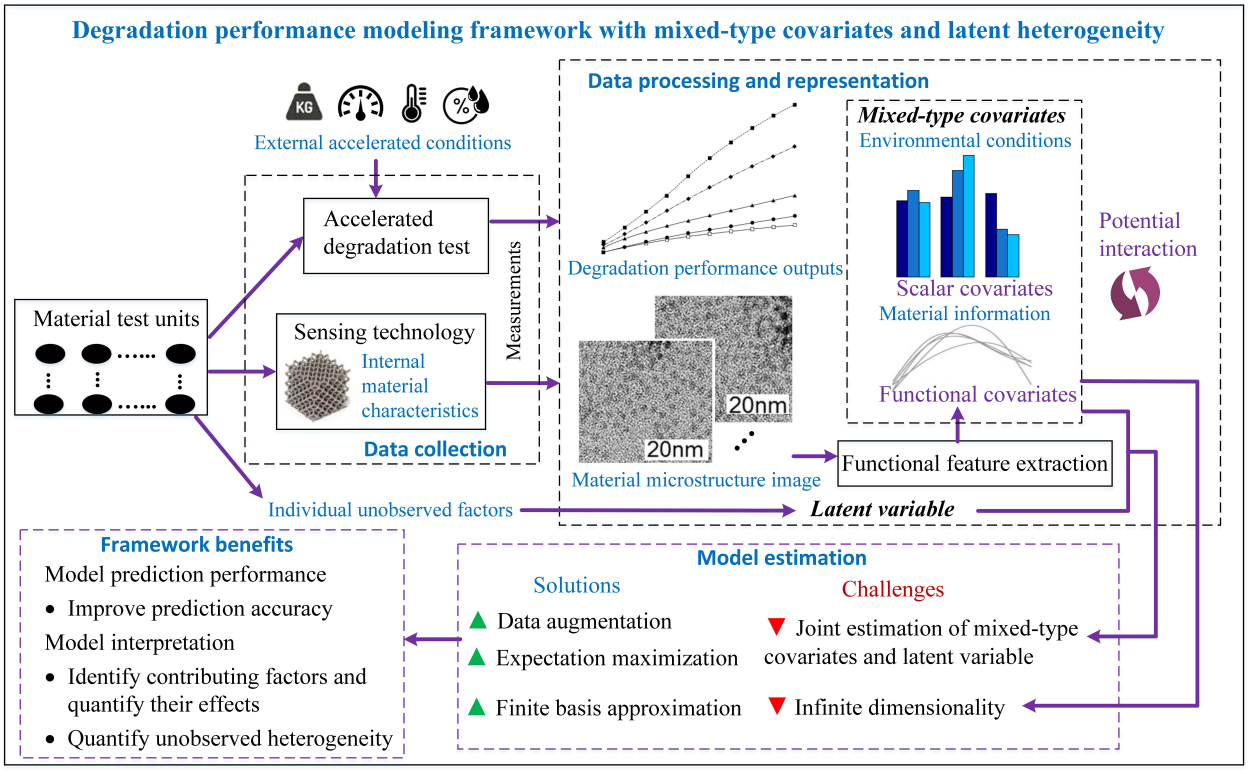

Figure 4.37: Overview of proposed modeling framework

are collected in the accelerated degradation test and are used as responses to develop the degradation performance model. Besides, the material microstructure information of each test unit is collected via advanced sensing technology. With the obtained microstructure images, we employ statistical measures to extract the functional features of material characteristics. We then use scalar covariates to represent external environmental conditions (e.g., temperature, loads and humidity) and utilize functional covariate to represent

internal material characteristics. The proposed framework incorporates both mixed-type (e.g., scalar and functional) covariates and accounts for their potential interaction as well as latent heterogeneity. Further, we employ finite basis approximation technique to address the infinity dimensionality issue of functional covariates and apply data augmentation technique with expectation maximization estimation method to jointly estimate both mixed-type covariates and latent variable. The proposed modeling framework can improve prediction accuracy via considering both influences of mixed-type covariates and latent heterogeneity. In addition, the proposed framework is able to identify important influencing factors and quantify their effects on product reliability performance (e.g., accelerating/decelerating degradation process). With the quantified effects of observed influencing factors, the proposed framework can facilitate optimal test design and further improve product reliability. Besides, the proposed framework can also quantify the latent heterogeneity of individual test unit and help with future data collection. The details will be elaborated in the following subsections.

4.2.2 Model Formulation

Considering a population of N test units, the observed degradation performance of test unit i at time t_{ij} is denoted as $y_{ij}, \forall i = 1, ..., N,\ j = 1, ..., m_i$ where m_i is total number of degradation performance measurements of test unit i. The degradation performance of each test unit may be influenced by both external factors, such as accelerated environmental conditions, and internal factors, such as the material characteristics. The former can often be characterized by scalar covariates to reflect a specific stress level of the accelerated environmental condition, while the latter can often be characterized by functional material descriptor due to their rich representation of material microstructure characteristics. In addition to the above influences of observed factors, it is still possible that each test unit may be influenced by a set of unobserved/unknown factors shared within each test unit, which causes the correlation among repeated degradation performance mea-

surements of single test unit over time. To simultaneously quantify both the influences of the observed mixed-type (i.e., scalar and functional) covariates, their potential interaction effect and the influence of unobserved/unknown factors shared within each test unit, the proposed bi-level degradation performance model is generically formulated as

$$y_{ij} = g_i(t_{ij}, \boldsymbol{\theta}_i, \boldsymbol{\Psi}) + \epsilon_{ij} \approx \sum_{l=0}^{L} \eta_{li}\phi_l(t_{ij}) + \epsilon_{ij}, \quad i = 1, ..., N, j = 1, ..., m_i \tag{4.25a}$$

$$\begin{aligned}\eta_{li} &= \nu_l + \boldsymbol{\beta}_l^{\mathrm{T}}\boldsymbol{x}_i + \sum_{s=1}^{S}\int_{\mathbb{R}_s} \alpha_{ls}(r)Z_{is}(r)\mathrm{d}r \\ &+ \sum_{p=1}^{P} x_{ip}\left(\sum_{s=1}^{S}\int_{\mathbb{R}_s}\rho_{lps}(r)Z_{is}(r)\mathrm{d}r\right) + \gamma_{li}, \quad i = 1, ..., N, l = 0, ..., L\end{aligned} \tag{4.25b}$$

At response level, the degradation performance outputs over time of test unit i can be captured by a unit-specific nonlinear function $g_i(\cdot)$ and an error term $\epsilon_{ij} \sim N(0, \sigma_\epsilon^2)$ where σ_ϵ^2 is the variance of measurement error. In the unit-specific nonlinear function mapping, $\boldsymbol{\Psi}$ is a vector of fixed effect parameters and $\boldsymbol{\theta}_i$ is a vector of random effect parameters of test unit i. To improve the model interpretation and estimation tractability, the nonlinear function $g_i(\cdot)$ can be further approximated by a set of basis functions, $\{\phi_l(\cdot), \forall l = 0, ..., L\}$ and unit-specific basis coefficients $\{\eta_{li}, \forall l = 0, ..., L\}$. $\phi_0(\cdot) = 1$ and η_{0i} is the grand mean function. Different basis functions, such as polynomial basis and spline basis, can be considered to capture the nonlinear curvature of degradation performance over time while unit-specific basis coefficients capture the individual heterogeneity of degradation performance. To further capture such individual heterogeneity, we decompose each coefficient η_{li} into five components at coefficient level, namely, (i) population-level component ν_l, which captures the population average degradation pattern at l^{th} coefficient level among all test units; (ii) the individual heterogeneity at l^{th} coefficient level explained by the marginal effect of observed scalar covariates $\boldsymbol{x}_i = [x_{i1}, ..., x_{iP}]^{\mathrm{T}}$ and covariates coefficients $\boldsymbol{\beta}_l = [\beta_{l1}, \beta_{l2}, ..., \beta_{lP}]^{\mathrm{T}}$; (iii) the individual heterogeneity at l^{th} coefficient level explained by the marginal effect of observed centered functional covariates $Z_{is}(r)$ with

support space $\mathbb{R}_s$ and covariates coefficient functions $\alpha_{ls}(r), \forall s = 1, ..., S$; (iv) the individual heterogeneity at l^{th} coefficient level explained by the interaction effect between observed scalar and centered functional covariates with covariates coefficient functions $\rho_{lps}(r), \forall p = 1, ..., P, s = 1, ..., S$, and (v) the unobserved heterogeneity at l^{th} coefficient level due to the influence of unobserved/unknown factors shared within each unit i, captured by the continuous latent variable γ_{li}, i.e., $\gamma_{li} \sim N(0, \sigma^2_{\gamma l})$ where $\sigma^2_{\gamma l}$ refers to the variance of latent variable.

The proposed model formulation is generic and several of the existing degradation performance models can be treated as the special cases of the proposed model. For instance, by neglecting the mixed-type covariates and their potential interaction, i.e., $\beta_{li} = 0, \alpha_{ls}(\cdot) = 0, \rho_{lps}(\cdot) = 0, \forall i = 1, ..., N, l = 0, ..., N, p = 1, ..., P, s = 1, ..., S$, the proposed model is reduced into the degradation path model in (Lu and Meeker, 1993). For another example, by neglecting the functional covariates and the interaction term as well as latent heterogeneity, i.e., $\alpha_{ls}(\cdot) = 0, \rho_{lps}(\cdot) = 0, \gamma_{li} = 0, \forall i = 1, ..., N, l = 0, ..., N, p = 1, ..., P, s = 1, ..., S$, the proposed model becomes the typical accelerated degradation model with constant stress factor. Moreover, by neglecting scalar covariates, potential interaction and latent heterogeneity, i.e., $\beta_{li} = 0, \rho_{lps}(\cdot) = 0, \gamma_{li} = 0, \forall i = 1, ..., N, l = 0, ..., N, p = 1, ..., P, s = 1, ..., S$, the proposed model becomes the degradation model with functional covariates introduced in (Si et al., 2019). Figure 4.38 further illustrates the hierarchical structure of the proposed bi-level degradation model. As shown in Figure 4.38, the rectangle nodes refer to the observed data, including the response data and the observed environmental/accelerated conditions as well as the measured material microstructure characteristics. Circle nodes represent either the unknown model parameters to be estimated or random variables. Triangle nodes represent deterministic functions. The solid and dashed lines indicate the deterministic and stochastic relationship between the connected nodes, respectively.

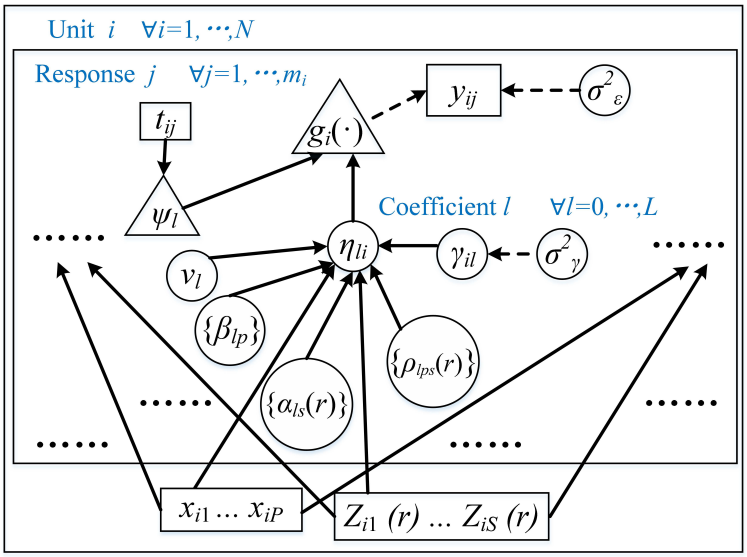

Figure 4.38: Visualization of proposed bi-level degradation model

4.2.3 Material Statistical Descriptor

Among mixed-type covariates in the above formulation, the centered functional covariates $Z_{is}(r), \forall i = 1, ..., N, s = 1, ..., S$ represent critical characteristics of material microstructure, such as spatial heterogeneity, which is known to have indispensable impacts on degradation performance (Singh et al., 2007). To evaluate the spatial heterogeneity of material microstructure at microscopic level, advanced sensing devices/technologies, such as transmission electron microscopy (TEM), are often available for the finer scale characterization of material microstructure. Figure 4.39a gives an example of a TEM image of a tested unit in the accelerated wear test considered in the paper. The gray part and black part represent two different phases of material unit, which have different compositions. As reflected in TEM images with two different colors, such material unit is two-phase and often exhibits spatial heterogeneity and non-uniformity. As compared to the two-phase unit, there is few color contrast or even single color in TEM image of test unit of single phase. The unit of single phase often exhibits homogeneous spatial patterns and uniformity. Figure 4.39a also illustrates a zoom-in view of spatial patterns of the red dot. To further extract and quantify spatial heterogeneity (or uniformity) patterns of TEM

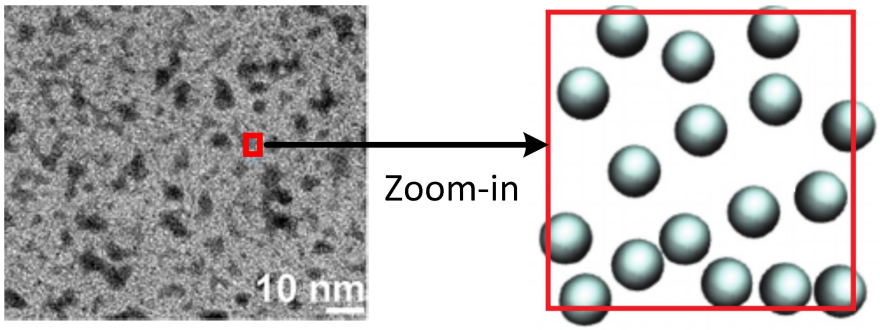

(a) Raw TEM image and zoom-in view

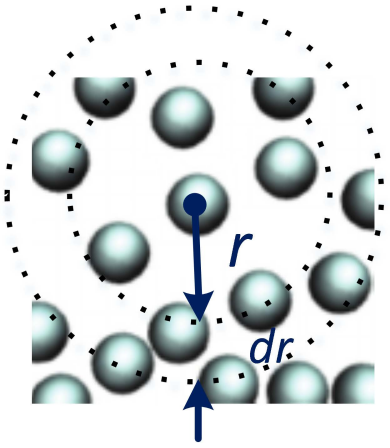

(b) Radial distribution function

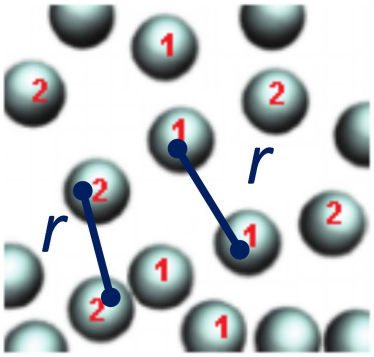

(c) Two-point correlation function

Figure 4.39: TEM image and diagrams of its functional descriptor

images at reduced complexity, the functional microstructure descriptors (Torquato, 2002), such as radial distribution function (RDF) and two-point correlation (TPC) function, are popular choices of correlation-based statistical measures. Unlike scalar covariates which summarize the spatial heterogeneity information at an aggregate level, the functional covariates (e.g., RDF, TPC) can capture the spatial heterogeneity patterns of of material microstructure more comprehensively. The details are elaborated as follows.

Radial distribution function (RDF) is an useful statistical measure to describe how particle density varies as a function of distance from a reference particle (Goel et al., 2012). Considering a material test unit of M particles in a volume V, RDF can be calculated as $g(\boldsymbol{r}) = \frac{1}{\kappa} \left\langle \sum_{m \neq 0} \delta(\boldsymbol{r} - \boldsymbol{r}_m) \right\rangle$ where $\kappa = \frac{M}{V}$ is the average number density of particles and $\langle \cdot \rangle$ is the ensemble averaging operator. $\boldsymbol{r}_m, \forall m = 1, ..., M$ refers to particle coordinates and $\delta(\cdot)$ is the Dirac delta function. Particularly, for a test unit with equivalent particles

$1, ..., M-1$, RDF calculation can be further simplified as $g(\boldsymbol{r}) = V\frac{M-1}{M}\langle\delta(\boldsymbol{r}-\boldsymbol{r}_1)\rangle$. As shown in Figure 4.39b, RDF is a distance dependent measure and determines how many particles are within a distance of r and $r+\mathrm{d}r$ away from the reference particle. If more particles in a material unit are uniformly distributed, the number of particles within a specified distance from the reference particle over the support range will be similar. This can further be reflected by the RDF values where less sharp changes are involved in the RDF curve. On the other side, if the particles concentrate on certain area of a test unit, the RDF values of different radius over the support range will become significantly different.

In addition to the RDF measure, we also introduce another measure called two-point correlation function (TPC) (Jiao et al., 2007) to describe microstructure characteristics of material test units. TPC is a statistical measure typically for material test units of two-phase. Considering a two-phase test unit with different material compositions in different phases, we define an indicator function $I^{(h)}(x), h = 1,2$ as $I^{(h)}(x) = \begin{cases} 1, & x \in V_h \\ 0, & x \in \bar{V}_h \end{cases}$ where V_h and $\bar{V}_h$ refer to the region occupied by phase h and the other phase, respectively. TPC then represents the probability of two randomly chosen points q_1 and q_2 are both in phase h, i.e., $S_2^{(h)}(q_1, q_2) = \left\langle I^{(h)}(q_1) I^{(h)}(q_2) \right\rangle$ where $\langle\cdot\rangle$ is the ensemble averaging operator over the support range of a test unit. Particularly, when a material test unit is statistically homogeneous, TPC can be calculated as $S_2^{(h)}(q_1, q_2) = \left\langle I^{(h)}(q_1) I^{(h)}(q_1 + r) \right\rangle$ where r is specified spatial distance, as depicted in Figure 4.39c. When the particles of same phase are uniformly distributed over a test unit, TPC values of different distances over the support range tend to be similar.

The aforementioned correlation method based material descriptors, such as RDF and TPC, are distance dependent functions and can be used to describe the spatial heterogeneity patterns of material microstructure effectively. The curve shape of these descriptors can be used to differentiate the non-uniformity structure such as clustering pattern from the uniform material structure. With advanced sensing technologies, these functional

descriptors become available and can help to investigate the influences of material characteristics on the degradation process.

4.2.4 Model Estimation

Considering a population of N deteriorating units are tested and m_i degradation performance measurements are collected on each unit $i, i = 1, ..., N$, the available data can be expressed as $\boldsymbol{D} = \{y_{ij}, t_{ij}, \boldsymbol{x}_i, Z_{is}(r), \forall i = 1, ..., N, j = 1, ..., m_i, s = 1, ..., S\}$. Let $\boldsymbol{\gamma}_i$ be a vector of latent variables of length $L+1$ with $\boldsymbol{\gamma}_i \sim N(0, \boldsymbol{\Sigma}_\gamma)$ where $\boldsymbol{\Sigma}_\gamma = \left[\sigma^2_{\gamma 0}, \sigma^2_{\gamma 1}, ..., \sigma^2_{\gamma L}\right] \mathbf{I}$. We further let $\boldsymbol{\Theta} = \{\nu_l, \boldsymbol{\beta}_l, \alpha_{ls}(\cdot), \rho_{lps}(\cdot), \sigma^2_\epsilon, \forall l = 0, ..., L, p = 1, ..., P, s = 1, ..., S\}$ be a set of unknown model parameters. Suppose the support space of extracted functional covariates from previous section is defined as $\mathbb{R}_s = [0, R]$, the original marginal likelihood function then becomes

$$
\begin{aligned}
L\left(\boldsymbol{\Theta}, \{\boldsymbol{\gamma}_i\}_{i=1}^N \mid \boldsymbol{D}\right) &= \prod_{i=1}^N \int \prod_{j=1}^{m_i} p\left(y_{ij} \mid \boldsymbol{\Theta}, \boldsymbol{\gamma}_i\right) p(\boldsymbol{\gamma}_i) \mathrm{d}\boldsymbol{\gamma}_i \\
&\propto \prod_{i=1}^N \int \cdots \int \left|\sigma^2_\epsilon \mathbf{I}_{m_i}\right|^{-\frac{1}{2}} \exp\{-\frac{1}{2\sigma^2_\epsilon} \sum_{j=1}^{m_i} (y_{ij} - \sum_{l=0}^{L} [\nu_l + \boldsymbol{\beta}_l^{\mathrm{T}} \boldsymbol{x}_i + \sum_{s=1}^{S} \int_0^R \alpha_{ls}(r) Z_{is}(r) \mathrm{d}r \\
&+ \sum_{p=1}^{P} x_{ip} \left(\sum_{s=1}^{S} \int_0^R \rho_{lps}(r) Z_{is}(r) \mathrm{d}r \right) + \gamma_{li}] \phi_l(t_{ij}))^2\} \, \mathrm{d}\gamma_{0i} \ldots \mathrm{d}\gamma_{Li}
\end{aligned} \tag{4.26}
$$

where $|\cdot|$ refers to the matrix determinant operator and $\mathbf{I}_{m_i}$ is $m_i \times m_i$ identity matrix. As shown in the above likelihood function, the intrinsic infinite dimensionality of functional data (Ramsay and Silverman, 2007) makes the parameters estimation mathematically intractable. In addition, as shown in Eq. (4.26), the latent variables will be integrated out via the marginal approach and cannot be estimated. To jointly estimate both the model parameters and the latent variables, we need to address these two key challenges. The solution details are elaborated as follows.

The functional data can be treated as a realization of stochastic process and intrinsically involves infinite dimensionality issue. To address such issue, we employ approxi-

mation method to reduce the dimensionality of functional data and facilitate parameter estimation. Based on Mercer's theorem, the covariance matrix of functional data can be expressed by orthogonal eigenfunctions and ordered nonnegative eigenvalues (Ramsay and Silverman, 2007). With these eigenfunctions, we can apply Karhunen-Loève expansion (Hsing and Eubank, 2015) on the centered functional covariates as well as the coefficient functions, and express them as linear combinations of the complete orthogonal basis functions, i.e., $Z_{is}(r) = \sum_{k=1}^{\infty} c_{isk}\psi_k(r)$, $\alpha_{ls}(r) = \sum_{k=1}^{\infty} b_{lsk}\psi_k(r)$ and $\rho_{lps}(r) = \sum_{k=1}^{\infty} b'_{lpsk}\psi_k(r), \forall i = 1,...,N, l = 0,...,L, p = 1,...,P, s = 1,...,S$ where c_{isk}, b_{lsk} and b'_{lpsk} are known as functional principle component scores of functional data (Ramsay and Silverman, 2007). Since the eigenvalues of covariance operator of functional data decrease and finally approximate to 0, it is often sufficient to use a small number of eigenfunctions whose eigenvalues are significantly nonzero to accurately approximate the functional data. The number of finite basis functions can be determined efficiently by the fraction of variance explained (FVE) in practice (Chen and Lei, 2015). With the truncated K basis functions, the centered functional covariates and the coefficient functions can then be approximated by $Z_{is}(r) \approx \sum_{k=1}^{K} c_{isk}\psi_k(r)$, $\alpha_{ls}(r) \approx \sum_{k=1}^{K} b_{lsk}\psi_k(r)$ and $\rho_{lps}(r) \approx \sum_{k=1}^{K} b'_{lpsk}\psi_k(r)$. The model parameters becomes $\boldsymbol{\Theta} = \{\nu_l, \boldsymbol{\beta}_l, b_{lsk}, b'_{lpsk}, \sigma^2_\epsilon, \forall l = 0,...,L, p = 1,...,P, s = 1,...,S, k = 1,...,K\}$. The joint likelihood can be rewritten as

$$L\left(\boldsymbol{\Theta}, \{\gamma_i\}_{i=1}^N \mid \boldsymbol{D}\right) \propto \prod_{i=1}^{N} \int \cdots \int \left|\sigma^2_\epsilon \mathbf{I}_{m_i}\right|^{-\frac{1}{2}} \exp\{-\frac{1}{2\sigma^2_\epsilon} \sum_{j=1}^{m_i} (y_{ij} - \sum_{l=0}^{L} [\nu_l + \boldsymbol{\beta}_l^{\mathrm{T}} \boldsymbol{x}_i + R(\sum_{s=1}^{S}\sum_{k=1}^{K} b_{lsk}c_{isk}) + R(\sum_{p=1}^{P} x_{ip}(\sum_{s=1}^{S}\sum_{k=1}^{K} b'_{lpsk}c_{isk})) + \gamma_{li}]\phi_l(t_{ij}))^2\} \, d\gamma_{0i} \ldots d\gamma_{Li} \tag{4.27}$$

In the above likelihood function, the infinite dimensionality issue of functional data is resolved and it is tractable to estimate $\boldsymbol{\Theta}$. We denote $\boldsymbol{\Lambda}_i$ as $m_i \times (L+1)$ design matrix of latent heterogeneity where $\boldsymbol{\Lambda}_i = \begin{pmatrix} \phi_0(t_{i1}) & \phi_1(t_{i1}) & ... & \phi_L(t_{i1}) \\ ... & ... & ... & \\ \phi_0(t_{im_i}) & \phi_1(t_{im_i}) & ... & \phi_L(t_{im_i}) \end{pmatrix}$. We then denote

$\boldsymbol{\Omega}_i$ as $m_i \times U$ design matrix of observed heterogeneity and denote $\boldsymbol{\zeta}$ as the corresponding coefficient vector of length U where $U = (L+1)(1+P+SK+PSK)$. $\boldsymbol{\Omega}_i$ can be manifested as $\boldsymbol{\Omega}_i = \begin{pmatrix} \boldsymbol{\Lambda}_i & \boldsymbol{A}_{2i} & \boldsymbol{A}_{3i} & \boldsymbol{A}_{4i} \end{pmatrix}$ where matrix details of $\boldsymbol{A}_{2i}$, $\boldsymbol{A}_{3i}$ and $\boldsymbol{A}_{4i}$ are presented in Appendix Section B.1.1. The coefficient vector of observed heterogeneity is written as $\boldsymbol{\zeta} = \left[\boldsymbol{\nu}^{\mathrm{T}}, \boldsymbol{\beta}_0^{\mathrm{T}}, ..., \boldsymbol{\beta}_L^{\mathrm{T}}, \boldsymbol{b}_{01}^{\mathrm{T}}, ..., \boldsymbol{b}_{LS}^{\mathrm{T}}, \boldsymbol{b}_{011}^{'\mathrm{T}}, ..., \boldsymbol{b}_{LPS}^{'\mathrm{T}}\right]^{\mathrm{T}}$ where vector details are described in Appendix Section B.1.1. The vector form of the proposed model can then be expressed as $\boldsymbol{y}_i = \boldsymbol{\Omega}_i\boldsymbol{\zeta} + \boldsymbol{\Lambda}_i\boldsymbol{\gamma}_i + \boldsymbol{\epsilon}_i,\ i = 1, ..., N$. The compact likelihood function is given by

$$
\begin{aligned}
&L(\boldsymbol{\Theta}, \{\boldsymbol{\gamma}_i\}_{i=1}^N \mid \boldsymbol{D}) \propto \\
&\prod_{i=1}^{N} \int \cdots \int \left|\sigma_\epsilon^2 \mathbf{I}_{m_i}\right|^{-\frac{1}{2}} \exp(-\frac{1}{2\sigma_\epsilon^2} \|\boldsymbol{y}_i - \boldsymbol{\Omega}_i\boldsymbol{\zeta} - \boldsymbol{\Lambda}_i\boldsymbol{\gamma}_i\|^2)\, d\gamma_{0i} \ldots d\gamma_{Li}
\end{aligned} \tag{4.28}
$$

In the above marginal approach, the latent variables $\boldsymbol{\gamma}_i, \forall i = 1, ..., N$ will be integrated out and cannot be estimated. To address the estimation issue of latent factors, We employ data augmentation technique (Wei and Tanner, 1990) and introduce the complete data, i.e., $\boldsymbol{D}^* = \{\boldsymbol{D}, \{\boldsymbol{\gamma}_i\}_{i=1}^N\}$. The model parameters can be specified as $\boldsymbol{\Theta} = \{\boldsymbol{\zeta}, \sigma_\epsilon^2, \boldsymbol{\Sigma}_\gamma\}$. Based on the augmented data $\boldsymbol{D}^*$, the joint likelihood can be derived as

$$
\begin{aligned}
L(\boldsymbol{\Theta} \mid \boldsymbol{D}^*) &= \prod_{i=1}^{N} p\left(\boldsymbol{y}_i \mid \boldsymbol{\Theta}, \boldsymbol{\gamma}_i\right) p(\boldsymbol{\gamma}_i \mid \boldsymbol{\Theta}) \\
&\propto \prod_{i=1}^{N} \left(\left|\sigma_\epsilon^2 \mathbf{I}_{m_i}\right|^{-\frac{1}{2}} \left|\boldsymbol{\Sigma}_\gamma\right|^{-\frac{1}{2}} \exp(-\frac{1}{2}{\boldsymbol{\gamma}_i}^{\mathrm{T}} \boldsymbol{\Sigma}_\gamma^{-1} \boldsymbol{\gamma}_i) \right) \cdot \exp\left(-\frac{1}{2\sigma_\epsilon^2} \left\|\boldsymbol{y} - \boldsymbol{\Omega}\boldsymbol{\zeta} - \boldsymbol{\Lambda}\boldsymbol{\gamma}\right\|^2 \right)
\end{aligned} \tag{4.29}
$$

where $\|\cdot\|$ is Euclidean norm operator. $\boldsymbol{y} = [\boldsymbol{y}_1^{\mathrm{T}}, ..., \boldsymbol{y}_N^{\mathrm{T}}]^{\mathrm{T}}$ is a vector of length $\sum_{i=1}^N m_i$ representing the degradation performance outputs for all units. $\boldsymbol{\Omega} = \begin{pmatrix} \boldsymbol{\Omega}_1^{\mathrm{T}} & ... & \boldsymbol{\Omega}_N^{\mathrm{T}} \end{pmatrix}^{\mathrm{T}}$ is a matrix of dimension $(\sum_{i=1}^N m_i)$ by U representing the design matrix of observed heterogeneity for all units. $\boldsymbol{\Lambda} = \begin{pmatrix} \boldsymbol{\Lambda}_1 & \mathbf{0} & ... & \mathbf{0} \\ \mathbf{0} & \boldsymbol{\Lambda}_2 & ... & \mathbf{0} \\ \mathbf{0} & \mathbf{0} & ... & \boldsymbol{\Lambda}_N \end{pmatrix}$ is a matrix of dimension $(\sum_{i=1}^N m_i) \times (L+1)N$ representing the design matrix of latent heterogeneity for all units. $\boldsymbol{\gamma} = [\boldsymbol{\gamma}_1^{\mathrm{T}}, \boldsymbol{\gamma}_2^{\mathrm{T}}, ..., \boldsymbol{\gamma}_N^{\mathrm{T}}]^{\mathrm{T}}$

is a vector of length $(L+1)N$ representing the latent variables among all units. Further, the log likelihood of augmented data can be written as $l(\boldsymbol{\Theta} \mid \boldsymbol{D}^*) \propto l_1(\boldsymbol{\zeta}, \sigma_\epsilon^2 \mid \boldsymbol{D}^*) + l_2(\boldsymbol{\Sigma}_\gamma \mid \boldsymbol{D}^*)$. $l_1(\boldsymbol{\zeta}, \sigma_\epsilon^2 \mid \boldsymbol{D}^*)$ can be manifested as $l_1(\boldsymbol{\zeta}, \sigma_\epsilon^2 \mid \boldsymbol{D}^*) = -\frac{\sum_{i=1}^N m_i}{2}\log(\sigma_\epsilon^2) - \frac{1}{2\sigma_\epsilon^2}(\|\boldsymbol{y} - \boldsymbol{\Omega}\boldsymbol{\zeta}\|^2 + \sum_{i=1}^N \text{Tr}(\boldsymbol{\Lambda}_i^\text{T}\boldsymbol{\Lambda}_i\boldsymbol{\gamma}_i\boldsymbol{\gamma}_i^\text{T}) - 2(\boldsymbol{y} - \boldsymbol{\Omega}\boldsymbol{\zeta})^\text{T}\boldsymbol{\Lambda}\boldsymbol{\gamma})$ where $\text{Tr}(\cdot)$ is the trace operator. $l_2(\boldsymbol{\Sigma}_\gamma \mid \boldsymbol{D}^*)$ can be expressed as $l_2(\boldsymbol{\Sigma}_\gamma \mid \boldsymbol{D}^*) = -\frac{N}{2}\log|\boldsymbol{\Sigma}_\gamma| - \frac{1}{2}\sum_{i=1}^N \boldsymbol{\gamma}_i{}^\text{T}\boldsymbol{\Sigma}_\gamma^{-1}\boldsymbol{\gamma}_i$. Given that $\boldsymbol{\gamma}$ is known, $\boldsymbol{\zeta}$ and σ_ϵ^2 can be obtained by maximizing $l_1(\boldsymbol{\zeta}, \sigma_\epsilon^2 \mid \boldsymbol{D}^*)$ and $\boldsymbol{\Sigma}_\gamma$ can be estimated by maximizing $l_2(\boldsymbol{\Sigma}_\gamma \mid \boldsymbol{D}^*)$. However, the latent factors are unknown in real world problem. Thus, we employ EM technique (Wei and Tanner, 1990; Wu et al., 1983) to develop the estimation algorithm to jointly estimate unknown model parameters and latent factors. At iteration τ, the Expectation step yields the conditional expectation of $l(\boldsymbol{\Theta} \mid \boldsymbol{D}^*)$, i.e., $Q(\boldsymbol{\Theta}, \boldsymbol{\Theta}^{(\tau-1)}) = \mathbb{E}_{S(\boldsymbol{\gamma})|\boldsymbol{D},\boldsymbol{\Theta}^{(\tau-1)}}[l(\boldsymbol{\Theta} \mid \boldsymbol{D}^*)]$ where $S(\boldsymbol{\gamma}) = \left(\boldsymbol{\gamma}_1, \boldsymbol{\gamma}_2, ..., \boldsymbol{\gamma}_N, \boldsymbol{\gamma}_1\boldsymbol{\gamma}_1^\text{T}, ..., \boldsymbol{\gamma}_N\boldsymbol{\gamma}_N^\text{T}\right)$ is a set of individual statistics and $\boldsymbol{\Theta}^{(\tau-1)}$ is a set of all obtained model parameters at iteration $\tau - 1$. The Q-function can be explicitly written as

$$
\begin{aligned}
Q(\boldsymbol{\Theta}, \boldsymbol{\Theta}^{(\tau-1)}) \propto & -\frac{\sum_{i=1}^N m_i}{2}\log(\sigma_\epsilon^2) - \frac{1}{2\sigma_\epsilon^2}(\|\boldsymbol{y} - \boldsymbol{\Omega}\boldsymbol{\zeta}\|^2 \\
& + \sum_{i=1}^N \text{Tr}(\boldsymbol{\Lambda}_i^\text{T}\boldsymbol{\Lambda}_i\mathbb{E}[\boldsymbol{\gamma}_i\boldsymbol{\gamma}_i^\text{T} \mid \boldsymbol{D}, \boldsymbol{\Theta}^{(\tau-1)}]) - 2(\boldsymbol{y} - \boldsymbol{\Omega}\boldsymbol{\zeta})^\text{T}\boldsymbol{\Lambda}\mathbb{E}[\boldsymbol{\gamma} \mid \boldsymbol{D}, \boldsymbol{\Theta}^{(\tau-1)}]) \\
& - \frac{N}{2}\log|\boldsymbol{\Sigma}_\gamma| - \frac{1}{2}\sum_{i=1}^N \mathbb{E}[\boldsymbol{\gamma}_i{}^\text{T}\boldsymbol{\Sigma}_\gamma^{-1}\boldsymbol{\gamma}_i \mid \boldsymbol{D}, \boldsymbol{\Theta}^{(\tau-1)}]
\end{aligned} \tag{4.30}
$$

where $\text{Tr}(\cdot)$ is the trace operator. The conditional expectation $\mathbb{E}[\boldsymbol{\gamma}_i \mid \boldsymbol{D}, \boldsymbol{\Theta}^{(\tau-1)}]$ and $\mathbb{E}[\boldsymbol{\gamma}_i\boldsymbol{\gamma}_i^\text{T} \mid \boldsymbol{D}, \boldsymbol{\Theta}^{(\tau-1)}]$ can be explicitly obtained as

$$
\begin{aligned}
&\mathbb{E}[\boldsymbol{\gamma}_i \mid \boldsymbol{D}, \boldsymbol{\Theta}^{(\tau-1)}] = \boldsymbol{\mu}_i^{(\tau-1)} = \frac{1}{\sigma_\epsilon^{2(\tau-1)}}\boldsymbol{V}_i^{(\tau-1)}\boldsymbol{\Lambda}_i^\text{T}(\boldsymbol{y}_i - \boldsymbol{\Omega}_i\boldsymbol{\zeta}^{(\tau-1)}), \forall i = 1, ..., N \\
&\mathbb{E}[\boldsymbol{\gamma}_i\boldsymbol{\gamma}_i^\text{T} \mid \boldsymbol{D}, \boldsymbol{\Theta}^{(\tau-1)}] = \boldsymbol{V}_i^{(\tau-1)} + \boldsymbol{\mu}_i^{(\tau-1)}\boldsymbol{\mu}_i^{(\tau-1)\text{T}}, i = 1, ..., N
\end{aligned} \tag{4.31}
$$

where $\boldsymbol{V}_i^{(\tau-1)} = (\boldsymbol{\Sigma}_\gamma^{-1(\tau-1)} + \frac{1}{\sigma_\epsilon^{2(\tau-1)}}\boldsymbol{\Lambda}_i^\text{T}\boldsymbol{\Lambda}_i)^{-1}$. The derivation details of conditional expectation are presented in Appendix Section B.1.2. We can further simplify the condi-

tional expectation as $\mathbb{E}[\boldsymbol{\gamma} \mid \boldsymbol{D}, \boldsymbol{\Theta}^{(\tau-1)}] = \boldsymbol{\mu}^{(\tau-1)} = [\boldsymbol{\mu}_1^{(\tau-1)\mathrm{T}}, \boldsymbol{\mu}_2^{(\tau-1)\mathrm{T}}, ..., \boldsymbol{\mu}_N^{(\tau-1)\mathrm{T}}]^{\mathrm{T}}$. With the calculated Q-function at current iteration, the Maximization step achieves the maximization of $Q(\boldsymbol{\Theta}, \boldsymbol{\Theta}^{(\tau-1)})$. The model parameters at iteration τ can then be updated by $\boldsymbol{\Theta}^{(\tau)} = \arg\max_{\boldsymbol{\Theta}} Q(\boldsymbol{\Theta}, \boldsymbol{\Theta}^{(\tau-1)})$. The maximization of $Q(\boldsymbol{\Theta}, \boldsymbol{\Theta}^{(\tau-1)})$ is mathematically tractable and the estimated model parameters at iteration τ can be derived as

$$\hat{\boldsymbol{\zeta}}^{(\tau)} = \left(\boldsymbol{\Omega}^{\mathrm{T}}\boldsymbol{\Omega}\right)^{-1}\boldsymbol{\Omega}^{\mathrm{T}}\left(\boldsymbol{y} - \boldsymbol{\Lambda}\boldsymbol{\mu}^{(\tau-1)}\right) \tag{4.32}$$

$$\hat{\boldsymbol{\Sigma}}_{\gamma}^{(\tau)} = \frac{1}{N}\sum_{i=1}^{N}\left((\hat{\boldsymbol{\Sigma}}_{\gamma}^{(\tau-1)-1} + \frac{1}{\hat{\sigma}_{\epsilon}^{2(\tau-1)}}\boldsymbol{\Lambda}_i^{\mathrm{T}}\boldsymbol{\Lambda}_i)^{-1} + \boldsymbol{\mu}_i^{(\tau-1)}\boldsymbol{\mu}_i^{(\tau-1)\mathrm{T}}\right) \tag{4.33}$$

$$\begin{aligned}\hat{\sigma}_{\epsilon}^{2(\tau)} = \frac{1}{\sum_{i=1}^{N} m_i}\Big(&\left\|\boldsymbol{y} - \boldsymbol{\Omega}\hat{\boldsymbol{\zeta}}^{(\tau)}\right\|^2 - 2\sum_{i=1}^{N}(\boldsymbol{y}_i - \boldsymbol{\Omega}_i\hat{\boldsymbol{\zeta}}^{(\tau)})^{\mathrm{T}}\boldsymbol{\Lambda}_i\boldsymbol{\mu}_i^{(\tau-1)} \\ &+ \sum_{i=1}^{N}\mathrm{Tr}(\boldsymbol{\Lambda}_i^{\mathrm{T}}\boldsymbol{\Lambda}_i((\hat{\boldsymbol{\Sigma}}_{\gamma}^{(\tau)-1} + \frac{1}{\hat{\sigma}_{\epsilon}^{2(\tau-1)}}\boldsymbol{\Lambda}_i^{\mathrm{T}}\boldsymbol{\Lambda}_i)^{-1} + \boldsymbol{\mu}_i^{(\tau-1)}\boldsymbol{\mu}_i^{(\tau-1)\mathrm{T}})))\end{aligned} \tag{4.34}$$

The derivation details of the above estimation procedure are provided in Appendix Sec-

Algorithm 5 Parameters estimation procedure of the proposed model

Initialization: $\boldsymbol{\Theta}^{(0)} = \{\boldsymbol{\zeta}^{(0)}, \sigma_{\epsilon}^{2(0)}, \boldsymbol{\Sigma}_{\gamma}^{(0)}\}$

procedure UPDATEESTIM

for $\iota \leftarrow 1, ..., \tau_{\max}$ **do**

Compute $\mathbb{E}[\boldsymbol{\gamma}_i \mid \boldsymbol{D}, \boldsymbol{\Theta}^{(\iota-1)}]$ and $\mathbb{E}[\boldsymbol{\gamma}_i\boldsymbol{\gamma}_i^{\mathrm{T}} \mid \boldsymbol{D}, \boldsymbol{\Theta}^{(\iota-1)}]$ based on Eq. (4.31)

Derive parameter estimates sequentially by maximizing $Q(\boldsymbol{\Theta}, \boldsymbol{\Theta}^{(\iota-1)})$

1. Obtain $\hat{\boldsymbol{\zeta}}^{(\iota)}$ based on Eq. (4.32)
2. Obtain $\hat{\boldsymbol{\Sigma}}_{\gamma}^{(\iota)}$based on Eq. (4.33)
3. Obtain $\hat{\sigma}_{\epsilon}^{2(\iota)}$ based on Eq. (4.34)

end for

end procedure

tion B.1.3. The estimation algorithm of the proposed model is summarized in Algorithm 5. In each iteration, the conditional expectations are computed first and the param-

eters are then updated sequentially via maximizing Q-function. The algorithm updates parameters iteratively till the maximum iteration $\tau_{\max}$ is achieved. The EM estimation technique greatly simplifies the computational difficulties in joint likelihood maximization. The merits of data augmentation method enables the closed-form parameter updating procedure. It is proved that the parameter estimates will converge to maximum likelihood estimates when the updating iteration increases (Wu et al., 1983).

4.3 Real Case Study

4.3.1 Experimental Data Description

To illustrate the proposed modeling framework and to further evaluate its prediction performance as well as model interpretation capability, we provide a real case study to analyze the tribological degradation performance data of copper alloys. Due to their exceptional mechanical properties and high strength, copper alloys have been widely considered in various mission and safety critical components (e.g., aircraft bearings and bushings) and systems (e.g., drilling and mining systems). The tribological degradation of copper alloys may be influenced by both external factors, such as load conditions, and internal factors, such as material microstructure information. We will utilize the proposed degradation performance model to quantify the influences of these observed factors as well as unobserved heterogeneity within each individual test unit. Specifically, accelerated wear tests of Cu-Ni-Sn alloys are carried out at elevated load conditions using the Koehler K93500 pin-on-disc tester (Singh et al., 2007), as shown in Figure 4.40. The test units consist of both as-received and annealed material specimens of Cu-Ni-Sn alloys. As compared to the as-received test units, the microstructure and physical/chemical properties of annealed test units are often altered considerably through the annealing process, and therefore the corresponding tribological degradation performance may also differ. For each test unit, its tribological degradation performance outputs (i.e., height loss in um) are measured over time (in seconds) by a linear variable displacement transducer

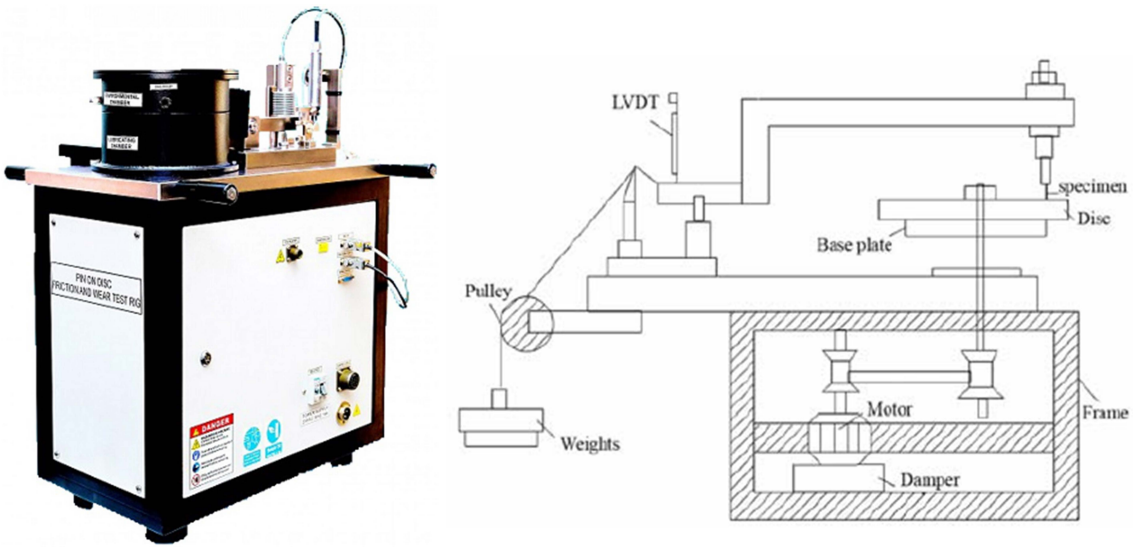

(a) The testing equipment (b) The diagram of wear test

Figure 4.40: The testing environment of the investigated accelerated wear test

(LVDT). Figure 4.41 shows degradation performance observations of four test units with

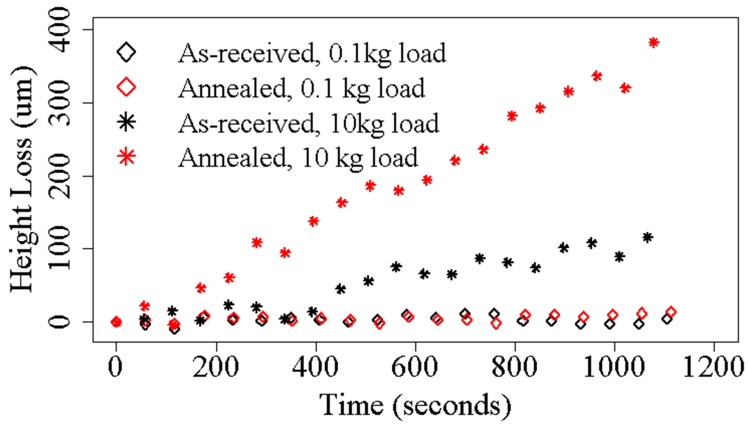

Figure 4.41: Degradation performance outputs of four test units

two different material types under different load conditions. The graphical visualization implies that both the internal factors (e.g., material types) and external factors (e.g., load conditions) play important roles in the degradation performance outputs and there is a need to explicitly quantify their effects.

With the advancement of material sensing and characterization techniques, it becomes readily available nowadays to obtain and extract more detailed information for test units

with different material types. In this paper, we utilize transmission electron microscopy (TEM) technique to characterize the microstructure of both as-received and annealed test units. The TEM images embrace useful information about material microstructure at finer scale. Particularly, we use grayscale TEM images at a nanometer-or-less length scale (20 nm) to characterize the microstructure properties of different types of copper alloys. Figure 4.42 shows two TEM images of as-received and annealed test units, respectively,

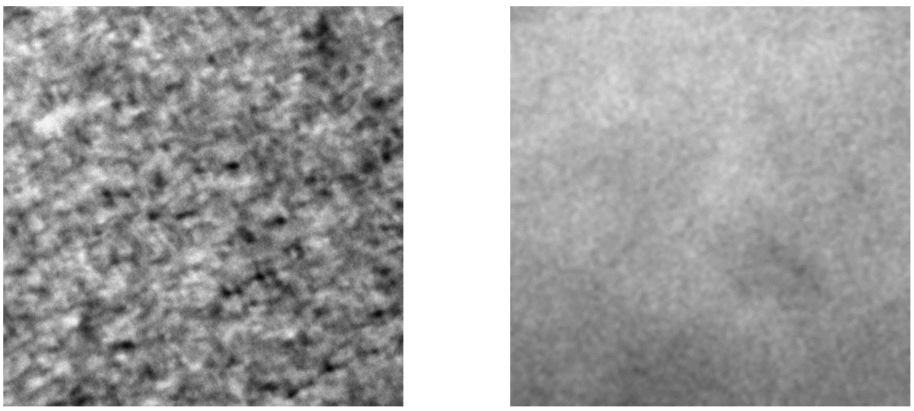

(a) As-received copper alloy (b) Annealed copper alloy

Figure 4.42: TEM micrographs of two different material types

which have significant visual difference. The texture pattern of the annealed test unit in Figure 4.42b has less spatial heterogeneity than that of the as-received test unit, indicating a more homogeneous microstructure with less distinct crystal structure and chemical composition. Such microstructure difference among different types of copper alloys is essentially due to the influence of the annealing process. After annealing at higher temperature, the primary two-phase microstructure in the as-received test unit has been converted into a single phase with alerted mechanical properties.

4.3.2 Functional Covariates Extraction

As shown in Figure 4.42, the microstructures of the test units with different material types exhibit different spatial heterogeneity patterns. To capture the spatial heterogeneity with rich spatial information, two functional microstructure descriptors, namely TPC and

RDF, are considered. As described in Section 4.2.3, the functional covariate $Z(r)$ is used to represent the material microstructure information where r is the distance measured at spatial scale in pixel. The distance measure for TPC function ranges from 0 to 200 pixels and the distance measure for RDF is between 0 and 250 pixels. Figure 4.43 shows

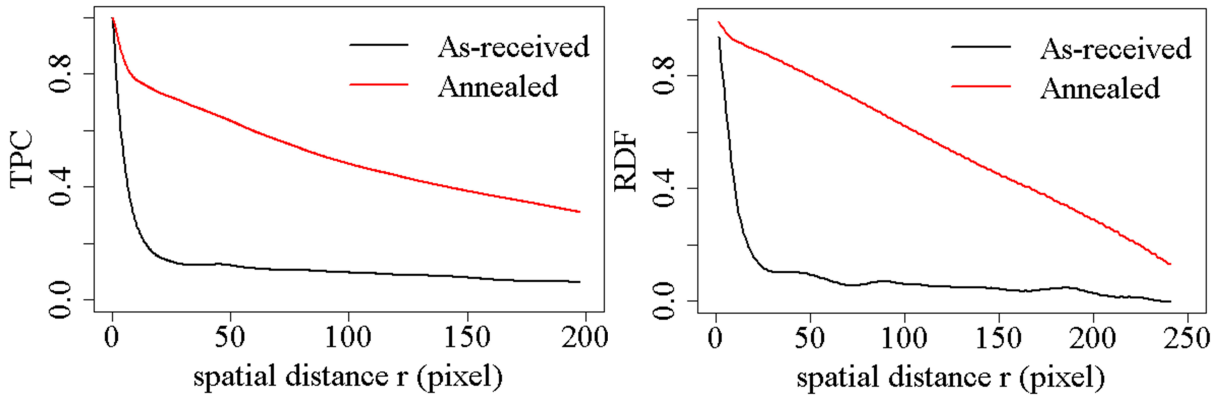

(a) TPC (b) RDF

Figure 4.43: Extracted functional descriptors

the corresponding functional covariates extracted based on TPC and RDF descriptors. Both descriptors are able to capture and differentiate the spatial heterogeneity patterns between annealed and as-received test units. The TPC (or RDF) value of an annealed test unit is uniformly larger than that of an as-received one at various spatial scales (measured in pixels), indicating a uniformly more homogeneous material microstructure. As the spatial distance r increases, the microstructures of both test units tend to become less homogeneous (with a smaller TPC or RDF value). When the spatial distance r is larger than 25 pixels, the TPC (or RDF) value of as-received test unit tends to approach 0, indicating that the cluster size in its TEM image is typically no larger than 25 pixels. Further, TPC is more sensitive than RDF in capturing and differentiating spatial heterogeneity of annealed unit at finer scale (e.g., smaller than 15 pixels).

4.3.3 Performance Comparison with Alternative Approaches

We first apply centering to the raw degradation performance data such that their baseline degradation performance (at $t = 0$) has been centered around 0, i.e., $\eta_{0i} = 0, \forall i = 1...12$. As shown in Figure 4.41, the degradation performance outputs exhibit approximately linear degradation path and thus we consider the first order polynomial basis function, i.e., $\phi_1(t_{ij}) = t_{ij}, \forall i = 1...12, j = 1...20$. We then decompose the basis coefficient η_{1i} into several parts, as described in Section 4.2.2. We use the extracted functional covariate $Z_{i1}(r), \forall i = 1...12$, as described in previous section, to represent the unit-specific microstructure pattern. In addition, we consider the scalar covariate x_{i1} to represent the load condition exerted on test unit i. By incorporating both $Z_{i1}(r)$ and x_{i1} as well as their interaction term into the proposed model, we further introduce a unit-specific latent variable γ_{1i} to capture the unobserved heterogeneity within each test unit i. The model specification using higher-order polynomial basis functions is also investigated and compared, which will be shown later in this section. Given a sample of test units available with observed degradation performance data (e.g., the height loss in um unit), we estimate the proposed model based on the estimation procedure described in Section 4.2.4. For basis function approximation in handling the infinite dimensionality of functional covariate during estimation, we select the optimal number of orthogonal basis functions based on the criterion of percentage of functional variation explained (FVE). The final number of basis functions for TPC functional approximation is two and the basis order for RDF functional approximation is three.

With the selected number of basis functions and the estimated models, we further evaluate the models with different functional descriptors (e.g., TPC and RDF) and compare their prediction performances. We partition the data into training (first 80% of degradation observations of each test unit) and testing data sets. We employ 5-fold cross-validation (CV) to evaluate and compare the prediction performance of the two models. The total CV error of all test units using model with TPC descriptor is smaller than the

total CV error of RDF-based model. Thus, we select TPC as microstructure descriptor to evaluate the performance of proposed modeling framework and further to compare it with other alternative models.

To demonstrate the superior modeling performance of the proposed modeling framework which incorporates mixed-type (i.e., both scalar and functional) covariates, their interaction as well as unobserved heterogeneity, we investigate and compare several alternative modeling approaches at various level of model complexity. First, to investigate

Table 4.12: Different degradation performance modeling approaches

Model	Observed factors				Unobserved heterogeneity	Order of polynomial basis	
	Material microstructure		Load condition	Interaction		first order	first and second orders
	Functional	Scalar	Scalar				
Model 1			✔			✔	
Model 2	✔					✔	
Model 3	✔		✔			✔	
Model 4	✔		✔	✔		✔	
Model 5	✔		✔	✔		✔	✔
Model 6		✔	✔	✔		✔	
Model 7	✔		✔	✔	✔	✔	

the importance of mixed-type covariates and their interaction, we consider the following set of alternative modeling approaches, namely (i) Model 1 which only considers scalar covariate of load condition, (ii) Model 2 which only considers functional covariate of material microstructure, (iii) Model 3 which considers mixed-type covariates but fails to consider their interaction, and (iv) Model 4 which considers both mixed-type covariates and their interaction but fails to consider unobserved heterogeneity. Among the first four modeling approaches, Model 4 is the most complex one. Based on Model 4, we further adjust its modeling complexity from the following three aspects, namely (i) adding higher order basis function in Model 5; (ii) replacing functional covariate with scalar covariate to represent material microstructure in Model 6; and (iii) incorporating latent variable to

represent unobserved heterogeneity in Model 7 (i.e., the proposed model). It is noticed that, for Model 6, we consider the scalar covariate of fractal dimension D_α to capture material microstructure, which is a popular choice of feature extraction method and often considered in microstructure image analysis (Chaudhuri and Sarkar, 1995). Table 4.12 summarizes the structure differences between the proposed modeling approach and six alternative modeling approaches.

To comprehensively evaluate and compare the modeling performance of the above models, we consider the following different performance evaluation criteria, namely (i) model goodness-of-fit criteria, e.g., R-squared and data log-likelihood; (ii) model selection criteria, e.g., Akaike Information Criterion (AIC) and Bayesian Information Criterion (BIC), and (iii) model prediction criteria, e.g., mean squared error (MSE) of both training and test data sets. The model selection criteria (e.g., AIC, BIC) can be unified as $C(\boldsymbol{\Theta}) = -2\ln L\left(\hat{\boldsymbol{\Theta}}, \{\hat{\gamma}_i\}_{i=1}^N \mid \boldsymbol{D}\right) + pk$, where $L\left(\hat{\boldsymbol{\Theta}}, \{\hat{\gamma}_i\}_{i=1}^N \mid \boldsymbol{D}\right)$ is the maximized joint likelihood and pk is the penalty term to leverage the model complexity. In particular, p is total number of estimated model parameters, $k = 2$ (for AIC) and $k = \ln N$ (for BIC).

Table 4.13: Model comparison results

Model	Results					Model structure
	R^2	$\log L$	AIC	BIC	($\bar{\Delta}_{\text{train}}$,$\bar{\Delta}_{\text{test}}$)	
Model 1	0.7303	-937.4	1880.8	1890.6	(1019.2, 3779.6)	$\boldsymbol{x}$
Model 2	0.5672	-982.3	1972.6	1985.6	(1626.8, 6646.2)	$Z(r)$
Model 3	0.9269	-811.042	1632.1	1648.4	(273.3, 1067.6)	$\boldsymbol{x} + Z(r)$
Model 4	0.9736	-712.1	1438.3	1461.1	(97.5, 248.9)	$\boldsymbol{x} \times Z(r)$
Model 5	0.9735	-712.1	1440.1	1466.2	(97.5, 253.6)	$\phi_1(t_{ij}) + \phi_2(t_{ij})$
Model 6	0.7304	-936.3	1882.7	1898.965	(1007.9, 3748.8)	Z
Model 7	0.9681	-698.7	1413.3	1439.4	(72.4, 156.3)	$\boldsymbol{x} \times Z(r) + \boldsymbol{\gamma}$

Based on the above criteria, Table 4.13 summarizes the results of performance comparison. Among all models, the proposed model achieves the best performance, in terms of both the largest goodness-of-fit, the smallest AIC/BIC and the smallest MSE values. Sev-

eral additional implications and discussions can be obtained as follows. First, by comparing Model 3 with Models 1 and 2, the model which only considers either external factor of environmental conditions (e.g., Model 1) or internal factor of material types (e.g., Model 2) has worse goodness-of-fit and prediction performance than the model which considers both internal and external factors (e.g., Model 3). Further, there exists interaction between these two factors and capturing such interaction (e.g., Model 4) will further improve the modeling performance. This implies the importance of incorporating both internal and external factors (as well as their potential interaction) during the degradation performance modeling. Second, by comparing Models 4 and 5, we explore the impact of higher order basis function on modeling performance improvement. Based on the training and testing MSE values, model with extra quadratic term (e.g., Model 5) has overfitting issue. Thus, in this study, the complex curvilinear model specification with higher order basis function will not provide additional modeling benefits and need to be avoided. Third, by comparing Models 4 and 6, Model 4 which considers mixed-type covariates (e.g., functional covariate of material microstructure and scalar covariate of load conditions) has superior modeling performance than Model 6 which only considers single-type covariates (e.g., scalar covariates). This emphasizes the benefits of incorporating mixed-type covariates in improving degradation performance modeling accuracy. The functional covariate carries richer material microstructure information than the conventional scalar covariate. Last, by comparing the proposed model which considers unobserved heterogeneity (e.g., Model 7) and Model 4 which fails to consider unobserved heterogeneity, both model goodness-of-fit and prediction results indicate the importance of considering both observed factors' influences and unobserved heterogeneity in developing the degradation performance model. The predicted degradation performance based on different models (e.g., Models 1-7) and the observed degradation performance of a single test unit are also shown in Figure 4.44. As compared to the alternative modeling approaches (e.g.,

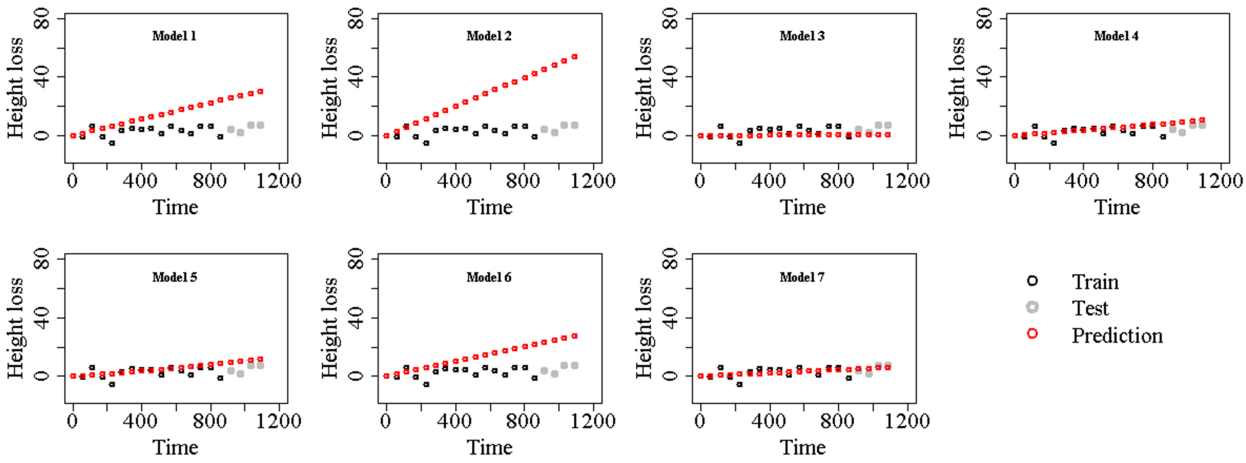

Figure 4.44: Prediction performance comparison among different models

Models 1-6), the predicted degradation performance values based on the proposed model (e.g., Model 7) are closer to the actual degradation performance observations over time.

4.3.4 Model Interpretation

Based on the above performance evaluation and comparison, the superior prediction performance of proposed modeling framework is demonstrated. We further investigate the model interpretability of the proposed work. The effects of different types of covariates on tribological degradation are discussed as below. The point estimates of model

Table 4.14: Model parameter estimation results

Parameter	Point Estimate	P-value	Parameter	Point Estimate	P-value
ν_1	0.01633	0.0038	β_{11}	0.02046	$<.0001$
b_{111}	0.000025	0.0235	b'_{1111}	0.00002	$<.0001$
b_{112}	-0.00047	0.4234	b'_{1112}	0.000326	0.3298

coefficients and their p-values are summarized in Table 4.14. As shown in Table 4.14, both $\hat{\nu}_1$ and $\hat{\beta}_{11}$ are significant at a significant level of 0.05. $\hat{\nu}_1$ captures the tribological degradation rate of studied alloy in absence of the influences of mixed-type covariates. A positive value of $\hat{\nu}_1$ indicates an increasing trend of degradation performance (i.e., material height loss) of copper alloys over time. $\hat{\beta}_{11}$ quantifies the marginal effects of scalar

covariate, i.e., load condition, on degradation performance output of test units. A positive value of $\hat{\beta}_{11}$ indicates that load condition is an effective stress factor in accelerating the tribological degradation process of copper alloys. Further, we investigate the marginal and interaction effect of functional covariates (i.e., TPC curves) of material microstructures on degradation performance output. As shown in Eq. (4.25b), $\int_0^R \alpha_{11}(r)Z_{i1}(r)dr$ captures the contributing marginal effects of functional covariate $Z_{i1}(r)$ on the slope of degradation performance, which can be written as $R(b_{111}c_{i11} + b_{112}c_{i12})$ via basis function approximation (in Section 4.2.4). A non-zero value of parameter b_{111} at a significance level of 0.05 indicates that there exists a marginal effect of material microstructures (captured by functional covariate) among different material types. Figure 4.45 shows the es-

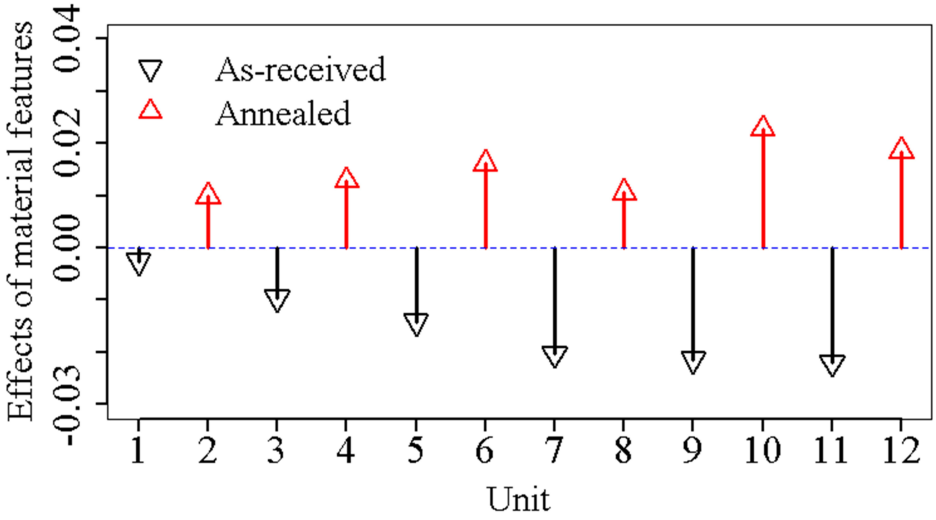

Figure 4.45: Effects of internal material characteristics among all test units

timated contributing marginal effects, $\int_0^R \alpha_{11}(r)Z_{i1}(r)dr$, among different test units with two different types of copper alloys. As shown in Figure 4.45, the microstructure effects of as-received test units are negative. It indicates that a less homogeneous microstructure yields greater hardness of the materials and ultimately reduces the corresponding tribological degradation rate. On the other side, the microstructure effects of annealed test units are positive, which indicates that a more uniformly homogeneous microstructure tends to accelerate the tribological degradation process of test units. In addition

to the significant marginal effect of functional covariate, the non-zero value of parameter b'_{1111} in Table 4.14 at a significance level of 0.05 also indicates that there exists an interaction effect between material microstructure (captured by functional covariate) and load condition (captured by scalar covariate) on the slope of degradation performance. Specifically, as shown in Eq. (4.25b), such interaction effect between scalar and functional covariates can be characterized as $x_{i1}\int_0^R \rho_{111}(r)Z_{i1}(r)dr$, which can further be approximated as $Rx_{i1}(b'_{1111}c_{i11} + b'_{1112}c_{i12})$ (as manifested in Section 4.2.4). Figure 4.46 shows the

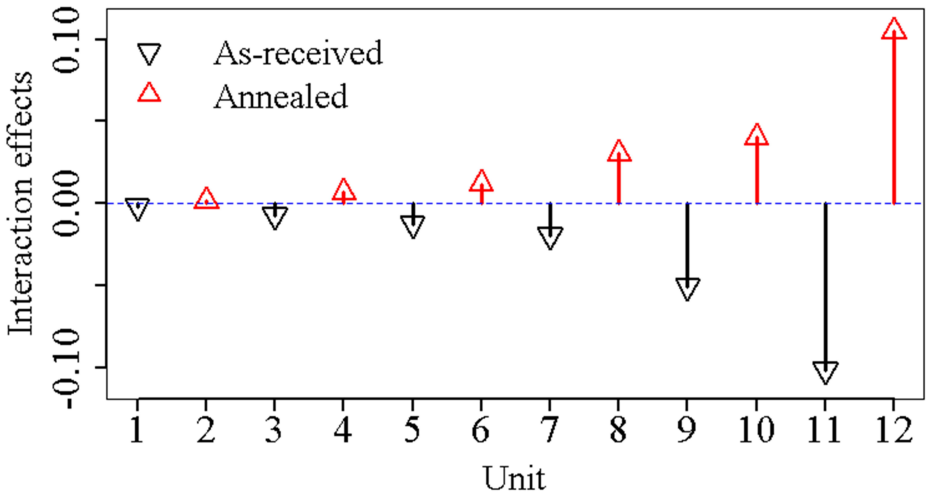

Figure 4.46: Interaction effect among all test units

estimated interaction effect, $x_{i1}\int_0^R \rho_{111}(r)Z_{i1}(r)dr$, among different test units. As shown in Figure 4.46, the interaction effect of material microstructure and load condition for as-received test units are negative. It implies that the degradation performance of as-received test units with less homogeneous microstructure is less sensitive to the accelerated load condition. On the other side, the interaction effect of material microstructure and load condition for annealed test units are positive. It implies that for more homogeneous microstructure, there exists a synergistic effect between material microstructure and accelerated load condition, which can further speed up the accelerated degradation test. All of the above rich model interpretations will inform the reliability engineers at product design and development stage to better identify the most appropriate material

types as well as accelerated conditions to improve the efficiency of accelerated testing as well as to improve the reliability performance of test units. In addition to the quantifica-

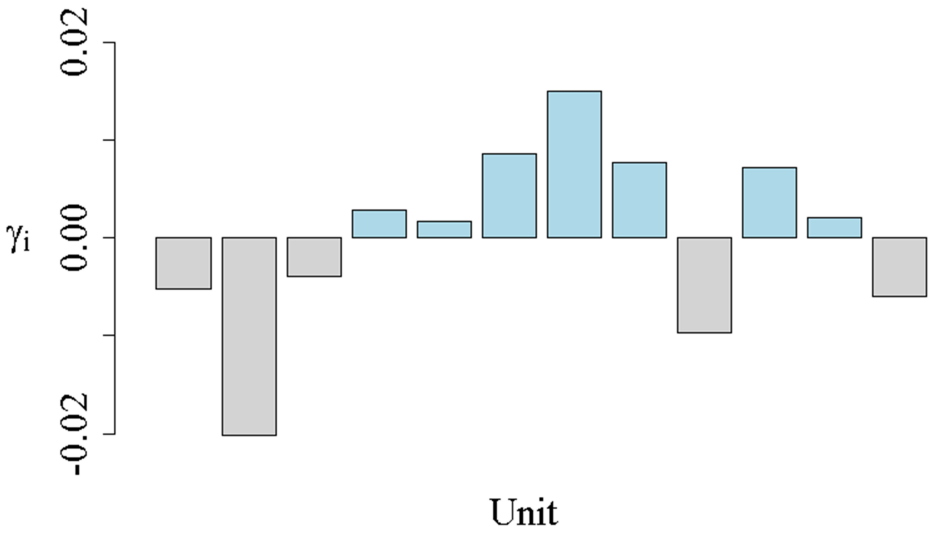

Figure 4.47: Quantification of individual latent heterogeneity

tion of the influences of the observed factors, the proposed work is able to quantify the unobserved heterogeneity, captured by γ_{1i}, within each test unit. As shown in Figure 4.47, the positive value of unobserved heterogeneity indicates a positive effect on the slope of degradation performance and vice versus. Such unobserved heterogeneity is essentially caused by unobserved/unknown factors shared within each test unit (e.g., the potential effect of accumulated wear debris on specimen contact surface). Such information can inform the reliability engineers to target specific test units which exhibit large unobserved heterogeneity and to investigate the potential contributing factors within each test unit via further data collection and analysis.

4.4 Conclusion Remarks

In this paper, we propose a degradation performance modeling framework with both generic model formulation and effective estimation algorithm to characterize heterogeneous degradation data with covariates. The proposed model formulation allows the incorporation of both mixed-type covariates and latent heterogeneity for improving the

prediction accuracy of degradation performance. The mixed-type covariates include both (i) the scalar covariates which represent the accelerated/environmental conditions; and (ii) the functional covariates which represent the material microstructure characteristics. The developed estimation algorithm further allows jointly quantifying the influences of mixed-type covariates and unobserved heterogeneity. In particular, basis function approximation technique is employed to address the infinite dimensionality issue of functional covariates. Data augmentation technique is further employed to simultaneously estimate the influences of the observed mixed-type covariates and the unobserved heterogeneity within each unit which is captured by the unit specific latent variable. A real case study is also presented to illustrate the proposed framework and to evaluate its performance via comprehensively comparing with several alternative modeling approaches. The proposed work demonstrates its superior prediction performance via using different performance metrics, such as goodness-of-fit, model selection criteria and model prediction criteria. With improved prediction accuracy of degradation performance, the proposed model also provides rich model interpretation. Both the marginal effects among mixed-type covariates, their interaction effect and unobserved heterogeneity within each test unit can be jointly quantified explicitly. Such modeling outputs will help to inform the reliability engineers to better identify the most influencing factors for improving reliability performance of product units and design more efficient accelerated tests in response to the varied material characteristics of product units.

Chapter 5

Heterogeneous Degradation Performance Modeling of Corroding Aluminum Alloys with Latent Heterogeneity and Fractional Dynamics

5.1 Introduction

With lightness, sound mechanical properties and relatively low cost (Liu et al., 2017; Mraied et al., 2016), aluminum (Al) alloys have been widely utilized in many mission-critical and safety-critical industries, such as marine and aerospace (Ezuber et al., 2008; Alexopoulos and Papanikos, 2008). However, in saline environments, such as sea water and salt-filled atmosphere of coastal shore bases and islands, the corrosion-induced degradation of Al alloys becomes a major concern and is a key failure cause of many critical engineering components, such as aircraft wing (Alexopoulos and Papanikos, 2008). It will significantly reduce the structural integrity and strength of materials and eventually leads to catastrophic failures and safety issues of the overall system. Thus, accurate modeling and assessment of corrosion-induced degradation performance of corroding Al-alloy units (e.g., specimens, components) becomes important[4]. Based on the laboratory or field testing data, successful degradation performance assessment of the test units will help improve reliability modeling and failure prediction accuracy, and further facilitate subsequent decision-making at design or operation stages, e.g., optimal design of experiments, cost-effective preventive maintenance.

To improve degradation performance assessment and modeling, a variety of data-driven models have been investigated in reliability literature, such as degradation path

[4]This chapter was published in Elsevier RESS (Sun et al., 2018). Copyright permission from the publisher is included in Appendix A.

models (Lu and Meeker, 1993; Gebraeel et al., 2005; Yuan et al., 2016; Bae et al., 2015), continuous stochastic process (Ye and Chen, 2014; Peng et al., 2014; Huynh et al., 2011; van Noortwijk, 2009; Ye et al., 2015) and Markov-based models (Kharoufeh, 2003; Bian et al., 2015). Many of these empirical approaches often assume that the degradation performance of the test units, e.g. the vibration signal of the bearings or the light intensity of the light-emitting diode lamps, can be directly observed. In corrosion-induced degradation, weight loss is often considered as a directly observed performance measure (Kirkland et al., 2012; Abiola and James, 2010). However, for Al-alloy units, weight loss is not a good performance indicator (Tabrizi et al., 1991). It is because in the course of Al-alloy corrosion, the corrosion products, e.g., Al oxides, often adheres to the alloy surface and thus the overall weight may not significantly decrease or may even slightly increase. Therefore, the actual degradation state becomes latent and cannot be directly observed. Such latent nature of degradation state makes the degradation performance assessment challenging and the above degradation models inapplicable.

To evaluate the corrosion-induced degradation performance of corroding units, electrochemical impedance spectroscopy (EIS) method (Mraied et al., 2016; He and Mansfeld, 2009; Hinderliter et al., 2006; Bierwagen et al., 2003; Kirkland et al., 2012) is considered as a popular non-destructive testing technique. By generating alternating potential stimulus signals to the test units, EIS instruments collect the frequency responses. Based on the frequency response data, EIS-based physical models, such as Randles circuit model (Hinderliter et al., 2006) and failed coating model (Bierwagen et al., 2003), can be established to investigate the corrosion-induced degradation process of the test units and to assess the latent degradation performance. Due to the complex physical failure mechanism of corroding Al-alloy units, the existing physical models are less generic and less flexible to characterize the highly nonlinear relationship between EIS responses and the latent degradation state.

In addition, existing EIS-based physical models have two major limitations. First, least squares estimation (LSE) method is mainly considered for the model estimation. However, due to the time-consuming data collection process and the limited laboratory testing resources (e.g. available sensing devices and/or operators), the available EIS data is often limited. It is important to quantify model parameters uncertainty due to the limited sample size of data, which is often neglected in LSE. Second, existing studies are mainly restricted to analyzing degradation behavior of an individual test unit. However, even for the same material, the degradation performance among multiple test units may not be identical. It may be attributed to the composition differences and micro-structural variations, and variability of manufacturing process is another source of variation. Thus, it will be also desirable to quantify degradation performance variability of the underlying population from which multiple test units are drawn. The resulting benefits of population level modeling are twofold. Population variability is an important metric to reflect material quality of suppliers and capability of the manufacturing process where test samples are produced. Moreover, when a test unit has sparse EIS measurements, it is difficult to assess its individual degradation performance. Leveraging information among multiple units will help resolve such issue.

To address the above limitations, Bayesian statistics provides appealing estimation and inference framework (Congdon, 2010). It has been successfully studied in reliability field to quantify estimation uncertainty and to improve reliability modeling as well as reliability assessment (Gebraeel et al., 2005; Hamada et al., 2008; Li and Liu, 2016; Qin et al., 2015; Zhang et al., 2014; Wang et al., 2013). However, due to the complex physical failure mechanism of Al-alloy units, Bayesian inference cannot be directly adopted due to its empirical nature. It will be desirable to integrate the physical model with Bayesian statistics to improve the modeling accuracy and further quantify both the parameters uncertainty and population variability.

To fill the above gaps, this work proposes a physical-statistical modeling approach to evaluating the latent degradation performance of corroding Al-alloy units by innovatively integrating complex physical failure mechanisms with Bayesian hierarchical modeling and computation. From the physical modeling aspect, the proposed model incorporates the fractional order system dynamics to improve the modeling accuracy of EIS data with more generic and flexible form than the conventional physical models. From the statistical modeling aspect, the proposed modeling framework not only quantifies the model parameters uncertainty of individual test unit, but also quantifies the population variability among multiple test units. The proposed population-level model further overcomes estimation difficulty of evaluating degradation performance of an individual unit when its available data is sparse and inadequate. In addition to improving the degradation performance assessment of test units of Al-alloy aircraft coatings (Alexopoulos and Papanikos, 2008), an additional case study is given to demonstrate the applicability of proposed model framework in other corroding metallic units, such as test units of magnesium (Mg) implants (Kirkland et al., 2012).

5.2 Framework Overview

Successful modeling and evaluating degradation performance of the corroding Al-alloy test units is important in both laboratory testing and field inspection for better reliability assessment. To characterize the latent degradation performance and further to quantify the parameters uncertainty (due to limited test data) as well as the performance variability (among multiple test units), we propose a modeling and quantification framework by innovatively integrating complex physical mechanisms with Bayesian statistical inference. Figure 5.48 gives an overview of the proposed framework. The nondestructive testing data is first collected via EIS instruments. Based on such data, both the individual-level and population-level degradation models are developed by integrating the fractional order system dynamics and Bayesian hierarchical structure. Physical mod-

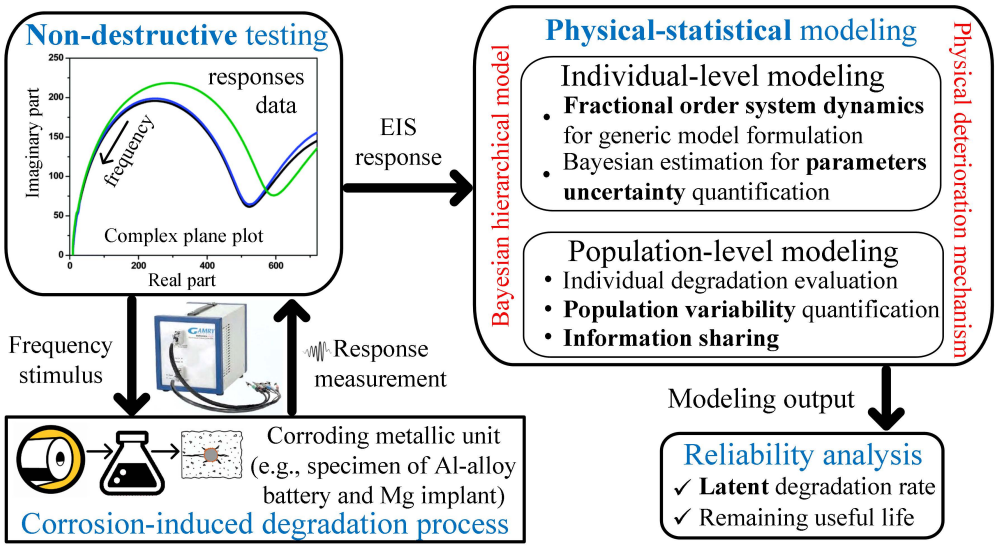

Figure 5.48: Overview of the proposed degradation modeling framework

eling improves the modeling accuracy while Bayesian inference delivers rich quantification results, such as parameters uncertainty and population variability. The estimated latent degradation performance can be used to calculate important reliability quantities, such as remaining useful life. The details will be elaborated as follows.

5.3 Model Formulation

5.3.1 Physical Background

Conventionally, the degradation performance evaluation of a corroding metallic unit, such as Zinc and Magnesium specimen, is realized by measuring the weight loss (Kirkland et al., 2012; Abiola and James, 2010). However, collecting weight loss data is often labor intensive and may incur extra costs, such as labor costs and material cleaning costs, since it requires manually terminating the corrosion process and measuring the unit outside the test environment. Moreover, for the corrosion-induced degradation of Al-alloy units in saline environment, such as in salt water, weight loss is not a good measure. It is because corrosion products may adhere to the surface during the degradation process, which often results in an insignificant decrease or even a slight increase of the overall

weight. To automatically evaluate the latent degradation performance, electrochemical impedance spectroscopy (EIS) method is a modern non-destructive testing technique to investigate the electrochemical system dynamics and to reflect the corrosion properties (e.g., corrosion resistance) of the structural deterioration process (Kirkland et al., 2012).

EIS testing is performed by stimulating alternating potential signals over a wide range of frequencies on the tested unit and collecting the responses. The corrosion process will not be interrupted during EIS testing. Based on the collected responses, physical models can be established to evaluate the latent degradation performance. In general, EIS-based degradation performance model can be represented as

$$\boldsymbol{y}(\omega) = g(\omega, R, \boldsymbol{\Theta}) + \boldsymbol{\epsilon} = \begin{bmatrix} |H(j\omega, R, \boldsymbol{\Theta})| \cos \angle H(j\omega, R, \boldsymbol{\Theta}) \\ \\ |H(j\omega, R, \boldsymbol{\Theta})| \sin \angle H(j\omega, R, \boldsymbol{\Theta}) \end{bmatrix} + \boldsymbol{\epsilon} \tag{5.35}$$

where $g(\cdot)$ is a function mapping from real frequency values to complex frequency responses and ω is the frequency of alternating potential stimulus which varies over a wide range. $\boldsymbol{y}(\omega) = [y^R(\omega), y^I(\omega)]^{\mathrm{T}}$ is the observed frequency response at w with $y^R(\omega)$ and $y^I(\omega)$ representing the real and imaginary parts. $H(j\omega, R, \boldsymbol{\Theta})$ is frequency response function at ω, i.e., $H(j\omega, R, \boldsymbol{\Theta}) = H(s, R, \boldsymbol{\Theta})|_{s=j\omega}$, where $H(s, R, \boldsymbol{\Theta})$ is the transfer function of the physical model established for characterizing the electrochemical system dynamics of the corrosion-induced degradation process. R and $\boldsymbol{\Theta}$ are model parameters of $H(s, R, \boldsymbol{\Theta})$, $|\cdot|$ and $\angle\cdot$ are response modulus operator and phase operator, respectively. $\boldsymbol{\epsilon}$ is a vector of error terms which represents the remainder not captured by the model, including measurement error and model mis-specification error. In $H(s, R, \boldsymbol{\Theta})$, model parameter R is the corrosion resistance to reflect the degradation performance. Based on Stern-Geary equation (Stern and Geary, 1957), degradation rate γ can be obtained as $\gamma = 10.9W/R$ $\mu\mathrm{m\,yr}^{-1}$, where $W = 52\,\mathrm{mV}$ is the Stern-Geary constant. It is noticed that the degradation rate γ cannot be directly measured and thus it is an unknown and latent variable, which

needs to be estimated from $H(s, R, \boldsymbol{\Theta})$. Therefore, it is referred to the latent degradation performance in this work.

Different forms of $H(s, R, \boldsymbol{\Theta})$ in Eq. (5.35) have been investigated to characterize the corrosion-induced degradation. Among them, the simplified Randles cell (SRC) model (Rosliza et al., 2010) is one of the most commonly utilized models. Its transfer function, $H_r(s, R, \boldsymbol{\Theta})$, can be expressed as

$$H_r(s, R, \boldsymbol{\Theta}) = \frac{B_r s + U_r}{E_r s + V_r} \tag{5.36}$$

where $s = j\omega$ is the alternating potential stimulus at certain frequency value ω, $\boldsymbol{\Theta} = \{R_1, C_1\}$, $B_r = RR_1C_1$, $U_r = R + R_1$, $E_r = RC_1$ and $V_r = 1$. Figure 5.49a illustrates the

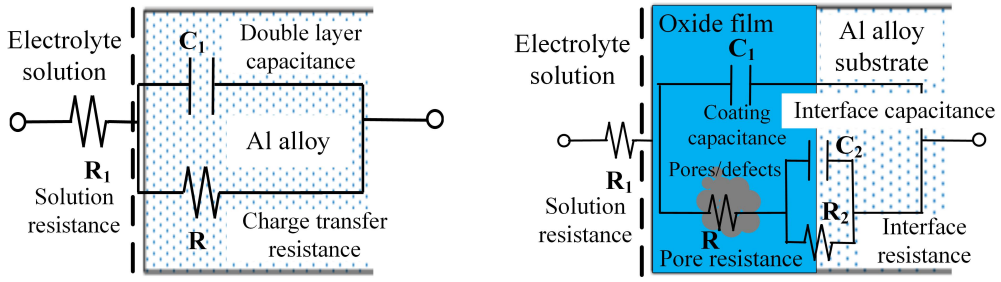

(a) SRC model (b) FC model

Figure 5.49: Conventional EIS based physical models

physical parameters $\{R, \boldsymbol{\Theta}\}$. For detailed physical mechanism, please refer to (Rosliza et al., 2010) and references therein. Although SRC model provides a simple representation, it does not consider the effect of extra layer, such as the passive film developed on corroding Al alloys, or the effect of corrosion products, such as Al oxides or hydroxide, which could adhere to the alloy surface. Thus, SRC model is too simple to capture the complex degradation process of corroding Al-alloy units.

To account for the effect from extra layer of Al alloys, previous studies investigated on failed coating (FC) model (González et al., 2003). The transfer function of FC model,

denoted as $H_c(s, R, \mathbf{\Theta})$, can be expressed as

$$H_c(s, R, \mathbf{\Theta}) = \frac{A_c s^2 + B_c s + U_c}{D_c s^2 + E_c s + V_c} \tag{5.37}$$

where $\mathbf{\Theta} = \{R_1, R_2, C_1, C_2\}$, $A_c = R_1 R_2 R C_1 C_2$, $B_c = R_1 C_1 (R + R_2) + R_2 C_2 (R + R_2)$, $U_c = R_1 + R_2 + R$, $D_c = R R_2 C_1 C_2$, $E_c = R_2 C_2 + R C_1 + R_2 C_1$ and $V_c = 1$. Figure 5.49b illustrates the model parameters. For physical mechanism details, please refer to (González et al., 2003) and references therein. Compared to SRC model, FC model considers the extra layer and attempts to describe the degree of structural deterioration on the extra layer. However, FC model fails to consider the effect from corrosion products on the surface of extra layer as well as the effect of penetrated solution on the interface of alloy substrate, which are often not negligible in the actual corrosion process of Al alloy units.

5.3.2 Individual-level Degradation Performance Modeling

In the aforementioned EIS-based physical models, the ideal capacitance parameters (e.g., C_1 and C_2) are considered to characterize the corrosion behavior. As a result, the orders of their transfer functions are all integers. The assumption about integer order of transfer function makes them less flexible in capturing the real and complex corrosion-induced degradation process of many metallic units, such as Al-alloy units. For instance, due to the defects in the extra layer of Al-alloy units, or the effects of corrosion product on the surface, the corrosion behavior near the surface cannot be captured by an ideal capacitance. Similarly, the capacitance at the interface of substrate may not be an ideal capacitance due to the effect of penetrated solution.

To relax the integer order assumption, fractional order system dynamics is employed as a promising avenue to model physical system with complex electrochemical dynamics (Wang et al., 2015; Elwakil, 2010). It allows both integer and non-integer orders in the transfer function and has been successfully utilized in many applications fields, such as

modeling human tissue or energy storage system, to capture the complex physical system behaviors. In the context of modeling corrosion-induced degradation, the constant phase elements (CPEs) (Elwakil, 2010) Λ_1 and Λ_2 are employed to capture the non-ideal capacitance behavior instead of the ideal capacitances C_1 and C_2, with $\Lambda_k = C_k(j\omega)^{\alpha_k}, k = 1, 2, 0 \leq \alpha_k \leq 1$ where α_k is fractional order parameter. When α_k approaches to 0, CPE behaves like a resistor; when α_k approaches to 1, CPE behaves like an ideal capacitor. As

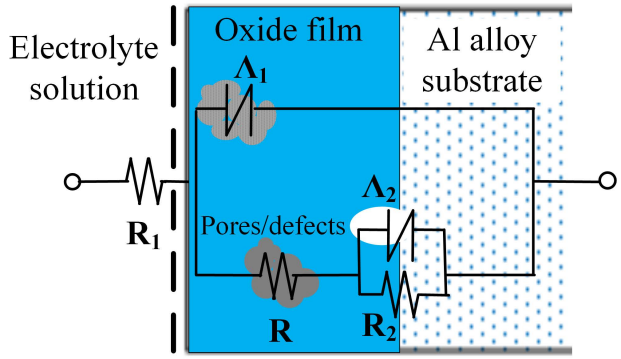

Figure 5.50: Proposed model based on fractional order system dynamics

shown in Figure 5.50, $\Lambda_1 = C_1(j\omega)^{\alpha_1}$ captures the non-ideal capacitance behavior due to the defects in extra layer or the effect of corrosion products. $\Lambda_2 = C_2(j\omega)^{\alpha_2}$ captures the non-ideal capacitance behavior at the substrate interface due to the effect of penetrated solution. Other model parameters, such as R, R_1 and R_2, are similar to those in FC model. The transfer function $H_f(s, R, \boldsymbol{\Theta})$ can be represented by a fractional order transfer function, written as

$$H_f(s, R, \boldsymbol{\Theta}) = \frac{A_f s^{\alpha_1+\alpha_2} + B_{f1} s^{\alpha_1} + B_{f2} s^{\alpha_2} + U_f s^0}{D_f s^{\alpha_1+\alpha_2} + E_{f1} s^{\alpha 1} + E_{f2} s^{\alpha_2} + V_f s^0} \tag{5.38}$$

where $\boldsymbol{\Theta} = \{R_1, R_2, \Lambda_1, \Lambda_2\} = \{R_1, R_2, C_1, C_2, \alpha_1, \alpha_2\}$, $A_f = RR_1R_2C_1C_2$, $B_{f1} = C_1R_1(R + R_2)$, $B_{f2} = C_2R_2(R + R_1)$, $U_f = R + R_1 + R_2$, $D_f = RR_2C_1C_2$, $E_{f1} = C_1(R + R_2)$, $E_{f2} = C_2R_2$ and $V_f = 1$. The derivation details are described in the Appendix Section B.2.1.

Now consider the corrosion-induced degradation process of an individual unit of Al alloy, with the modified fractional order transfer function, the degradation performance

model of single unit becomes Bayesian non-hierarchical model with only one layer. The proposed individual-level model can be formulated as

$$
\begin{aligned}
&\boldsymbol{y}_k \mid \boldsymbol{\Theta}_1, \boldsymbol{\Theta}_2, R, \omega_k \sim MVN(\boldsymbol{\zeta}_k, \sigma^2 I) \\
&\boldsymbol{\zeta}_k = g_f(\boldsymbol{\Theta}_1, \boldsymbol{\Theta}_2, R, \omega_k) = \begin{bmatrix} \left|H_f(j\omega_k, R, \boldsymbol{\Theta})\right| \cos \angle H_f(j\omega_k, R, \boldsymbol{\Theta}) \\ \\ \left|H_f(j\omega_k, R, \boldsymbol{\Theta})\right| \sin \angle H_f(j\omega_k, R, \boldsymbol{\Theta}) \end{bmatrix} \\
&\gamma = 10.9W/R
\end{aligned} \tag{5.39}
$$

where $\boldsymbol{y}_k, k = 1, ..., m$ is the observed response collected by alternating potential stimulus at frequency value ω_k with m total measurements. $\boldsymbol{\Theta} = \{\boldsymbol{\Theta}_1, \boldsymbol{\Theta}_2\}$ is the model parameters of transfer function $H_f(j\omega_k, R, \boldsymbol{\Theta})$ with $\boldsymbol{\Theta}_1 = \{R_1, R_2, C_1, C_2\}$ and $\boldsymbol{\Theta}_2 = \{\alpha_1, \alpha_2\}$. $MVN(\cdot)$ stands for multivariate normal distribution, and I is the 2×2 identity matrix. In the proposed individual-level model, $g_f(\cdot)$ is a nonlinear function mapping, which consists of the magnitude of response $|H(j\omega_k, R, \boldsymbol{\Theta})| = \sqrt{\frac{K_1(\omega_k,R)^2 + K_2(\omega_k,R)^2}{K_3(\omega_k,R)^2 + K_4(\omega_k,R)^2}}$ and the phase of response as $\angle H(j\omega_k, R, \boldsymbol{\Theta}) = \tan^{-1} \frac{K_2(\omega_k,R)}{K_1(\omega_k,R)} - \tan^{-1} \frac{K_4(\omega_k,R)}{K_3(\omega_k,R)}$, where the derivation details of $K_1(\omega_k, R)$ to $K_4(\omega_k, R)$ can be found in the Appendix Section B.2.2. The degradation performance, namely the degradation rate γ, of a test unit can be evaluated based on Eq. (5.39). The proposed individual-level model is not limited to corroding Al-alloy unit. The same model structure can be employed for other corroding metallic unit by replacing $H_f(\cdot)$ with the transfer function of the investigated metallic unit.

Compared to the existing physical models, the proposed fractional order transfer function provides a more generic and flexible representation to characterize the complex electrochemical degradation process of corroding Al alloys. SRC model and FC model can be considered as special cases of the proposed model. Their relationships can be explicitly summarized in the following theorem.

Theorem: The proposed fractional order transfer function $H_f(s, R, \mathbf{\Theta})$ can be reduced into $H_c(s, R, \mathbf{\Theta})$ and $H_r(s, R, \mathbf{\Theta})$, respectively, if the following conditions hold:
(i) When $\alpha_1 = 1, \alpha_2 = 0$, $H_f(s, R, \mathbf{\Theta})$=$H_r(s, R', \mathbf{\Theta})$ with $R' = R + \frac{R_2}{R_2 C_2 + 1}$, $B_r = A_f + B_{f1}$, $U_r = B_{f2} + U_f$, $E_r = D_f + E_{f1}$ and $V_r = V_f + E_{f2}$;
(ii) When $\alpha_1 = 1, \alpha_2 = 1$, $H_f(s, R, \mathbf{\Theta})$=$H_c(s, R, \mathbf{\Theta})$ with $A_c = A_f$, $B_c = B_{f1} + B_{f2}$, $U_c = U_f$, $D_c = D_f$, $E_c = E_{f1} + E_{f2}$, and $V_c = V_f$.

5.3.3 Population-level Degradation Performance Modeling

Existing studies mainly assess the degradation performance of an individual test unit. When multiple units are provided by the supplier or produced from the manufacturing process, their degradation performance cannot be identical and may vary from one to another due to material inhomogeneity and/or manufacturing variation. It will be desirable to develop a population-level degradation performance model to evaluate and quantify their underlying population variability, which is not available in individual-level modeling. Successful quantification of such variability can serve as a good metric to evaluate the quality of a material supplier and/or a manufacturing process. In addition, when the number of EIS response data is sparse, e.g., the number of observations is smaller than the number of model parameters, it may be difficult, if not impossible, to estimate the individual-level model and evaluate the degradation performance of an individual test unit. However, the population-level model is able to automatically and effectively pool information from other test units with more available data to compensate for the data scarcity and make individual-level model estimation possible (Gelman et al., 2013).

Considering K Al-alloy units of the same material type drawing from a large population, they are tested under the same environmental condition. The proposed population-level degradation performance model is essentially a three-level Bayesian hierarchical model and can be formulated as follows.

The level 1 model is specified for individual corroding Al-alloy unit. It is expressed as

$$
\begin{aligned}
&\boldsymbol{y}_{ik} \mid \boldsymbol{\Theta}_1, \boldsymbol{\Theta}_2, R_i, \omega_{ik} \sim MVN(\boldsymbol{\zeta}_{ik}, \sigma^2 I) \\
&\boldsymbol{\zeta}_{ik} = g_f(\boldsymbol{\Theta}_1, \boldsymbol{\Theta}_2, R_i, \omega_{ik}) = \begin{bmatrix} \left|H_f(j\omega_{ik}, R_i, \bar{\boldsymbol{\Theta}})\right| \cos \angle H_f(j\omega_{ik}, R_i, \bar{\boldsymbol{\Theta}}) \\ \\ \left|H_f(j\omega_{ik}, R_i, \bar{\boldsymbol{\Theta}})\right| \sin \angle H_f(j\omega_{ik}, R_i, \bar{\boldsymbol{\Theta}}) \end{bmatrix} \\
&\gamma_i = 10.9W/R_i
\end{aligned} \tag{5.40}
$$

where I is 2×2 identity matrix, and $\boldsymbol{y}_{ik}$, $i = 1, ..., K$, $k = 1, ..., m_i$ is the observed response of test unit i measured by frequency stimulus at frequency value ω_{ik}. There are m_i measurements totally collected for each unit i. R_i and γ_i are individual specific corrosion resistance and degradation rate of unit i, respectively. $\bar{\boldsymbol{\Theta}} = \{\boldsymbol{\Theta}_1, \boldsymbol{\Theta}_2\}$ represents the rest of unknown parameters shared among all units. $\boldsymbol{\Theta}_1, \boldsymbol{\Theta}_2$ are same to those defined in Eq. (5.39) of individual-level model. Prior distributions can be assigned to $\boldsymbol{\Theta}_1$, $\boldsymbol{\Theta}_2$, which will be elaborated in Section 5.4. The frequency response magnitude and phase can be written as $\left|H_f(j\omega_{ik}, R_i, \bar{\boldsymbol{\Theta}})\right| = \sqrt{\frac{r_{1i}(\omega_{ik}, R_i)^2 + r_{2i}(\omega_{ik}, R_i)^2}{r_{3i}(\omega_{ik}, R_i)^2 + r_{4i}(\omega_{ik}, R_i)^2}}$ and $\angle H_f(j\omega_{ik}, R_i, \bar{\boldsymbol{\Theta}}) = \left(\tan^{-1} \frac{r_{2i}(\omega_{ik}, R_i)}{r_{1i}(\omega_{ik}, R_i)} - \tan^{-1} \frac{r_{4i}(\omega_{ik}, R_i)}{r_{3i}(\omega_{ik}, R_i)}\right)$, respectively. The derivation details of $r_{1i}(\omega_{ik}, R_i)$ to $r_{4i}(\omega_{ik}, R_i)$ can be found in the Appendix Section B.2.2. The population-sharing parameters $\bar{\boldsymbol{\Theta}}$ can be justified from the following three aspects. First, units are tested under the same environmental conditions, such as the same solution concentration levels and pH values. Thus, model parameters, such as solution resistance R_1 among units, will be almost identical. Second, for other model parameters, such as capacitance parameters and fractional orders, due to the same material of units, they may not vary significantly. Moreover, since they are not the major parameters of interest in directly determining the degradation rate, in this work, they are specified as common parameters, which can be interpreted as the population average model parameters. Third, based on the population-sharing parameter specification, it becomes mathematically feasible to auto-

matically leverage information among units to compensate for the data scarcity and overcome estimation difficulty for those individual units with sparse response data.

The level 2 model is specified for multiple units drawn from the same underlying population. It can be expressed as

$$R_i \mid \boldsymbol{\theta}_R \sim G_{\boldsymbol{\theta}}(\cdot \mid \boldsymbol{\theta}_R) \tag{5.41}$$

where $G_{\boldsymbol{\theta}}(\cdot \mid \boldsymbol{\theta}_R)$ represents the distribution of the underlying population where multiple test units are drawn and $\boldsymbol{\theta}_R$ is a collection of population-level parameters. $G_{\boldsymbol{\theta}}(\cdot \mid \boldsymbol{\theta}_R)$ can be analogous to the distribution specified for the random effects in the mixed-effects models. In this work, to account for the positive support of R and the estimation convenience, we specify $G_{\boldsymbol{\theta}}(\cdot \mid \boldsymbol{\theta}_R)$ as log-normal distribution, i.e., $LN(\mu_R, \sigma_R^2)$. With $\boldsymbol{\theta}_R = \{\mu_R, \sigma_R^2\}$, the population average corrosion resistance and its population variability can be quantified explicitly as $E(R) = \exp(\mu_R + \frac{\sigma_R^2}{2})$ and $Var(R) = (\exp(\sigma_R^2) - 1)\exp(2\mu_R + \sigma_R^2)$, respectively. Based on the delta method (Oehlert, 1992), the corresponding mean and variability of degradation rate for the underlying population can be approximated as $\mathrm{E}(\gamma) = 10.9W/\exp(\mu_R + \frac{\sigma_R^2}{2})$ and $\mathrm{Var}(\gamma) = 118.81W^2 e^{-2\mu_R}(1 - e^{-\sigma_R^2})$.

The level 3 model is specified for hyper-prior of population quantity, written as

$$\boldsymbol{\theta}_R \mid \boldsymbol{\phi} \sim \pi(\boldsymbol{\theta}_R \mid \boldsymbol{\phi}) \tag{5.42}$$

where $\pi(\boldsymbol{\theta}_R \mid \boldsymbol{\phi})$ is the joint hyper-prior density for the population-level parameters $\boldsymbol{\theta}_R$ and $\boldsymbol{\phi}$ is a collection of hyper-parameters. In this work, independent normal prior $N(\mu, \tau^2)$ and inverse gamma prior $IG(\rho, \beta)$ are specified for μ_R and σ_R^2, respectively, due to their conjugate relationship with $G_{\boldsymbol{\theta}}(\cdot \mid \boldsymbol{\theta}_R)$, where μ and τ^2 are mean and variance of $N(\cdot)$, ρ and β are shape and scale parameters of $IG(\cdot)$.

Both the proposed individual-level and population-level models can be also viewed from the directed acyclic graph (DAG) perspective, as shown in Figure 5.51. They are

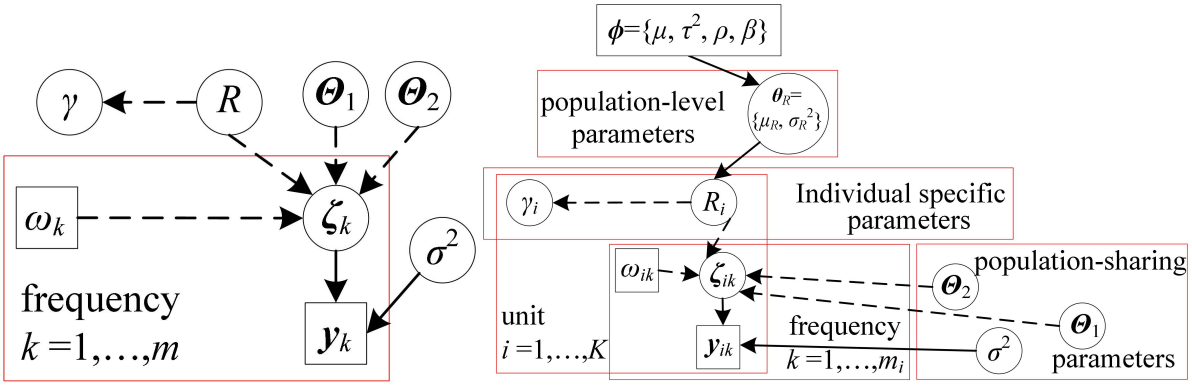

(a) DAG of individual-level model (b) DAG of population-level model

Figure 5.51: Graphical representations of proposed models

one-level and three-level Bayesian hierarchical models, respectively. Square nodes represent either the observed response data or the specified hyper-parameter settings. Circle nodes represent the unknown model parameters to be estimated. The solid and dashed lines indicate the stochastic and deterministic relationship between the connected nodes, respectively. Compared to the conventional Bayesian hierarchical models where empirical relationship is often constructed among different nodes, the proposed models incorporate the complex physical failure mechanism of the corrosion-induced degradation process into the first level of the model structure. Therefore, they can be viewed as a hybrid model with both physical and statistical modeling features. It is also noticed that the transfer function $H_f(\cdot)$ is considered to capture the complex degradation process of corroding Al-alloy units. For other corroding metallic units, $H_f(\cdot)$ can be replaced with other material specific transfer function and the model structure will remain the same as the proposed individual-level and population-level models.

5.4 Model Estimation

To estimate the model parameters, nonlinear least squares (NLS) estimation (Ran et al., 2010) is mainly utilized in the existing EIS-based corrosion studies. Moreover, the degradation performance assessment is restricted to an individual test unit. In this work,

Bayesian estimation method is employed to estimate both individual- and population-level models. Bayesian estimation is considered because (i) it allows the quantification of model parameters (e.g., corrosion resistance, degradation rate, etc.) uncertainty due to the limited sample size of EIS data (Qin et al., 2015; Zhang et al., 2014; Wang et al., 2013), and (ii) it further provides richer estimation results (e.g., both point and interval estimation) than NLS method. For NLS, point estimation is often obtained with parameters uncertainty quantification neglected. At population level, Bayesian estimation also enables the information sharing among multiple test units to overcome the NLS estimation difficulty in evaluating an individual test unit when its available data is sparse. The details of developed estimation algorithms for both individual-level and population-level models under Bayesian estimation framework will be elaborated as follows.

5.4.1 Individual-level Model Estimation

Considering an individual corroding Al-alloy test unit with m frequency response observations, the available data for estimating individual-level model can be denoted as $\mathbf{D}_{\text{ind}} = \{\boldsymbol{y}_k, \omega_k\}_{k=1}^{m}$, where $\boldsymbol{y}_k$ represents the observed real and imaginary parts of frequency response at stimulus with frequency ω_k, i.e., $\boldsymbol{y}_k = [y^R(\omega_k), y^I(\omega_k)]^{\mathrm{T}}$. Based on the proposed model in Eq. (5.39), the corresponding likelihood function $L(\boldsymbol{\Theta}, R, \sigma^2 \mid \mathbf{D}_{\text{ind}})$ can be written as

$$L(\boldsymbol{\Theta}, R, \sigma^2 \mid \mathbf{D}_{\text{ind}}) = \prod_{k=1}^{m} \frac{1}{2\pi\sigma^2} \exp\left[-\frac{\chi}{2\sigma^2}\right] \tag{5.43}$$

where $\chi = \left(\boldsymbol{y}_k - g_f(\omega_k, R, \boldsymbol{\Theta})\right)^{\mathrm{T}} \left(\boldsymbol{y}_k - g_f(\omega_k, R, \boldsymbol{\Theta})\right)$. Under Bayesian estimation and inference framework, the joint posterior $\pi(\boldsymbol{\Theta}, R, \sigma^2 \mid \mathbf{D}_{\text{ind}})$ of the individual-level model can be written as

$$\pi(\boldsymbol{\Theta}, R, \sigma^2 \mid \mathbf{D}_{\text{ind}}) \propto (\sigma^2)^{-m} \exp\left(-\frac{\Xi_1}{2\sigma^2}\right) \pi(\boldsymbol{\Theta})\pi(R)\pi(\sigma^2) \tag{5.44}$$

where $\Xi_1 = \sum_{k=1}^{m} \left(\boldsymbol{y}_k - g_f(\omega_k, R, \boldsymbol{\Theta})\right)^{\mathrm{T}} \left(\boldsymbol{y}_k - g_f(\omega_k, R, \boldsymbol{\Theta})\right)$ and $\pi(\cdot)$ denotes an arbitrary probability density function. $\pi(R)$, $\pi(\boldsymbol{\Theta})$ and $\pi(\sigma^2)$ are prior distribution densities for the corrosion resistance R, the rest of model parameters $\boldsymbol{\Theta}$ and the variance of error term, respectively. Since $\boldsymbol{\Theta}_1$ and R are positive and $\boldsymbol{\Theta}_2$ is between 0 and 1, truncated normal and uniform distributions are assumed, respectively. When prior knowledge is not available, a less-informative truncated normal prior with large variance can be specified for $\boldsymbol{\Theta}_1$ or R, while a non-informative prior, such as $Unif(0,1)$ can be specified for $\boldsymbol{\Theta}_2$. Conjugate prior is available for σ^2, which can be specified as the inverse gamma distribution, i.e., $\sigma^2 \sim IG(a,b)$, where a and b are shape and scale parameters, respectively. When no prior knowledge is available, a less-informative prior can be utilized with small values of a and b being specified. The full conditional posterior distribution for σ^2 can then be conveniently written as

$$\pi(\sigma^2 \mid \boldsymbol{\Theta}, R, \mathbf{D}_{\text{ind}}) \sim IG\left(a + m, b + \frac{\Xi_1}{2}\right) \tag{5.45}$$

Due to the highly nonlinear model structure in $H_f(\cdot)$, there are no conjugate priors available for physical model parameters R and $\boldsymbol{\Theta}$. Thus, we consider the general purpose of Metropolis-Hastings (M-H) algorithm (Roberts and Sahu, 1997). It is also noticed that when other corroding metallic units are investigated by replacing H_f with other form of transfer function, the M-H sampling procedure will remain the same. The Bayesian sampling algorithm for individual-level model estimation is summarized in Algorithm 6. The model parameters R and $\boldsymbol{\Theta}$ are initialized based on prior physical knowledge. $\iota_{\max}$ is the maximum number of iterations. Heidelberg and Welch diagnostic test (Heidelberger and Welch, 1983) are considered to identify the burn-in iterations and further ensure sampling convergence. The outputs of Algorithm 6 are posterior samples of R and $\boldsymbol{\Theta}$. Bayesian point estimates (e.g., posterior mean) and interval estimates (e.g., 95% credible interval) can be calculated conveniently from the posterior samples. Based on Stern-Geary equa-

Algorithm 6 Sampling algorithm of individual model

Initialization: $\boldsymbol{\Theta}^{(0)}$, $R^{(0)}$, $\sigma^{2^{(0)}} \sim \pi(\sigma^2)$

procedure DRAWSAMPLES

for $\iota \leftarrow 1, \iota_{\max}$ **do**

generate $R^{(\iota)}$ from $R \mid \boldsymbol{\Theta}^{(\iota-1)}, \sigma^{2^{(\iota-1)}}, \mathbf{D}_{\text{ind}}$ by M-H algorithm

generate $\boldsymbol{\Theta}^{(\iota)}$ from $\boldsymbol{\Theta} \mid R^{(\iota)}, \sigma^{2^{(\iota-1)}}, \mathbf{D}_{\text{ind}}$ by M-H algorithm

generate $\sigma^{2^{(\iota)}}$ from $\sigma^2 \mid \boldsymbol{\Theta}^{(\iota)}, R^{(\iota)}, \mathbf{D}_{\text{ind}}$ by Eq. (5.45)

calculate degradation rate $\gamma^{(\iota)}$ by Eq. (5.39)

end for

end procedure

tion $\gamma = 10.9W/R$, posterior samples of latent degradation rate γ can also be obtained from the posterior samples of R.

5.4.2 Population-level Model Estimation

To further estimate the population-level model, a sample of K Al-alloy units are considered and tested. For unit i, m_i response observations are collected by EIS instrument. The available data for population-level modeling are denoted as $\mathbf{D}_{\text{pop}} = \{\boldsymbol{y}_{ik}, \omega_{ik}\}_{i=1,\ldots,K}^{k=1,\ldots,m_i}$, where $\boldsymbol{y}_{ik}$ is the frequency response of unit i at stimulus with frequency ω_{ik}. The available data of individual unit i are defined as $\mathbf{D}_{\text{ind},i} = \{\boldsymbol{y}_{ik}, \omega_{ik}\}_{k=1}^{m_i}$. Based on the proposed population-level model, conventional maximum likelihood estimation method aims to maximize the marginalized likelihood function, which can be written as

$$L(\boldsymbol{\theta}_R, \bar{\boldsymbol{\Theta}}, \sigma^2 \mid \mathbf{D}_{\text{pop}}) = \prod_{i=1}^{K} \int_0^{\infty} \prod_{k=1}^{m_i} \frac{1}{2\pi\sigma^2} \exp(-\frac{\chi_i}{2\sigma^2}) \pi(R_i) \mathrm{d}R_i \tag{5.46}$$

where $\chi_i = \big(\boldsymbol{y}_{ik} - g_f(\omega_{ik}, R_i, \bar{\boldsymbol{\Theta}})\big)^{\mathrm{T}} \big(\boldsymbol{y}_{ik} - g_f(\omega_{ik}, R_i, \bar{\boldsymbol{\Theta}})\big)$. As shown in Eq. (5.46), the individual corrosion resistances R_i's (or equivalently, the latent degradation rates γ_i's) are not estimated. To jointly estimate the individual parameters R_i's and γ_i as well as

the population-level parameters $\boldsymbol{\theta}_R = \{\mu_R, \sigma_R^2\}$, a full Bayesian approach is considered. Specifically, the joint posterior density $\pi(\boldsymbol{\theta}_R, \bar{\boldsymbol{\Theta}}, \sigma^2, \{R_i\}_{i=1}^K \mid \mathbf{D}_{\text{pop}})$ can be written as

$$\pi(\boldsymbol{\theta}_R, \bar{\boldsymbol{\Theta}}, \sigma^2, \{R_i\}_{i=1}^K \mid \mathbf{D}_{\text{pop}}) \propto (\sigma^2)^{-\sum_{i=1}^K m_i} \exp\left(-\frac{\Xi_2}{2\sigma^2}\right) \pi(\bar{\boldsymbol{\Theta}})\pi(\sigma^2) \cdot \prod_{i=1}^K G_\theta(R_i \mid \boldsymbol{\theta}_R) \cdot \pi(\boldsymbol{\theta}_R) \tag{5.47}$$

where $\Xi_2 = \sum_{i=1}^K \sum_{k=1}^{m_i} \left(\boldsymbol{y}_{ik} - g_f(\omega_{ik}, R_i, \bar{\boldsymbol{\Theta}})\right)^{\mathrm{T}} \left(\boldsymbol{y}_{ik} - g_f(\omega_{ik}, R_i, \bar{\boldsymbol{\Theta}})\right)$. $G_\theta(R_i \mid \boldsymbol{\theta}_R)$ is specified as a log-normal distribution, as described in Eq. (5.41). $\pi(\bar{\boldsymbol{\Theta}})$ and $\pi(\sigma^2)$ are prior distribution densities for the population-sharing parameters and the variance of error term, respectively. Conjugate prior is available for σ^2, e.g., $\sigma^2 \sim IG(a, b)$. Due to the log-normal distribution form assumed for $G_\theta(R_i \mid \boldsymbol{\theta}_R)$, conjugate priors are also available for μ_R and σ_R^2. They are specified as normal and inverse gamma priors, respectively. When prior knowledge is not available, less-informative priors can be specified similarly to those discussed in Section 5.4.1. With the above conjugate priors, the full conditional posterior densities can then be conveniently written as

$$\mu_R \mid \{R_i\}_{i=1}^K, \sigma_R^2 \sim N\left(\frac{\left(\sum_{i=1}^K \ln R_i\right)\tau^2 + \mu\sigma_R^2}{K\tau^2 + \sigma_R^2}, \frac{\sigma_R^2\tau^2}{K\tau^2 + \sigma_R^2}\right) \tag{5.48}$$

$$\sigma_R^2 \mid \{R_i\}_{i=1}^K, \mu_R \sim IG\left(\rho + \frac{K}{2}, \beta + \frac{1}{2}\sum_{i=1}^K (\ln R_i - \mu_R)^2\right) \tag{5.49}$$

$$\sigma^2 \mid \bar{\boldsymbol{\Theta}}, \{R_i\}_{i=1}^K, \mathbf{D}_{\text{pop}} \sim IG\left(a + \sum_{i=1}^K m_i, b + \frac{1}{2}\Xi_2\right) \tag{5.50}$$

For other parameters, e.g., $\bar{\boldsymbol{\Theta}} = \{R_1, R_2, C_1, C_2, \alpha_1, \alpha_2\}$, conjugate priors are not available, since high nonlinearity is involved in the relationship between the degradation performance and EIS response data, as captured by the function mapping $g_f(\cdot)$ in Eq. (5.40). Thus, M-H sampling method is considered to draw samples of these parameters. The overall sampling algorithm for the population-level model is summarized in Algorithm 7.

Algorithm 7 Sampling algorithm of population model

Initialization: $\bar{\boldsymbol{\Theta}}^{(0)}$, $(\sigma^{2^{(0)}}, \mu_R^{(0)}, \sigma_R^{2^{(0)}}) \sim \pi(\sigma^2, \mu_R, \sigma_R^2)$

$R_i^{(0)} \sim LN(\mu_R^{(0)}, \sigma_R^{2^{(0)}}), \forall i = 1, ..., K$

procedure DRAWSAMPLES

for $\iota \leftarrow 1, \iota_{\max}$ **do**

generate $\bar{\boldsymbol{\Theta}}^{(\iota)}$ from $\bar{\boldsymbol{\Theta}} | \sigma^{2^{(\iota-1)}}, \{R_i^{(\iota-1)}\}_{i=1}^K, \mathbf{D}_{\text{pop}}$ by M-H algorithm

generate $R_i^{(\iota)}$ from $R_i \mid \bar{\boldsymbol{\Theta}}^{(\iota)}, \mu_R^{(\iota-1)}, \sigma_R^{2^{(\iota-1)}}, \sigma^{2^{(\iota-1)}}, \mathbf{D}_{\text{ind},i}, \forall i$ by M-H algorithm

generate $\mu_R^{(\iota)}$ from $\mu_R \mid \{R_i^{(\iota)}\}_{i=1}^K, \sigma_R^{2^{(\iota-1)}}$ by Eq. (5.48)

generate $\sigma_R^{2^{(\iota)}}$ from $\sigma_R^2 \mid \{R_i^{(\iota)}\}_{i=1}^K, \mu_R^{(\iota)}$ by Eq. (5.49)

generate $\sigma^{2^{(\iota)}}$ from $\sigma^2 \mid \bar{\boldsymbol{\Theta}}^{(\iota)}, \{R_i^{(\iota)}\}_{i=1}^K, \mathbf{D}_{\text{pop}}$ by Eq. (5.50)

calculate individual degradation rate $\{\gamma_i^{(\iota)}\}_{i=1}^K$ by Eq. (5.40)

end for

end procedure

Similar to Algorithm 6, Heidelberg and Welch diagnostic test is performed to ensure the algorithm convergence. Posterior samples of unknown parameters can be also extracted to make Bayesian inference and to quantify uncertainty of model parameters.

Based on the proposed population-level model, both the parameters uncertainty of degradation performance for an individual unit and the population variability of degradation performance for the underlying population can be explicitly quantified. Specifically, the parameters uncertainty of existing individual unit i under investigation is characterized by the posterior density $\pi(\gamma_i|\mathbf{D}_{\text{pop}})$. The corrosion resistance variability of the underlying population where a finite number of existing units are drawn from is characterized by $LN(\hat{\mu}_R, \hat{\sigma}_R^2)$, where $\hat{\mu}_R$ and $\hat{\sigma}_R^2$ are point estimates (e.g., posterior mode) calculated from their corresponding posterior densities $\pi(\mu_R|\mathbf{D}_{\text{pop}})$ and $\pi(\sigma_R^2|\mathbf{D}_{\text{pop}})$. The mean and variance of degradation rate for the underlying population can be approximately quantified (based on the delta method) as $\mathrm{E}(\gamma) = 10.9W/\exp(\hat{\mu}_R + \frac{\hat{\sigma}_R^2}{2})$ and $\mathrm{Var}(\gamma) = 118.81W^2 e^{-2\hat{\mu}_R}(1 - e^{-\hat{\sigma}_R^2})$. For any future test unit drawn from the same pop-

ulation, $LN(\hat{\mu}_R, \hat{\sigma}_R^2)$ can be also viewed as the prior knowledge elicited, i.e., $R_{\text{new}} \sim LN(\hat{\mu}_R, \hat{\sigma}_R^2)$, where R_{new} is the corrosion resistance of a future test unit. Such prior can be utilized as informative prior knowledge to guide the experimental data collection of future test units and achieve the same estimation precision with a smaller sample size of test data (Li et al., 2017b).

Another feature of the population-level model is its capability of borrowing information from multiple test units to overcome the difficulty of estimating individual-level model when the test data of the individual test unit is sparse. The rationale is that in Algorithm 7, population-sharing parameters are estimated and updated by all available data $\mathbf{D}_{\text{pop}}$ pooled together from multiple test units. The remaining individual specific parameter R_i can be estimated and updated with the individual data $\mathbf{D}_{\text{ind},i}$ and previously updated $\hat{\hat{\mathbf{\Theta}}}$. In the case that $\mathbf{D}_{\text{ind},i}$ is sparse and has a smaller number of observations than the number of model parameters in the individual-level model, e.g., Eq. (5.39), nevertheless, it is adequate to estimate a single parameter R_i in the population-level model. It is also noticed that both Algorithm 6 and Algorithm 7, are generic and applicable to estimating EIS-based models of other corroding metallic units, such as Magnesium-alloy.

5.4.3 Reliability Analysis

The estimated degradation performance can be further utilized to calculate important reliability quantities, such as the reliability function of remaining useful life (RUL). Given a fixed thickness ν_d of the Al-alloy unit, the corrosion-induced failure will occur when the corrosion depth exceeds the thickness of Al-alloy. The RUL T_c refers to the remaining time elapsed until the occurrence of such failure given the current corrosion depth ν_l. The estimated reliability function of unit i can be expressed as

$$\begin{aligned}\hat{S}_i(t_c \mid \mathbf{D}_{\text{ind}}) &= \Pr(T_c > t_c \mid \mathbf{D}_{\text{ind}}) = \Pr(\nu_l + \gamma_i t_c < \nu_d \mid \mathbf{D}_{\text{ind}}) \\ &= \Pr(\nu_l + \frac{10.9 W t_c}{R_i} < \nu_d \mid \mathbf{D}_{\text{ind}}) \end{aligned} \tag{5.51}$$

where R_i is drawn from $\pi(R_i \mid \mathbf{D}_{\text{ind}})$. Individual reliability estimate incorporates parameters uncertainty of an individual unit. The estimated reliability function of the overall population can be expressed as

$$\begin{aligned}\hat{S}(t_c \mid \mathbf{D}_{\text{pop}}) &= \Pr(T_c > t_c \mid \mathbf{D}_{\text{pop}}) = \Pr(\nu_l + \gamma t_c < \nu_d \mid \mathbf{D}_{\text{pop}}) \\ &= \Pr(\nu_l + \frac{10.9Wt_c}{R} < \nu_d \mid \mathbf{D}_{\text{pop}}) \end{aligned} \tag{5.52}$$

where $R \sim LN(\hat{\mu}_R, \hat{\sigma}_R^2)$. The population reliability estimate incorporates the population variability. Consider a new unit from the underlying population, $LN(\hat{\mu}_R, \hat{\sigma}_R^2)$ can be further utilized as its prior before testing and data collection are performed. Eq. (5.52) can be also viewed as the prior reliability function of a new test unit. Once its testing is performed and individual data is incorporated for model estimation, the posterior reliability function becomes Eq. (5.51).

5.4.4 Discussion

The development of the proposed models and estimation procedures is motivated by the degradation performance assessment of corroding Al-alloy units. Thus, it can be widely applied to corrosion testing/inspection of many mission-critical engineering components made of Al-alloy, such as aircraft wing, high-speed train gearbox, low-cost fuel cell and nuclear reactor. In addition, the proposed work also has several general implications, which allow its great potential in improving degradation performance assessment of other corroding metallic units at different phases, ranging from the laboratory testing of bio-degradable Magnesium (Mg) at early design phase to the field inspection of rebar corrosion in deteriorating bridges at field operational phase.

First, the fractional order system dynamics is considered in this work to relax the integer order assumption in the conventional EIS-based physical models (e.g., Eq. (5.36) and Eq. (5.37) described in Section 5.3.1). With its more generic and flexible transfer func-

tion form, the modeling accuracy will be improved. This concept not only holds for Al-alloy units, but also for other corroding metallic units, such as Mg implants utilized in biomedical field (e.g., Mg-based bone screws, plates and anchors (Kirkland et al., 2012; Windhagen et al., 2013)). Mg implants are promising alternatives to permanent metallic implants widely used in orthopedic surgeries for bone fracture healing and repairs nowadays. They offer the great benefit of avoiding secondary surgery intervention. One critical issue in developing reliable Mg implants is their rapid corrosion-induced degradation. To assess the degradation performance of Mg implants, conventional EIS-based model, such as SRC model in Section 5.3.1, is often utilized. We will give a real case study to demonstrate that by incorporating fractional order system dynamics, the modeling accuracy can be improved with better goodness-of-fit to real EIS data.

Second, the proposed population-level model in Eq. (5.40) is quite generic and not problem specific. The transfer function $H_f(\cdot)$ can be replaced by any other form of transfer function as long as the transfer function adopted could successfully capture the corrosion complexity of the investigated test units. Therefore, the application context of the proposed work will not be constrained to a specific type of corroding unit (e.g., Al-alloy unit). It can be broadly applied to different types of corroding units using EIS testing. Moreover, Bayesian estimation also advances the conventional least squares estimation method which is widely adopted in most of EIS data analysis. It quantifies the model parameters uncertainty due to the limited sample size of available test data. It also allows information sharing among multiple test units to overcome the estimation difficulty in evaluating an individual test unit when its EIS data is sparse. These appealing features are also generic and can be beneficial to EIS-based degradation performance assessment of different corroding units in general.

5.5 Case Study

To illustrate the proposed Bayesian physical-statistical model and to demonstrate its effectiveness and generality in assessing and quantifying degradation performance of corroding metallic units, two types of test units, namely, Al-alloy specimens for aircraft coatings and Mg-alloy specimens for biomedical implants, are considered.

5.5.1 Case I: Corrosion-induced Degradation of Al-alloy

Alloying pure Al with appropriate transition metal, such as manganese (Mn), is found to be an effective method in improving the strength of the material and has been widely utilized to develop high-strength aircraft coatings for the purpose of environmental protections. However, alloying may significantly affect the corrosion-induced degradation of Al-alloy units in saline environments due to the change of its micro-structure. To evaluate the degradation performance, corrosion immersion tests for Al-Mn units with the same Mn composition of 20.5 at.% (atomic percentage) are carried out in NaCl solution with the same concentration level of 3.5 wt.% (weight percentage). Due to the limited laboratory testing resources available, EIS data of four Al-Mn test units are measured using non-destructive testing technique, with sample size ranging from six to thirty-six measurements per test unit.

5.5.1.1 Individual-level Performance Evaluation

For an individual Al-Mn unit, the performance of the proposed individual-level model is first evaluated and compared with some existing alternative models, such as SRC model and FC model. Figure 5.52a displays the comparison results in the complex plane (He and Mansfeld, 2009), where the horizontal axis refers to real part of EIS response data and vertical axis refers to imaginary part. Compared to the predicted response curves based on the conventional SRC model (in dashed black) and FC model (in dashed blue),

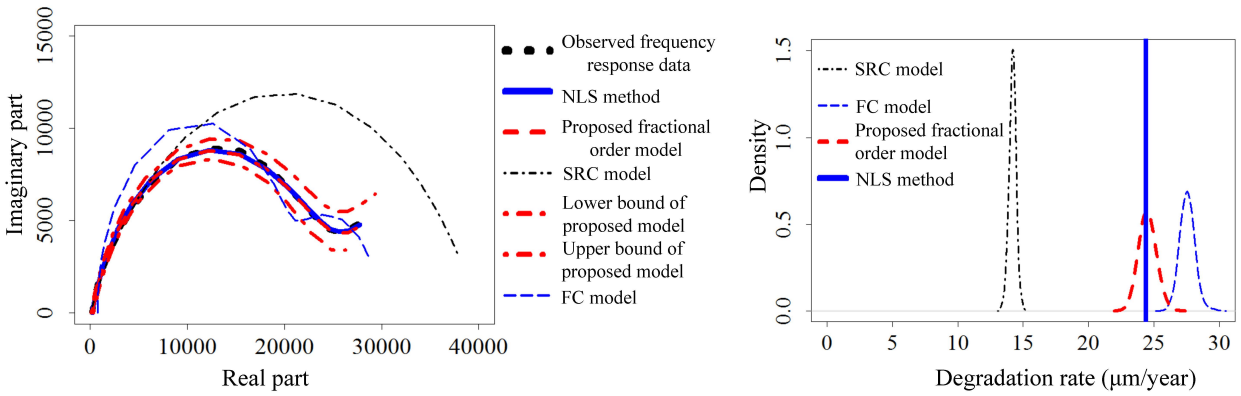

(a) Prediction comparison

(b) Degradation rate comparison

Figure 5.52: Performance comparison of different modeling approaches

the predicted curve based on the proposed model (in dashed red) is closer to the observed EIS responses (in black dot) and exhibits superior prediction performance. It is mainly attributed to its more generic and flexible representation using fractional order system dynamics in characterizing more realistic degradation behavior of corroding Al-Mn unit. Figure 5.52a further compares the prediction performances of the proposed model using different estimation methods, namely, the proposed Bayesian method and the conventional NLS method commonly adopted in commercial EIS software, such as Gamry and Metrohm. The prediction results based on Bayesian point estimates (e.g., posterior mode) in dashed red curve and predicted performance based on NLS estimates in solid blue curve are similar and they are both close to the observed responses. Compared to NLS method, which only delivers point estimates, Bayesian estimation method allows richer estimation results by quantifying exactly the parameters uncertainty, which can be characterized by 95% credible intervals of predicted performance (in red dot), as shown in Figure 5.52a. The lower and upper bounds of predicted curves completely cover the observed EIS curve. Figure 5.52b compares the estimated degradation rates using different models and estimation methods. SRC and FC models underestimate and overestimate the degradation rate of Al-Mn unit. The proposed model under Bayesian estimation and

inference framework is able to quantify the parameters uncertainty and can give richer information than the conventional models using NLS method.

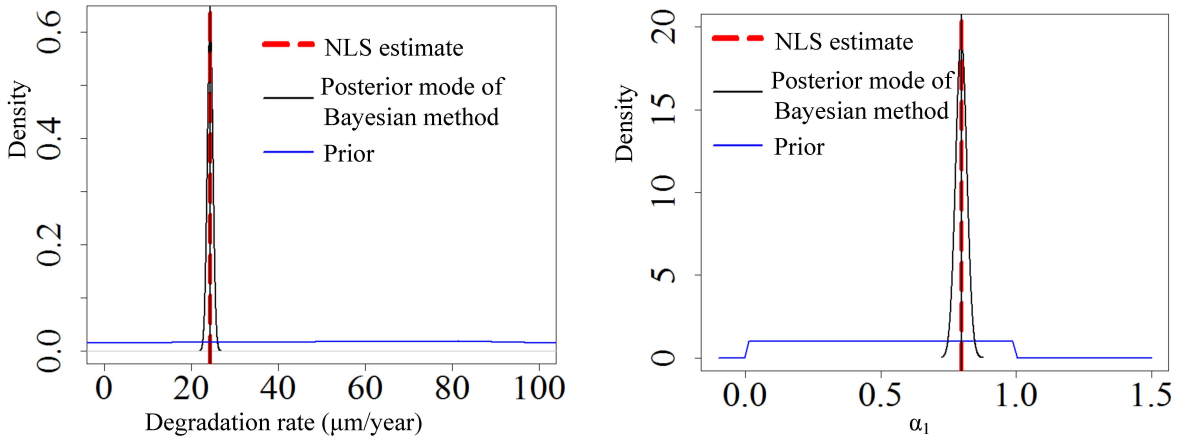

(a) Estimated degradation rate γ (b) Estimated fractional order parameter α_1

Figure 5.53: Results comparison based on different estimation methods

Figure 5.53 further shows the prior and posterior densities of model parameters γ and α_1. Non-informative priors are specified, i.e., $R \sim TN(0, 10^{20})$ and $\alpha_1 \sim Unif(0,1)$. As shown in Figure 5.53, posterior densities are mainly dominated by the EIS data while non-informative priors play less significant roles in final estimation results. Therefore, point estimates between Bayesian and NLS methods are similar.

Table 5.15: Estimation results of individual-level model

Parameters	Point estimation from NLS method	Proposed method	
		Posterior mean	95% Credible interval
$R_1(\Omega)$	1.991×10^{-2}	2.154×10^{-2}	1.629×10^{-2}, 2.768×10^{-2}
$R(\Omega)$	2.321×10^{4}	2.327×10^{4}	2.239×10^{4}, 2.364×10^{4}
$R_2(\Omega)$	3.364×10^{6}	1.009×10^{6}	0.315×10^{6}, 3.814×10^{6}
α_1	0.799	0.797	0.790, 0.812
C_1(F)	1.346×10^{-5}	1.349×10^{-5}	1.302×10^{-5}, 1.376×10^{-5}
α_2	0.417	0.411	0.367, 0.451
C_2(F)	5.000×10^{-4}	4.835×10^{-4}	3.964×10^{-4}, 5.706×10^{-4}
$\gamma(\mu m\, yr^{-1})$	2.442×10^{1}	2.435×10^{1}	2.396×10^{1}, 2.477×10^{1}

Table 5.15 summarizes the estimation results for all model parameters. It is noticed that we run the Bayesian sampling algorithm for 22000 iterations and the first 2000 iterations are selected as burn-in iterations. Thus, both of the posterior mean and the 95% credible internals are calculated based on the remaining 20000 posterior samples. Bayesian convergence tests, such as Heidelberg and Welch diagnostic tests (Heidelberger and Welch, 1983), are further performed to ensure the good convergence of the algorithm. Posterior means of the estimated model parameters are similar to NLS results since less informative priors are specified. In addition, Bayesian interval estimates completely cover the NLS results. It is also noticed that for fractional order parameters, such as α_1 and α_2, both of the posterior means and the 95% credible intervals are between zero and one. Analytically, based on the proposed Theorem, it implies that the reduced model structures, such as SRC and FC models with integer orders, are not appropriate in characterizing the actual degradation performance of corroding Al-Mn unit. Physically, it implies that in the actual degradation of corroding Al-Mn unit, the corrosion products at surface of extra layer and the penetrated solution at the substrate interface have non-negligible effects on electrons transfer.

5.5.1.2 Population-level Performance Evaluation

To further evaluate the degradation performance variability of the underlying population, the population-level degradation model is considered to jointly analyze the EIS data of 4 available Al-Mn test units. One test unit (denoted as unit 1), has 6 EIS measurements, which is smaller than the number of model parameters. It becomes difficult to estimate the individual-level model due to the inadequate available data. The proposed Bayesian population-level model, however, is able to overcome such data sparsity issue and evaluate the individual degradation performance by information sharing among multiple units of the underlying population. Figure 5.54 shows the estimated degradation rates for all 4 units. For unit 1, NLS estimation becomes infeasible while the population-level model

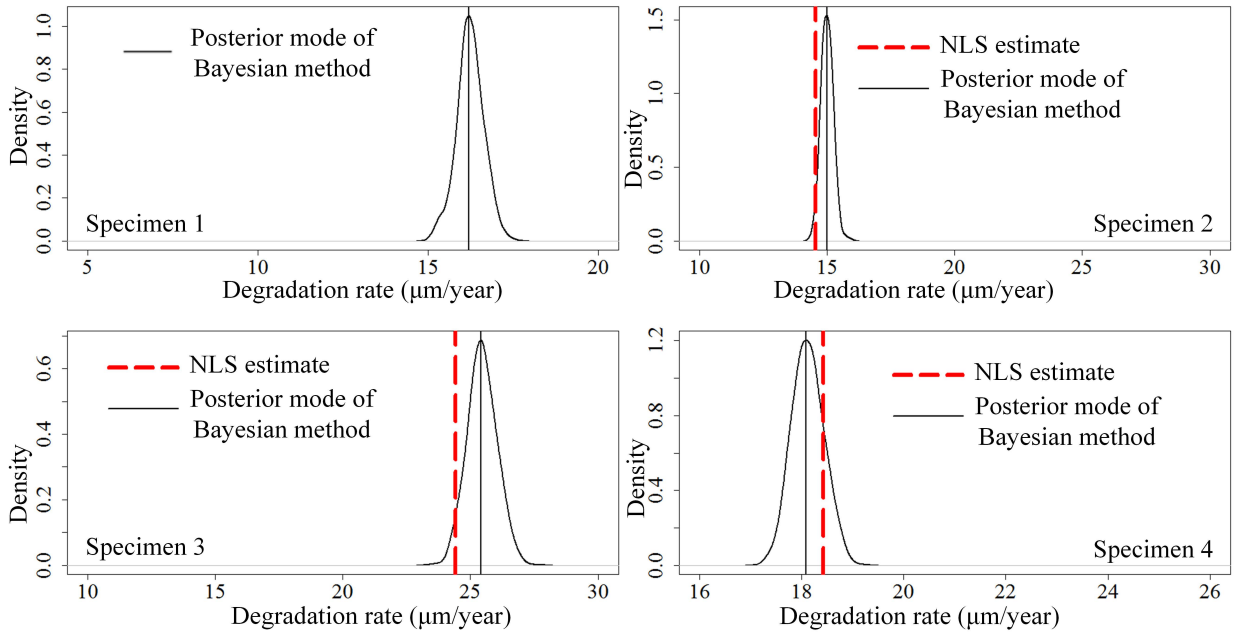

Figure 5.54: Estimated degradation rates comparison

can give valid estimation. For units 2-4, the estimated degradation performances obtained from the proposed population-level model are slightly different from the results of individual-level model using NLS method. Such slight discrepancy is mainly attributed to the effects of population-sharing parameters specified in the population-level model. However, the discrepancy between the point estimates is small, and the interval estimates (e.g., 95% credible intervals) can still completely cover the NLS estimation results.

Figure 5.55 further shows the predicted EIS curves of population-level model in the complex plane. The predicted EIS curves are obtained based on Bayesian posterior mode of model parameters. They successfully capture the overall trend of the observed data. The overall model complexity of proposed population-level model is reduced by utilizing population-sharing parameters.Figure 5.55 shows that such reduction of model complexity does not affect the prediction performance and the goodness-of-fit of EIS data is satisfactory. Moreover, due to sparse EIS data of unit 1 with low frequency data not collected, its EIS curve pattern is different from other units. Figure 5.55a demonstrates that the estimation result of unit 1 is valid. It is noticed that the goodness-of-fit of unit 1 is

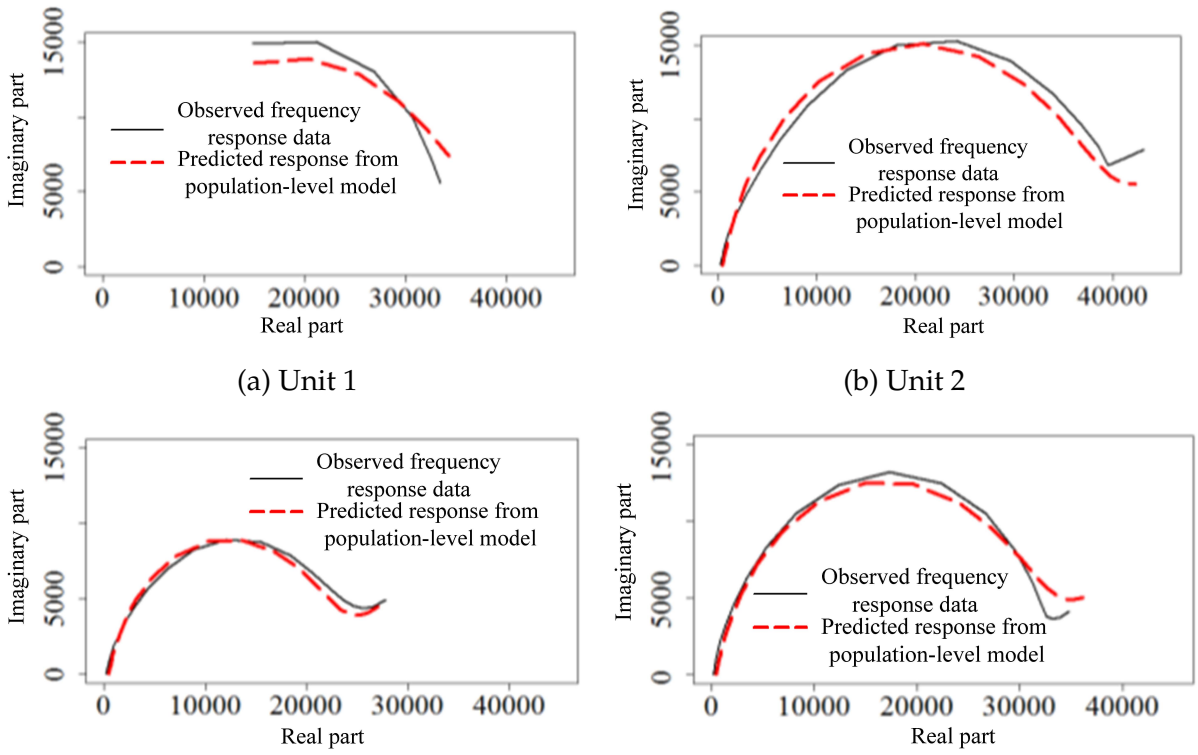

(a) Unit 1 (b) Unit 2

(c) Unit 3 (d) Unit 4

Figure 5.55: Prediction performance evaluation of population-level model

not as good as other units which have sufficient available data. It is mainly because even though the propagated information can make estimation feasible, they cannot be treated as equally important as the observed data of unit 1 itself.

Another appealing feature of the population-level model is its capability of estimating the population-level quantities, such as the estimated average corrosion resistance $\exp(\hat{\mu}_R + \frac{\hat{\sigma}_R^2}{2})$ and the estimated corrosion resistance variability $(\exp(\hat{\sigma}_R^2) - 1)\exp(2\hat{\mu}_R + \hat{\sigma}_R^2)$, which cannot be obtained from individual-level model. Approximated by delta method, the estimated average degradation performance and its population variability can then be quantified as $\mathrm{E}(\gamma) = 10.9W/\exp(\hat{\mu}_R + \frac{\hat{\sigma}_R^2}{2})$ and $\mathrm{Var}(\gamma) = 118.81W^2e^{-2\hat{\mu}_R}(1 - e^{-\hat{\sigma}_R^2})$, respectively. The proposed population-level model has the capability of quantifying both parameters uncertainty of every individual unit and the population variability of multiple units. Figure 5.56 shows both parameters uncertainty of each unit, which is captured by the corresponding posterior density $\pi(\gamma_i|\mathbf{D}_{\text{pop}})$, and the population-level quan-

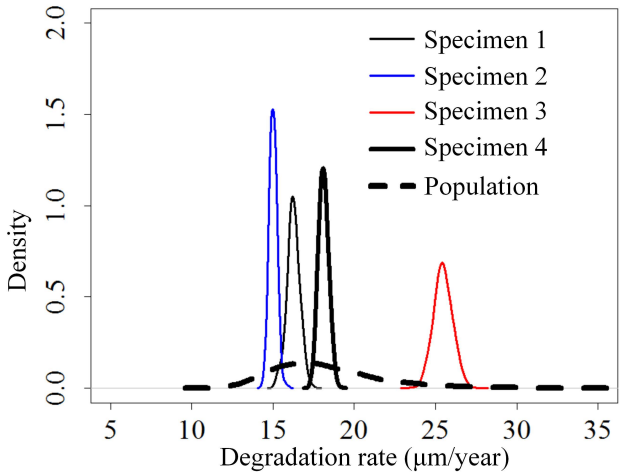

Figure 5.56: Quantification of parameter uncertainty and population variability

tities such as $E(\gamma) \approx 17.7$ micrometer per year (μm/year) and $Var(\gamma) \approx 9.0\ \mu m^2$/year. The quantified population variability can also be utilized as the prior knowledge of degra-

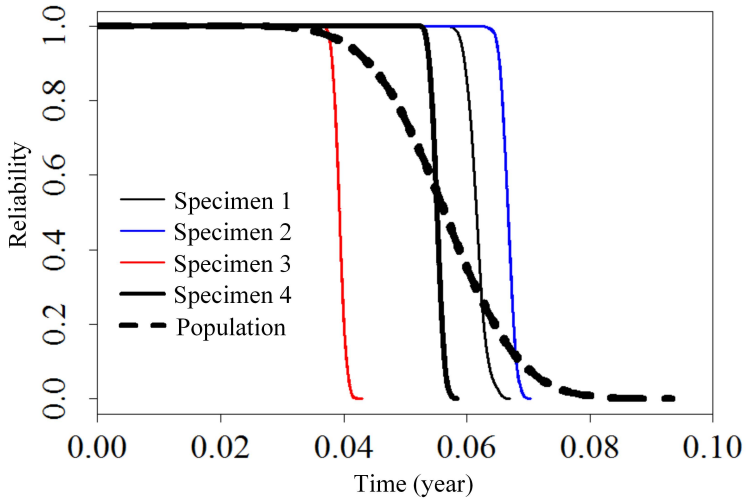

Figure 5.57: K-M curves for individual units RUL and population average RUL

dation performance for a new individual unit before collecting its response data. Assuming the overall thickness of each unit as $\nu_d = 1.5\mu$m and the existing corrosion depth as $\nu_l = 0.5\mu$m, the reliability curves of each individual unit's RUL and the overall population RUL can also be calculated, as described in Eq. (5.51) and Eq. (5.52), respectively. Figure 5.57 shows both the corresponding Kaplan-Meier (K-M) curves of individual units and the overall population.

5.5.2 Case II: Corrosion-induced Degradation of Mg-alloy

To show that the proposed model framework is also beneficial to assess degradation performance of other metallic units, a second real case study on Mg-alloy specimens for developing the next-generation bio-degradable medical implants is further conducted. EIS instruments are utilized to collect the non-destructive testing data of 3 Mg-alloy units. The sample size of EIS measurements of 3 units varies from 26 to 31. Figure 5.58 com-

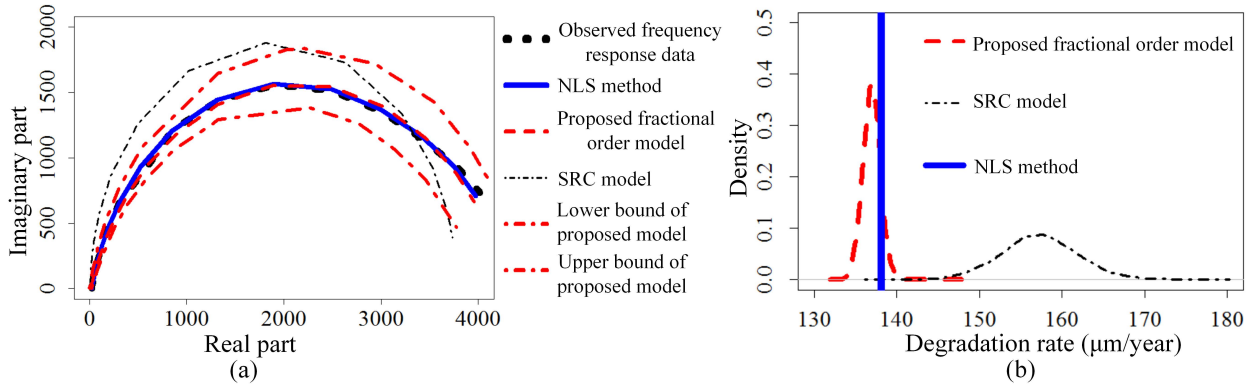

Figure 5.58: Prediction comparison results of individual unit of Mg-alloy

pares the prediction performance between the proposed individual-level model which considers the fractional order and the conventional modeling approach. Since no extra layer is developed during corrosion process of Mg-alloy unit, the conventional SRC model is considered as the benchmark. The proposed fractional order model outperforms SRC model with constant order.Figure 5.58 also shows that the proposed model under NLS and Bayesian estimation methods exhibit similar prediction performance (since non-informative priors are specified), and they are both close to the observed data. In addition, Bayesian estimation gives richer information than NLS based method and the predicted intervals totally cover the observed data. Similar to Al-alloy units, the parameters uncertainty of individual unit and the population variability of multiple units can be simultaneously quantified by the population-level model, as shown in Figure 5.59. Figure 5.60 further shows the K-M curves of individual units and the underlying population from where multiple test units are drawn. The estimated reliability information can pro-

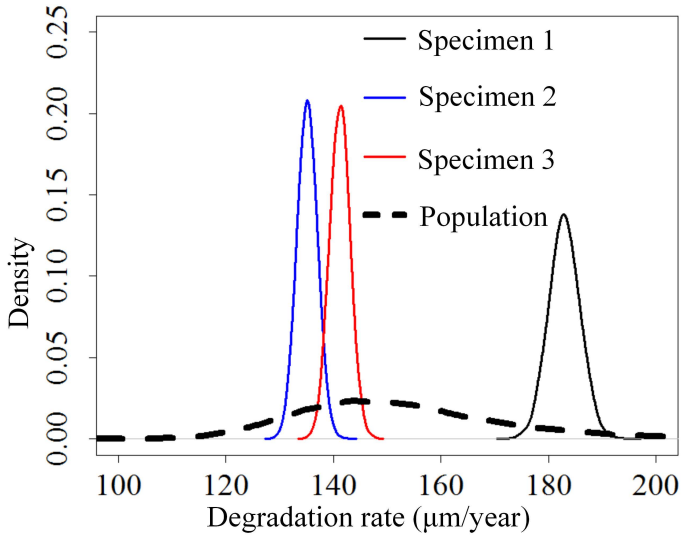

Figure 5.59: Quantification of uncertainty and variability for Mg units

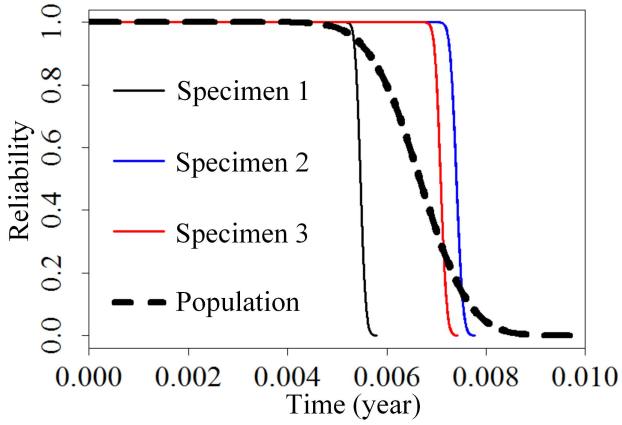

Figure 5.60: Reliability estimates of individual units and underlying population

vide useful information with regarding to whether the desired reliability requirement has been satisfied or not at the product development stage.

5.6 Conclusion Remarks

In this work, a physical-statistical modeling approach is proposed to evaluate the latent degradation performance of corroding Al-alloy units. The proposed framework innovatively integrates the physical failure mechanism with Bayesian hierarchical modeling and computation. Fractional order physical model is first employed with more

generic and flexible form in characterizing the complex degradation process of corroding Al-alloy units. Bayesian individual- and population-level models are further developed and estimated to evaluate the degradation performance of an individual test unit as well as the underlying population of multiple test units, respectively. The effectiveness of the proposed work and its potential applications to other corroding metallic units are further demonstrated by two real case studies. The proposed work is more accurate than conventional SRC and FC models in representing real EIS data. The proposed Bayesian model and estimation procedure also allow the quantification of model parameters uncertainty as well as population variability, which are not available in conventional EIS data modeling and estimation. In addition, the population-level model is capable of evaluating degradation performance of an individual unit with sparse measurement data by information sharing among multiple units. In future work, we will investigate more efficient Bayesian sampling algorithms for both individual- and population-level models. In addition, we will apply the proposed work to other corroding units deployed in the field, e.g., rebar corrosion of aging infrastructure.

Chapter 6

Conclusion and Future Work

In this dissertation, a generic modeling framework of characterizing the heterogeneous performance of individual units (e.g., patients, product units) with different types of data structure is proposed to advance the statistical modeling approaches in both health systems engineering and reliability engineering. Specifically, under the proposed modeling framework, I develop a series of modeling approaches for characterizing three main types of complex performance data in health systems engineering and reliability engineering, namely the heterogeneous time-to-event data, the heterogeneous trajectory data and the heterogeneous frequency response data. The proposed work provides a set of modeling approaches and analytical tools for the stakeholders (e.g., healthcare practitioners and policymakers, reliability engineers) to improve the scientific understanding via identifying the contributing factors and quantifying their influences on the heterogeneous performance of individual units. Moreover, the proposed framework improves the prediction performance and further facilitates the development of proactive and adaptive decisions (e.g., healthcare resource preparedness decision, product maintenance policy) in both healthcare practice and reliability engineering.

Chapter 2 focuses on modeling the heterogeneous time-to-event data of elderly adults to investigate their heterogeneous service utilizations in multiple different healthcare settings. Specifically, I develop modeling approach for heterogeneous time-to-readmission data and time-to-discharge data with Bayesian statistics and latent survival analysis. The proposed approach accounts for both the observed heterogeneity and the unobserved heterogeneity due to the lack of detailed physiological information in claims data. The pro-

posed model considers multiple competing healthcare facilities as well. Real case studies on time-to-readmission of older adults in assisted living facility with multiple healthcare settings (e.g., hospital, nursing home) and time-to-discharge of hospital patients demonstrate the effectiveness of proposed work.

Chapter 3 focuses on modeling the heterogeneous service demand of NH residents and further developing a resource planning decision support platform to meet the service demand of a heterogeneous population of NH residents. Specifically, I first develop a predictive model to characterize heterogeneous length-of-stay of NH residents. Further, I develop a generic predictive model with mixed-type latent heterogeneity to capture the temporal dynamics and temporal heterogeneity of service need trajectory of NH residents. Then, I integrate the developed predictive analytics with computer simulation and stochastic optimization to investigate the impact of service demand heterogeneity on NH resource planning decisions. In addition, an analytics-based decision support platform is developed to facilitate the managerial decisions in response to varied residents census composition and varied service demand scenarios.

Chapter 4 focuses on modeling the heterogeneous trajectory data of tribological degradation performance of test units in accelerated degradation test. Specifically, I develop a generic degradation model with mixed-type covariates and latent heterogeneity to simultaneously quantify the influences of both scalar covariates of external accelerated conditions and functional covariates of internal material characteristics, and the influence of their potential interaction as well as the influence of the unobserved factors shared within each unit. Further, I develop estimation algorithm to address the estimation challenge induced by functional covariates and to achieve the joint quantification of the influences of mixed-type covariates and latent variables. A real case study on tribological degradation performance of cooper alloy units in an accelerated wear test is provided to demonstrate the effectiveness of proposed work and to illustrate its superior modeling performance

via comprehensive comparison. The results also demonstrate sound model interpretability of the proposed approach.

Chapter 5 focuses on modeling the heterogeneous frequency response data of corroding units of aluminum alloy in reliability engineering. Specifically, I develop a physical-statistical modeling approach for heterogeneous corrosion performance assessment signals in frequency domain by integrating Bayesian statistics with fractional order system dynamics. The proposed work can capture the complex physical mechanisms of corroding material units and nonlinear relationships between frequency responses and latent degradation state. The proposed hierarchical models and estimation methods can quantify both parameter uncertainty and population variability. In addition, the proposed approach enables information sharing among different units from same underlying population. Real case studies with corrosion performance assessment via non-destructive testing technique on corroding aluminum alloy units and corroding magnesium units are provided. The proposed work demonstrates superior prediction performance and improved reliability evaluation as compared to conventional methods.

For future research plan, several aspects remain to be further investigated. First, although current framework is generic for three different types of heterogeneous performance data, it will be ideal to extend the framework for handling the combination of some of these data types, such as joint modeling the heterogeneous time-to-event data and the heterogeneous trajectory data. Second, since computation efficiency is not the major focus in this dissertation, there is still research opportunity in high-performance computing, such as developing efficient algorithm to investigate the heterogeneity of streaming data via incorporating parallel computation technique. Third, considering a heterogeneous system with the individual latent heterogeneity changing over time, the current framework can be further developed to explore the dynamics of the influence of individual unobserved factors and the impact of such time-varying latent heterogeneity on dynamic decision making. In addition, the proposed framework in this dissertation

is readily applicable for other applications in health systems engineering and reliability engineering, such as the modeling of heterogeneous treatment responses of patients for personalized medical decision making, or problems in other application domain with the same data structure of performance data, such as the modeling of heterogeneous performance outcomes of students in education system.

References

Abiola, O. K. and James, A. (2010). The effects of aloe vera extract on corrosion and kinetics of corrosion process of zinc in hcl solution. *Corrosion Science*, 52(2):661–664.

Agrawal, R., Srikant, R., et al. (1994). Fast algorithms for mining association rules. In *Proc. 20th int. conf. very large data bases, VLDB*, volume 1215, pages 487–499.

Akritas, M. G. (1986). Bootstrapping the kaplan—meier estimator. *Journal of the American Statistical Association*, 81(396):1032–1038.

Alavi, S. M. M., Mahdi, A., Payne, S. J., and Howey, D. A. (2016). Identifiability of generalized randles circuit models. *IEEE Transactions on Control Systems Technology*, 25(6):2112–2120.

Alexopoulos, N. and Papanikos, P. (2008). Experimental and theoretical studies of corrosion-induced mechanical properties degradation of aircraft 2024 aluminum alloy. *Materials Science and Engineering: A*, 498(1):248–257.

Bae, S. J., Yuan, T., Ning, S., and Kuo, W. (2015). A bayesian approach to modeling two-phase degradation using change-point regression. *Reliability Engineering & System Safety*, 134:66–74.

Bagdonavicius, V. and Nikulin, M. S. (2001). Estimation in degradation models with explanatory variables. *Lifetime Data Analysis*, 7(1):85–103.

Bard, J. F. and Purnomo, H. W. (2005). Short-term nurse scheduling in response to daily fluctuations in supply and demand. *Health Care Management Science*, 8(4):315–324.

Bender, A., Groll, A., and Scheipl, F. (2018). A generalized additive model approach to time-to-event analysis. *Statistical Modelling*, 18(3-4):299–321.

Bentler, P. M. and Weeks, D. G. (1980). Linear structural equations with latent variables. *Psychometrika*, 45(3):289–308.

Bernatz, J. T., Tueting, J. L., and Anderson, P. A. (2015). Thirty-day readmission rates in orthopedics: a systematic review and meta-analysis. *PloS one*, 10(4):e0123593.

Bian, L., Gebraeel, N., and Kharoufeh, J. P. (2015). Degradation modeling for real-time estimation of residual lifetimes in dynamic environments. *IIE Transactions*, 47(5):471–486.

Bierwagen, G., Tallman, D., Li, J., He, L., and Jeffcoate, C. (2003). Eis studies of coated metals in accelerated exposure. *Progress in Organic Coatings*, 46(2):149–158.

Bowblis, J. R. (2011). Staffing ratios and quality: An analysis of minimum direct care staffing requirements for nursing homes. *Health services research*, 46(5):1495–1516.

Bowblis, J. R. and Ghattas, A. (2017). The impact of minimum quality standard regulations on nursing home staffing, quality, and exit decisions. *Review of Industrial Organization*, 50(1):43–68.

Burdett, R. and Kozan, E. (2016). A multi-criteria approach for hospital capacity analysis. *European Journal of Operational Research*, 255(2):505–521.

Centers For Medicare & Medicaid Services (2013). Time Study (STRIVE). https://www.cms.gov/Medicare/Medicare-Fee-for-Service-Payment/SNFPPS/TimeStudy. Online; accessed 19 October 2020.

Chaudhuri, B. B. and Sarkar, N. (1995). Texture segmentation using fractal dimension. *IEEE Transactions on pattern analysis and machine intelligence*, 17(1):72–77.

Chen, K. and Lei, J. (2015). Localized functional principal component analysis. *Journal of the American Statistical Association*, 110(511):1266–1275.

Chen, P. and Ye, Z.-S. (2018). Uncertainty quantification for monotone stochastic degradation models. *Journal of Quality Technology*, 50(2):207–219.

Chiu, C.-J. and Wray, L. A. (2011). Physical disability trajectories in older americans with and without diabetes: The role of age, gender, race or ethnicity, and education. *The Gerontologist*, 51(1):51–63.

Congdon, P. D. (2010). *Applied Bayesian hierarchical methods*. CRC Press.

Dadlani, A., Kumar, M. S., Murugan, S., and Kim, K. (2014). System dynamics of a refined epidemic model for infection propagation over complex networks. *IEEE Systems Journal*, 10(4):1316–1325.

Debón, A. and Garcia-Díaz, J. C. (2012). Fault diagnosis and comparing risk for the steel coil manufacturing process using statistical models for binary data. *Reliability Engineering & System Safety*, 100:102–114.

Dellefield, M. E. (2006). Using the resource utilization groups (rug-iii) system as a staffing tool in nursing homes. *Geriatric Nursing*, 27(3):160–165.

Dhillon, I. S., Mallela, S., and Kumar, R. (2003). A divisive information-theoretic feature clustering algorithm for text classification. *Journal of machine learning research*, 3(Mar):1265–1287.

Efron, B. and Morris, C. (1973). Stein's estimation rule and its competitors—an empirical bayes approach. *Journal of the American Statistical Association*, 68(341):117–130.

Elwakil, A. S. (2010). Fractional-order circuits and systems: An emerging interdisciplinary research area. *IEEE Circuits and Systems Magazine*, 10(4):40–50.

Ezuber, H., El-Houd, A., and El-Shawesh, F. (2008). A study on the corrosion behavior of aluminum alloys in seawater. *Materials & Design*, 29(4):801–805.

Fang, G., Pan, R., and Hong, Y. (2020). Copula-based reliability analysis of degrading systems with dependent failures. *Reliability Engineering & System Safety*, 193:106618.

Fernández-Alemán, J. L., Señor, I. C., Lozoya, P. Á. O., and Toval, A. (2013). Security and privacy in electronic health records: A systematic literature review. *Journal of biomedical informatics*, 46(3):541–562.

Gardner, R. L., Sarkar, U., Maselli, J. H., and Gonzales, R. (2007). Factors associated with longer ed lengths of stay. *The American journal of emergency medicine*, 25(6):643–650.

Gebraeel, N. (2006). Sensory-updated residual life distributions for components with exponential degradation patterns. *IEEE Transactions on Automation Science and Engineering*, 3(4):382–393.

Gebraeel, N. Z., Lawley, M. A., Li, R., and Ryan, J. K. (2005). Residual-life distributions from component degradation signals: A bayesian approach. *IIE Transactions*, 37(6):543–557.

Gehrke, J., Ganti, V., Ramakrishnan, R., and Loh, W.-Y. (1999). Boat—optimistic decision tree construction. In *Proceedings of the 1999 ACM SIGMOD international conference on Management of data*, pages 169–180.

Gelman, A., Carlin, J. B., Stern, H. S., Dunson, D. B., Vehtari, A., and Rubin, D. B. (2013). *Bayesian data analysis*. CRC press.

Goel, S., Luo, X., and Reuben, R. L. (2012). Molecular dynamics simulation model for the quantitative assessment of tool wear during single point diamond turning of cubic silicon carbide. *Computational Materials Science*, 51(1):402–408.

González, S., Cáceres, F., Fox, V., and Souto, R. (2003). Resistance of metallic substrates protected by an organic coating containing aluminum powder. *Progress in organic coatings*, 46(4):317–323.

Goodhew, P. J. and Humphreys, J. (2000). *Electron microscopy and analysis*. CRC Press.

Gorjian, N., Ma, L., Mittinty, M., Yarlagadda, P., and Sun, Y. (2010). A review on degradation models in reliability analysis. In *Engineering Asset Lifecycle Management*, pages 369–384. Springer.

Hamada, M. S., Wilson, A., Reese, C. S., and Martz, H. (2008). *Bayesian reliability*. Springer Science & Business Media.

HASTINGS, W. (1970). Monte carlo sampling methods using markov chains and their applications. *Biometrika*, 57(1):97–109.

He, Z. and Mansfeld, F. (2009). Exploring the use of electrochemical impedance spectroscopy (eis) in microbial fuel cell studies. *Energy & Environmental Science*, 2(2):215–219.

Heidelberger, P. and Welch, P. D. (1983). Simulation run length control in the presence of an initial transient. *Operations Research*, 31(6):1109–1144.

Hinderliter, B., Croll, S., Tallman, D., Su, Q., and Bierwagen, G. (2006). Interpretation of eis data from accelerated exposure of coated metals based on modeling of coating physical properties. *Electrochimica Acta*, 51(21):4505–4515.

Hsing, T. and Eubank, R. (2015). *Theoretical foundations of functional data analysis, with an introduction to linear operators*, volume 997. John Wiley & Sons.

Huynh, K. T., Barros, A., Berenguer, C., and Castro, I. T. (2011). A periodic inspection and replacement policy for systems subject to competing failure modes due to degradation and traumatic events. *Reliability Engineering & System Safety*, 96(4):497–508.

Hyer, K., Thomas, K. S., Branch, L. G., Harman, J. S., Johnson, C. E., and Weech-Maldonado, R. (2011). The influence of nurse staffing levels on quality of care in nursing homes. *The Gerontologist*, 51(5):610–616.

Janiszewski Goodin, H. (2003). The nursing shortage in the united states of america: an integrative review of the literature. *Journal of advanced nursing*, 43(4):335–343.

Jasti, H., Mortensen, E. M., Obrosky, D. S., Kapoor, W. N., and Fine, M. J. (2008). Causes and risk factors for rehospitalization of patients hospitalized with community-acquired pneumonia. *Clinical infectious diseases*, 46(4):550–556.

Jiao, Y., Stillinger, F., and Torquato, S. (2007). Modeling heterogeneous materials via two-point correlation functions: Basic principles. *Physical Review E*, 76(3):031110.

Kansagara, D., Englander, H., Salanitro, A., Kagen, D., Theobald, C., Freeman, M., and Kripalani, S. (2011). Risk prediction models for hospital readmission: a systematic review. *Jama*, 306(15):1688–1698.

Kharoufeh, J. P. (2003). Explicit results for wear processes in a markovian environment. *Operations Research Letters*, 31(3):237–244.

Kharoufeh, J. P. and Cox, S. M. (2005). Stochastic models for degradation-based reliability. *IIE Transactions*, 37(6):533–542.

Kharoufeh, J. P., Solo, C. J., and Ulukus, M. Y. (2010). Semi-markov models for degradation-based reliability. *IIE Transactions*, 42(8):599–612.

Kim, K. and Mehrotra, S. (2015). A two-stage stochastic integer programming approach to integrated staffing and scheduling with application to nurse management. *Operations Research*, 63(6):1431–1451.

Kirkland, N., Birbilis, N., and Staiger, M. (2012). Assessing the corrosion of biodegradable magnesium implants: a critical review of current methodologies and their limitations. *Acta biomaterialia*, 8(3):925–936.

Kleywegt, A. J., Shapiro, A., and Homem-de Mello, T. (2002). The sample average approximation method for stochastic discrete optimization. *SIAM Journal on Optimization*, 12(2):479–502.

Konetzka, R. T., Stearns, S. C., and Park, J. (2008). The staffing-outcomes relationship in nursing homes. *Health services research*, 43(3):1025–1042.

Kunkel, A. and McLay, L. A. (2013). Determining minimum staffing levels during snowstorms using an integrated simulation, regression, and reliability model. *Health care management science*, 16(1):14–26.

Laird, N. M. and Ware, J. H. (1982). Random-effects models for longitudinal data. *Biometrics*, pages 963–974.

Lee, E. W. (2012). Selecting the best prediction model for readmission. *Journal of Preventive Medicine and Public Health*, 45(4):259.

Lee, E. W., Wei, L., and Ying, Z. (1993). Linear regression analysis for highly stratified failure time data. *Journal of the American Statistical Association*, 88(422):557–565.

Li, M. and Liu, J. (2016). Bayesian hazard modeling based on lifetime data with latent heterogeneity. *Reliability Engineering & System Safety*, 145:183–189.

Li, M., Meng, H., and Zhang, Q. (2017a). A nonparametric bayesian modeling approach for heterogeneous lifetime data with covariates. *Reliability Engineering & System Safety*, 167:95–104.

Li, M., Zhang, W., Hu, Q., Guo, H., and Liu, J. (2017b). Design and risk evaluation of reliability demonstration test for hierarchical systems with multilevel information aggregation. *IEEE Transactions on Reliability*, 66(1):135–147.

Li, Y., Zhang, Y., Kong, N., and Lawley, M. (2016). Capacity planning for long-term care networks. *IIE Transactions*, 48(12):1098–1111.

Lin, J. (1991). Divergence measures based on the shannon entropy. *IEEE Transactions on Information theory*, 37(1):145–151.

Liu, K., Coughlin, T., and McBride, T. (1991). Predicting nursing-home admission and length of stay: A duration analysis. *Medical Care*, pages 125–141.

Liu, Y., Sun, Q., Li, W., Adair, K. R., Li, J., and Sun, X. (2017). A comprehensive review on recent progress in aluminum–air batteries. *Green Energy & Environment*, 2(3):246–277.

Lu, C. J. and Meeker, W. O. (1993). Using degradation measures to estimate a time-to-failure distribution. *Technometrics*, 35(2):161–174.

Lyu, J. and Chen, M.-N. (2008). Gauge capability studies for attribute data. *Quality and Reliability Engineering International*, 24(1):71–82.

Ma, G. and Demeulemeester, E. (2013). A multilevel integrative approach to hospital case mix and capacity planning. *Computers & Operations Research*, 40(9):2198–2207.

Manton, K. G., Liu, K., and Cornelius, E. S. (1985). An analysis of the heterogeneity of us nursing home patients. *Journal of Gerontology*, 40(1):34–46.

McGilchrist, C. and Aisbett, C. (1991). Regression with frailty in survival analysis. *Biometrics*, pages 461–466.

Meeker, W. Q. and Escobar, L. A. (2014). *Statistical methods for reliability data*. John Wiley & Sons.

Meeker, W. Q., Escobar, L. A., and Lu, C. J. (1998). Accelerated degradation tests: modeling and analysis. *Technometrics*, 40(2):89–99.

Méndez-González, L. C., Rodríguez-Picón, L. A., Valles-Rosales, D. J., Romero-López, R., and Quezada-Carreón, A. E. (2017). Reliability analysis for electronic devices using beta-weibull distribution. *Quality and Reliability Engineering International*, 33(8):2521–2530.

Meng, H., Dobbs, D., Wang, S., and Hyer, K. (2013). Hospice use and public expenditures at the end of life in assisted living residents in a f lorida medicaid waiver program. *Journal of the American Geriatrics Society*, 61(10):1777–1781.

Mraied, H., Cai, W., and Sagüés, A. A. (2016). Corrosion resistance of al and al–mn thin films. *Thin Solid Films*, 615:391–401.

Mueller, C., Arling, G., Kane, R., Bershadsky, J., Holland, D., and Joy, A. (2006). Nursing home staffing standards: Their relationship to nurse staffing levels. *The Gerontologist*, 46(1):74–80.

National Center For Health Statistics (2019). Long-Term Care Providers and Services Users in the United States: Data From the National Study of Long-Term Care Providers. https://www.cdc.gov/nchs/npals. Online; accessed 19 October 2020.

Oehlert, G. W. (1992). A note on the delta method. *The American Statistician*, 46(1):27–29.

Park, J. and Stearns, S. C. (2009). Effects of state minimum staffing standards on nursing home staffing and quality of care. *Health services research*, 44(1):56–78.

Park, J. S., Lee, S. M., Joo, B. S., and Jang, H. (2017). The effect of material properties on the stick–slip behavior of polymers: A case study with pmma, pc, ptfe, and pvc. *Wear*, 378:11–16.

Peng, W., Huang, H.-Z., Li, Y., Zuo, M. J., and Xie, M. (2013). Life cycle reliability assessment of new products-a bayesian model updating approach. *Reliability Engineering & System Safety*, 112:109–119.

Peng, W., Li, Y.-F., Yang, Y.-J., Huang, H.-Z., and Zuo, M. J. (2014). Inverse gaussian process models for degradation analysis: A bayesian perspective. *Reliability Engineering & System Safety*, 130:175–189.

Punnakitikashem, P., Rosenberber, J. M., and Buckley-Behan, D. F. (2013). A stochastic programming approach for integrated nurse staffing and assignment. *IISE Transactions*, 45(10):1059–1076.

Qin, H., Zhou, W., and Zhang, S. (2015). Bayesian inferences of generation and growth of corrosion defects on energy pipelines based on imperfect inspection data. *Reliability Engineering & System Safety*, 144:334–342.

Ramsay, J. O. and Silverman, B. W. (2007). *Applied functional data analysis: methods and case studies*. Springer.

Ran, L., Junfeng, W., Haiying, W., and Gechen, L. (2010). Prediction of state of charge of lithium-ion rechargeable battery with electrochemical impedance spectroscopy theory. In *Industrial Electronics and Applications (ICIEA), 2010 the 5th IEEE Conference on*, pages 684–688. IEEE.

Ridge, J., Jones, S., Nielsen, M., and Shahani, A. (1998). Capacity planning for intensive care units. *European journal of operational research*, 105(2):346–355.

Roberts, G. O. and Sahu, S. K. (1997). Updating schemes, correlation structure, blocking and parameterization for the gibbs sampler. *Journal of the Royal Statistical Society: Series B (Statistical Methodology)*, 59(2):291–317.

Rondeau, V., Commenges, D., and Joly, P. (2003). Maximum penalized likelihood estimation in a gamma-frailty model. *Lifetime data analysis*, 9(2):139–153.

Rondeau, V., Filleul, L., and Joly, P. (2006). Nested frailty models using maximum penalized likelihood estimation. *Statistics in medicine*, 25(23):4036–4052.

Rosliza, R., Nora'Aini, A., and Nik, W. W. (2010). Study on the effect of vanillin on the corrosion inhibition of aluminum alloy. *Journal of applied electrochemistry*, 40(4):833–840.

Sakib, N., Sun, X., Kong, N., Meng, H., and Li, M. (2017). Bi-level heterogeneity modeling of functional performance degradation for the aging population. *IISE Transactions on Healthcare Systems Engineering*, 7(3):156–167.

Salamzadeh, J., Wong, I., Hosker, H., and Chrystyn, H. (2003). A cox regression analysis of covariates for asthma hospital readmissions. *Journal of Asthma*, 40(6):645–652.

Saliba, D., Jones, M., Streim, J., Ouslander, J., Berlowitz, D., and Buchanan, J. (2012). Overview of significant changes in the minimum data set for nursing homes version 3.0. *Journal of the American Medical Directors Association*, 13(7):595–601.

Shafiee, M., Finkelstein, M., and Bérenguer, C. (2015). An opportunistic condition-based maintenance policy for offshore wind turbine blades subjected to degradation and environmental shocks. *Reliability Engineering & System Safety*, 142:463–471.

Shu, M.-H., Hsu, B.-M., and Kapur, K. C. (2010). Dynamic performance measures for tools with multi-state wear processes and their applications for tool design and selection. *International journal of production research*, 48(16):4725–4744.

Si, W., Yang, Q., and Wu, X. (2019). Material degradation modeling and failure prediction using microstructure images. *Technometrics*, 61(2):246–258.

Siferd, S. P. and Benton, W. (1992). Workforce staffing and scheduling: Hospital nursing specific models. *European Journal of Operational Research*, 60(3):233–246.

Singh, J., Cai, W., and Bellon, P. (2007). Dry sliding of cu–15 wt% ni–8 wt% sn bronze: Wear behaviour and microstructures. *Wear*, 263(1-6):830–841.

Spiegelhalter, D. J., Best, N. G., Carlin, B. P., and Van Der Linde, A. (2002). Bayesian measures of model complexity and fit. *Journal of the royal statistical society: Series b (statistical methodology)*, 64(4):583–639.

Spilsbury, K., Hewitt, C., Stirk, L., and Bowman, C. (2011). The relationship between nurse staffing and quality of care in nursing homes: a systematic review. *International journal of nursing studies*, 48(6):732–750.

Stephens, M. A. (1970). Use of the kolmogorov–smirnov, cramer–von mises and related statistics without extensive tables. *Journal of the Royal Statistical Society: Series B (Methodological)*, 32(1):115–122.

Stern, M. and Geary, A. L. (1957). Electrochemical polarization i. a theoretical analysis of the shape of polarization curves. *Journal of the electrochemical society*, 104(1):56–63.

Sun, X., Cai, W., Zhang, Q., and Li, M. (2021a). A degradation performance model with mixed-type covariates and latent heterogeneity. *arXiv preprint arXiv:2101.03671*.

Sun, X., Li, M., Meng, C., Kong, N., Meng, H., and Hyer, K. (2017a). Data-driven simulation for healthcare facility utilization modeling and evaluation. In *2017 Winter Simulation Conference (WSC)*, pages 2869–2880. IEEE.

Sun, X., Lou, Z., Li, M., Kong, N., and Parikh, P. J. (2017b). Predictive modeling of care demand and transition. *Stochastic modeling and analytics in healthcare delivery systems. Singapore: World Scientific Publishing*, pages 135–166.

Sun, X., Mraied, H., Cai, W., Zhang, Q., Liang, G., and Li, M. (2018). Bayesian latent degradation performance modeling and quantification of corroding aluminum alloys. *Reliability Engineering & System Safety*, 178:84–96.

Sun, X., Sakib, N., Kong, N., Meng, H., Hyer, K., Masterson, C., and Li, M. (2021b). An analytics-based decision support system for resource planning under heterogeneous service demand of nursing home residents. *arXiv preprint arXiv:2102.02069*.

Tabrizi, M., Lyon, S., Thompson, G., and Ferguson, J. (1991). The long-term corrosion of aluminium in alkaline media. *Corrosion science*, 32(7):733–742.

Torquato, S. (2002). Statistical description of microstructures. *Annual review of materials research*, 32(1):77–111.

van Eeden, K., Moeke, D., and Bekker, R. (2016). Care on demand in nursing homes: a queueing theoretic approach. *Health care management science*, 19(3):227–240.

van Noortwijk, J. M. (2009). A survey of the application of gamma processes in maintenance. *Reliability Engineering & System Safety*, 94(1):2–21.

Verburg, I. W., de Keizer, N. F., de Jonge, E., and Peek, N. (2014). Comparison of regression methods for modeling intensive care length of stay. *PloS one*, 9(10):e109684.

Wang, B., Li, S. E., Peng, H., and Liu, Z. (2015). Fractional-order modeling and parameter identification for lithium-ion batteries. *Journal of Power Sources*, 293:151–161.

Wang, L., Pan, R., Li, X., and Jiang, T. (2013). A bayesian reliability evaluation method with integrated accelerated degradation testing and field information. *Reliability Engineering & System Safety*, 112:38–47.

Wei, G. C. and Tanner, M. A. (1990). A monte carlo implementation of the em algorithm and the poor man's data augmentation algorithms. *Journal of the American statistical Association*, 85(411):699–704.

Windhagen, H., Radtke, K., Weizbauer, A., Diekmann, J., Noll, Y., Kreimeyer, U., Schavan, R., Stukenborg-Colsman, C., and Waizy, H. (2013). Biodegradable magnesium-based screw clinically equivalent to titanium screw in hallux valgus surgery: short term results of the first prospective, randomized, controlled clinical pilot study. *Biomedical engineering online*, 12(1):62.

Wu, C. J. et al. (1983). On the convergence properties of the em algorithm. *The Annals of statistics*, 11(1):95–103.

Yankovic, N. and Green, L. V. (2011). Identifying good nursing levels: A queuing approach. *Operations research*, 59(4):942–955.

Ye, Z.-S. and Chen, N. (2014). The inverse gaussian process as a degradation model. *Technometrics*, 56(3):302–311.

Ye, Z.-S., Chen, N., and Shen, Y. (2015). A new class of wiener process models for degradation analysis. *Reliability Engineering & System Safety*, 139:58–67.

Ye, Z.-S. and Xie, M. (2015). Stochastic modelling and analysis of degradation for highly reliable products. *Applied Stochastic Models in Business and Industry*, 31(1):16–32.

Yuan, T., Bae, S. J., and Zhu, X. (2016). A bayesian approach to degradation-based burn-in optimization for display products exhibiting two-phase degradation patterns. *Reliability Engineering & System Safety*, 155:55–63.

Yuan, T. and Ji, Y. (2014). A hierarchical bayesian degradation model for heterogeneous data. *IEEE Transactions on Reliability*, 64(1):63–70.

Zhang, S., Zhou, W., Al-Amin, M., Kariyawasam, S., and Wang, H. (2014). Time-dependent corrosion growth modeling using multiple in-line inspection data. *Journal of Pressure Vessel Technology*, 136(4):041202.

Zhang, T. and Xie, M. (2011). On the upper truncated weibull distribution and its reliability implications. *Reliability Engineering & System Safety*, 96(1):194–200.

Zhang, X. and Grabowski, D. C. (2004). Nursing home staffing and quality under the nursing home reform act. *The Gerontologist*, 44(1):13–23.

Zhang, Y., Puterman, M. L., Nelson, M., and Atkins, D. (2012). A simulation optimization approach to long-term care capacity planning. *Operations research*, 60(2):249–261.

Zhao, X., He, S., and Xie, M. (2018). Utilizing experimental degradation data for warranty cost optimization under imperfect repair. *Reliability Engineering & System Safety*, 177:108–119.

Zimmer, Z., Martin, L. G., Nagin, D. S., and Jones, B. L. (2012). Modeling disability trajectories and mortality of the oldest-old in china. *Demography*, 49(1):291–314.

Zonderland, M. E., Boucherie, R. J., Carter, M. W., and Stanford, D. A. (2015). Modeling the effect of short stay units on patient admissions. *Operations research for health care*, 5:21–27.

Appendix A Copyright Permissions

A.1 Permission for Chapter 2

Data-driven simulation for healthcare facility utilization modeling and evaluation

Conference Proceedings: 2017 Winter Simulation Conference (WSC)

Author: Xuxue Sun

Publisher: IEEE

Date: Dec. 2017

Copyright © 2017, IEEE

Thesis / Dissertation Reuse

The IEEE does not require individuals working on a thesis to obtain a formal reuse license, however, you may print out this statement to be used as a permission grant:

Requirements to be followed when using any portion (e.g., figure, graph, table, or textual material) of an IEEE copyrighted paper in a thesis:

1) In the case of textual material (e.g., using short quotes or referring to the work within these papers) users must give full credit to the original source (author, paper, publication) followed by the IEEE copyright line © 2011 IEEE.
2) In the case of illustrations or tabular material, we require that the copyright line © [Year of original publication] IEEE appear prominently with each reprinted figure and/or table.
3) If a substantial portion of the original paper is to be used, and if you are not the senior author, also obtain the senior author's approval.

Requirements to be followed when using an entire IEEE copyrighted paper in a thesis:

1) The following IEEE copyright/ credit notice should be placed prominently in the references: © [year of original publication] IEEE. Reprinted, with permission, from [author names, paper title, IEEE publication title, and month/year of publication]
2) Only the accepted version of an IEEE copyrighted paper can be used when posting the paper or your thesis on-line.
3) In placing the thesis on the author's university website, please display the following message in a prominent place on the website: In reference to IEEE copyrighted material which is used with permission in this thesis, the IEEE does not endorse any of [university/educational entity's name goes here]'s products or services. Internal or personal use of this material is permitted. If interested in reprinting/republishing IEEE copyrighted material for advertising or promotional purposes or for creating new collective works for resale or redistribution, please go to http://www.ieee.org/publications_standards/publications/rights/rights_link.html to learn how to obtain a License from RightsLink.

If applicable, University Microfilms and/or ProQuest Library, or the Archives of Canada may supply single copies of the dissertation.

BACK CLOSE WINDOW

RE: Request for permission to reuse part of a chapter in dissertation

Rights <rights@wspc.com>
Sun 12/20/2020 10:59 PM

To: Sun, Xuxue <xuxuesun@usf.edu>
Cc: Li, Mingyang <mingyangli@usf.edu>

Dear Xuxue Sun

Thanks for getting in touch.

We will be pleased to grant you the permission of including your own final version of the concerned book chapter in your dissertation, provided that full credit been given to the original source in the following format:

Title of the Work, Author (s) and/or Editor(s) Name (s), Copyright @ year and name of the publisher

With regards
Tu Ning

From: Sun, Xuxue <xuxuesun@usf.edu>
Sent: 2020年12月10日 4:25
To: Rights <rights@wspc.com>
Cc: Li, Mingyang <mingyangli@usf.edu>
Subject: Request for permission to reuse part of a chapter in dissertation

Hello,

My name is Xuxue Sun. I am a PhD candidate at the University of South Florida. My advisor is Dr. Mingyang Li.

I am writing to request for an authorization of publication of the following work in a dissertation titled 'Heterogeneity Modeling with Applications in Healthcare and Reliability Engineering ' with an expected presentation date at the beginning of 2021:

Chapter 6: Predictive Modeling of Care Demand and Transition
Book: Stochastic Modeling and Analytics in Healthcare Delivery Systems
Authors: Xuxue Sun, Zhouyang Lou, Mingyang Li, Nan Kong and Pratik J. Parikh
DOI: https://doi.org/10.1142/9789813220850_0006
Publisher: World Scientific

It is greatly appreciated if the permission can be granted, or you can give further guidance if additional work needs to be done.

Thank you!

A.2 Permissions for Chapter 3 and Chapter 4

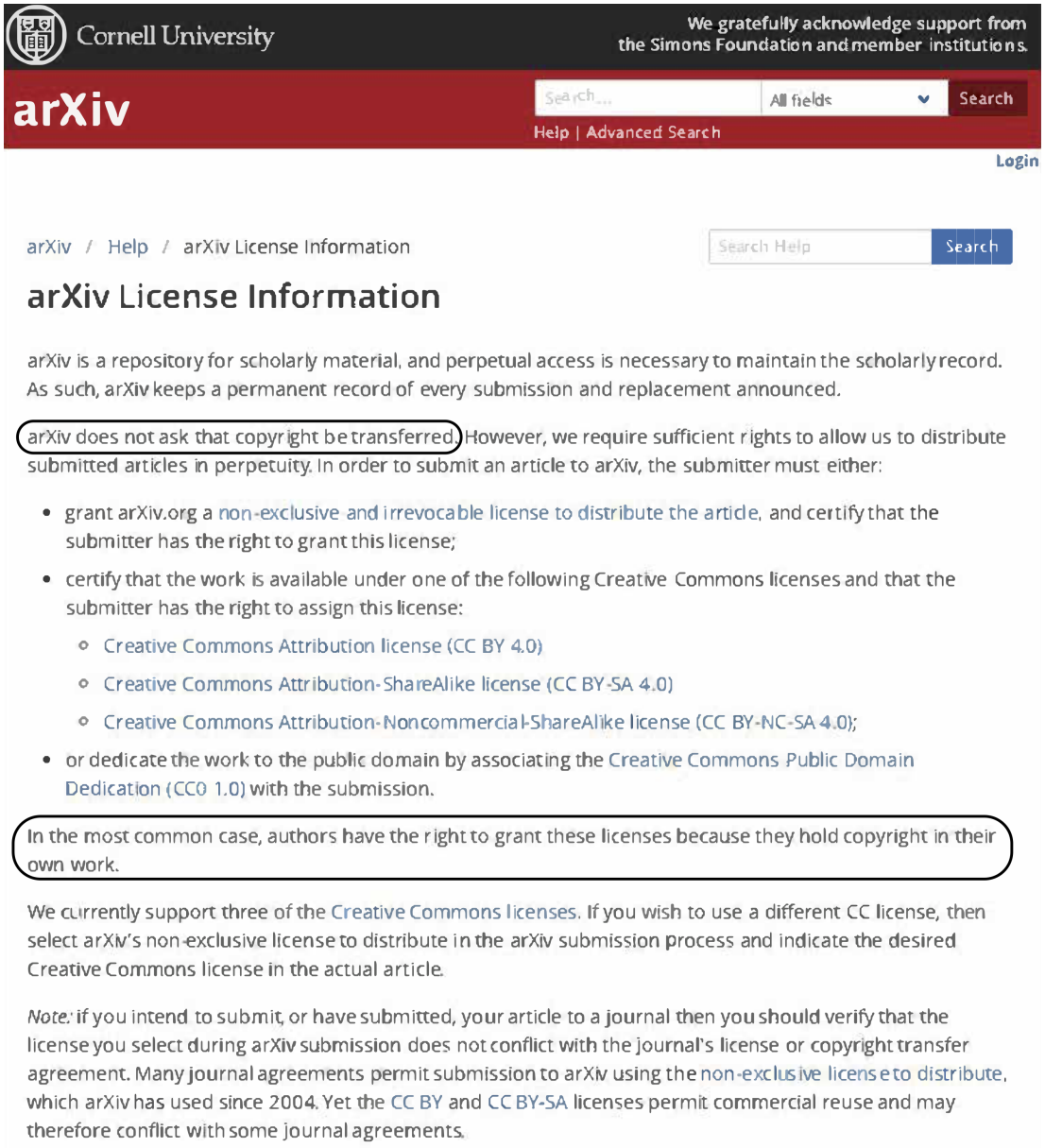

Cornell University

We gratefully acknowledge support from the Simons Foundation and member institutions.

arXiv

Search... All fields Search

Help | Advanced Search

Login

arXiv / Help / arXiv License Information

Search Help Search

arXiv License Information

arXiv is a repository for scholarly material, and perpetual access is necessary to maintain the scholarly record. As such, arXiv keeps a permanent record of every submission and replacement announced.

arXiv does not ask that copyright be transferred. However, we require sufficient rights to allow us to distribute submitted articles in perpetuity. In order to submit an article to arXiv, the submitter must either:

- grant arXiv.org a non-exclusive and irrevocable license to distribute the article, and certify that the submitter has the right to grant this license;
- certify that the work is available under one of the following Creative Commons licenses and that the submitter has the right to assign this license:
  - Creative Commons Attribution license (CC BY 4.0)
  - Creative Commons Attribution-ShareAlike license (CC BY-SA 4.0)
  - Creative Commons Attribution-Noncommercial-ShareAlike license (CC BY-NC-SA 4.0);
- or dedicate the work to the public domain by associating the Creative Commons Public Domain Dedication (CC0 1.0) with the submission.

In the most common case, authors have the right to grant these licenses because they hold copyright in their own work.

We currently support three of the Creative Commons licenses. If you wish to use a different CC license, then select arXiv's non-exclusive license to distribute in the arXiv submission process and indicate the desired Creative Commons license in the actual article.

Note: if you intend to submit, or have submitted, your article to a journal then you should verify that the license you select during arXiv submission does not conflict with the journal's license or copyright transfer agreement. Many journal agreements permit submission to arXiv using the non-exclusive license to distribute, which arXiv has used since 2004. Yet the CC BY and CC BY-SA licenses permit commercial reuse and may therefore conflict with some journal agreements.

A.3 Permission for Chapter 5

Bayesian latent degradation performance modeling and quantification of corroding aluminum alloys

Author: Xuxue Sun,Hesham Mraied,Wenjun Cai,Qiong Zhang,Guoyuan Liang,Mingyang Li

Publication: Reliability Engineering & System Safety

Publisher: Elsevier

Date: October 2018

Appendix B Supplemental Materials

B.1 Appendix for Chapter 4

B.1.1 Details of Vector Form of Proposed Model

Based on Eq. (4.27), the degradation performance responses can be fully expressed as

$$y_{ij} = \sum_{l=0}^{L}[\nu_l + \boldsymbol{\beta}_l^{\mathrm{T}}\boldsymbol{x}_i + R\left(\sum_{s=1}^{S}\sum_{k=1}^{K} b_{lsk}c_{isk}\right) + R\left(\sum_{p=1}^{P} x_{ip}\left(\sum_{s=1}^{S}\sum_{k=1}^{K} b'_{lpsk}c_{isk}\right)\right) + \gamma_{li}]\phi_l(t_{ij}) + \epsilon_{ij}, i = 1, ..., N, j = 1, ..., m_i$$

where y_{ij} is degradation performance output of test unit i measured at time t_{ij} and ϵ_{ij} is the error term. We denote the vector form as $\boldsymbol{y}_i = [y_{i1}, ..., y_{im_i}]^{\mathrm{T}}$ and $\boldsymbol{\epsilon}_i = [\epsilon_{i1}, ..., \epsilon_{im_i}]^{\mathrm{T}}$. ν_l is the population-level average degradation performance at l^{th} decomposition, $\forall l = 0, ..., L$. Let $\boldsymbol{\nu} = [\nu_0 ... \nu_L]^{\mathrm{T}}$ be a vector of population-level average degradation performance at all decomposition levels. x_{ip} is the p^{th} scalar covariate of unit i and $\boldsymbol{x}_i = [x_{i1}, ..., x_{iP}]$ is a vector of all P observed scalar covariates. $\boldsymbol{\beta}_l = [\beta_{l1} ... \beta_{lP}]^{\mathrm{T}}$ is a vector of the coefficients of total P scalar covariates at l^{th} decomposition, $\forall l = 0, ..., L$. R is the range of spatial distance and c_{isk} is the k^{th} basis coefficient for s^{th} functional covariate of unit i. b_{lsk} and b'_{lpsk} are k^{th} basis coefficients for coefficient function of s^{th} functional covariate and the interaction terms, respectively. We denote $\boldsymbol{b}_{ls} = [b_{ls1}, ..., b_{lsK}]^{\mathrm{T}}$ and $\boldsymbol{b}'_{lps} = [b'_{lps1}, ..., b'_{lpsK}]^{\mathrm{T}}, \forall l = 0, ..., L, p = 1, ..., P, s = 1, ..., S$. γ_{li} is the latent factor of unit i at l^{th} decomposition and let $\boldsymbol{\gamma}_i = [\gamma_{0i}, ..., \gamma_{Li}]^{\mathrm{T}}$ be a vector of latent variables of unit i at all decomposition levels. $\phi_l(\cdot)$ is basis function at l^{th} decomposition.

The design matrix of unobserved heterogeneity can be expressed as

$$\boldsymbol{\Lambda}_i = \left(w_{uv}^{1i} \right) \in \mathbb{R}^{m_i \times (L+1)}$$

where $w_{uv}^{1i} = \phi_v(t_{iu}), \forall u = 1, ..., m_i, v = 0, ..., L$ is the element at u^{th} row and v^{th} column.

Further, we let $\boldsymbol{A}_{2i}$, $\boldsymbol{A}_{3i}$ and $\boldsymbol{A}_{4i}$ be the block matrices, i.e.,

$$\boldsymbol{A}_{2i} = \begin{pmatrix} \boldsymbol{A}_{20i} & \boldsymbol{A}_{21i} & ... & \boldsymbol{A}_{2Li} \end{pmatrix} \in \mathbb{R}^{m_i \times (L+1)P}$$

where $\boldsymbol{A}_{2li} = \left(w_{uv}^{2li} \right) \in \mathbb{R}^{m_i \times P}, \forall l = 0, ..., L$ is the submatrix and the element at u^{th} row and v^{th} column is expressed as $w_{uv}^{2li} = x_{iv}\phi_l(t_{iu}), \forall u = 1, ..., m_i, v = 1, ..., P$.

$$\boldsymbol{A}_{3i} = \begin{pmatrix} \boldsymbol{A}_{30i} & \boldsymbol{A}_{31i} & ... & \boldsymbol{A}_{3Li} \end{pmatrix} \in \mathbb{R}^{m_i \times (L+1)SK}$$

where each submatrix $\boldsymbol{A}_{3li} \in \mathbb{R}^{m_i \times SK}$ can be expressed as $\boldsymbol{A}_{3li} = \begin{pmatrix} \boldsymbol{A}_{3li1} & ... & \boldsymbol{A}_{3liS} \end{pmatrix}, \forall l = 0, ..., L$. Each submatrix $\boldsymbol{A}_{3lis}$ can be written as $\boldsymbol{A}_{3lis} = \left(w_{uv}^{3lis} \right) \in \mathbb{R}^{m_i \times K}, \forall s = 1, ..., S$ where $w_{uv}^{3lis} = Rc_{isv}\phi_l(t_{iu}), \forall u = 1, ..., m_i, v = 1, ..., K$ is the element at u^{th} row and v^{th} column of the submatrix.

$$\boldsymbol{A}_{4i} = \begin{pmatrix} \boldsymbol{A}_{40i} & \boldsymbol{A}_{41i} & ... & \boldsymbol{A}_{4Li} \end{pmatrix} \in \mathbb{R}^{m_i \times (L+1)PSK}$$

where $\boldsymbol{A}_{4li} = \begin{pmatrix} \boldsymbol{A}_{4li1} & ... & \boldsymbol{A}_{4liP} \end{pmatrix} \in \mathbb{R}^{m_i \times PSK}, \forall l = 0, ..., L$ is the submatrix. Each submatrix $\boldsymbol{A}_{4lip}, \forall p = 1, ..., P$ can be expressed as $\boldsymbol{A}_{4lip} = \begin{pmatrix} \boldsymbol{A}_{4lip1} & ... & \boldsymbol{A}_{4lipS} \end{pmatrix} \in \mathbb{R}^{m_i \times SK}$. Finally, the submatrix $\boldsymbol{A}_{4lips}, \forall s = 1, ..., S$ is written as $\boldsymbol{A}_{4lips} = \left(w_{uv}^{4lips} \right) \in \mathbb{R}^{m_i \times K}$ where $w_{uv}^{4lips} = Rx_{ip}c_{isv}\phi_l(t_{iu}), \forall u = 1, ..., m_i, v = 1, ..., K$ is the element at u^{th} row and v^{th} column.

With the above block matrices, the design matrix of observed heterogeneity can then be manifested as

$$\boldsymbol{\Omega}_i = \begin{pmatrix} \boldsymbol{\Lambda}_i & \boldsymbol{A}_{2i} & \boldsymbol{A}_{3i} & \boldsymbol{A}_{4i} \end{pmatrix} \in \mathbb{R}^{m_i \times U}$$

where $U = (L+1)(1+P+SK+PSK)$.

Further, we denote $\boldsymbol{\zeta} = \left[\boldsymbol{\nu}^{\mathrm{T}}, \boldsymbol{\beta}_1^{\mathrm{T}}, ..., \boldsymbol{\beta}_L^{\mathrm{T}}, \boldsymbol{b}_{01}^{\mathrm{T}} ... \boldsymbol{b}_{LS}^{\mathrm{T}}, \boldsymbol{b}_{011}^{'\mathrm{T}} ... \boldsymbol{b}_{LPS}^{'\mathrm{T}}\right]^{\mathrm{T}}$ as a vector of coefficients for the design matrix of observed heterogeneity. With the above notations, we can simplify the proposed model into the vector form, i.e., $\boldsymbol{y}_i = \boldsymbol{\Omega}_i\boldsymbol{\zeta} + \boldsymbol{\Lambda}_i\boldsymbol{\gamma}_i + \boldsymbol{\epsilon}_i,\ i = 1, ..., N$.

B.1.2 Derivation of Eq. (4.31)

The measurements of specimen i are normally distributed, i.e., the marginal density can be expressed as $\boldsymbol{y}_i \sim N(\boldsymbol{\Omega}_i\boldsymbol{\zeta}, \boldsymbol{\Lambda}_i\boldsymbol{\Sigma}_\gamma\boldsymbol{\Lambda}_i^{\mathrm{T}} + \sigma_\epsilon^2\mathbf{I}_{m_i})$. Given that $\boldsymbol{\gamma}_i$ is known, the conditional distribution becomes $\boldsymbol{y}_i \mid \boldsymbol{\gamma}_i \sim N(\boldsymbol{\Omega}_i\boldsymbol{\zeta} + \boldsymbol{\Lambda}_i\boldsymbol{\gamma}_i, \sigma_\epsilon^2\mathbf{I}_{m_i})$. Based on Bayes rule, the conditional distribution of $\boldsymbol{\gamma}_i \mid \boldsymbol{D}$ can be calculated as

$$
\begin{aligned}
p(\boldsymbol{\gamma}_i \mid \boldsymbol{D}) &= p(\boldsymbol{\gamma}_i \mid \boldsymbol{y}_i, \boldsymbol{\Theta}) = \frac{p(\boldsymbol{y}_i \mid \boldsymbol{\gamma}_i, \boldsymbol{\Theta}) p(\boldsymbol{\gamma}_i \mid \boldsymbol{\Theta})}{p(\boldsymbol{y}_i \mid \boldsymbol{\Theta})} \\
&= \frac{C_{11}\frac{1}{\sigma_\epsilon}\left|\Sigma_\gamma\right|^{-\frac{1}{2}} \exp\left[-\frac{1}{2\sigma_\epsilon^2}\left\|\boldsymbol{y}_i - \boldsymbol{\Omega}_i\boldsymbol{\zeta} - \boldsymbol{\Lambda}_i\boldsymbol{\gamma}_i\right\|^2 - \frac{1}{2}\boldsymbol{\gamma}_i^{\mathrm{T}}\boldsymbol{\Sigma}_\gamma^{-1}\boldsymbol{\gamma}_i\right]}{C_{12}\left|\boldsymbol{\Lambda}_i\boldsymbol{\Sigma}_\gamma\boldsymbol{\Lambda}_i^{\mathrm{T}} + \sigma_\epsilon^2\mathbf{I}_{m_i}\right|^{-\frac{1}{2}} \exp\left[-\frac{1}{2}(\boldsymbol{y}_i - \boldsymbol{\Omega}_i\boldsymbol{\zeta})^{\mathrm{T}}(\boldsymbol{\Lambda}_i\boldsymbol{\Sigma}_\gamma\boldsymbol{\Lambda}_i^{\mathrm{T}} + \sigma_\epsilon^2\mathbf{I}_{m_i})^{-1}(\boldsymbol{y}_i - \boldsymbol{\Omega}_i\boldsymbol{\zeta})\right]}
\end{aligned}
$$

where C_{11} and C_{12} are normalizing constant. With the expansion of Euclidean norm, i.e., $\|\boldsymbol{y}_i - \boldsymbol{\Omega}_i\boldsymbol{\zeta} - \boldsymbol{\Lambda}_i\boldsymbol{\gamma}_i\|^2 = \|\boldsymbol{y}_i - \boldsymbol{\Omega}_i\boldsymbol{\zeta}\|^2 + \|\boldsymbol{\Lambda}_i\boldsymbol{\gamma}_i\|^2 - 2(\boldsymbol{y}_i - \boldsymbol{\Omega}_i\boldsymbol{\zeta})^{\mathrm{T}}\boldsymbol{\Lambda}_i\boldsymbol{\gamma}_i$, the conditional density can be further represented as

$$
\begin{aligned}
p(\boldsymbol{\gamma}_i \mid \boldsymbol{y}_i, \boldsymbol{\Theta}) &\propto \frac{\left|\sigma_\epsilon^2\boldsymbol{\Sigma}_\gamma\right|^{-\frac{1}{2}}}{\left|\boldsymbol{\Lambda}_i\boldsymbol{\Sigma}_\gamma\boldsymbol{\Lambda}_i^{\mathrm{T}} + \sigma_\epsilon^2\mathbf{I}_{m_i}\right|^{-\frac{1}{2}}} \exp[-\frac{1}{2\sigma_\epsilon^2}((\boldsymbol{y}_i - \boldsymbol{\Omega}_i\boldsymbol{\zeta})^{\mathrm{T}}(\boldsymbol{y}_i - \boldsymbol{\Omega}_i\boldsymbol{\zeta}) + \boldsymbol{\gamma}_i^{\mathrm{T}}\boldsymbol{\Lambda}_i^{\mathrm{T}}\boldsymbol{\Lambda}_i\boldsymbol{\gamma}_i \\
&- 2(\boldsymbol{y}_i - \boldsymbol{\Omega}_i\boldsymbol{\zeta})^{\mathrm{T}}\boldsymbol{\Lambda}_i\boldsymbol{\gamma}_i) - \frac{1}{2}\boldsymbol{\gamma}_i^{\mathrm{T}}\boldsymbol{\Sigma}_\gamma^{-1}\boldsymbol{\gamma}_i + \frac{1}{2}(\boldsymbol{y}_i - \boldsymbol{\Omega}_i\boldsymbol{\zeta})^{\mathrm{T}}(\boldsymbol{\Lambda}_i\boldsymbol{\Sigma}_\gamma\boldsymbol{\Lambda}_i^{\mathrm{T}} + \sigma_\epsilon^2\mathbf{I}_{m_i})^{-1}(\boldsymbol{y}_i - \boldsymbol{\Omega}_i\boldsymbol{\zeta})] \\
&\propto \left|(\boldsymbol{\Sigma}_\gamma^{-1} + \frac{\boldsymbol{\Lambda}_i^{\mathrm{T}}\boldsymbol{\Lambda}_i}{\sigma_\epsilon^2})^{-1}\right|^{-\frac{1}{2}} \exp[-\frac{1}{2}(\boldsymbol{y}_i - \boldsymbol{\Omega}_i\boldsymbol{\zeta})^{\mathrm{T}}(\boldsymbol{\Lambda}_i\boldsymbol{\Sigma}_\gamma\boldsymbol{\Lambda}_i^{\mathrm{T}} + \sigma_\epsilon^2\mathbf{I}_{m_i})^{-1}(\frac{\boldsymbol{\Lambda}_i\boldsymbol{\Sigma}_\gamma\boldsymbol{\Lambda}_i^{\mathrm{T}}}{\sigma_\epsilon^2} + \mathbf{I}_{m_i}) \\
&\cdot (\boldsymbol{y}_i - \boldsymbol{\Omega}_i\boldsymbol{\zeta}) + \frac{1}{2}(\boldsymbol{y}_i - \boldsymbol{\Omega}_i\boldsymbol{\zeta})^{\mathrm{T}}(\boldsymbol{\Lambda}_i\boldsymbol{\Sigma}_\gamma\boldsymbol{\Lambda}_i^{\mathrm{T}} + \sigma_\epsilon^2\mathbf{I}_{m_i})^{-1}(\boldsymbol{y}_i - \boldsymbol{\Omega}_i\boldsymbol{\zeta}) - \frac{1}{2}\boldsymbol{\gamma}_i^{\mathrm{T}}\frac{\boldsymbol{\Lambda}_i^{\mathrm{T}}\boldsymbol{\Lambda}_i}{\sigma_\epsilon^2}\boldsymbol{\gamma}_i \\
&+ \frac{1}{\sigma_\epsilon^2}(\boldsymbol{y}_i - \boldsymbol{\Omega}_i\boldsymbol{\zeta})^{\mathrm{T}}\boldsymbol{\Lambda}_i\boldsymbol{\gamma}_i - \frac{1}{2}\boldsymbol{\gamma}_i^{\mathrm{T}}\boldsymbol{\Sigma}_\gamma^{-1}\boldsymbol{\gamma}_i]
\end{aligned}
$$

$$
\begin{aligned}
&\propto \left|(\boldsymbol{\Sigma}_\gamma^{-1} + \frac{\boldsymbol{\Lambda}_i^{\mathrm{T}}\boldsymbol{\Lambda}_i}{\sigma_\epsilon^2})^{-1}\right|^{-\frac{1}{2}} \exp[-\frac{1}{2}(\boldsymbol{y}_i - \boldsymbol{\Omega}_i\boldsymbol{\zeta})^{\mathrm{T}}(\boldsymbol{\Lambda}_i\boldsymbol{\Sigma}_\gamma\boldsymbol{\Lambda}_i^{\mathrm{T}} + \sigma_\epsilon^2\mathbf{I}_{m_i})^{-1}\frac{\boldsymbol{\Lambda}_i\boldsymbol{\Sigma}_\gamma\boldsymbol{\Lambda}_i^{\mathrm{T}}}{\sigma_\epsilon^2}(\boldsymbol{y}_i - \boldsymbol{\Omega}_i\boldsymbol{\zeta}) \\
&- \frac{1}{2}\boldsymbol{\gamma}_i^{\mathrm{T}}(\boldsymbol{\Sigma}_\gamma^{-1} + \frac{\boldsymbol{\Lambda}_i^{\mathrm{T}}\boldsymbol{\Lambda}_i}{\sigma_\epsilon^2})\boldsymbol{\gamma}_i + \frac{(\boldsymbol{y}_i - \boldsymbol{\Omega}_i\boldsymbol{\zeta})^{\mathrm{T}}\boldsymbol{\Lambda}_i}{\sigma_\epsilon^2}\boldsymbol{\gamma}_i] \\
&\propto |\boldsymbol{V}_i|^{-\frac{1}{2}} \exp\left[-\frac{1}{2}(\boldsymbol{\gamma}_i - \boldsymbol{\mu}_i)^{\mathrm{T}}\boldsymbol{V}_i^{-1}(\boldsymbol{\gamma}_i - \boldsymbol{\mu}_i)\right]
\end{aligned}
$$

where $\boldsymbol{\mu}_i = \frac{1}{\sigma_\epsilon^2}\boldsymbol{V}_i\boldsymbol{\Lambda}_i^{\mathrm{T}}(\boldsymbol{y}_i - \boldsymbol{\Omega}_i\boldsymbol{\zeta})$ and $\boldsymbol{V}_i = (\boldsymbol{\Sigma}_\gamma^{-1} + \frac{\boldsymbol{\Lambda}_i^{\mathrm{T}}\boldsymbol{\Lambda}_i}{\sigma_\epsilon^2})^{-1}$. Thus, $\boldsymbol{\gamma}_i \mid \boldsymbol{y}_i, \boldsymbol{\Theta}$ follows normal distribution with mean $\boldsymbol{\mu}_i$ and variance $\boldsymbol{V}_i$. The conditional expectation quantities can then be derived as

$$
\begin{aligned}
&\mathbb{E}[\boldsymbol{\gamma}_i \mid \boldsymbol{D}, \boldsymbol{\Theta}] = \boldsymbol{\mu}_i = \frac{1}{\sigma_\epsilon^2}\boldsymbol{V}_i\boldsymbol{\Lambda}_i^{\mathrm{T}}(\boldsymbol{y}_i - \boldsymbol{\Omega}_i\boldsymbol{\zeta}) \\
&\mathbb{E}[\boldsymbol{\gamma}_i\boldsymbol{\gamma}_i^{\mathrm{T}} \mid \boldsymbol{D}, \boldsymbol{\Theta}] = \mathbb{V}(\boldsymbol{\gamma}_i \mid \boldsymbol{D}, \boldsymbol{\Theta}) + \mathbb{E}[\boldsymbol{\gamma}_i \mid \boldsymbol{D}, \boldsymbol{\Theta}]\left(\mathbb{E}[\boldsymbol{\gamma}_i \mid \boldsymbol{D}, \boldsymbol{\Theta}]\right)^{\mathrm{T}} = \boldsymbol{V}_i + \boldsymbol{\mu}_i\boldsymbol{\mu}_i^{\mathrm{T}}
\end{aligned}
$$

Further, the conditional expectation can be simplified as

$$
\mathbb{E}[\boldsymbol{\gamma} \mid \boldsymbol{D}, \boldsymbol{\Theta}] = \boldsymbol{\mu} = \begin{pmatrix} \mathbb{E}[\boldsymbol{\gamma}_1 \mid \boldsymbol{D}, \boldsymbol{\Theta}] \\ \mathbb{E}[\boldsymbol{\gamma}_2 \mid \boldsymbol{D}, \boldsymbol{\Theta}] \\ \cdots \\ \mathbb{E}[\boldsymbol{\gamma}_N \mid \boldsymbol{D}, \boldsymbol{\Theta}] \end{pmatrix} = \begin{pmatrix} \boldsymbol{\mu}_1 \\ \boldsymbol{\mu}_2 \\ \cdots \\ \boldsymbol{\mu}_N \end{pmatrix} = \left(\boldsymbol{\mu}_1^{\mathrm{T}}\boldsymbol{\mu}_2^{\mathrm{T}}\ldots\boldsymbol{\mu}_N^{\mathrm{T}}\right)^{\mathrm{T}}
$$

B.1.3 Derivation of Eq. (4.32), Eq. (4.33) and Eq. (4.34)

The model parameters $\boldsymbol{\Theta}$ can be obtained by maximizing Q function $Q(\boldsymbol{\Theta}, \boldsymbol{\Theta}^{(\tau-1)})$. We will show how to derive the estimates of $\hat{\boldsymbol{\zeta}}$, $\hat{\boldsymbol{\Sigma}}_\gamma$ and $\hat{\sigma}_\epsilon^2$ respectively.

The parameter $\hat{\boldsymbol{\zeta}}$ at iteration τ can be obtained by $\hat{\boldsymbol{\zeta}}^{(\tau)} = \arg\max_{\boldsymbol{\zeta}} Q(\boldsymbol{\Theta}, \boldsymbol{\Theta}^{(\tau-1)})$. This can be further explicitly written as

$$
\begin{aligned}
\frac{\partial Q}{\partial \boldsymbol{\zeta}} = -\frac{1}{2\sigma_\epsilon^2}(&\frac{\partial \boldsymbol{\zeta}^{\mathrm{T}}\boldsymbol{\Omega}^{\mathrm{T}}\boldsymbol{\Omega}\boldsymbol{\zeta}}{\partial \boldsymbol{\zeta}} - \frac{\partial \boldsymbol{\zeta}^{\mathrm{T}}\boldsymbol{\Omega}^{\mathrm{T}}\boldsymbol{y}}{\partial \boldsymbol{\zeta}} - \frac{\partial \boldsymbol{y}^{\mathrm{T}}\boldsymbol{\Omega}\boldsymbol{\zeta}}{\partial \boldsymbol{\zeta}} + \frac{\partial \mathbb{E}[\boldsymbol{\gamma}^{\mathrm{T}} \mid \boldsymbol{D}, \boldsymbol{\Theta}^{(\tau-1)}]\boldsymbol{\Lambda}^{\mathrm{T}}\boldsymbol{\Omega}\boldsymbol{\zeta}}{\partial \boldsymbol{\zeta}} \\
&+ \frac{\partial \boldsymbol{\zeta}^{\mathrm{T}}\boldsymbol{\Omega}^{\mathrm{T}}\boldsymbol{\Lambda}\mathbb{E}[\boldsymbol{\gamma}^{\mathrm{T}} \mid \boldsymbol{D}, \boldsymbol{\Theta}^{(\tau-1)}]}{\partial \boldsymbol{\zeta}}) = 0
\end{aligned}
$$

The above equation can be simplified as

$$2\boldsymbol{\Omega}^{\mathrm{T}}\boldsymbol{\Omega}\boldsymbol{\zeta} + 2\boldsymbol{\Omega}^{\mathrm{T}}\boldsymbol{\Lambda}\mathbb{E}[\boldsymbol{\gamma} \mid \boldsymbol{D}, \boldsymbol{\Theta}^{(\tau-1)}] - 2\boldsymbol{\Omega}^{\mathrm{T}}\boldsymbol{y} = 0$$

To solve the above equation, we obtain parameter estimate as

$$\hat{\boldsymbol{\zeta}}^{(\tau)} = (\boldsymbol{\Omega}^{\mathrm{T}}\boldsymbol{\Omega})^{-1}\boldsymbol{\Omega}^{\mathrm{T}}(\boldsymbol{y} - \boldsymbol{\Lambda}\mathbb{E}[\boldsymbol{\gamma} \mid \boldsymbol{D}, \boldsymbol{\Theta}^{(\tau-1)}]) = (\boldsymbol{\Omega}^{\mathrm{T}}\boldsymbol{\Omega})^{-1}\boldsymbol{\Omega}^{\mathrm{T}}(\boldsymbol{y} - \boldsymbol{\Lambda}\boldsymbol{\mu}^{(\tau-1)})$$

Similarly, the parameter $\hat{\boldsymbol{\Sigma}}_\gamma$ at iteration τ can be obtained by maximizing Q function, i.e., $\hat{\boldsymbol{\Sigma}}_\gamma^{(\tau)} = \arg\max_{\boldsymbol{\Sigma}_\gamma} Q(\boldsymbol{\Theta}, \boldsymbol{\Theta}^{(\tau-1)})$. This can be achieved by solving the following equation

$$\frac{\partial Q}{\partial \boldsymbol{\Sigma}_\gamma} = -\frac{N}{2}\frac{\partial \log|\boldsymbol{\Sigma}_\gamma|}{\partial \boldsymbol{\Sigma}_\gamma} - \frac{1}{2}\sum_{i=1}^{N}\left(\frac{\partial \mathbb{E}[\boldsymbol{\gamma}_i{}^{\mathrm{T}}\boldsymbol{\Sigma}_\gamma^{-1}\boldsymbol{\gamma}_i \mid \boldsymbol{D}, \boldsymbol{\Theta}^{(\tau-1)}]}{\partial \boldsymbol{\Sigma}_\gamma}\right) = 0$$

The parameter estimate of $\boldsymbol{\Sigma}_\gamma$ can then be obtained as

$$\begin{aligned}\hat{\boldsymbol{\Sigma}}_\gamma^{(\tau)} &= \frac{1}{N}\sum_{i=1}^{N}\mathbb{E}[\boldsymbol{\gamma}_i\boldsymbol{\gamma}_i^{\mathrm{T}} \mid \boldsymbol{D}, \boldsymbol{\Theta}^{(\tau-1)}] = \frac{1}{N}\sum_{i=1}^{N}\left(\boldsymbol{V}_i^{(\tau-1)} + \boldsymbol{\mu}_i^{(\tau-1)}\boldsymbol{\mu}_i^{(\tau-1)\mathrm{T}}\right) \\ &= \frac{1}{N}\sum_{i=1}^{N}\left((\hat{\boldsymbol{\Sigma}}_\gamma^{(\tau-1)-1} + \frac{1}{\hat{\sigma}_\epsilon^{2(\tau-1)}}\boldsymbol{\Lambda}_i^{\mathrm{T}}\boldsymbol{\Lambda}_i)^{-1} + \boldsymbol{\mu}_i^{(\tau-1)}\boldsymbol{\mu}_i^{(\tau-1)\mathrm{T}}\right)\end{aligned}$$

Based on the updated estimates of $\hat{\boldsymbol{\zeta}}^{(\tau)}$ and $\hat{\boldsymbol{\Sigma}}_\gamma^{(\tau)}$, the parameter $\hat{\sigma}_\epsilon^2$ at iteration τ can be obtained by $\hat{\sigma}_\epsilon^{2(\tau)} = \arg\max_{\sigma_\epsilon^2} Q(\boldsymbol{\Theta}, \boldsymbol{\Theta}^{(\tau-1)})$. The parameter $\hat{\sigma}_\epsilon^{2(\tau)}$ can be estimated by solving the following equation

$$\begin{aligned}\frac{\partial Q}{\partial \sigma_\epsilon^2} = &-\frac{\sum_{i=1}^{N} m_i}{2}\frac{\partial \log(\sigma_\epsilon^2)}{\partial \sigma_\epsilon^2} - \frac{\partial \frac{1}{2\sigma_\epsilon^2}}{\partial \sigma_\epsilon^2}\Big(\left\|\boldsymbol{y} - \boldsymbol{\Omega}\hat{\boldsymbol{\zeta}}^{(\tau)}\right\|^2 + \sum_{i=1}^{N}\mathrm{Tr}(\boldsymbol{\Lambda}_i^{\mathrm{T}}\boldsymbol{\Lambda}_i\mathbb{E}[\boldsymbol{\gamma}_i\boldsymbol{\gamma}_i^{\mathrm{T}} \mid \boldsymbol{D}, \boldsymbol{\Theta}^{(\tau-1)}]) \\ &- 2(\boldsymbol{y} - \boldsymbol{\Omega}\hat{\boldsymbol{\zeta}}^{(\tau)})^{\mathrm{T}}\boldsymbol{\Lambda}\mathbb{E}[\boldsymbol{\gamma} \mid \boldsymbol{D}, \boldsymbol{\Theta}^{(\tau-1)}]) = 0\end{aligned}$$

The closed form of parameter estimate of σ_ϵ^2 then becomes

$$\begin{aligned}\hat{\sigma}_\epsilon^{2(\tau)} &= \frac{1}{\sum_{i=1}^{N} m_i}\Big(\Big\|\boldsymbol{y} - \boldsymbol{\Omega}\hat{\boldsymbol{\zeta}}^{(\tau)}\Big\|^2 - 2\sum_{i=1}^{N}(\boldsymbol{y}_i - \boldsymbol{\Omega}_i\hat{\boldsymbol{\zeta}}^{(\tau)})^{\mathrm{T}}\boldsymbol{\Lambda}_i\mathbb{E}[\boldsymbol{\gamma}_i \mid \boldsymbol{D}, \boldsymbol{\Theta}^{(\tau-1)}] \\ &+ \sum_{i=1}^{N}\mathrm{Tr}(\boldsymbol{\Lambda}_i^{\mathrm{T}}\boldsymbol{\Lambda}_i\mathbb{E}[\boldsymbol{\gamma}_i\boldsymbol{\gamma}_i^{\mathrm{T}} \mid \boldsymbol{D}, \boldsymbol{\Theta}^{(\tau-1)}])\Big) \\ &= \frac{1}{\sum_{i=1}^{N} m_i}\Big(\Big\|\boldsymbol{y} - \boldsymbol{\Omega}\hat{\boldsymbol{\zeta}}^{(\tau)}\Big\|^2 - 2\sum_{i=1}^{N}(\boldsymbol{y}_i - \boldsymbol{\Omega}_i\hat{\boldsymbol{\zeta}}^{(\tau)})^{\mathrm{T}}\boldsymbol{\Lambda}_i\boldsymbol{\mu}_i^{(\tau-1)} \\ &+ \sum_{i=1}^{N}\mathrm{Tr}(\boldsymbol{\Lambda}_i^{\mathrm{T}}\boldsymbol{\Lambda}_i((\hat{\boldsymbol{\Sigma}}_\gamma^{(\tau)-1} + \frac{1}{\hat{\sigma}_\epsilon^{2(\tau-1)}}\boldsymbol{\Lambda}_i^{\mathrm{T}}\boldsymbol{\Lambda}_i)^{-1} + \boldsymbol{\mu}_i^{(\tau-1)}\boldsymbol{\mu}_i^{(\tau-1)\mathrm{T}})))\end{aligned}$$

Based on the above derived closed forms, the estimation procedure will iteratively update the parameters through expectation step and maximization step.

B.2 Appendix for Chapter 5

B.2.1 Derivations of Eq. (5.38) and $K_1(R,\omega)$-$K_4(R,\omega)$

Based on the proposed equivalent circuit model in Figure 5.50, the overall impedance Z of the circuit model can be calculated based on the series and parallel configurations of circuit elements as

$$Z = R_1 + \frac{\frac{1}{C_1 s^{\alpha_1}}\left(R + \frac{R_2}{C_2 s^{\alpha_2}}/(\frac{1}{C_2 s^{\alpha_2}} + R_2)\right)}{\frac{1}{C_1 s^{\alpha_1}} + R + \frac{R_2}{C_2 s^{\alpha_2}}/(\frac{1}{C_2 s^{\alpha_2}} + R_2)}$$

which can be further simplified into $H_f(s, R, \boldsymbol{\Theta})$ in Eq. (5.38). The corresponding frequency response of transfer function becomes

$$H_f(s, R, \boldsymbol{\Theta})\mid_{s=j\omega} = \Psi_1(j\omega)/\Psi_2(j\omega)$$

where $\Psi_1(j\omega) =$ is expressed as

$$\Psi_1(j\omega) = A_f(j\omega)^{\alpha_1+\alpha_2} + B_{f1}(j\omega)^{\alpha_1} + B_{f2}(j\omega)^{\alpha_2} + U_f(j\omega)^0$$

$\Psi_2(j\omega)$ is expressed as

$$\Psi_2(j\omega) = D_f(j\omega)^{\alpha_1+\alpha_2} + E_{f1}(j\omega)^{\alpha_1} + E_{f2}(j\omega)^{\alpha_2} + V_f(j\omega)^0$$

Based on Euler's formula, we can show that $(j\omega)^\alpha = \omega^\alpha(\cos\frac{\pi}{2} + j\sin\frac{\pi}{2})^\alpha = \omega^\alpha(\cos\frac{\pi}{2}\alpha + j\sin\frac{\pi}{2}\alpha)$. Thus, $\Psi_1(j\omega)$ and $\Psi_2(j\omega)$ can be further written as

$$\begin{aligned}
\Psi_1(j\omega) &= A_f\omega^{\alpha_1+\alpha_2}\left(\cos\frac{\pi}{2}(\alpha_1+\alpha_2) + j\sin\frac{\pi}{2}(\alpha_1+\alpha_2)\right) \\
&\quad + B_{f1}\omega^{\alpha_1}\left(\cos\frac{\pi}{2}\alpha_1 + j\sin\frac{\pi}{2}\alpha_1\right) + B_{f2}\omega^{\alpha_2}\left(\cos\frac{\pi}{2}\alpha_2 + j\sin\frac{\pi}{2}\alpha_2\right) + U_f \\
\Psi_2(j\omega) &= D_f\omega^{\alpha_1+\alpha_2}\left(\cos\frac{\pi}{2}(\alpha_1+\alpha_2) + j\sin\frac{\pi}{2}(\alpha_1+\alpha_2)\right) \\
&\quad + E_{f1}\omega^{\alpha_1}\left(\cos\frac{\pi}{2}\alpha_1 + j\sin\frac{\pi}{2}\alpha_1\right) + E_{f2}\omega^{\alpha_2}\left(\cos\frac{\pi}{2}\alpha_2 + j\sin\frac{\pi}{2}\alpha_2\right) + V_f
\end{aligned}$$

Denote $G_1(\alpha,\omega) = \omega^\alpha\cos\frac{\pi}{2}\alpha$ and $G_2(\alpha,\omega) = \omega^\alpha\sin\frac{\pi}{2}\alpha$, $\Psi_1(j\omega)$ and $\Psi_2(j\omega)$ can be further simplified as $K_1(R,\omega) + jK_2(R,\omega)$ and $K_3(R,\omega) + jK_4(R,\omega)$, respectively. $K_1(R,\omega)$ to $K_4(R,\omega)$ can be explicitly written as

$$\begin{aligned}
K_1(\omega_k,R) &= A_fG_1(\alpha_1+\alpha_2,\omega_k) + B_{f1}G_1(\alpha_1,\omega_k) + B_{f2}G_1(\alpha_2,\omega_k) + U_f \\
K_2(\omega_k,R) &= A_fG_2(\alpha_1+\alpha_2,\omega_k) + B_{f1}G_2(\alpha_1,\omega_k) + B_{f2}G_2(\alpha_2,\omega_k) \\
K_3(\omega_k,R) &= D_fG_1(\alpha_1+\alpha_2,\omega_k) + E_{f1}G_1(\alpha_1,\omega_k) + E_{f2}G_1(\alpha_2,\omega_k) + V_f \\
K_4(\omega_k,R) &= D_fG_2(\alpha_1+\alpha_2,\omega_k) + E_{f1}G_2(\alpha_1,\omega_k) + E_{f2}G_2(\alpha_2,\omega_k)
\end{aligned}$$

where $G_1(\eta, \omega_k) = \omega_k^\eta \cos\frac{\pi}{2}\eta$, $G_2(\eta, \omega_k) = \omega_k^\eta \sin\frac{\pi}{2}\eta$, and $A_f = RR_1R_2C_1C_2$, $B_{f1} = RC_1R_1 + C_1R_1R_2$, $B_{f2} = RC_2R_2 + C_2R_2R_1$, $U_f = R_1 + R_2 + R$, $D_f = RR_2C_1C_2$, $E_{f1} = RC_1 + C_1R_2$, $E_{f2} = C_2R_2$, $V_f = 1$.

B.2.2 Derivation of $r_{1i}(\omega, R_i)$-$r_{4i}(\omega, R_i)$

Similar to the above impedance calculation, the transfer function $H_f(s, R_i, \bar{\mathbf{\Theta}})$ of individual unit i in the population-level model can be written as

$$H_f(s, R_i, \bar{\mathbf{\Theta}}) = \frac{A_i s^{\alpha_1+\alpha_2} + B_{1i} s^{\alpha_1} + B_{2i} s^{\alpha_2} + U_i s^0}{D_i s^{\alpha_1+\alpha_2} + E_{1i} s^{\alpha 1} + E_{f2} s^{\alpha_2} + V_f}$$

where $A_i = R_iR_1R_2C_1C_2$, $B_{1i} = C_1R_1(R_i + R_2)$, $B_{2i} = C_2R_2(R_i + R_1)$, $U_i = R_i + R_1 + R_2$, $D_i = R_iR_2C_1C_2$, $E_{1i} = C_1(R_i + R_2)$, $E_{f2} = C_2R_2$ and $V_f = 1$. The corresponding frequency response of transfer function becomes $H_f(s, R_i, \bar{\mathbf{\Theta}}) \mid_{s=j\omega} = \Psi_{1i}(j\omega)/\Psi_{2i}(j\omega)$. With similar denotation of $G_1(\alpha, \omega)$ and $G_2(\alpha, \omega)$ as written in Section B.2.1, $\Psi_{1i}(j\omega)$ and $\Psi_{2i}(j\omega)$ can be explicitly represented as

$$\begin{aligned}
\Psi_{1i}(j\omega) &= A_i \left(G_1(\alpha_1+\alpha_2, \omega) + jG_2(\alpha_1+\alpha_2, \omega)\right) \\
&\quad + B_{1i} \left(G_1(\alpha_1, \omega) + jG_2(\alpha_1, \omega)\right) + B_{2i} \left(G_1(\alpha_2, \omega) + jG_2(\alpha_2, \omega)\right) + U_i \\
&= \left(A_iG_1(\alpha_1+\alpha_2, \omega) + B_{1i}G_1(\alpha_1, \omega) + B_{2i}G_1(\alpha_2, \omega) + U_i\right) \\
&\quad + j \left(A_iG_2(\alpha_1+\alpha_2, \omega) + B_{1i}G_2(\alpha_1, \omega) + B_{2i}G_2(\alpha_2, \omega)\right), \\
\Psi_{2i}(j\omega) &= D_i \left(G_1(\alpha_1+\alpha_2, \omega) + jG_2(\alpha_1+\alpha_2, \omega)\right) \\
&\quad + E_{1i} \left(G_1(\alpha_1, \omega) + jG_2(\alpha_1, \omega)\right) + E_{f2} \left(G_1(\alpha_2, \omega) + jG_2(\alpha_2, \omega)\right) + V_f \\
&= \left(D_iG_1(\alpha_1+\alpha_2, \omega) + E_{1i}G_1(\alpha_1, \omega) + E_{f2}G_1(\alpha_2, \omega) + V_f\right) \\
&\quad + j \left(D_iG_2(\alpha_1+\alpha_2, \omega) + E_{1i}G_2(\alpha_1, \omega) + E_{f2}G_2(\alpha_2, \omega)\right)
\end{aligned}$$

Let $r_{1i}(\omega, R_i)$ and $r_{2i}(\omega, R_i)$ represent the real and imaginary parts of $\Psi_{1i}(j\omega)$, and let $r_{3i}(\omega, R_i)$ and $r_{4i}(\omega, R_i)$ represent the real and imaginary parts of $\Psi_{2i}(j\omega)$, the derivation is completed. $r_{1i}(\omega, R_i)$ to $r_{4i}(\omega, R_i)$ can be explicitly written as

$$
\begin{aligned}
r_{1i}(\omega_{ik}, R_i) &= A_i G_1(\alpha_1 + \alpha_2, \omega_{ik}) + B_{1i} G_1(\alpha_1, \omega_{ik}) + B_{2i} G_1(\alpha_2, \omega_{ik}) + U_i \\
r_{2i}(\omega_{ik}, R_i) &= A_i G_2(\alpha_1 + \alpha_2, \omega_{ik}) + B_{1i} G_2(\alpha_1, \omega_{ik}) + B_{2i} G_2(\alpha_2, \omega_{ik}) \\
r_{3i}(\omega_{ik}, R_i) &= D_i G_1(\alpha_1 + \alpha_2, \omega_{ik}) + E_{1i} G_1(\alpha_1, \omega_{ik}) + E_{f2} G_1(\alpha_2, \omega_{ik}) + V_f \\
r_{4i}(\omega_{ik}, R_i) &= D_i G_2(\alpha_1 + \alpha_2, \omega_{ik}) + E_{1i} G_2(\alpha_1, \omega_{ik}) + E_{f2} G_2(\alpha_2, \omega_{ik})
\end{aligned}
$$